Imperial College of Science, Technology and Medicine
University of London

PULSATING FLOW BEHAVIOUR IN A TWIN-ENTRY VANELESS RADIAL INFLOW TURBINE

by

J. H. YEO

January 1990

This thesis forms part of the requirements for the Doctor of Philosophy degree of the University of London and the Diploma of Imperial College

Abstract

This investigation is aimed at understanding more fully the fluid dynamic basis of the pulse flow behaviour of twin-entry radial-inflow turbines. Although turbocharger turbines operate under highly unsteady flow conditions, tests on these turbines are usually carried out in steady flow conditions. A survey of flow investigations on radial inflow-turbines reveal very little information on unsteady flow testing. An extensive experimental investigation of the flow in a vaneless twin-entry radial-inflow turbocharger turbine is presented for both steady and unsteady flow conditions.

Using a Laser Two Focus (L2F) velocimeter it has been possible to measure the flow in the turbine housing immediately upstream of the rotor, and in the exhaust pipe downstream of it. The instrumented turbine allows measurements to be made at different azimuth angles. In addition, mirrors can be accommodated to deflect the L2F beam so that it is possible to measure the same point in the flow from different angles, and hence to investigate the presence of axial components of velocity at rotor inlet. In the unsteady flow condition measurements are phase-locked with the pulse generator so that the variation in flow conditions through a pulse in these important regions can be studied.

Results are presented for steady flow tests with equal and partial admission flow conditions. These show significant changes in incidence at rotor entry as the flow condition varies. At the rotor exit, a large component of swirl is observed at off-design flow conditions.

Unsteady flow tests also reveal large variations of incidence

through a pulse at rotor entry, and similarly large changes in rotor exit swirl, even when operating at a nominal design condition. The interaction of the flows in the two volute entries when both are pulsed in anti-phase (simulating a common pulse turbocharging arrangement) are very clearly seen.

It has been possible from these measurements to deduce and correlate the time-varying velocity triangles with time-varying power developed by rotor, and turbine efficiency.

From these investigations it has been possible to understand more fully the origin of the losses associated with pulsating flow, to indicate the areas where further research is required, and to suggest how it may be possible to modify the turbine design to make better use of the engine exhaust pulse energy.

Acknowlegements

The author wishes to thank Dr. N.C.Baines under whose supervision this project was conducted, for his advice, guidance, patience and encouragement.

To Dr. E.Tzanatos, whom the author worked very closely with during the early stages of the experimental work, the author is grateful for his patience, thoughtfulness and contribution in the work.

The author also wishes to thank J.David for his precision work in instrumenting the turbine housing and building up the dynamometer, and A.Dale and C.Hall for support and technical advise.

The author is also indebted to Garrett Automotive Europe and the Science and Engineering Research Council for a Research Studentship covering from January 1987 to January 1990.

This thesis is dedicated to Siang and Michael

CONTENTS

Title Page	1
Abstract	2
Acknowledgements	4
Contents	6
Notation	9
CHAPTER 1 : Introduction	10
1.1 Principle of Turbocharging	10
1.2 Energy Transfer in a Radial Turbine Rotor	14
1.3 Objectives	19
CHAPTER 2 : Literature Survey	25
2.1 Flow Field Survey in a Volute	25
2.1.1 Volute survey	25
2.1.2 Rotor exit survey	29
2.2 Test and Performance	32
2.2.1 Steady Flow Conditions	33
2.2.2 Unsteady Flow Conditions	35
2.3 Application of Laser Velocimetry on Turbomachinery	37
2.4 Conclusions from Literature Survey	40
CHAPTER 3 : Laser Two Focus Velocimetry	60
3.1 Laser Velocimetry Technique	60
3.1.1 LDV Principle	60
3.1.2 L2F Principle	61
3.1.3 Comparison between LDV and L2F	61
3.2 L2F Technique	62
3.3 L2F Optical System	64
3.4 L2F Signal Processing	66
3.5 L2F Periodic Flow Mapping	67
3.6 Signal Quality of the L2F Velocimeter	69
3.7 Summary	71

CHAPTER 4 : Experimental Facilities 79
4.1 Test Rig Facilities 79
4.2 Automatic Data Logging for Steady State 83
4.3 Instrumented Turbine Housing 84
4.4 Measuring Concept 86
4.4.1 Measuring the same point within a flow from two direction 86
4.4.2 Measurements made with L2F beam directed in axial direction 87
4.4.3 Measurements made with L2F beam directed via the mirror 88
4.4.4 Flow Angle Orientation 88

CHAPTER 5 : Steady Flow Test Results and Discussion 106
5.1 Introduction 106
5.1.1 Phase One 107
5.1.2 Phase Two 108
5.2 Rotor Inlet,Equal Admission Flow,3 Flow Conditions Azimuth Angle = 20°,90°,180° and 270° 110
5.2.1 Through-flow velocity 110
5.2.2 Axial velocity component 112
5.2.3 Conclusion from equal admission flow 114
5.3 Rotor Inlet,Equal and Partial Admission Flow 114
5.3.1 One limb fully closed 115
5.3.1.1 Through-flow velocity 115
5.3.1.2 Axial velocity component 116
5.3.2 Mass Flow Ratio ($^{inner}/_{outer}$) = 1.5 and 2.0 116
5.3.3 Mass Flow Ratio ($^{inner}/_{outer}$) = o.5 and 0.67 119
5.3.4 Conclusion from partial admission flow 120
5.4 Rotor Exit,Equal and Partial Admission Flow 121
5.4.1 Equal admission flow,three flow conditons 122
5.4.2 Equal and partial admission flow condition 125
5.5 Rotor Inlet,Equal Admission Flow with Different Divider Depth 126

5.6 Rotor Inlet,Series of Partial Admission Flow with Different Divider Depth 128
5.6.1 Introduction 128
5.6.2 Flow characteristics with different dividers 128
5.7 Gas Flow Characteristics and Turbine Performance with Partial and Equal Admission Flow 131
5.8 Measurement Close to Rotor Exit 134

CHAPTER 6 : Unsteady Flow Test Results and Discussion 192
6.1 Introduction 192
6.2 Rotor Inlet,3 Flow Conditions,Through-flow Velocity 194
6.3 Rotor Inlet,Axial Velocity of Components 199
6.4 Rotor Exit,3 Flow Conditions 202
6.5 Rotor Inlet,Azimuth Angle = 20°,90°,180° and 270° with Different Divider Depth 204
6.6 Turbine Performance under Unsteady Flow Conditions 207
6.6.1 Power Developed by Rotor 207
6.6.2 Fixed Absolute Flow Angle 211

CHAPTER 7 : Summary of Achievements,Conclusions and Suggestions for Future Work 261
7.1 Summary of Achievements 261
7.2 Conclusions 263
7.2.1 Steady Flow Tests 263
7.2.2 Unsteady Flow Tests 265
7.3 Future Work 269
7.4 Final Remarks 273

References 275

Appendix A 283
Appendix B 290
Appendix C 295
Appendix D 297

Notation

A	cross-sectional area	m^2
C	velocity	m/s
C_P	specific heat at constant pressure	J
dx	element width at rotor inlet	m
dr	element width at rotor exit	m
m	mass flow rate	kg/s
p	pressure	N/m^2
r	radius	m
R	radius referring to rotor and separating wall plate	m
R	gas constant	KJ/KgK
T	temperature	K
TQ	torque	Nm
U	blade speed	m/s
W	work done, relative velocity	KJ;m/s
α,δ,θ	flow angle	deg
β	incidence angle	deg
ρ	density	kg/m^3
γ	specific heat ratio	
δm	mass flow rate in each streamtube	kg/s
δw	power developed by rotor in each streamtube	watt
ω	angular velocity	rad/s
α_3	angle deviation from radial plane	deg

Subscript

a,r,θ	axial radial and tangential direction
1	rotor inlet
2	rotor exit
tip	rotor tip

Abbreviation

SWϕ	separating wall diameter
LDV	laser doppler velocimeter
L2F	laser two focus

CHAPTER 1

Introduction

1.1 Principles of turbocharging

The principal objective of turbocharging is to increase the power output of an internal combustion engine. This is accomplished by using a compressor to raise the inlet air density, so that a greater mass of air (or air-fuel mixture) can be introduced into the engine cylinder during the induction process than is normally the case with naturally aspirated engines. With more air in the cylinders, a proportional increase in fuel can be burnt to raise the engine power output.

Supercharging generally refers to using a compressor driven by gears or belts directly from the crankshaft of the engine. Turbocharging is a specific method of supercharging, using a turbine coupled to the compressor to form a self-contained unit called turbocharger. Fig.1.1 illustrates the principle of turbocharging. A typical automotive turbocharger is shown in Fig.1.2. In turbocharging, the exhaust energy (which would otherwise be wasted) is used to drive the turbine which in turn drives the compressor. The advantage of turbocharging is greater efficiency than with a supercharger. Today, turbocharging the engine is the better known method of achieving substantial gains in power to weight ratio, volume and cost ratio, improvement on fuel economy and exhaust emissions. Continuous improvement on performance of turbocharger will have a positive effect on engine performance in the future.

A reciprocating engine is basically an unsteady flow device, in which the cylinders exhaust a continuous pulse flow. The turbocharger turbine can accept such unsteady flow, but operates more efficiently under steady flow condition.
The type of turbocharging system applied is either constant pressure turbocharging or pulse turbocharging.

With constant pressure turbocharging, the cylinders exhaust to a common manifold sufficiently large to damp down the unsteady flow before entering the turbine. This system is commonly applied in highly rated engines designed for constant speed and load such as marine engines. The disadvantage of this system is that it does not fully utilize the high kinetic energy of the gases leaving the exhaust valve.
In pulse turbocharging, the objective is to maximise the use of this high pressure and temperature gas at the exhaust valve opening. This creates a highly unsteady flow through the turbine causing a reduction to its efficiency. The loss of turbine efficiency due to partial admission and high unsteady flow is usually more than offset by the additional energy available at the turbine, hence the pulse system is by far the more widely used. Unlike constant pressure turbocharging, the small volume of the exhaust manifold of pulse system, results in rapid transfer of energy by pressure waves to the turbine, and hence a superior acceleration response of the system when fast load changes occur. Also the lighter and more compact exhaust manifold is important in itself e.g for automotive applications. In addition, pulse turbocharging of a four stroke engine produces higher torque in the low speed range. At part load operation, higher efficiency is achieved. These important features are the main reasons why present day automotive turbocharged engine apply the pulse system. Fig.1.3 shows the difference between constant pressure and pulse turbocharging.

The two main components of a turbocharger are the compressor and turbine. Rotodynamic compressors and turbines are used since they are efficient at higher pressure ratios and are very compact. The typical turbocharger operating speed range for small engine is 90000 - 120000 RPM.
A radial outflow compressor is generally used in turbocharger while the type of turbine used depends on the application. Axial flow turbines are used in larger turbochargers in rail traction, industrial engines and for marine purposes. Radial inflow turbines are usually applied in small and medium size turbochargers. All vehicle engine turbochargers currently use radial inflow turbine. Their advantages over the conventional axial turbine of the same size are simplicity, low cost, ease of manufacturing and installation and relatively high performance. The radial turbine is also more robust and less sensitive in small sizes to tip clearance compared with an equivalent axial turbine.

The component parts of a radial turbine are shown in Fig.1.4. The volute of a typical turbocharger turbine either can be vaneless or can have a vaned nozzle. Nozzled turbines are not usually applied to automotive turbochargers. Though they have higher peak efficiencies, the mass flow range is more limited. A more flexible flow range requirement led to the development of the variable geometry turbocharger (Fig.1.4) but this incurs an additional cost and complexity in design. Automotive turbocharged engines are required to operate over a large mass flow range and the vaneless volute turbine can cope with this requirement with reasonable efficiency over a wide mass flow range. The vaneless volute has the advantage of mechanical and manufacturing simplicity, and hence low cost. Without the nozzle, the vaneless volute will be required to perform the following functions :

a) distribute the flow around the periphery of the turbine rotor

b) to accelerate the flow around to the desired velocity and flow angle at the rotor tip.

Automotive turbocharged engines have multi-cylinders and most operating on pulse system will have the cylinders arranged with two exhaust manifolds feeding a twin-entry turbine. For twin-entry turbine, the turbine housing can either be twin-flow or double-flow, see Fig.1.5. The twin-flow housing has the volute divided meridionally over the whole circumference. The rotor is fed by the two adjacent spirals in parallel over the whole circumference. This system allows more interference between each branch of the engine exhaust manifold. In pulse turbocharging, when the unequal mass flows are passing through each sector (or limb), the flows may mix out before reaching the rotor blade. Even under extreme conditions when one sector has zero flow, there will always be substantial gas flow around the whole circumference of the rotor. The same is not true for the double-flow housing which has the volute split into two sectors with each entry feeding a 180° sector of the rotor entry. When there is momentarily zero flow in one entry, half the rotor will be windmilling. Double-flow housings are generally with nozzle rings, and usually for larger turbines only. Twin-flow housings are always vaneless.
Investigation shows that in terms of efficiency, the twin flow housing, while being inferior at equal admission flow, becomes superior with partial admission flow. Because the twin-flow housing feeds the rotor circumferentially all the time, it reduces flow unsteadiness on the rotor itself. Thus most automotive turbocharged engines use the twin-flow housing.

In summary, most automotive turbocharged engines employ pulse

turbocharging, using twin-entry turbines. For low cost and simplicity in design and manufacturing, these are usually vaneless type. Fig.1.6 shows a typical vaneless twin-entry radial inflow turbine.

The housing of the turbine has the function of distributing the flow around the turbine rotor and accelerating the flow. In the turbine rotor, work is done. This work done is dependent on the flow characteristics at inlet to the rotor. Therefore it is important to understand these characteristics and to be able to link them to the performance of the turbine.

1.2 Energy transfer in a radial turbine rotor

In the following, the energy transfer and velocity triangles of the turbine rotor are presented to give the reader an impression of the effect of the flow characteristics on rotor work.

In the radial flow turbine energy is transferred from the fluid to the rotor in passing from a large radius to a small radius. The specific energy transfer in the rotor can be derived from the velocity triangles at the rotor inlet and exit. As energy transfer takes place from the fluid, there is a drop in enthalpy, pressure and absolute velocity.

1.2.1 Velocity Triangles

The velocity triangles of a radial flow turbine are given in Fig.1.7. The figure shows a typical off-design velocity triangle at the rotor entry. After entering the rotor, the gas is constrained by the blade passage to have a purely radial relative velocity (for a one dimensional flow model of a radial bladed rotor), and hence the actual gas angle is rapidly

changed. In a real rotor the incidence angle between the gas and the rotor blade may cause flow to separate from the blades and there will be a subsequent mixing loss within the impeller. This loss is called an incidence loss in the one dimensional flow model. Incidence loss can be defined as the sum of work done in turning the fluid through the incidence angle and the mixing loss if separation occurs. Ideally this will be zero at the design point and will rapidly increase as conditions change.

At rotor exit, the gas will have axial and tangential velocity components. The fluid discharging from it may have a considerable velocity C_2 and an axial diffuser (exit duct) would be considered as a means of recovering most of the energy, $^1/_2(C_2)^2$ which would otherwise be wasted. But in automotive applications the constraints of the installation rarely permits an exhaust diffuser. Ideally at the design point C_2 is a minimum and the exit flow angle (α_2) is zero. This is usually not the case according to experimental results.

1.2.2 Energy Transfer

The rate of change of angular momentum is equal to the sum of the moments of external forces (that is, the torque TQ). Since angular momentum is the moment of linear momentum, the rate of change will be given by the product of the mass flow times velocity. The torque becomes;

$$TQ = m (r_1C_{\theta 1} - r_1C_{\theta 2}) \quad \ldots\ldots\ldots\ldots\ldots\ldots\ldots\ldots \quad (1)$$

The energy transfer will be given by the product of torque and angular velocity (ω) , hence

$$W = \omega . TQ$$

$$W = \omega.(m\ (r_1 C_{\theta 1} - r_2 C_{\theta 2}))$$

since $U = \omega.r$

$$W = m.(U_1.C_{\theta 1} - U_2.C_{\theta 2}) \quad \ldots\ldots\ldots\ldots\ldots\ldots (2)$$

This is the basic equation for energy transfer in the turbine rotor.

Rewriting (2) becomes

$$2.(W/m) = 2\ (U_1.C_{\theta 1} - U_2.C_{\theta 2})$$

$$= (U_1^2 + C_{\theta 1}^2 - (C_{\theta 1} - U_1)^2) - (U_2^2 + C_{\theta 2}^2 - (C_{\theta 2} - U_2)^2)$$

From velocity triangle

$$C_{\theta 1} - U_1 = a$$

$$(C_{\theta 1} - U_1)^2 = a^2$$

$$(C_{\theta 1} - U_1)^2 = W_1^2 - C_{r1}^2 \qquad \text{since} \quad a^2 = W_1^2 - C_{r1}^2$$

Thus

$$2.(W/m) = (U_1^2 + C_{\theta 1}^2 - (W_1^2 - C_{r1}^2)) - (U_2^2 + C_{\theta 2}^2 - (W_2^2 - C_{r2}^2))$$

$$2.(W/m) = (U_1^2 - W_1^2 + C_1^2) - (U_2^2 - W_2^2 + C_2^2)$$

hence specific work

$$W/m = 0.5\ ((U_1^2 - U_2^2) - (W_1^2 - W_2^2) + (C_1^2 - C_2^2)) \ldots\ldots\ldots (3)$$

The three bracketed terms in equation (3) illustrate key features of a radial inflow turbine.

1st term $+(U_1^2 - U_2^2)$: This represents a large contribution to

the turbine work due to the change in radius (not present in an axial turbine)

2^{nd} term $-(W_1^2 - W_2^2)$: For positive work, W_2 must exceed W_1, that is the flow must accelerate through the rotor, relative to the rotor.

3^{rd} term $+(C_1^2 - C_2^2)$: The absolute exit velocity must be minimised since this is a direct loss of potential turbine work. It is for this reason that exit swirl should be zero or at least kept to minimum. Exit swirl is undesirable but this is almost unavoidable at off-design operation. It increases the exit kinetic energy for a fixed mass flow rate, thus reducing the potential turbine work.
From the velocity triangles, it is evident that the flow characteristics play an important role in the rotor specific work and hence turbine efficiency. Turbine efficiency affects the overall turbocharger efficiency and hence engine performance.

Most small and medium size diesel vehicles use pulse turbocharging to better utilize the exhaust pulse energy. The turbine is then exposed to a highly unsteady flow, and operates off-design for most of the engine cycle. The problem can be made less severe by grouping the cylinders, and a common configuration is to split the exhaust manifold into two, and have each half feeding a separate entry to the turbine. By grouping the cylinders appropriately, with regards to firing order and exhaust valve timing, it may be possible to make the pulses in each entry anti-phase, thereby removing the worst of the unsteadiness, Fig.1.8.

Despite this, under the pulse system the turbine is still exposed to a highly unsteady flow. Normal twin-entry radial

inflow turbine design is based on steady flow information with continuous turbine-compressor equilibrium, and therefore takes no account of the unsteady pulse flow conditions which exist in actual turbocharger operation. Thus the plotting of mean values (using steady flow testing) on the turbine map for matching and design purposes can be quite misleading. Hence it becomes important to know the turbine performance under pulsating conditions which are representative of an engine and to use these data for matching and design. However, to assess accurately the operating range on a turbine would require plots of instantaneous gas flow, pressure ratio, blade speed ratio and efficiency. This information is very difficult to measure, which is the main reason why all current turbocharging matching and design continue to use steady state data. It is not until recently that full instantaneous performance data have been measured by Dale and Watson.[38] Here the characteristics of the turbine under steady and unsteady flow conditions were analysed and compared, and the results revealed the importance of pulse flow testing.

Pulse flow testing of turbocharger turbines for performance has now been studied by these authors. As far as the author is aware, however,there is an absence of knowledge of the internal gas flow characteristics of a turbocharging turbine operating under pulsating flow.

1.3 Objectives

In view of limited knowledge on gas flow characteristics of radial-inflow turbines under steady flow, and more importantly no study so far on unsteady gas flow characteristics, the objectives of this project were set as follows:

(1)
To investigate the gas flow characteristics of a twin-entry radial turbine at rotor inlet and exit under steady flow with a series of different mass flow ratios between each entry.

(2)
To investigate the gas flow characteristics of the same turbine at rotor inlet and exit under unsteady flow with conditions representative of a turbocharger operation .

(3)
To link these with the turbine performance.

This project is a continuation of Dale and Watson's work. This investigation involves extensive experimental work carried out using a laser two focus velocimeter. Detailed flow measurement have been made at both the rotor inlet and exit for a range of operating conditions at steady and unsteady flow. Flows at different azimuth angles around the volute were also studied. Different divider depths (meridional divider wall) have been applied in the flow measurement and studied.

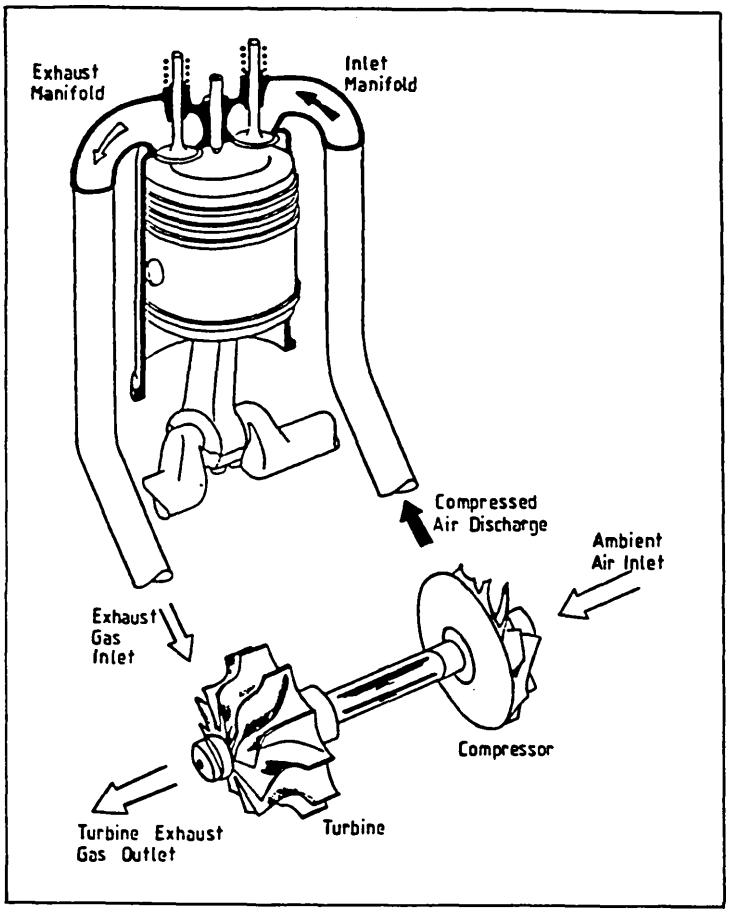


Fig. 1.1

Principle of Turbocharging

Exhaust gas energy drives the turbine which in turn drives the compressor to increase the air inlet density to the engine cylinder during the induction process.

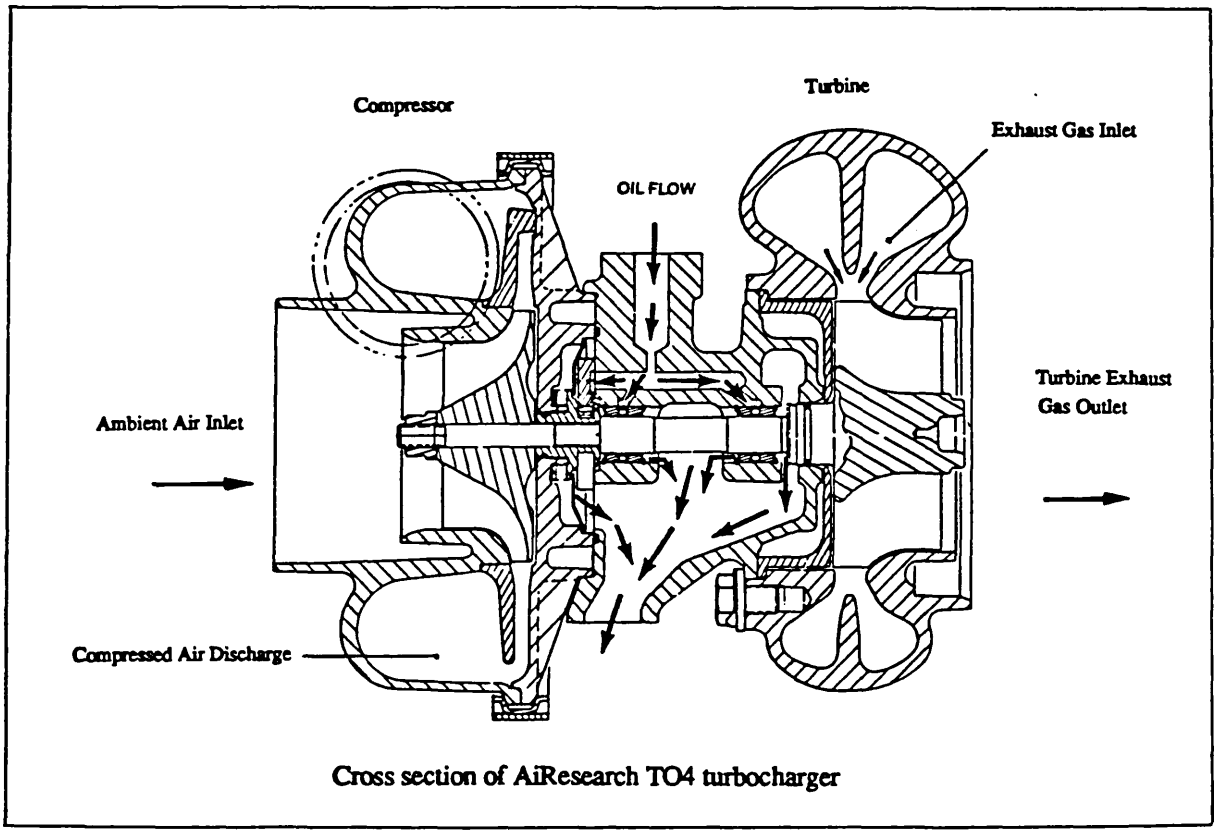


Fig. 1.2 A typical Automotive Turbocharger

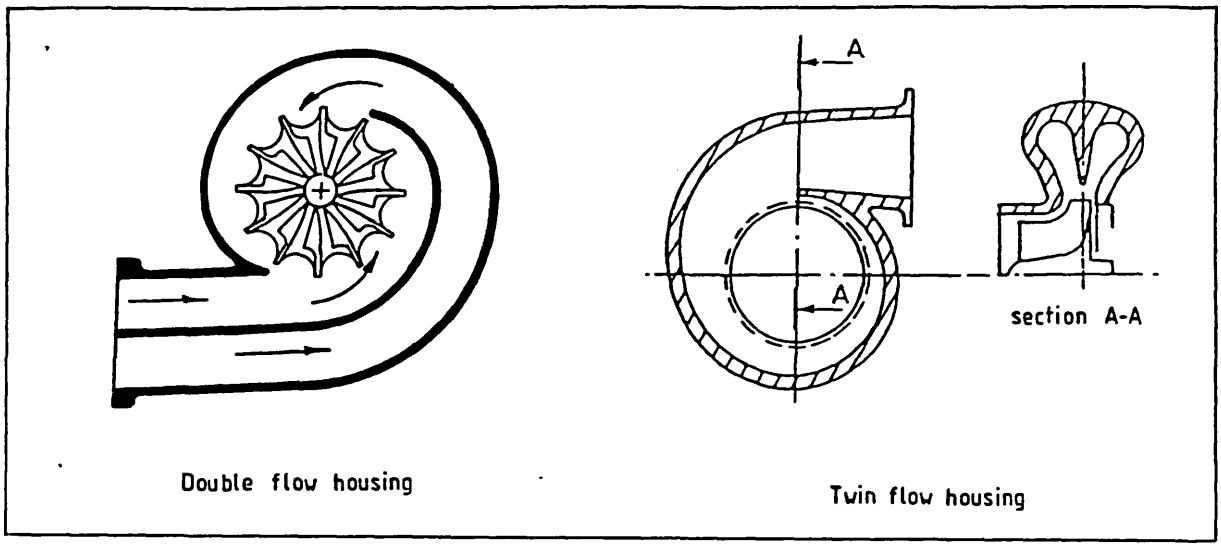


Fig. 1.5 Two types of twin-entry radial inflow turbine

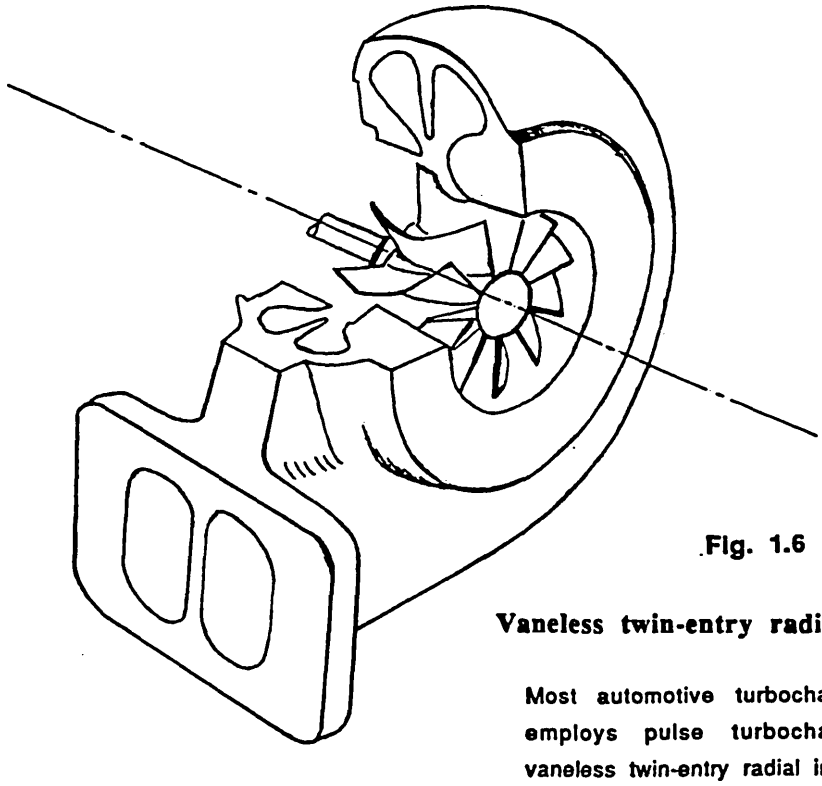


Fig. 1.6

Vaneless twin-entry radial inflow turbine

Most automotive turbocharged engines employs pulse turbocharging, using vaneless twin-entry radial inflow turbine.

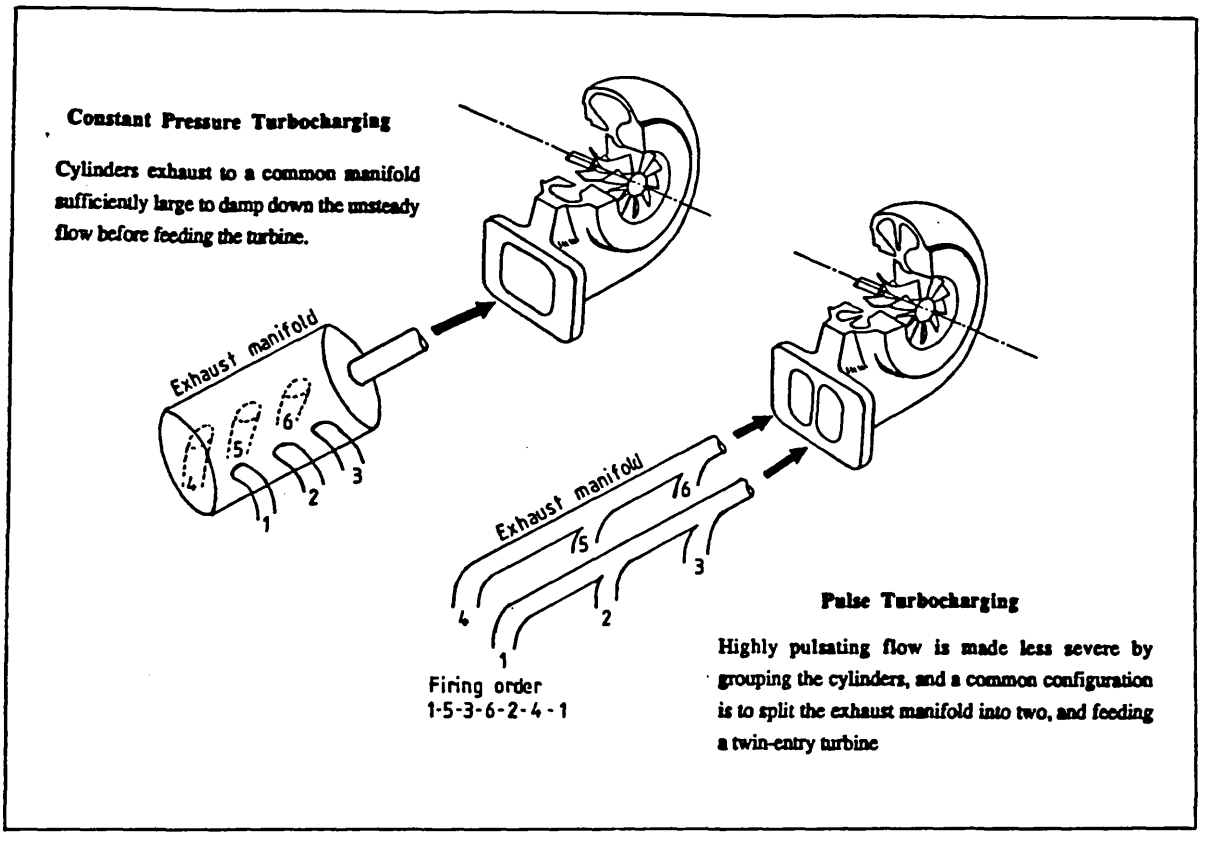


Fig. 1.3 Turbocharging System

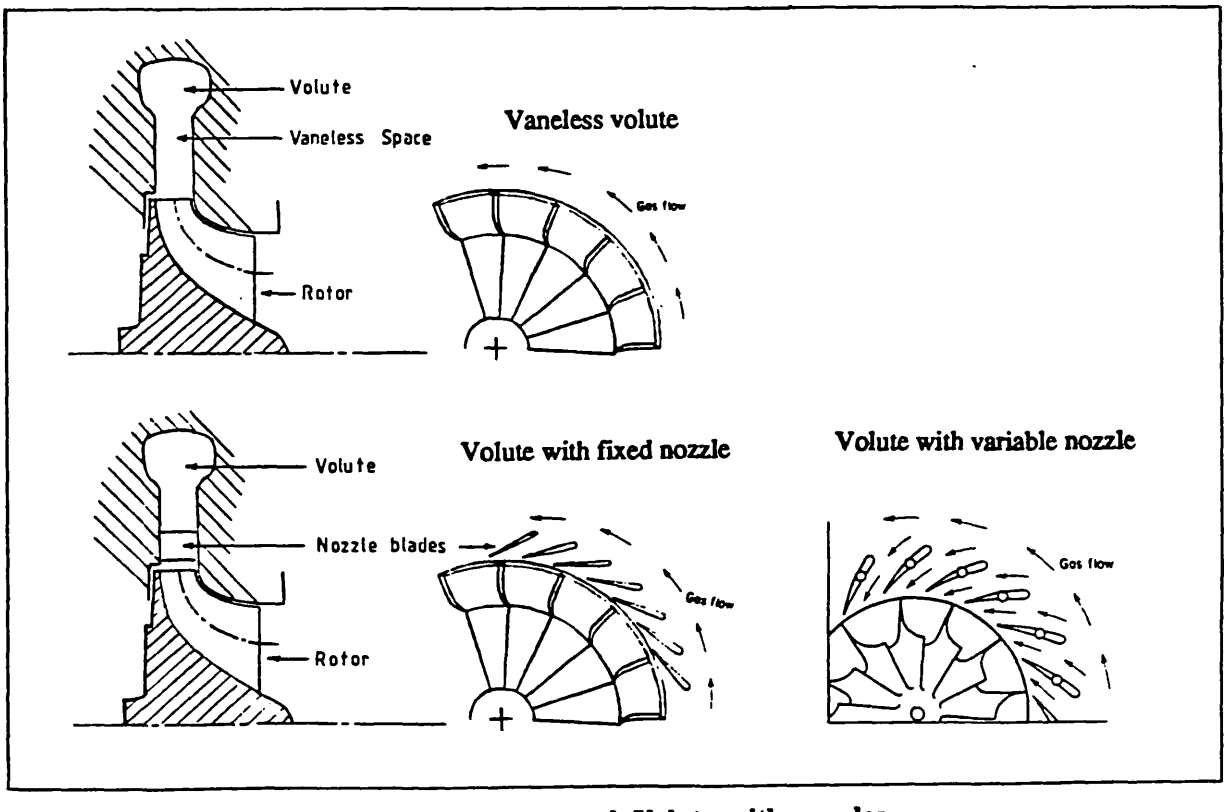


Fig. 1.4 Vaneless volute and Volute with nozzles

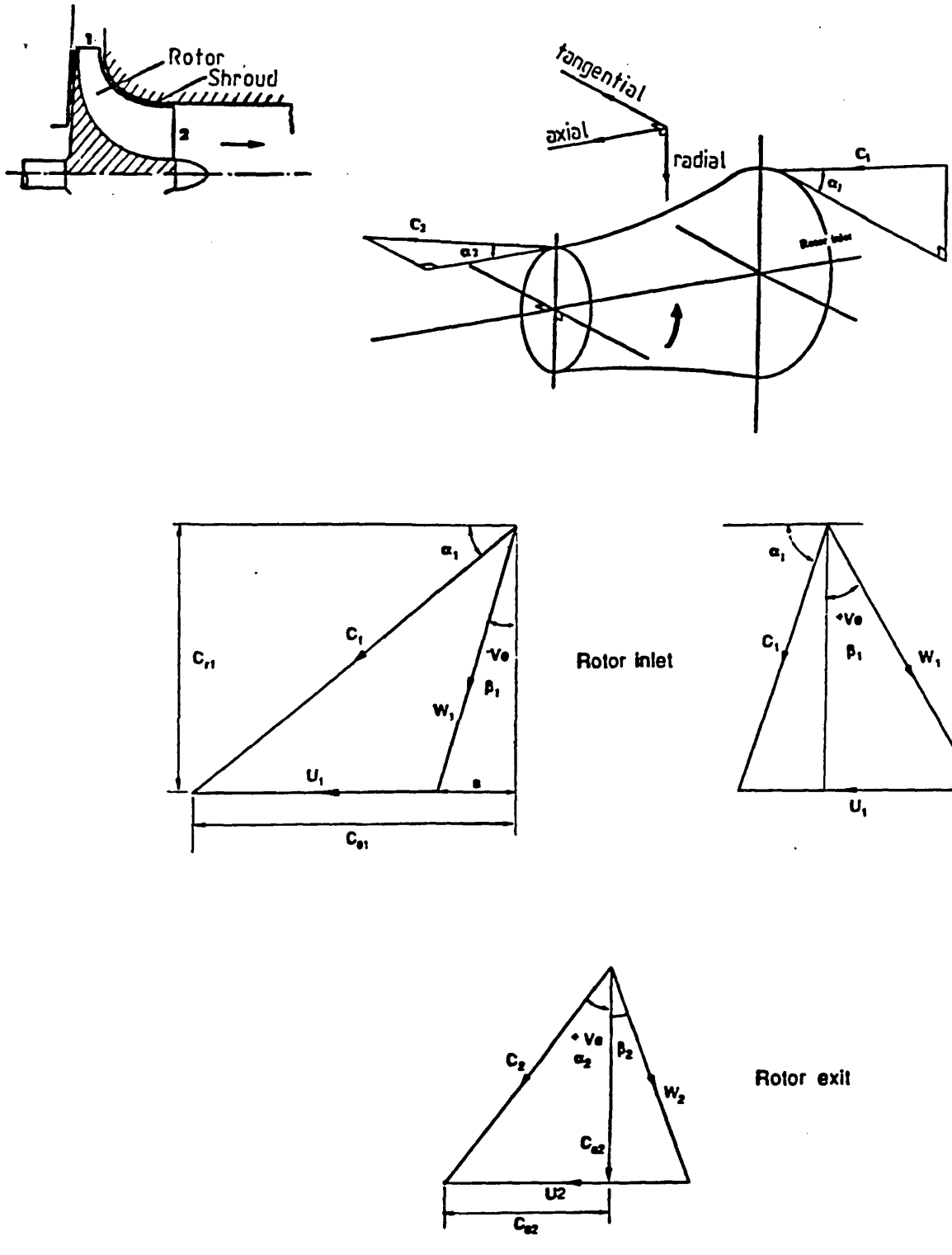
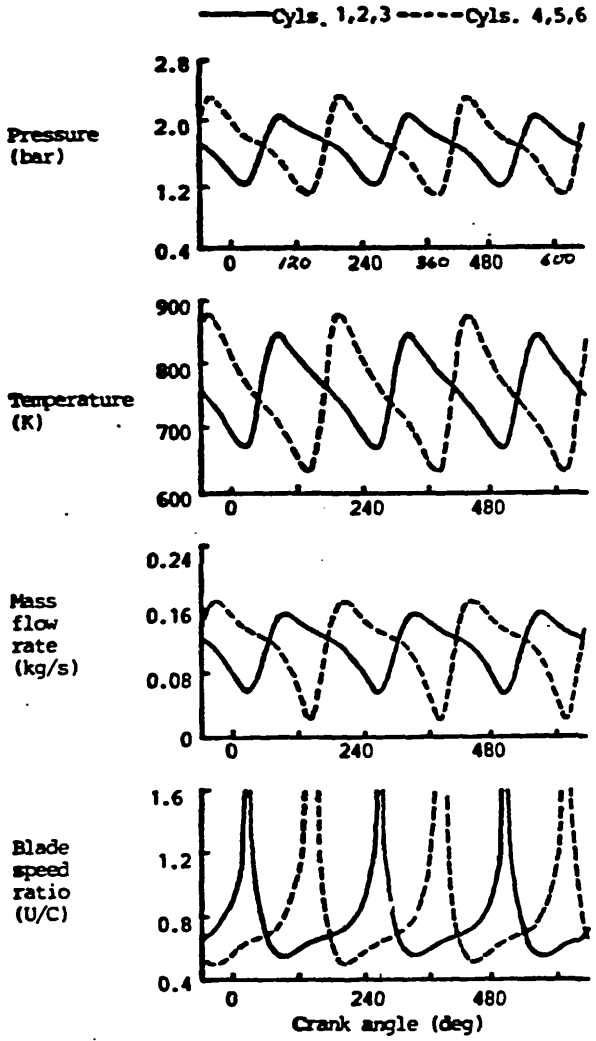


Fig. 1.7 Velocity triangles of a turbine rotor



Turbocharger turbine operating conditions at steady engine speed, maximum torque. Six cylinder engine, twin-entry turbine

Fig 1.8 Turbocharger Turbine Operating Condition

Chapter 2

Literature Survey

This chapter contains a literature survey of related work carried out on radial-inflow turbines, in particular for automotive applications. This survey is presented in the following sections:

2.1 Flow field investigation in the volute
2.2 Test and Performance
2.3 Laser velocimeter application on turbomachinery

2.1 Flow field investigation in the volute

2.2.1 Volute Survey

The function of the volute will depend on whether or not the turbine has inlet nozzle vanes. If it has, then the volute must simply deliver a uniform gas flow to the nozzles. However, most automotive turbocharger turbines have the inlet nozzles eliminated so that the volute must take over the function of flow guidance at entry to the rotor in addition to flow distribution and acceleration. The geometry of the volute must therefore determine the gas angle at volute exit. Designers have combined one dimensional analysis with free vortex theory to determine the geometry of the volute (volute cross-section area or A/R ratio) for optimum gas angle with respect to the turbine performance.

Several studies have been conducted to develop methods for predicting radial inflow turbine aerodynamics performance (1-

7). These methods are mainly based on one dimensional flow analysis with free vortex theory and a combination of appropriate loss models in the inlet volute, vaned and/or vaneless nozzle, rotor and exit duct. While the purpose of these design methods is to provide uniform flow conditions around the nozzle periphery of rotor tip (in the case of vaneless volute), Bhinder (8) reported that the measured flow angle in a vaneless turbine designed using this method showed significant variation around the rotor, Fig.2.1. There were other investigations (e.g 9,10) carried out and they also showed variation of flow properties around the exit of the volute, Fig.2.2.

A group of researchers from the University of Cincinnati have contributed a considerable amount of theoretical and experimental work on the analysis of the flow in radial inflow turbine volutes. Their investigations (11,12,13) reveal that the flow in the radial inflow turbine is actually three dimensional and is also complicated by the interaction between the rotor and nozzle. In these investigations, Tabakoff et al (11,12,13) obtained hot-wire measurements in scrolls of different cross sectional geometries and revealed the presence of two counter rotating vortices at three different scroll cross section. Khalil et al (14) presented maps of the total pressure, Mach numbers, and flow angles at the inlet and exit of the vaned nozzle. These measurements clearly demonstrate the three dimensional flow behaviour in this component.

In 1986, Malak et al (15) presented the results of an experimental study of the three dimensional flow field in a radial inflow turbine scroll using a two colour Laser Doppler Velocimeter system. The three components of velocity were measured at 758 points lying on 7 azimuth sections of a square cross section non-symmetrical scroll. The purpose of this study

is to obtain detailed measurements of the three velocity components through the scroll and the vaneless nozzles. The results showed clearly the formation and development of the free vortex pattern at the different scroll cross sections. The cross-stream velocities showed the presence of one vortex, not the familiar two counter rotating vortices existing in the curved ducts.

Miller et al (16) presented a three dimensional flow survey at the rotor inlet. Experiments were performed using a five hole cobra probe traversing axially (measuring 4 points) at 12 azimuth sections to determine the rotor inlet flow properties at design flow conditions, Fig.2.3a. This investigation, taking into account the three dimensional components of velocity, reported that flow properties were generally uniform in the axial direction and around the turbine housing for azimuth angle = 60° to 300°, Fig.2.3b. The very small variation in the axial direction may be a consequence of symmetrical volute. In the tongue region (azimuth angle = 330° to 30°), significant variations in velocity and absolute flow angle were noted.

So far the work carried out on radial inflow turbine has been mainly on single entry volutes. Very little information, however, can be found of the flow details in a twin-entry volute. An internal report by Miller et al (17) presented some information on the flow field of a twin-entry radial inflow turbine with equal inlet pressures in each entry. This corresponds to a full admission condition. The rotor inlet flow field in the axial direction exhibited the influence of the divider wall in a wake effect. Fig.2.4a shows the variation of absolute flow velocity in the axial direction at volute exit for several azimuth angles. Around the middle of the volute exit (directly below the divider wall tip) the lower absolute velocity is probably due to the wake shade by the dividing wall. Similarly this

effect is also observed in the absolute flow angles, Fig.2.4b. The pattern of behaviour at azimuth angles, θ_2 = 30° and 330° is less clear, and this is probably due to the effect of the tongue. Distribution of the static pressure around the volute is showed in Fig.2.4c. The sudden variation of static pressure at azimuth angle 0°, 360° represents the effect of the tongue. This observation at the tip of the tongue is consistent with Scrimshaw's investigation (10).

The more recent publication of volute flow field surveys by Lymberopoulos (18) presents the numerical analysis and experimental measurements of flows in the vaneless volute of a radial inflow turbine. Cases of single and twin-entry volutes were studied. For the twin-entry volute, the turbine inlet conditions were varied to study the partial admission effects. In addition, different separating wall diameters were applied to study its effects. Fig.2.5a shows the flow angle measurement arrangement and the single and twin-entry volutes.
The variation of flow angle and total pressure across the volute exit for separating wall diameters, SWϕ = 78 and 86mm are shown in Fig.2.5b and Fig.2.5c respectively. For the case of equal flows (P_{01} =P_{02} = 1.25 bar), in the middle of the volute exit, the flow angle (Fig. 2.5c) is higher, which could be due to the wake shed of the dividing wall. The total pressure also falls, but less so for SWϕ = 86mm than 78mm, and this is presumably caused by the mixing loss of the wake.
For unequal inlet total pressures in the two entries, SWϕ = 78mm, Fig.2.5b shows values of negative flow angles representing reverse flow. With SWϕ = 86mm, reverse flow is not observed under partial admission condition, Fig.2.5c. This is likely to be due to the mixing of the two streams taking place earlier at a higher radius, so that there is more time for the flows to mix before arriving at the measuring plane. These findings show that the two streams exert a powerful influence

on one another, which is predicted in the numerical analysis, to lead to reversal and recirculation in extreme cases where one of the entry has zero flow. These results are very interesting in that they show that the flowfield around the rotor inlet varies significantly under partial admission conditions which is the normal case of turbocharger turbine operation.

2.1.2 Rotor Exit Survey

The above survey so far contains information on flow properties at the rotor inlet. Some investigation at the rotor exit had been carried out (17,19-24). From equation (3) in Chapter 1, the exit flow characteristics from the rotor are important in that they determine the swirl at the rotor exit, and hence the work done by the fluid and ultimately the efficiency of the turbine. In NASA reports (19-23), the exit flow angles were measured as a function of radius ratio at some point downstream of the rotor. Fig.2.6 shows the measuring arrangement at the rotor exit. In the experiment, a centrebody (cylindrical tube) was used at the rotor exit in order to obtain measurement of hub static pressure and to provide a flow area at the measuring station equal to the flow area at the rotor passage exit. All measurements were done using pneumatic probes and these have slow response. As a result, the measurements are average values rather than the blade-to-blade variation. Measurements of the flow angle at the turbine exit were obtained by the use of a self aligning probe and actuator. Fig.2.7 shows the definition of the exit flow angle.

A general observation shows large variations of exit flow angle across the measurement section from shroud to hub, Fig.2.8. Milton et al (19) measured the variations of the exit flow angle and static pressure with radius ratio and indicated that there was a non-uniform work distribution from hub to shroud,

with minimum work occuring along the outer wall. This further suggested that minimum losses occured near the hub region and the losses increased towards the shroud. This may be due to the blade unloading which resulted from tip leakage and from low momentum fluid being centrifuged to this region. This observation is supported by Samuel et al (21,22) in which large positive flow angle with low velocity are observed near the shroud with large tip leakages.

A general observation on the rotor exit flow angle (19-22) show that the angle changes from negative (around the hub region) to positive (around the shroud region). The positive angle indicates a flow velocity with a component in the direction of rotation, Fig.2.7a. As a result of this change in the exit flow angle, the tangential component also changes in direction (with respect to direction of rotation), from hub to shroud. Milton et al (20) calculated the local total efficiency at each of the radial positions on the basis of the change in tangential momentum through the rotor and the measured values of total pressure and temperature at the rotor exit. The result shows a maximum variation of 10 points in efficiency, with maximum efficiency corresponding to minimum flow exit angle in the hub region. The lowest local turbine efficiency was calculated to be in the shroud region.

More detailed measurements on rotor exit were made by Miller (17). Measurements in several radial planes (different circumferentially locations) at 0.506" away from the rotor exit blade were made using a five hole probe. Fig.2.9 shows that the absolute velocity V_3 increases by 100 ft/s (30 m/s) from hub to shroud. The presence of exit swirl is indicated by the absolute flow angle a_3 which increases from -15° at the hub to 25° at the shroud. These results are consistent with the experiments carried out in NASA (19-23), showing large variation of rotor exit flow angle.

The rotor exit survey radial (shroud to hub) were made at several circumferential planes, θ_3 = 0° to 360° at 30° intervals. For θ_3 = 330° and 0°, which is in the tongue region, the absolute velocity is generally lower. This effect can also be observed in the exit flow angle though it is less significant.

A rotor exit flow survey by Mizumachi et al (24) was carried out with the objective of obtaining experimentally the relative exit flow angle and velocity coefficient of the radial turbine blades during rotation, Fig.2.10. The experiment was carried out by traversing a five hole yaw meter along the radius of the turbine exit, and the direction and exit flow absolute velocity C_2 were measured. The experiments were carried out on several types of rotor having different numbers of blades and different profiles of exducers. The experiment showed that the relative exit flow angles vary from hub to the shroud. In addition, the exit flow angles measured differed considerably from the rotor exit blade angle. However the distance between the axis of measurement and the rotor trailing edge is not clear. This distance may affect the measured flow angle.

Fig.2.11 gives a general survey of the flow field investigations of radial inflow turbines. A general observation shows that relatively little work has been carried out to investigate the flow in the rotor exit region. It is obvious that flow field surveys in twin-entry volutes are even more sparse. Narrowing the subject to unsteady flow in a twin-entry turbine will practically eliminate all references. The nearest reference which the author can find, relating to unsteady flow investigation is by Tindal et al (25). The investigation was carried out on single entry volute of 3 geometrically similar radial inflow turbines. Pulsations in the inlet flow were generated by means of a rotary valve. The air velocity was

measured using hot-wire anemometer and a fast data logging system. Instantaneous velocity profiles measured during the unsteady flow test are shown in Fig.2.12. The instantaneous velocity measured in the middle of the volute exit shows fluctuations which Tindal suggests are probably associated with a change of flow direction when the rotary valve opens. This investigation shows that the instantaneous velocity does vary in the unsteady flow. However no measurement of the instantaneous flow angle was made.

2.2 Test and Performance

This section presents the survey of twin-entry vaneless radial inflow turbines on test and performance. The test conditions can either be steady or unsteady flow. Under steady flow conditions, full admission implies that the absolute pressure ratio between the two turbine inlets is equal to one. By restricting the flow to one of the turbine inlets, partial admission conditions result and the pressure ratio is not unity.

When testing under unsteady flow conditions, the pressure to the turbine inlet is pulsed. Under this condition, partial admission conditions can still be applicable depending on the phase of the pressure pulse. For instance, when the pressure pulses in each inlet are in phase, the result is the effect of unsteady flow on full admission. This can also represent a single entry turbine being fed by pulsating flow. With the pressure pulses set 180° out of phase, it will simulate the effect of unsteady flow on partial and full admission.

The survey on steady and unsteady flow conditions will be presented in separate sections.

2.2.1 Steady Flow Conditions

Fig.2.13 presents an outline of the surveys on test and performance on radial inflow turbines that had been carried out since 1965. This survey shows that in the 1960s and early 1970s, all the work carried out was mainly on the twin-entry, double-flow housing type of radial turbine (2,26-29). In addition, tests were done on a nozzled turbine.

The more commonly used twin-flow housing was not investigated until 1977 when Pischinger (30) made a study to compare the performance of twin-flow and double-flow types of housing. These test were conducted under steady and partial admission conditions. Pischinger presented the turbine efficiency versus the ratio, C^2/U^2, for both housings tested under full admission, Fig.2.14. The double-flow turbine is 2 to 3% superior to the twin-flow housing. However this does not necessary mean a superiority in engine performance because of the importance of the partial admission behaviour (most of the time the turbine is fed by on partial admission conditions) which is not characterized in Fig.2.14. Thus partial admission conditions were applied up to the limits of zero flow in either entry. The results presented in Fig.2.15 show that in terms of efficiency, the twin-flow housing while being inferior at full admission becomes superior when there is a significant difference between the two entry conditions.

After Pischinger's work on the twin-flow and double-flow housings of a radial turbine, there appears to have been little further investigation on double-flow housings. The most recent investigation of test and performance of a twin-flow, vaneless radial turbine was presented by Dale (38,39,40)

A specially designed high-speed eddy current dynamometer made possible the direct measurement of turbine torque over a wide load range. The dynamometer is capable of measuring efficiency over a load range equivalent to blade speed ratio (u/c) of 0.2

to 0.9. This is in contrast to the earlier work of Pischinger (30), in which a compressor was used as the loading device. This greatly limits the test range of the turbine, unless special measures are taken (e.g using a range of compressor impellers of different diameter, or throttling the compressor inlet). When testing under partial admission condition, so that the pressure ratio between the entries is varied, Dale (38) concluded that the flow in each entry is significantly affected by the pressure ratio in the other. The efficiency characteristics are also influenced by the unequal conditions at the two entries. Maximum efficiency does not necessarily occur with equal inlet conditions, even with a housing of symmetrical cross-section. However, the lowest efficiency occurs at extreme partial admission conditions where one entry has no flow, Fig.2.16. Relative to full admission data, the turbine efficiency with partial admission, ranged from +5% to -12% (the lower efficiency being at zero flow in one entry). Dale (30) found that the maximum efficiency occurs when M_a/M_b = 1.5 where M_a and M_b are the mass flows in the two entries.

The latest information on twin-entry vaneless turbine test and performance was presented by Acton (42), in which the work carried out is similar to that done by Dale (38). Full and partial admission flow tests were conducted. However in this investigation the turbine work was evaluated by applying the conventional method of coupling a compressor to the turbine to absorb and measure the turbine work and also adding losses due to the bearing. Wallace et al (27) researched with a wide range of compressors to brake the turbine and reported that this method would require ± 0.05K accuracy on thermocouple measurements to satisfy efficiency. To achieve such accuracy with thermocouples would require extreme care in manufacture, calibration, and placement to ensure that the measured temperature is a representative one. In the investigation by Acton (42), the method of calculation of efficiency under

partial admission conditions is not clear. Nevertheless similar results as Dale (38) were obtained, showing that partial admission efficiencies were lower than full admission by about 10% to 15%, Fig.2.17. The maximum efficiency in this case occurs at full admission, which differs from Dale's finding (38) under similar conditions. Without the full details of the calculation of partial admission efficiencies it is not possible at present to resolve this difference.

2.2.2 Unsteady Flow Conditions

Unsteady flow tests began at around the same time as investigations on steady, partial admission work, see Fig.2.13. The conventional approach towards the analysis of unsteady flow performance utilizes a quasi-steady flow assumption in which the turbine is assumed to operate as if the flow were instantaneouly steady. In this way, provided the boundary conditions (pressure ratio, mass flow and speed) were known at any instant in time, the turbine efficiency can be found from its steady-state performance. An improvement on this basis was to use the steady-state characteristics as a basis, but correct the results using empirically-derived factors.

Benson (37) tested a single entry vaneless turbine under unsteady flow conditions and attempted to take into account of the wave action of the flow pulsation, but did not make progress due to the complexity and lack of understanding of the flow within the turbine under such conditions.

Fig.2.13 shows again that early unsteady flow investigation was mainly done on double-flow housings (26-29,33,34), and that all the turbines are nozzled except in (38). Single and multiple entries turbines with nozzles were also among those tested under unsteady flow conditions (31,32).

The latest unsteady flow test and performance on vaneless twin-entry radial turbine was presented by Acton (42). In this

investigation the turbine mean flow characteristics were determined on the basis of the average values (pressure, temperature, mass flow and torque) in the pulse cycle. The analysis of the unsteady flow thus still utilizes the quasi-steady flow assumption. Capobianco (41) conducted a similar investigation, using a single entry vaneless turbine. A compressor was used as a means of power absorption and the mean unsteady flow characteristics were determined from averaged values of temperature, pressure, mass flow and torque.

So far in the unsteady flow investigation, only instantaneous pressures had been measured. These are insufficient for a full unsteady analysis of the turbine performance. Unsteady flow performance testing of a twin-entry,vaneless turbine was first presented by Dale (38). The high speed eddy current dynamometer mentioned above is capable of measuring efficiency under unsteady as well as steady flow conditions. Instantaneous pressure, mass flow and dynamometer torque were measured, producing for the first time a full set of instantaneous performance data. Details of the development of the test facility are given in (39,40). This investigation has revealed the importance of making a full set of instantaneous measurements when testing under unsteady flow conditions. The results showed that the instantaneous mass flow departs significantly from that measured under steady flow conditions, Fig.2.18. The instantaneous efficiency plotted against turbine blade-speed ratio with steady state data superimposed shows that the instantaneous efficiency departs from the steady state data, forming an efficiency loop, Fig.2.19. It is note worthy that the instantaneous efficiency is significantly lower than the steady-state efficiency over much of the cycle. These results were obtained with a single-entry turbine. When a twin-entry turbine was used, the pulses were 180° out of phase, Fig.2.20 shows the instantaneous flow locus under these

conditions. It is clear that mass flows predicted by a quasi-steady assumption can be seriouly in error in some parts of the loop.

From Fig.2.13 the survey shows that the testing of twin-entry turbine is narrowing towards twin-flow type housing. The ability to measure the instantaneous torque, pressure and mass flow under unsteady flow, and hence a full set of instantaneous performance data has produced important information for turbocharger engineer. This technique has so far not been applied elsewhere thus its result remain unique. Due to lack of facilities, steady flow information will still continue to be applied by turbocharger designer for matching and design, and further investigation on unsteady flow characteristics will still apply conventional methods and quasi-steady flow assumption for analysis.

2.3 Application of laser velocimetry on turbomachinery

The laser doppler velocimeter (LDV) has been established long before the development of laser two focus (L2F) method. Its measuring technique has been successfully applied in wind tunnels, free jets, liquid flow, flames etc. However its application to turbomachines has met with considerable difficulties especially in small machines and in high speed flows. This leads to the search for other techniques of optical velocimeter measurement, and subsequently the development of L2F technique.

This L2F method in small, high-speed turbomachines was first pioneered by research engineers in DFVLR (43,44,45,46). Its capability to measure close to wall surfaces and the high speed flow range have been compared favourably with the LDV, Schodl (43,44). Flow investigation in an axial and a centrifugal

compressor have proved that the L2F method works successfully even under very severe conditions (44). With its sychronizing facility, it is possible to take measurements between blades of turbomachinery. The measurements have yielded a lot of information on the real flow in compressors, especially inside the rotating impeller which otherwise is not possible with conventional methods.

The application of the L2F technique on turbomachinery has gained popularity. In 1981, IHI Research Institute had introduced its L2F velocimeter (47) and evaluated the accuracy of the flow velocity to be within 1% and the flow angle to be within 0.5 degree, compared with measurements performed with the standard pitot tube. Measurements of the flow distribution within a centrifugal impeller have also been successfully applied using a sychronizing facility.

Elder et al (48) investigated the application of doppler and transit (L2F) laser anemometry on turbomachinery. In this investigation, the L2F was used to study flow at the stator outlet in a small transonic fan. The measurements were phase locked to the blade passing frequency in order to ascertain the rotor unsteadiness transmitted through the stator. It was reported that the degree of unsteadiness transmitted was surprisingly large. This measurement would not be possible using conventional measuring technique. A typical problem encountered in this investigation is fouling of optical window. This is caused by the deposit of seeding (oil particles) on the window thus the signal quality transmitted is drastically reduced hence measurements become tedious.

Forster et al (49) evaluated the L2F measurements in unsteady turbine flow. Measurements were made within and near the rotor blade channels of a single-stage turbine. In this

investigation, seeding was used to improve the signal rate and thus reducing measuring time. It was observed that this improvement in signal rate was not the same at all measuring locations. Close to the wall and especially in separation zones a reduced data rate was obtained because of the lower mass entrainment of seeding particles from the main flow. In such flow regions the measuring time increased significantly. This may also affect the signal quality and hence no measurements can be possible.

Young et al (50) used an L2F velocimeter to take measurements within the blades of a turbocharger compressor. The sychronising mode was applied and the space between the blades divided into sixteen individual measurements. Fig.2.21 shows the velocity and turbulence measurements made at the best efficiency point and near surge. For measurements at best efficiency point, all sixteen individual measurements yielded results with a maximum turbulence intensity of 10%. When tested to the surge point, the turbulence intensity level reached as high as 49% in which case no velocity measurements were possible. It was suggested that the high turbulence level associated with these measurement indicated the region of significant flow recirculation. A characteristic of the L2F velocimeter is that in a region of recirculating flow, mean velocity and angle measurements are not possible as a result of high level of turbulence.

The L2F technique is so far the most developed and promising method for measurements in small and high speed turbomachinery. Its application on turbomachinery has been proven and is becoming more widely used, in particular its sychronising facility that enables measurements to be made within rotating blades.

2.4 Conclusions from literature survey

The survey shows that very little information is available on the commonly used twin-entry vaneless radial inflow turbine for turbocharger application. Dale's work (38,39,40) on performance testing has provided useful information on steady and unsteady flow, and full and partial admission test conditions. In particular, the unsteady flow tests have yielded some important turbine characteristics and further investigation of the unsteady gas flow characteristics will be necessary to have a complete understanding of the unsteady flow effects of radial turbines.

Information of the flow field surveys of vaneless twin-entry radial turbines is limited. So far only Lymberopoulos (18) and Miller (16,17) have investigated in this area but under steady flow conditions. Tindal (25) investigated the flow at the rotor inlet, measuring the instantaneous velocity under unsteady flow conditions using a hot-wire,but no measurements on the instantaneous flow angle were made. No measurements of instantaneous velocity as well as flow angle under unsteady flow conditions has been carried out as far as the author is aware. Therefore, there is an absence of information on unsteady gas flow characteristics.

The application of L2F velocimetry on turbomachinery started in early 1970's (43). Since then, its application on turbomachinery has been successful with regard to its accuracy and reliability. Its synchronizing facility which enables measurements to be phase locked, has been successfully applied to allow flow measurements to be made within compressor impellers. This feature can be applied to the present test rig facility so that the measurement is phase locked to the pulse frequency to study the unsteady gas flow characteristics. This is another application of the L2F sychronising facility that has not previously been tested.

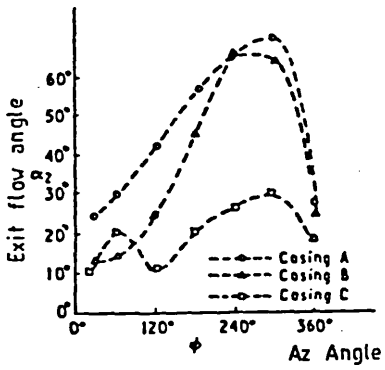
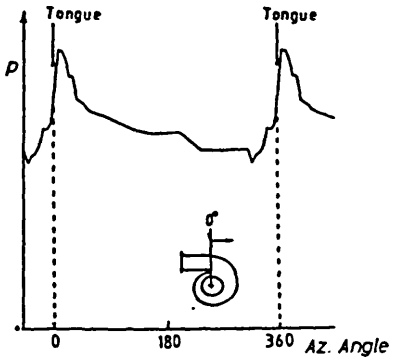
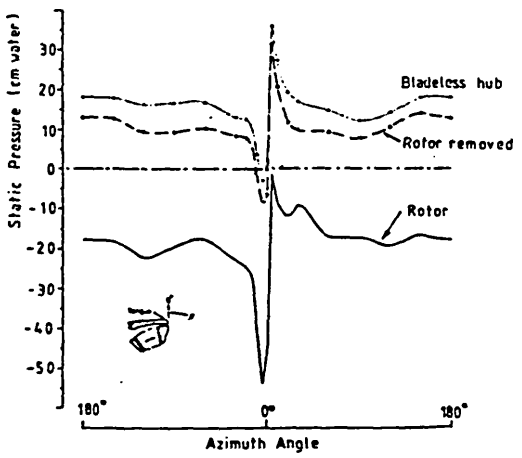


Fig. 2.1

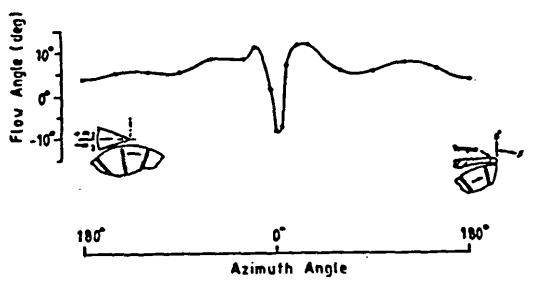
Volute Exit Flow Angle versus Azimuth Angle
(Bhinder (8))



Static Pressure Distribution at Volute Exit
(Ellison et al (9))

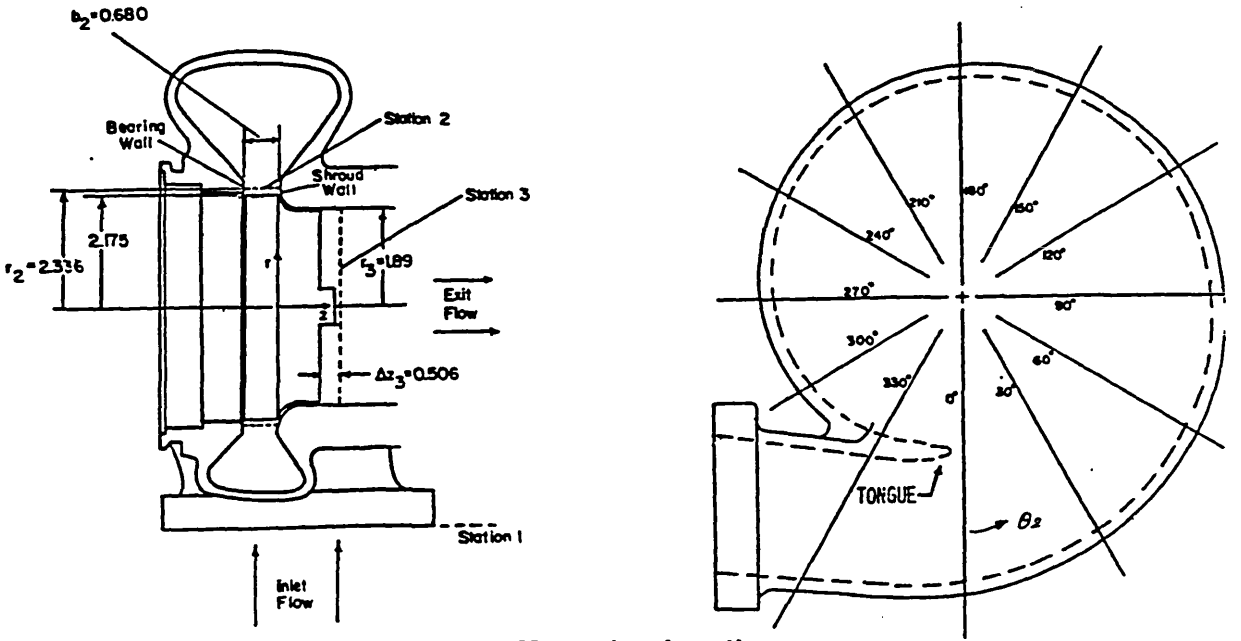


Static Pressure Distribution at Volute Exit
(Scrimshaw (10))



Volute Exit Flow Angle Distribution
at Volute Exit (Scrimhaw (10))

Fig. 2.2



Measuring Locations

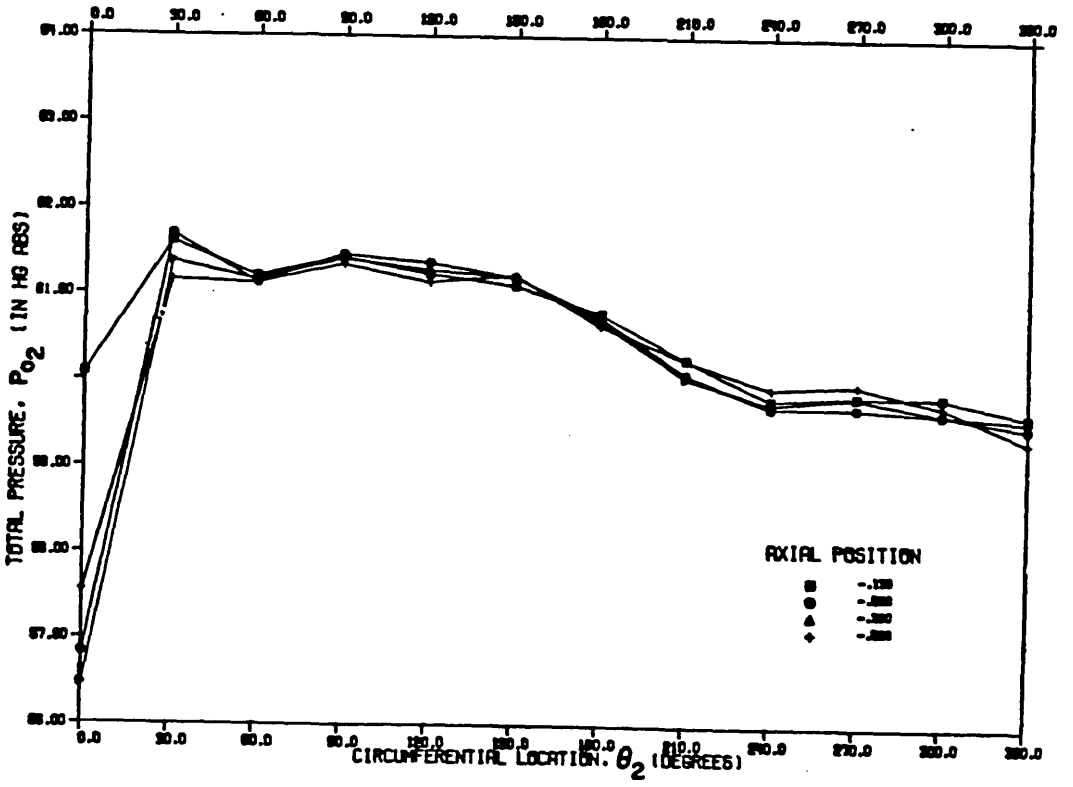


Fig 2.3a Circumferential Distribution of Rotor Inlet Total Pressure (Miller et al (17))

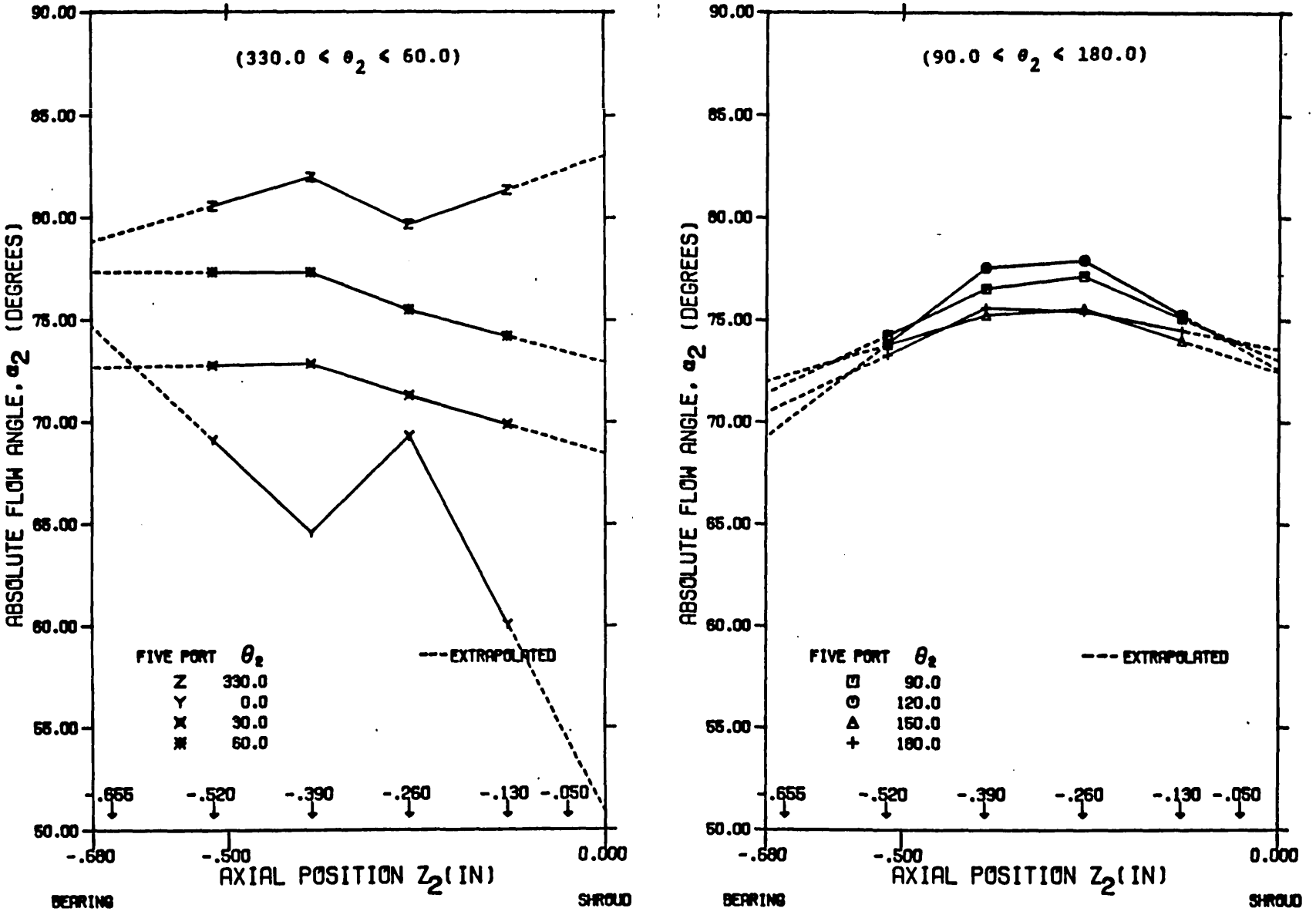


Fig 2.3b Flowfield Survey at Rotor Inlet of a Single Entry Nozzleless Turbine (Miller et al (17))

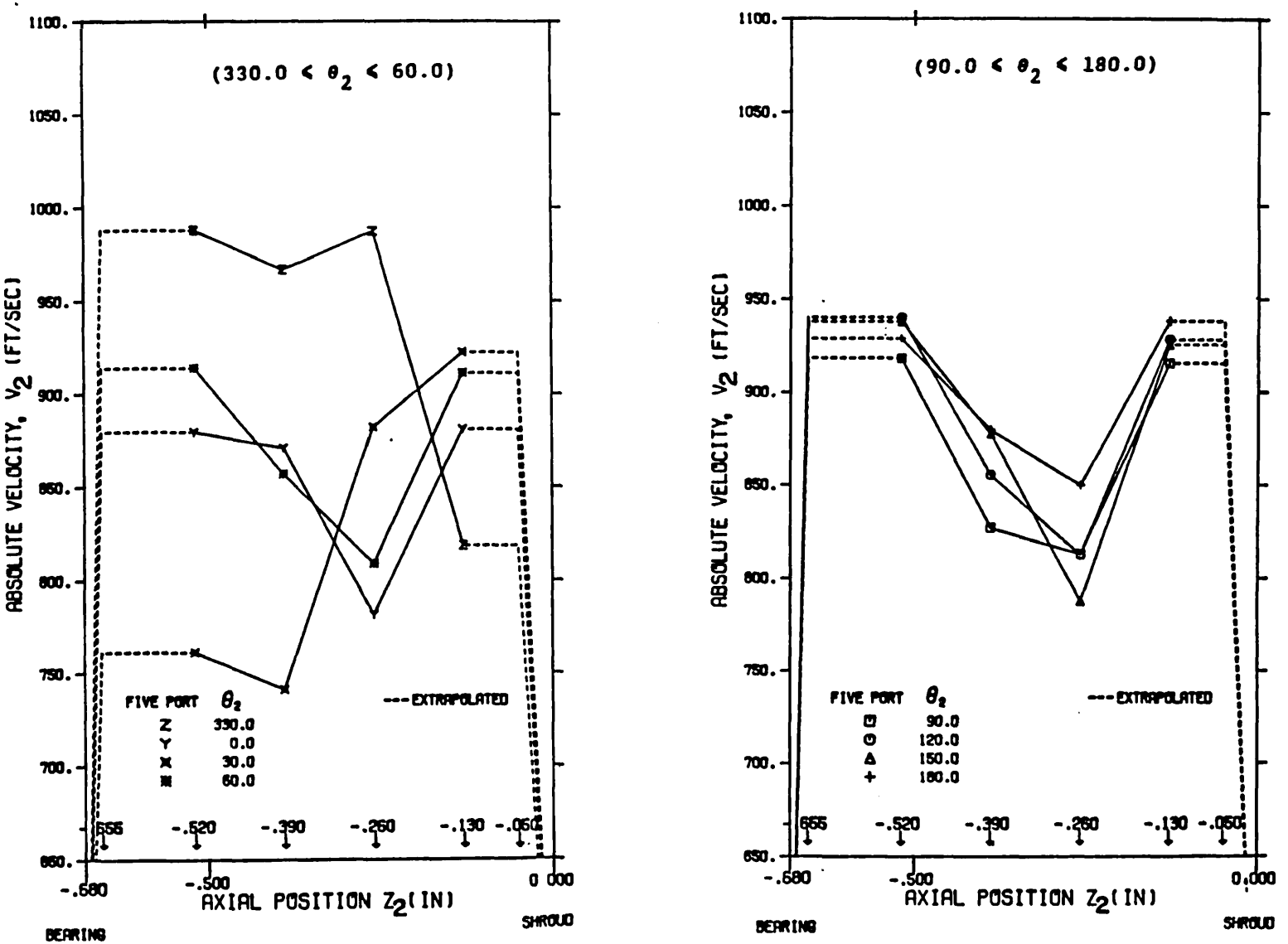


Fig 2.4a Axial Distribution of Rotor Inlet Absolute Velocity in a Twin Flow Housing (Miller et al (17))

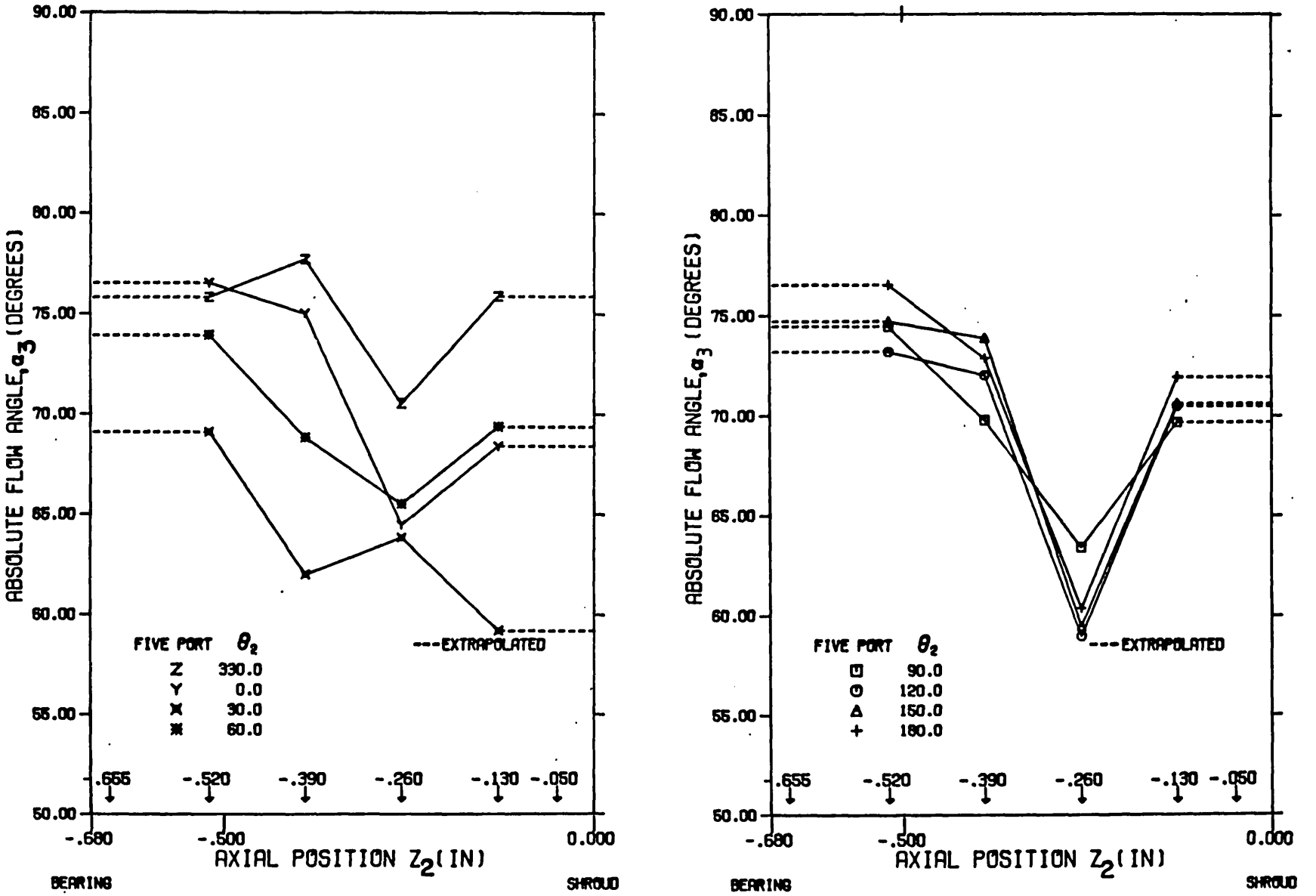


Fig 2.4b Axial Distribution of Rotor Inlet Absolute Flow Angle in a Twin Flow Housing (Miller et al (17))

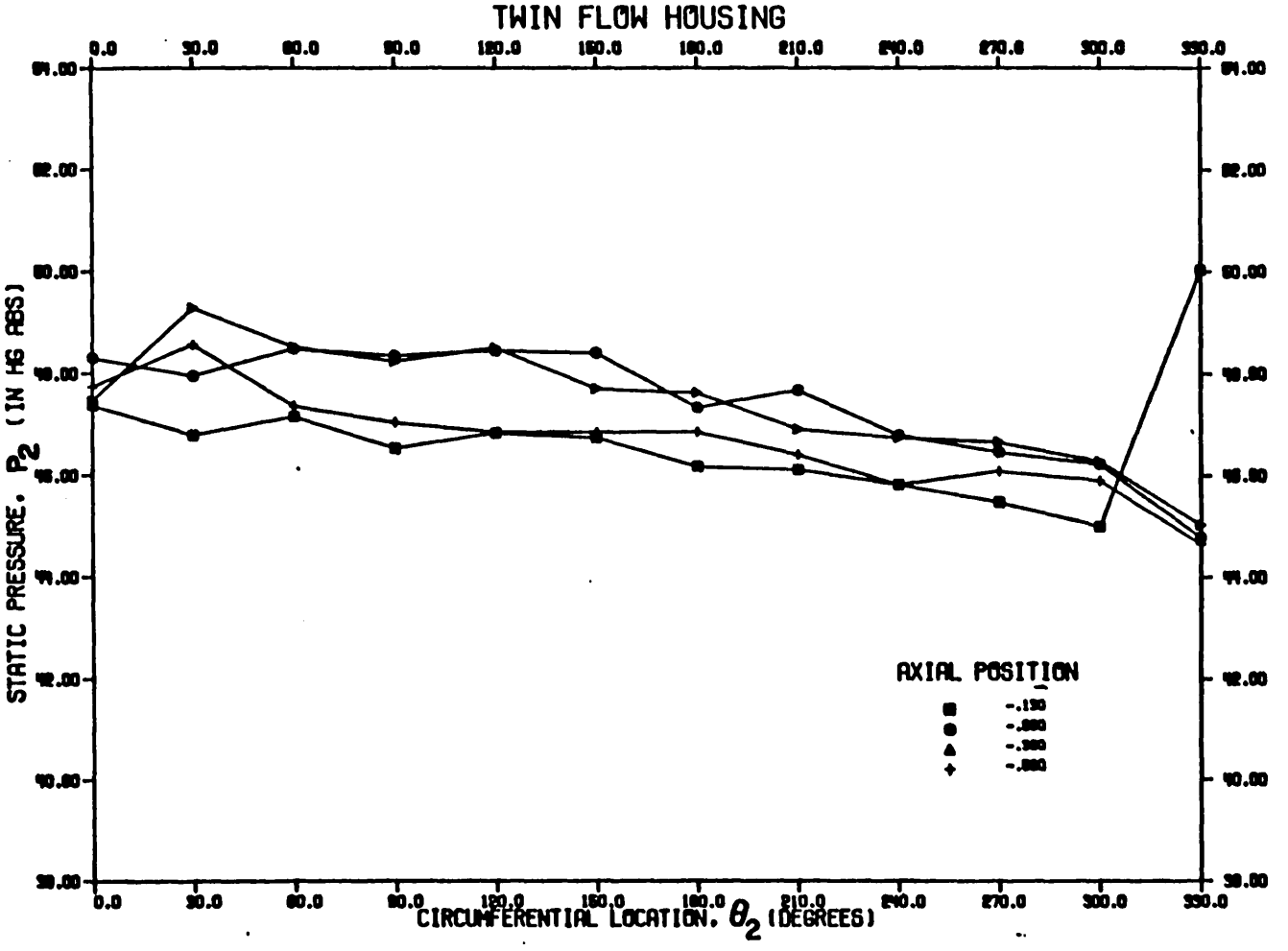
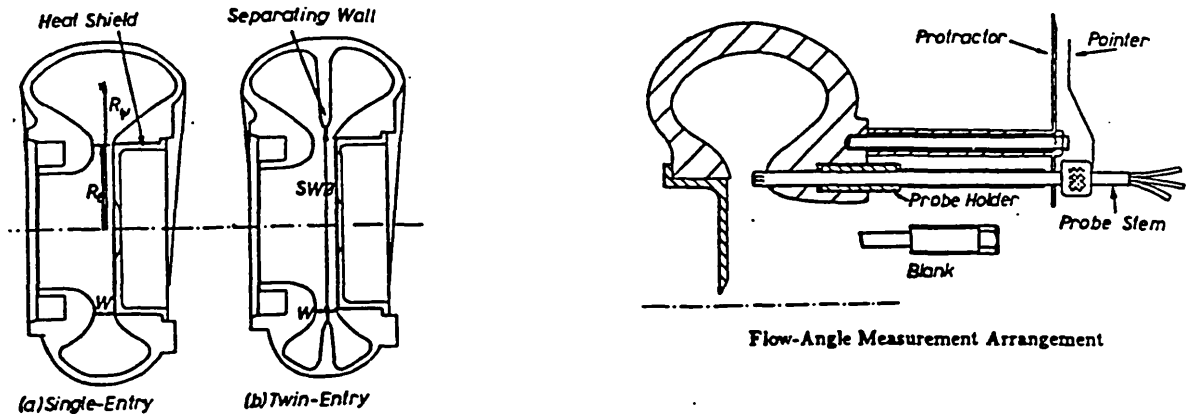


Fig 2.4c Static Pressure Distribution at Volute exit (Miller et al (17))



(a) Flow angle arrangement for single and twin entry volute

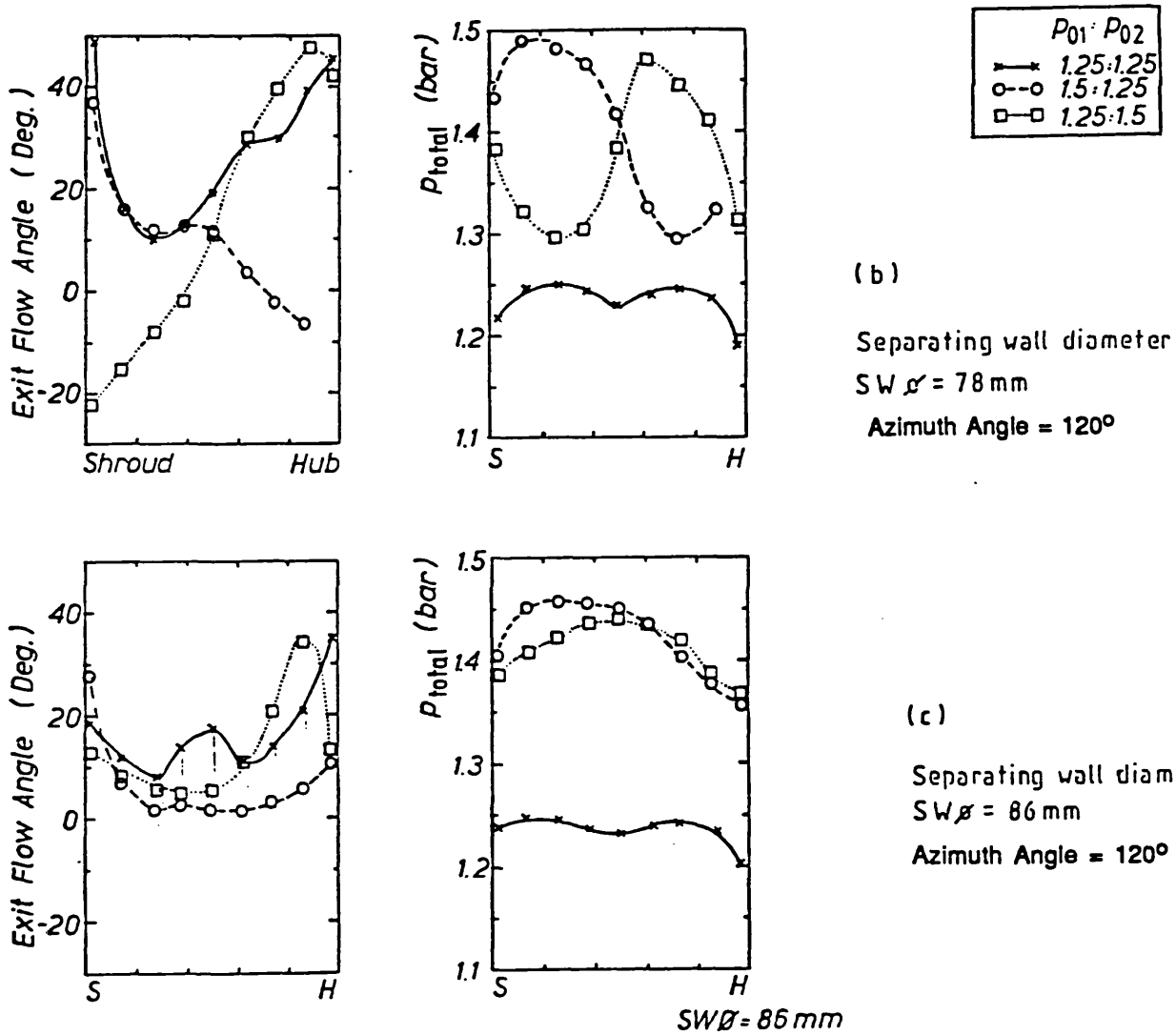


Fig. 2.5 Flowfield Survey at Rotor Inlet of a Twin-Entry Nozzleless Turbine (Lymberoupolos (18))

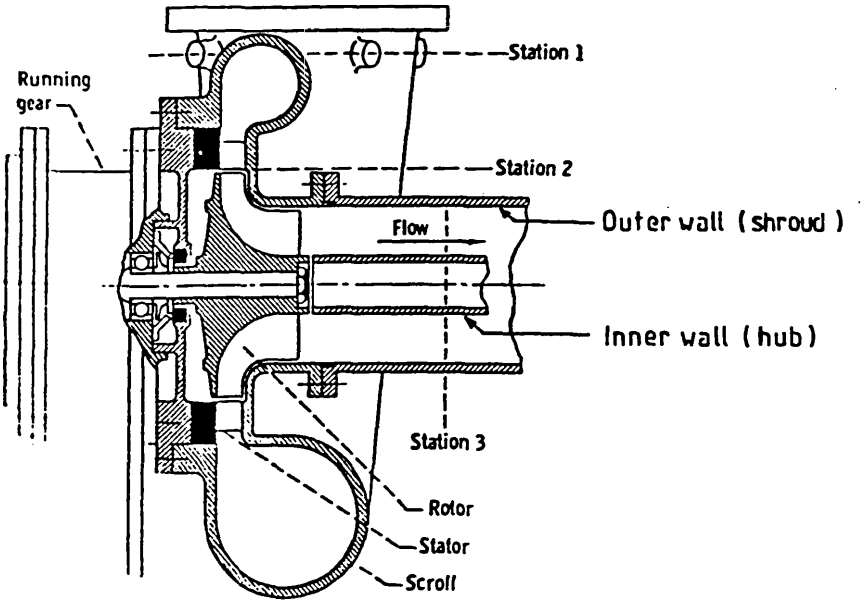


Fig. 2.6 Measuring Location at Rotor Exit (Milton et al (19))

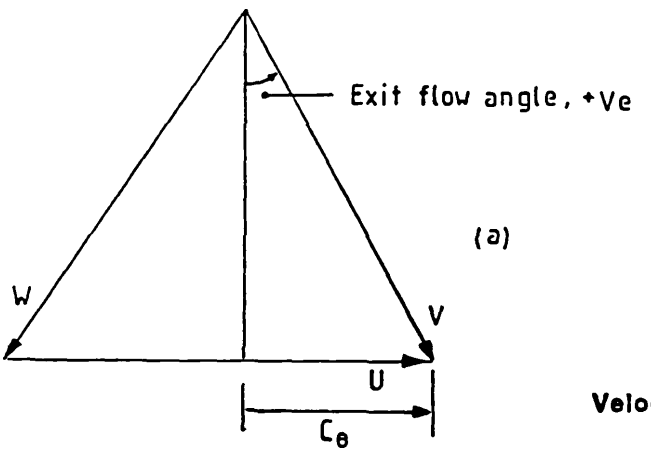
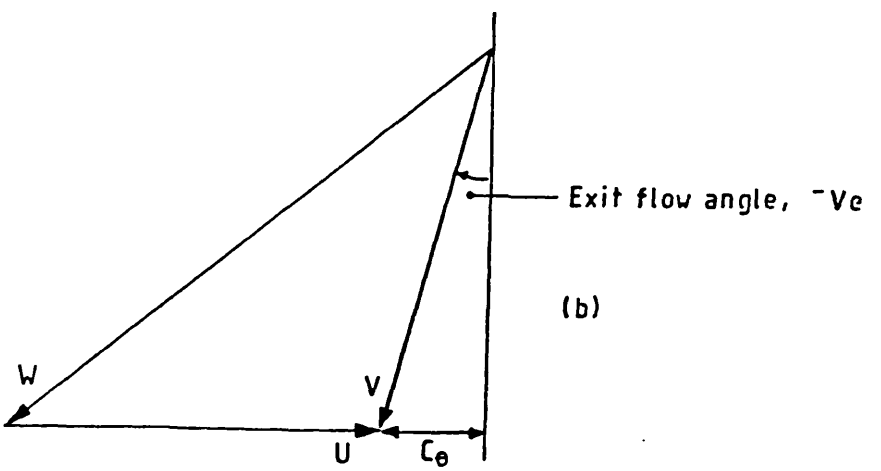
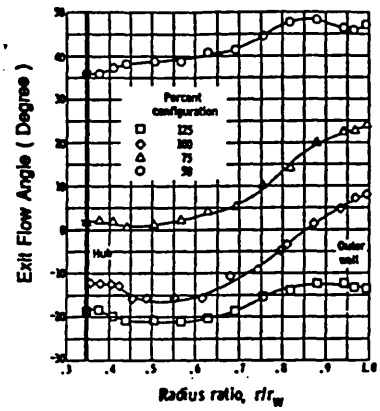


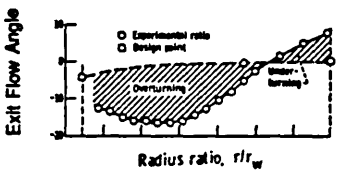
Fig. 2.7
Velocity Triangles at Rotor Exit
(Milton et al (19))



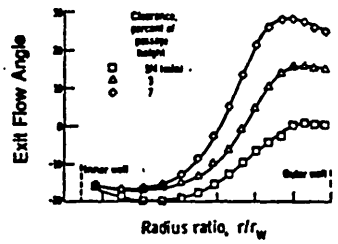


Stator throat area nominally 50, 75, 100 and 125% of design

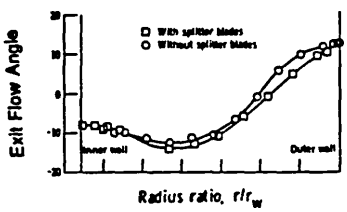
Milton et al (19)



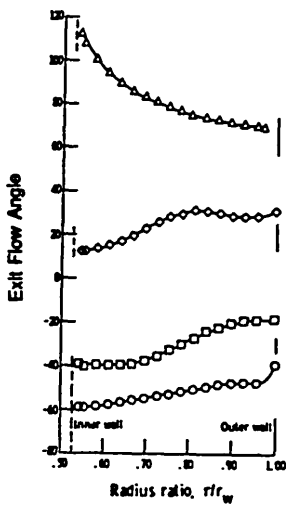
Milton et al (20)



Samuel et al (21)



Samuel et al (22)



Variation of exit flow angle with radius ratio at equivalent design speed and pressure ratio; with rotor extension.

Milton et al (23)

Fig. 2.8 Variation of Exit Flow Angle from outer to inner wall

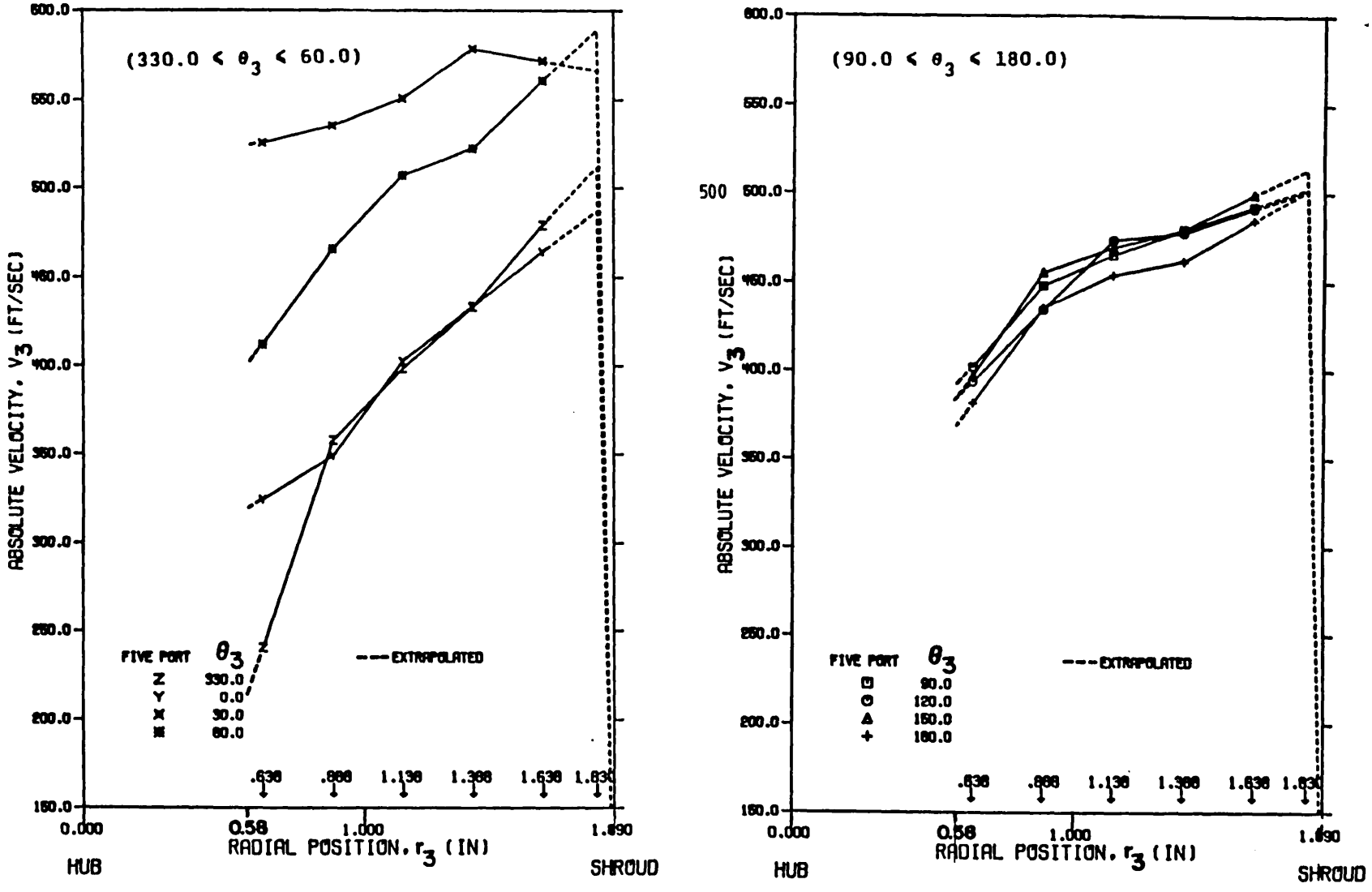


Fig 2.9a Radial Distribution of Rotor Exit Absolute Velocity (Miller et al (17))

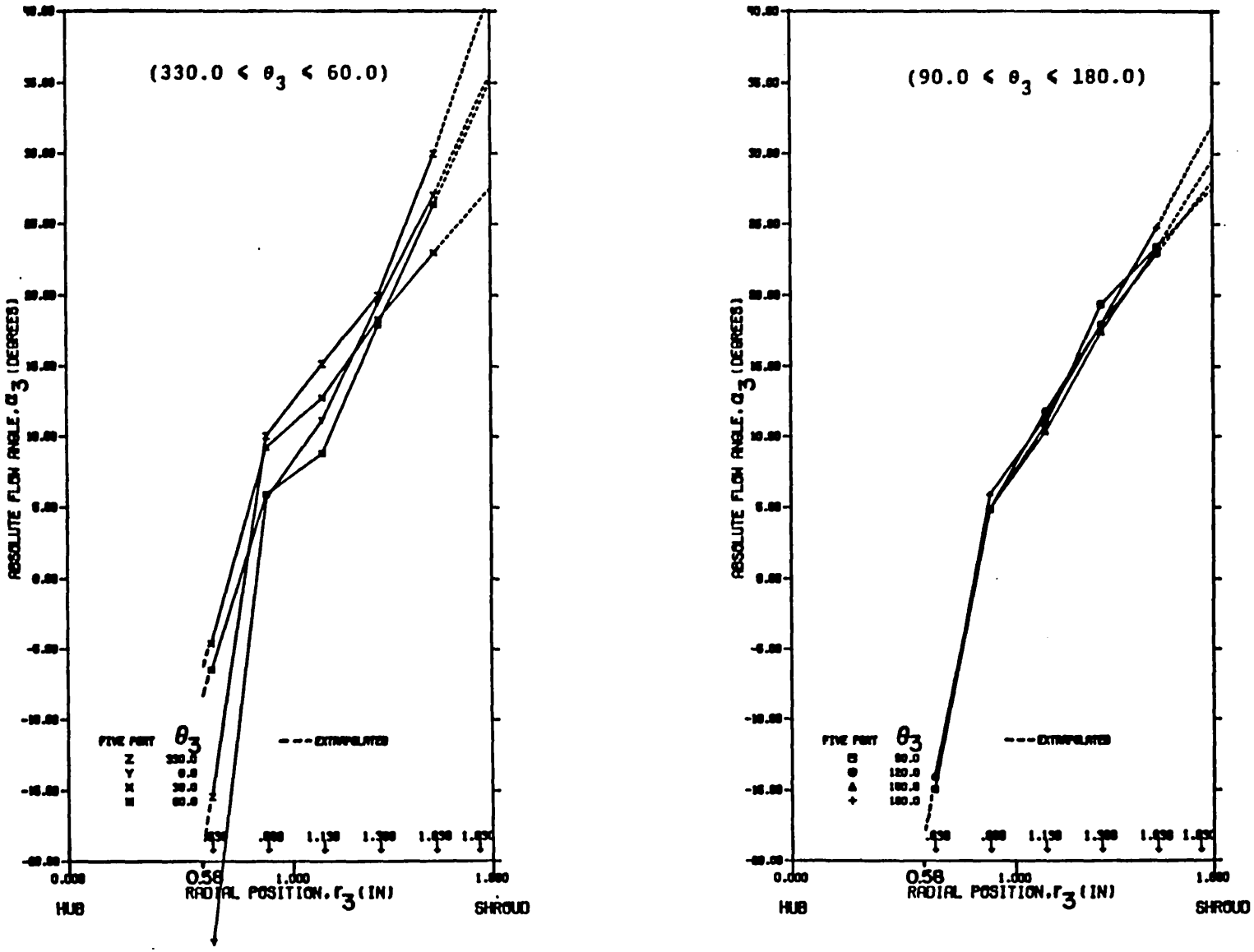
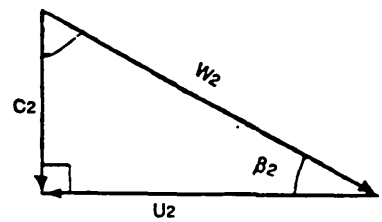
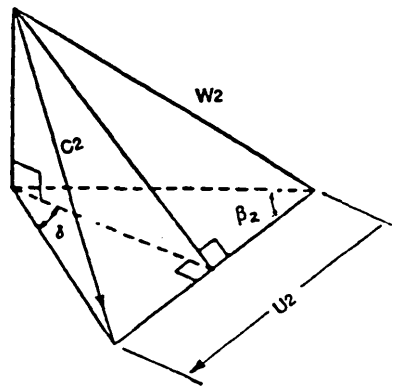


Fig 2.9b Radial Distribution of Rotor Exit Absolute Flow Angle (Miller et al (17)).

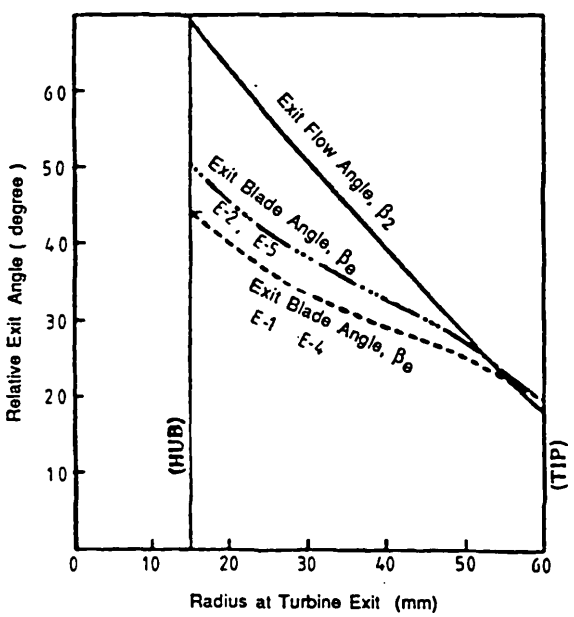


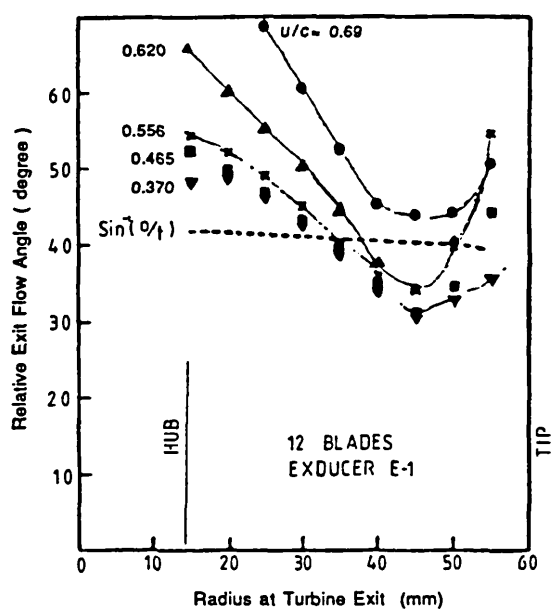
Velocity diagram at blade exit

(at design point)



Velocity diagram at turbine exit





β_2 = Relative exit flow angle

β_e = Relative exit blade angle

Fig. 2.10 Relative Exit Flow Angle Variation
(Mizumachi et al (24))

Flowfield Survey at Rotor Inlet

Steady Flow Test

1969	Bhinder et al	(8)	Single Entry, Nozzleless Turbine
1976	Khalil et al	(14)	Single-Entry, Nozzleld Turbine
1978	Ellison et al	(9)	Twin-Entry, Nozzleless Turbine
1981	Scrimshaw	(10)	Single-Entry, Nozzleless Turbine
1982	Tabakoff et al	(11)	Single-Entry, Nozzled Turbine
1982	Tabakoff et al	(12)	Single-Entry, Nozzleless Turbine
1984	Tabakoff et al	(13)	Single-Entry, Nozzled Turbine
1985	Miller et al	(17)	Single & Twin-Entry, Nozzleless Turbine
1986	Malak et al	(15)	Single-Entry, Nozzleless Turbine
1987	Miller et al	(16)	Single-Entry, Nozzleless
1987	Tindal et al	(25)	Single-Entry, Nozzleless

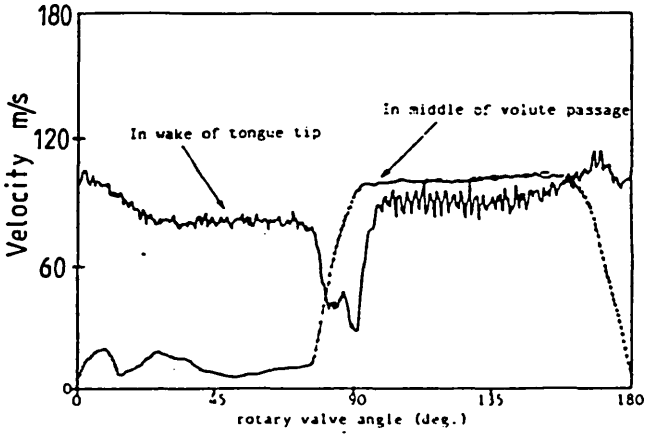
Unsteady flow test

1987	Tindal et al	(25)	Single-Entry, Nozzleless

Flowfield Survey at Rotor Exit

1966	Milton et al	(19)	
1969	Milton et al	(20)	
1970	Samuel et al	(21)	Exit Flow Angle and
1970	Samuel et al	(22)	Pressure measurement
1972	Milton et al	(23)	
1975	Mizumachi et al	(24)	
1985	Miller et al	(17)	

Fig. 2.11 Flowfield Survey of Radial Inflow Turbine

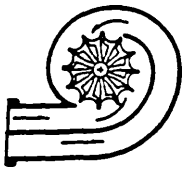


Velocity diagrams obtained in the centre of the volute entry and in the wake of the entry tongue. 101.6 mm diameter turbine. Rotor velocity 380 r.p.s.

Fig. 2.12 Instantaneous Flow Velocity (Tindal et al (25))

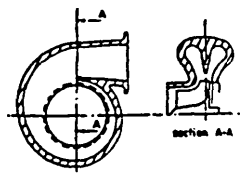
STEADY FLOW TEST

Double-Flow Housing
Equal & Partial Admission



1965	Benson et al	(26)	Nozzled Turbine
1965	Wallace et al	(27)	Nozzled Turbine
1968	Timmis et al	(28)	Nozzled Turbine
1969	Wallace et al	(2)	Nozzled Turbine
1977	Pischinger et al	(30)	Nozzled Turbine
1979	Mizumachi et al	(29)	Nozzled Turbine

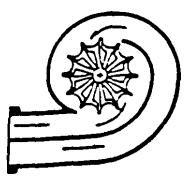
Twin-Flow Housing
Equal & Partial Admission



1977	Pischinger et al	(30)	Nozzleless Turbine
1986	A. Dale et al	(38,39,40)	Nozzleless Turbine
1987	Acton et al	(42)	Nozzleless Turbine

UNSTEADY FLOW TEST

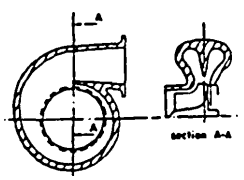
Double-Flow Housing



1965	Benson et al	(26)	Nozzled Turbine
1965	Wallace et al	(27)	Nozzled Turbine
1968	Timmis et al	(28)	Nozzled Turbine
1974	Mayashita et al	(34)	Nozzled Turbine
1974	Benson et al	(33)	Nozzleless Turbine
1979	Mizumachi et al	(29)	Nozzled Turbine

3 entries volute with 3 separate supply pipes	1969	Wallace et al	(31)	Nozzled Turbine
1,2 and 3 entries volute	1970	Wallace et al	(32)	Nozzled Turbine

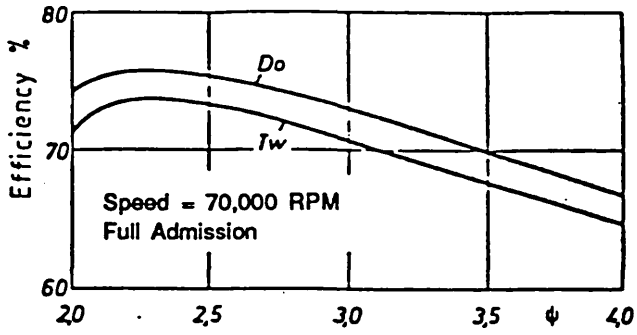
Twin-Flow Housing



1984	A.Dale et al	(38,39)	Nozzleless Turbine
1987	Acton et al	(42)	Nozzleless Turbine

Single Entry Turbine	1976	Kosuge et al	(35)	Nozzled Turbine
	1989	Capobianco et al	(41)	Nozzleless

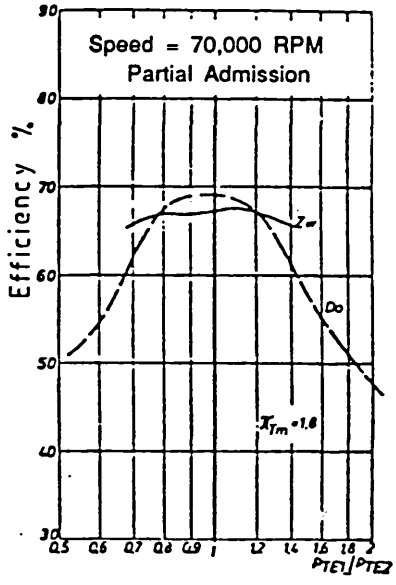
Fig. 2.13 Test and Performance of Radial Inflow Turbine



$\psi = C^2/U^2$

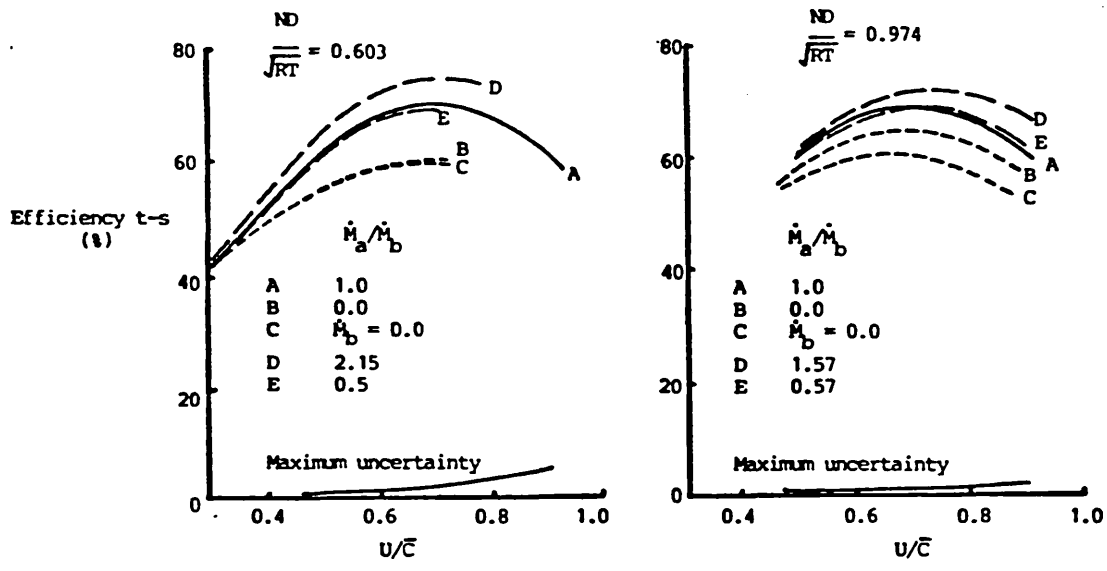
Isentropic turbine efficiency versus pressure number, ψ , for two different types of turbine at full admission. Inlet temperature at 900K
Tw = Twin-flow housing Do = Double-flow housing

FIG. 2.14 Comparison of Turbine Efficiency between twin-flow and double-flow housing, at full admission (Pischinger et al (30))



Isentropic turbine efficiency versus inlet pressure ratio, P_{TE}/P_{TE2} for two different types of turbine housing. Inlet temperature at 900K.
Tw = Twin-flow housing Do = Double-flow housing

FIG. 2.15 Comparison of Turbine Efficiency between twin-flow and double-flow housing, at partial admission (Pischinger et al (30))



Efficiency characteristic with unequal admission, at two speeds ($\bar{C}$ is the energy mean isentropic exit velocity)

Fig. 2.16 Turbine efficiency characteristics with partial admission (Dale et al (38))

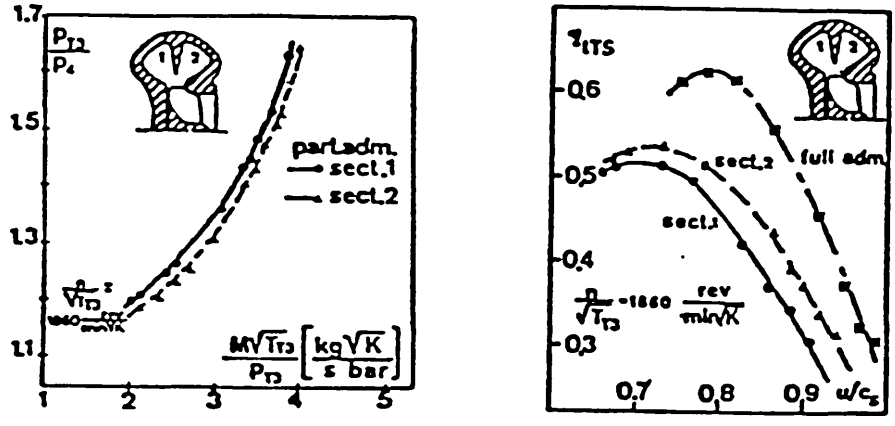
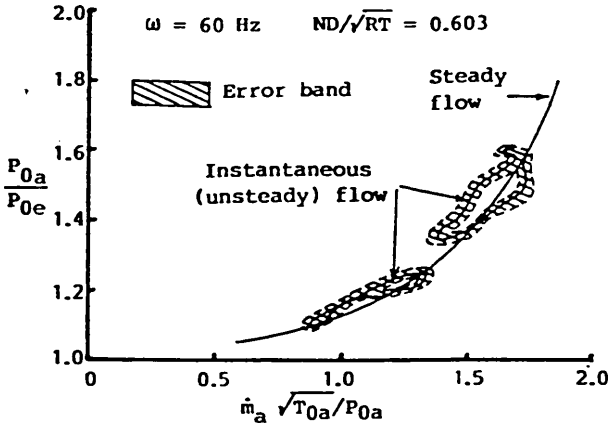


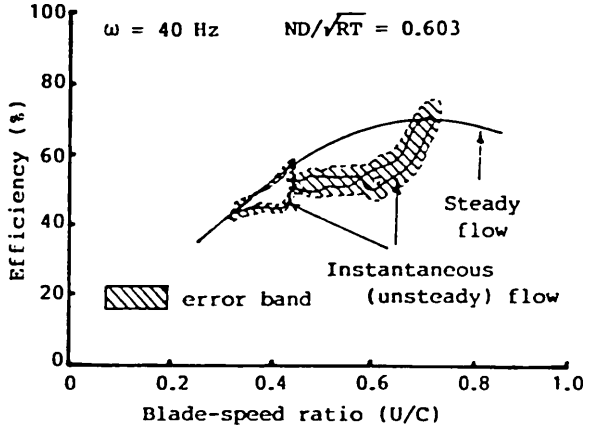
Fig. 2.17 Turbine efficiency characteristics with partial admission (Acton et al (42))



Locus of instantaneous flow under pulsed inlet conditions superimposed on steady-flow data (for two mean inlet pressures, single-entry turbine)

Fig. 2.18

Instantaneous mass flow (Dale (39))

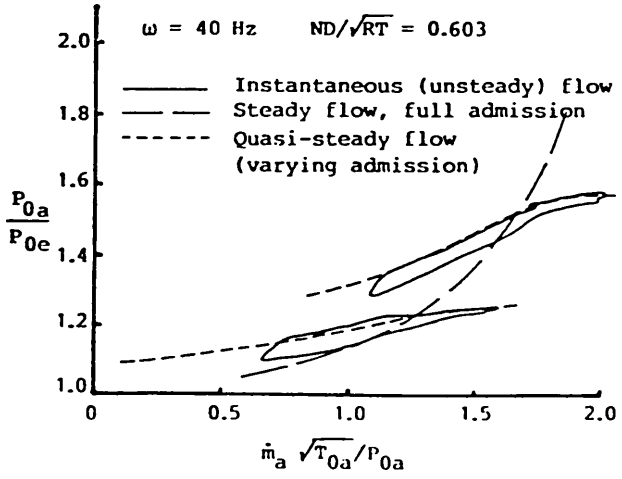


Locus of instantaneous efficiency under pulsed inlet conditions superimposed on steady-flow data (for two mean inlet pressures, single-entry turbine)

Fig. 2.19

Instantaneous turbine efficiency

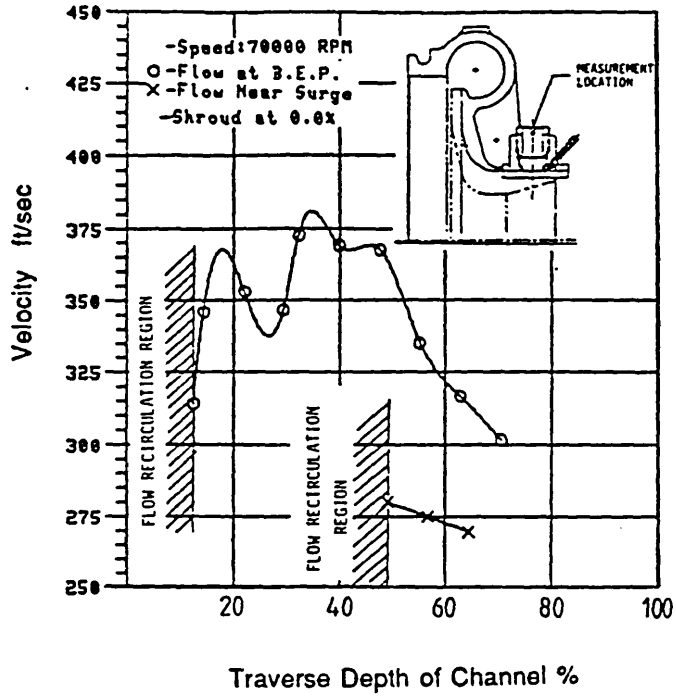
(Dale (39))



Instantaneous flow locus, at one entry, with out-of-phase flows at each entry of a twin-entry turbine (for two mean inlet pressures)

Fig. 2.20

Instantaneous mass flow (Dale (39))



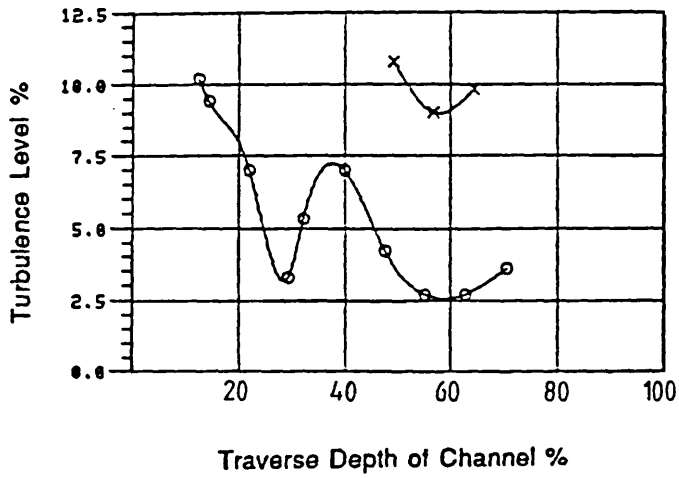


Fig. 2.21 Flow measurements within impeller of a turbocharger compressor using L2F velocimeter (Young et al (50))

CHAPTER 3

Laser Two Focus Velocimetry

The basic idea of laser velocimetry is that the velocity of the flow can be determined by measuring the speed of small particles in the fluid. The particles are assumed to follow the flow path of the real flow. Thus, the flow direction can be deduced from the direction of the particles. The particles are illuminated by a laser beam and the light scattered by the particles is registered by very sensitive optical photo multiplier detectors.
The main components of a laser velocimeter are : a transmitting device by which laser beams are directed to a distinct point in the flow, a receiving device aligned with the probe volume that registers the scattered light from the particles, and an electronic device that processes the photo multiplier signals and delivers the velocity and turbulence information which is finally required. There are basically two types of laser velocimeters, namely Laser Doppler Velocimeter (LDV) and Laser Two Focus (L2F).

3.1 Laser velocimeter techniques

3.1.1 LDV Principle

The concept of LD-velocimetry is indicated in Fig.3.1. Two coherent light beams intersect, producing an alternating system of bright and dark interference fringes. The distance,s, between the fringes depends on the intersection angles, β, and on the wavelength, ℓ, of the light. A particle moving through this fringe system emits periodic light signals, and the

frequency of these signals is directly proportional to the velocity component perpendicular to the fringe system. The component parallel to the fringes of Fig.3.1 can be measured by an additional fringe system using light of a different wavelength oriented perpendicular to the fringes of Fig.3.1.

3.1.2 L2F Principle

In the L2F velocimetry, the fringe is replaced by two distinct light beams which create a light gate, Fig.3.2. The velocity component perpendicular to the laser beam axis is derived from the time a particle takes to pass the two indicated spots and from their separation, S. As in the LD-velocimetry, the velocity component parallel to the laser beam axis cannot be measured by this approach. However, if the laser beam is rotated to explore different flow direction, then a two dimensional flowfield is obtained.

3.1.3 Comparison between LDV and L2F

The main difference between the laser Doppler and the two focus systems is the light intensity concentration in the probe volume. Since the probe volume of the laser two focus system is significantly smaller than the probe volume dimensions of the LD-velocimeter (Fig.3.3), a much higher intensity concentration is obtained in the probe volume of the L2F velocimeter. This results in an increased signal amplitude of the detected scattered light for the L2F system. Therefore the use of the L2F system is most appropriate if small particles have to be used to follow the flow. Very small particles are necessary for measurements in highly accelerated flow, measurements close to the wall, and for measurements in narrow flow channels where the background flare results in a strong signal noise.

Because in most turbomachinery applications it is impossible to install the the photo multiplier behind the test rig, the laser velocimetry system is designed to receive the back scatter rather than the forward scatter light from the particle. Therefore, only the weak backscatter intensity of the particles is detected by the photo multiplier, giving only low amplitude signals. Furthermore the intensity of the scattered light decreases with the particle size. Hence a high particle concentration at the probe volume is necessary to ensure an adequate signal amplitude. For these reasons, the L2F system is superior to the LD system in many turbomachinery applications, and has achieved importance in the experimental fluid flow analysis.

3.2 L2F Technique

The L2F measuring device generates in its probe volume two highly focused light beams. A particle trajectory passing through both the light beams in the focused section, along the focal plane produces two successive pulses of the scattered light. Fig.3.4 illustrates the event. The first signal pulse derived from the scattered light starts a clock. The same particle when it passes the second focal volume stops the clock. The time of flight is the time interval between the start and stop pulse of the same particle.

Taking a single measurement of the time interval between the scattered light pulses, one is never sure of the right measurement. The reason is that the two succeeding pulses can be generated in two different ways as is shown in Fig.3.5. First by one particle crossing both the beams and causing a useful measurement; second by two different particles independently passing the two beams causing incorrect measurement. Therefore a large number of time interval

measurements have to be made such that correlated time interval measurements are reinforced while erroneous measurements are averaged as background noise.

The measurement direction is in a plane which contains the focal volumes. As the diameter of these volumes is small compared to their distance apart, the L2F has a highly directional measuring volume.

In Fig.3.6, the angular measurement is made possible when the stop trigger beam rotates about the axis of the start trigger beam. A stepping motor facilitates this rotation at a preselected angular interval. By rotating the two spots, more velocity histograms can be accumulated. This yields a two dimensional probability histogram as in Fig.3.7.

The histograms taken at different angular positions have to be normalized to a reference value. In the L2F system, the number of particles entering the start-probe volume are taken as this reference. They are counted with a particle counter that can be preset to a selectable number of counts. When the count limit is reached the data accumulation will be stopped automatically. A new angular position is then set and a new measurement is made.

Fig.3.8 shows an example of a velocity and angular data distribution during a test run with a turbine rotor.

Turbulence intensity in a 2-D flow is defined as :

$$Tu_i = \frac{\sqrt{\sum(u_i - \bar{u}_i)^2}}{u}$$

where $$u = \sqrt{(u_1)^2 + (u_2)^2}$$

u_i = velocity component in the i^{th} direction

$\bar{u}_i$ = mean value of component velocity

The L2F velocimeter can only be applied to flows with a turbulence level smaller than about 30%. Higher than this value, it is difficult to estimate the mean values with any accuracy on the basis of a very broad histogram.
In Fig.3.8a, the low turbulence nature of the flow is characterised by a distinct peak in the velocity data, giving a low velocity turbulence intensity level. High turbulence flow is indicated by a more broadly spread distribution yielding a higher velocity turbulence intensity level, Fig.3.8a. A high noise level in the low velocity region is also evident from the distribution. This is a typical characteristic of turbulent flow. The turbulent nature of the flow can also be seen from the angular data distributions, Figs.3.8c and d.

3.3 L2F Optical System

The optical system of the L2F velocimeter is illustrated in Fig.3.9. For the L2F technique it is necessary to produce two laser beam waists separated by a known distance in the measuring volume. A Rochon prism is used to divide the incoming laser beam into two collimated beams. One beam emerges essentially undeviated while the other beam deviates at a small angle with respect to the optical axis.
A $\lambda/4$ wave retarder, A, between the laser and the Rochon prism is required to convert the linearly polarized laser light to circular polarized light. The beam splitter, B, is followed by a lens, C, placed at one focal length behind it. As the splitting face of the beam splitter prism is in the front focal plane of the lens, C the collimated beams are brought to two focal spots in the second plane of the lens, D. These focal volumes are relayed via two deflection mirrors, E and the transceiver lens, F, into the probe volume, G, at some distance from the optical head.

The transceiver lens is a combination of two back to back collimator lenses. These can be changed to allow variable working distances. The following is a list of lenses that were available:

L2F Optical Head	Spot Separation µm	Spot Diameter µm	Working Distance mm	Focal Length mm
L2F 0 4412	209	9	276	350
L2F 0 4413	291	12	473	500
L2F 0 4414	541	20	898	800

When a particle trajectory passes the probe volume in the focal plane, light is scattered. The backscattered light is collected by the transceiver lens and focused onto the plane, I. The image of the focal volumes generated in this plane is enlarged with the objective, J and imaged onto the dual pin holes, K. Light passing this pair of pin holes is detected by two very sensitive wide band photo multiplier tubes, converting it into electrical pulses.

The function of the dual pin holes and the light gate at H is to reject light from all sources except those scattered from the moving particles in the measuring volume.The small diameter of the pin holes and the high resolution of the optical system gives sensitivity to particles as small as 0.5mm in diameter.

By rotating the beam splitter B, the dual pin holes and other stops rotate simultaneously. Thus setting the two spots in the probe volume to rotate, allows measurements for more than one flow direction. A stepping motor is coupled to the beam splitter and other stops through a toothed belt drive. Due to the highly precise construction, excellent mechanical correspondence between the output and return image is achieved.

3.4 L2F Signal Processing

The output pulses from the photo multiplier tubes are generally noisy images of the intensity of the focal volumes. Special pulse processing techniques are therefore required in order to maintain a good time of flight resolution. The photo multiplier is a combined unit containing a very sensitive broad band photo multiplier tube and a low noise, fast rise time preamplifier. This allows a fast timing and photon counting signal processing technique to be used.

The preamplified signals are transmitted over the signal cables to the L2F signal processor. The signal conditioning electronics are the pulse shaper and constant fraction discriminator, Fig.3.10. To measure exactly the time of flight for a particle that passes from one focal volume to the other, logic signals whose times of generation are precisely related to the peaks of the scattered light pulses have to be generated. Two basic factors may cause inaccuracies in the time measurement, jitter and walk. Jitter is introduced by noise on the signal. The noise riding in the signal changes the absolute points at which a discriminator responds. Timing uncertainties caused by jitter are reduced by the pulse shaper. The pulse shaper is also necessary to restore useful signal amplitudes when high voltages supplied to the photo multiplier tube have to be reduced. This is always the case when measuring takes place close to the solid wall (surfaces), where there is a lot of flare.

The major problem, however, is the time uncertainties, or walk, due to variation of amplitude or variation in rise time. This is, for example, caused by particles of different sizes or of different refractive index across the two focal volumes. Walk is minimised by the constant fraction discriminator. A variable threshold for signal acceptance can be adjusted in order to reject noise events and to boost the 'real event' rate. A

secondary discriminator level allows the rejection of signals from big particles which do not follow the flow because of their high inertia, for example in the region of high acceleration.
To measure the time of flight, a time to pulse height converter (TPHC) generates an output pulse which is proportional to the time interval between a start and a stop pulse. The output of the TPHC is fed to the analogue to digital converter (ADC) of a multi-channel analyser (MCA) which digitizes the pulse amplitude for acceptance by the MCA's logic circuitry. The MCA produces a spectrum of height from the subsequent input pulses and hence a spectrum of the time of flight. Fig.3.11 shows an example of a typical spectrum of the time of flight during a test with a turbine rotor under steady flow conditions.

3.5 L2F Periodic Flow Mapping

The L2F signal processor used has the capability to produce periodic mapping, where measurements are made for example in rotating components of turbomachines or in reciprocating engines. In the periodic flow mapping, it is necessary to relate the measured velocity function to the time phase of the periodic phenomenon. For example, when measurements in the intra-rotor region of turbomachinery are made, the measuring volume sweeps out a circumferential path within the rotating blade row.
With its built-in routing circuit the L2F Signal Processor can assign the measured data automatically to separate memory stacks each containing 256 channels of the MCA's memory. Together with the measured data, the L2F Control Processor loads the digital representation of the angular position of the rotor into its internal buffer for data processing. The circumferential path in a blade row can be divided into a fixed

number of the line segments, called time windows. Fig.3.12 shows a typical time of flight distribution obtained from 16 different windows during a test run with a turbine rotor with pulsating flow.

The L2F system for multi window and automatic operation capability is illustrated in Fig.3.13. The synchronizer is used for the periodic flow mapping described earlier. It operates as an electronic shaft angle encoder, to generate the correct angular position (or to tag each time interval measurement with the proper phase of the periodic flow). The synchronizer uses a trigger pulse from the object under investigation to produce a digital word which corresponds to the current angular position.

The encoded angular position is produced by two phase lock looped circuits. In the first stage, the frequency of the input signal (once per revolution) is multiplied by the number of blades to generate the once per blade pulses (blade frequency). The blade frequency is then mutiplied by a factor of 32 in the second stage. Therefore the blade to blade period is divided into 32 equal angular increments. This count is further divided to yield the required number of time windows (2,4,8 or 16). The maximum number of time windows possible is 16. If a line segment is drawn across two successive blades it can be divided into 2,4,8 or 16 equal angular position for the time of flight. The time of flight increments are tagged with the location of the line segment in which it occured and the resulting data is sorted in the MCA. Thus it is possible to accumulate many multi-channel analysis functions (up to 16) each from a line segment of the blade to blade period or in this application, of a pulse period.

Another feature of the synchronizer is the possiblilty of gating the laser beam when a light chopper is used. This acousto-optical light chopper is used to turn off the laser beam periodically in order to prevent the intense laser light

hitting the blades as they pass the probe volume, so that light reflected from the blades cannot drive the PM-detector into saturation. This feature not only keeps the signal-to-noise ratio constant but also improves it because the photocathodes of the PM-tubes recover during the laser-off-time.

3.6 Signal Quality of the L2F Velocimeter

The actual detection volume is defined as the region from which scattered light is used for the time of flight measurement. This volume is reduced when the scattered light is gated by the optical stops like the dual pin hole aperture. A threshold is applied so that the constant fraction discriminator will only process signals if they exceed a certain amplitude. This reduces the measuring volume further.

In most cases, the length, ℓ, and the spot separation, S, of the actual measuring volume are about the same. Thus angle, Ψ is approximately 45° (see Fig.3.14a). The measuring volume is defined as (s x 2ℓ) . Particles crossing this measuring volume will give rise to a signal.

The focused laser beam has a Gaussian intensity profile, so that particles which do not cross the measuring volume at right angles to the optical axis can also give rise to a signal. However the maximum output signal occurs when the particles cross perpendicularly to the optical axis. Fig.3.14b illustrates this. Consider two trajectories A and B crossing the two spots. One particle moving at right angle covering the distance S, the other touching the two spots tangentially covering the distance S*. Both give rise to a signal.

$$S^* = S.\cos\left(\sin^{-1} d/S\right)$$

$$e = (S - S^*)/S \qquad \text{Relative Error}$$

This error reduces as the S:d ratio increases. A S:d ratio of more than 20 ensures that only particles following trajectories of small α are detected as a dual peak events, thus avoiding the broadening of L2F velocity data from particles with large α.

The beam transit probability is defined as the probability with which the same particle produces a start and a stop pulse. As the flow turbulence increases, the beam transit probabilty decreases. The beam transit probability is also affected by the S:d ratio. Fig.3.15 shows the beam transit probability as a function of turbulence intensity and the beam distance to diameter ratio.

In the experiment, a 500mm nominal focal length lens was used.

Spot separation = 290μm Spot Diameter = 12μm

Thus S:d = 24

From Fig.3.15 the turbulence intensity and S:d ratio are used to estimate the beam transit probability. As the turbulence intensity increases, the beam transit probability decreases.

Table below gives examples of beam transit probability estimated from Fig.3.15 with typical turbulence intensity values.

Turbulence Intensity %	S : d	Turbulence Intensity * (S:d)	Beam Transit Probability % from Fig 3.15
5	24	1.2	97
10	24	2.4	88
15	24	3.6	78
20	24	4.8	67
30	24	7.2	50

3.7 Summary

Laser velocimeters are classified as optical instruments for making non-intrusive measurements of gas and liquid flow. Generally laser velocimetry is superior to the probe measurement method because there is no interference with the flow. The relationship between the fluid velocity and the signal is linear over the entire measurement range. This relationship is independent of the properties of the material and environmental conditions such as temperature, pressure and density. Calibration is not necessary as the laser velocimetry is an absolute method. The volume in which the measurements are made is very small and is limited only by optical means so that measurements can be made even in the boundary layers and at places that cannot be reached by probes. It is because of these advantages that laser velocimetry stands out as the most effective system for measuring the flow in turbomachinery over the entire range of velocities from low to high.

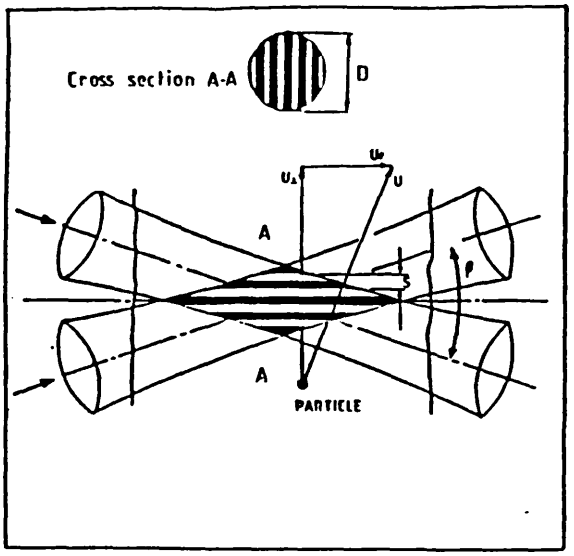


Fig. 3.1 Principle of Laser Doppler Velocimeter

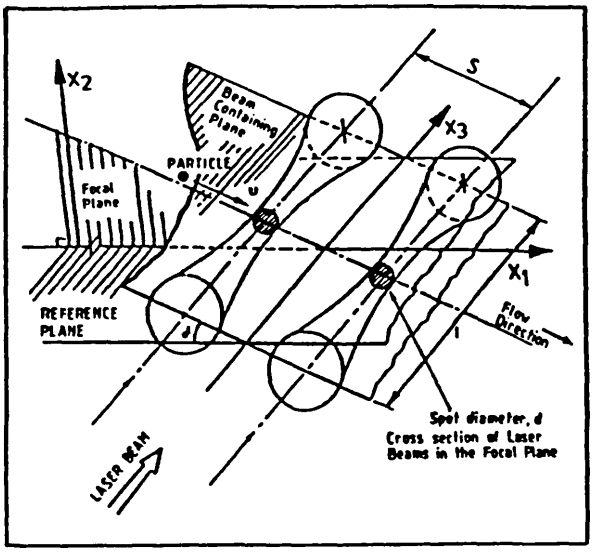
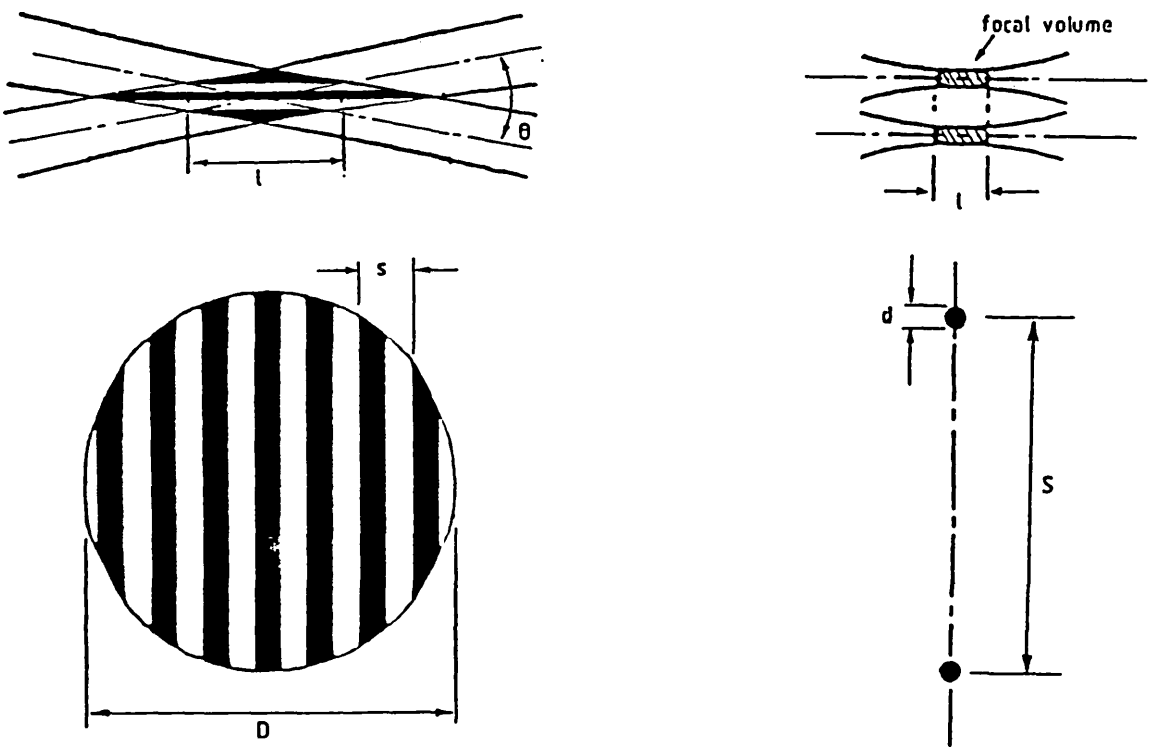
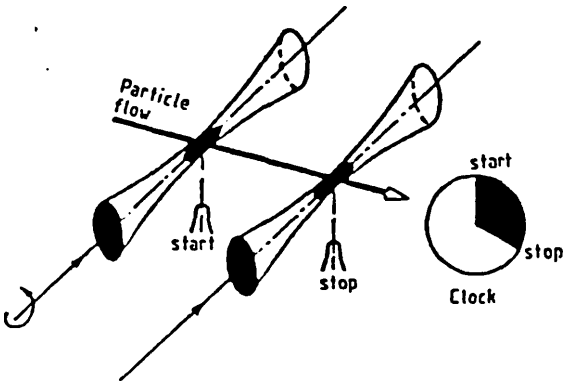


Fig. 3.2 Principle of Laser Two Focus



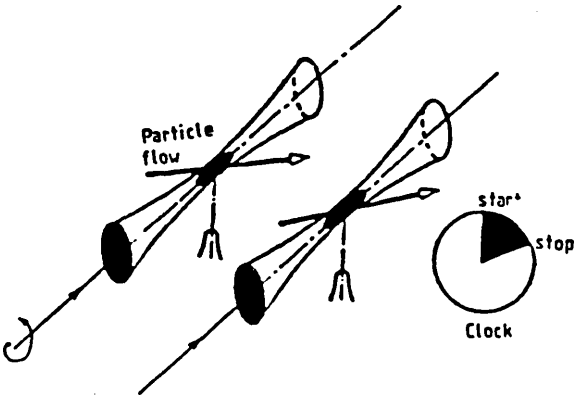
Comparison of LD and L2F Probe Volume Dimension

Fig. 3.3



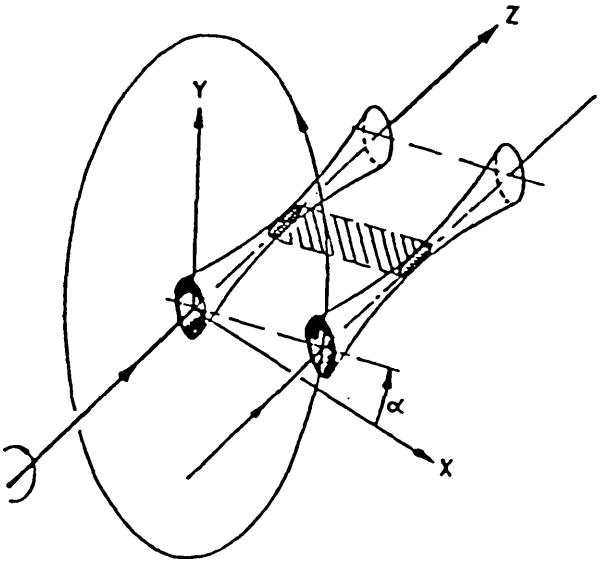
Useful time of flight caused by the same particle

Fig. 3.4



Incorrect time of flight caused by two independent particles

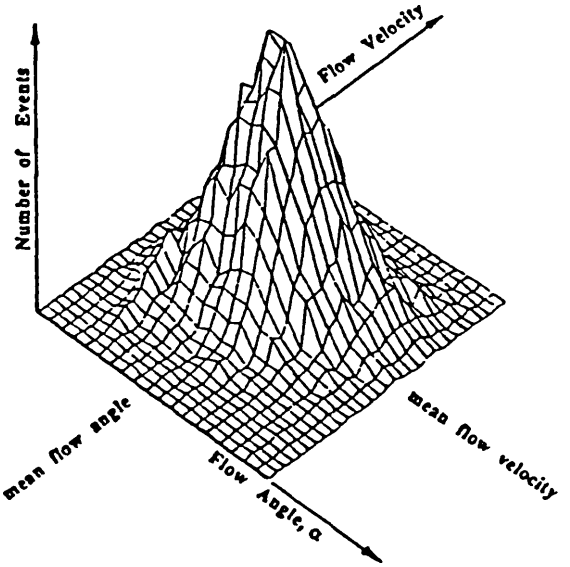
Fig. 3.5



Rotation of Measurement Direction

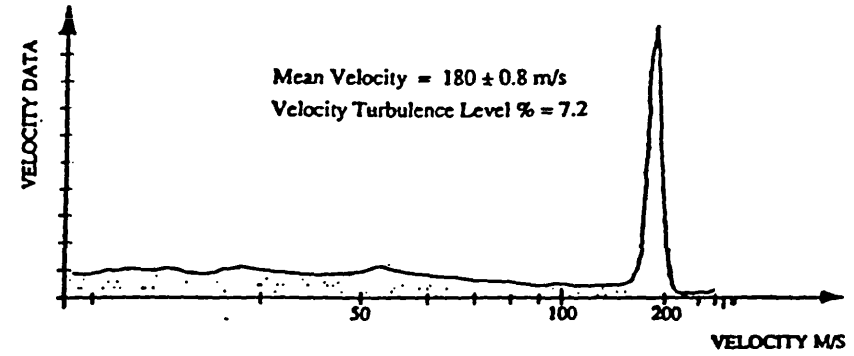
The stop trigger beam rotates about the axis of start trigger beam.

Fig. 3.6

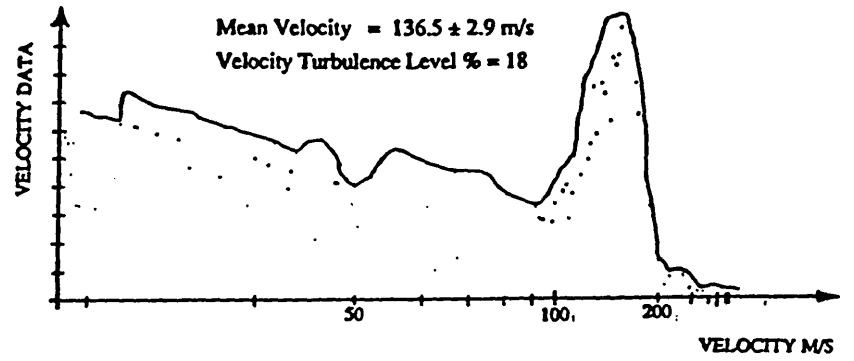


Two Dimensional Velocity Distribution

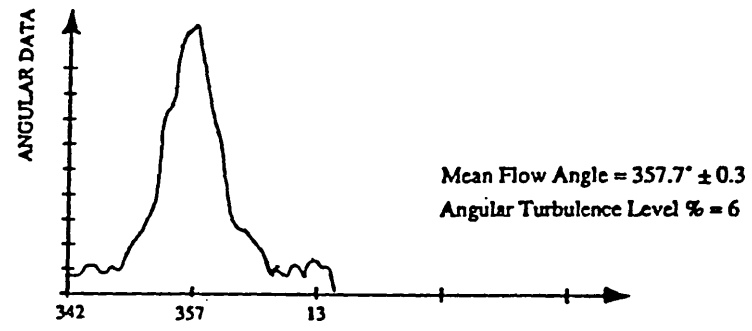
Fig. 3.7



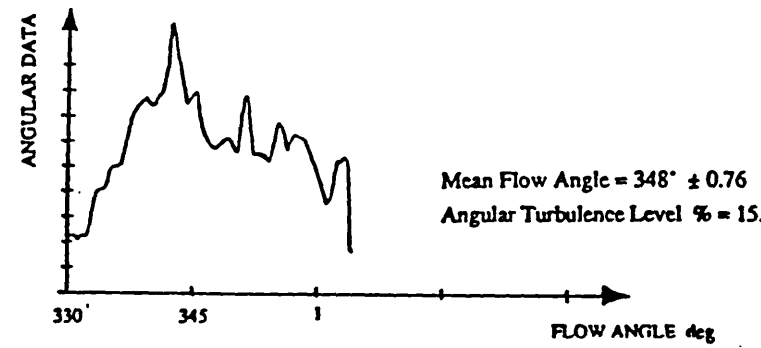
(a)



(b)

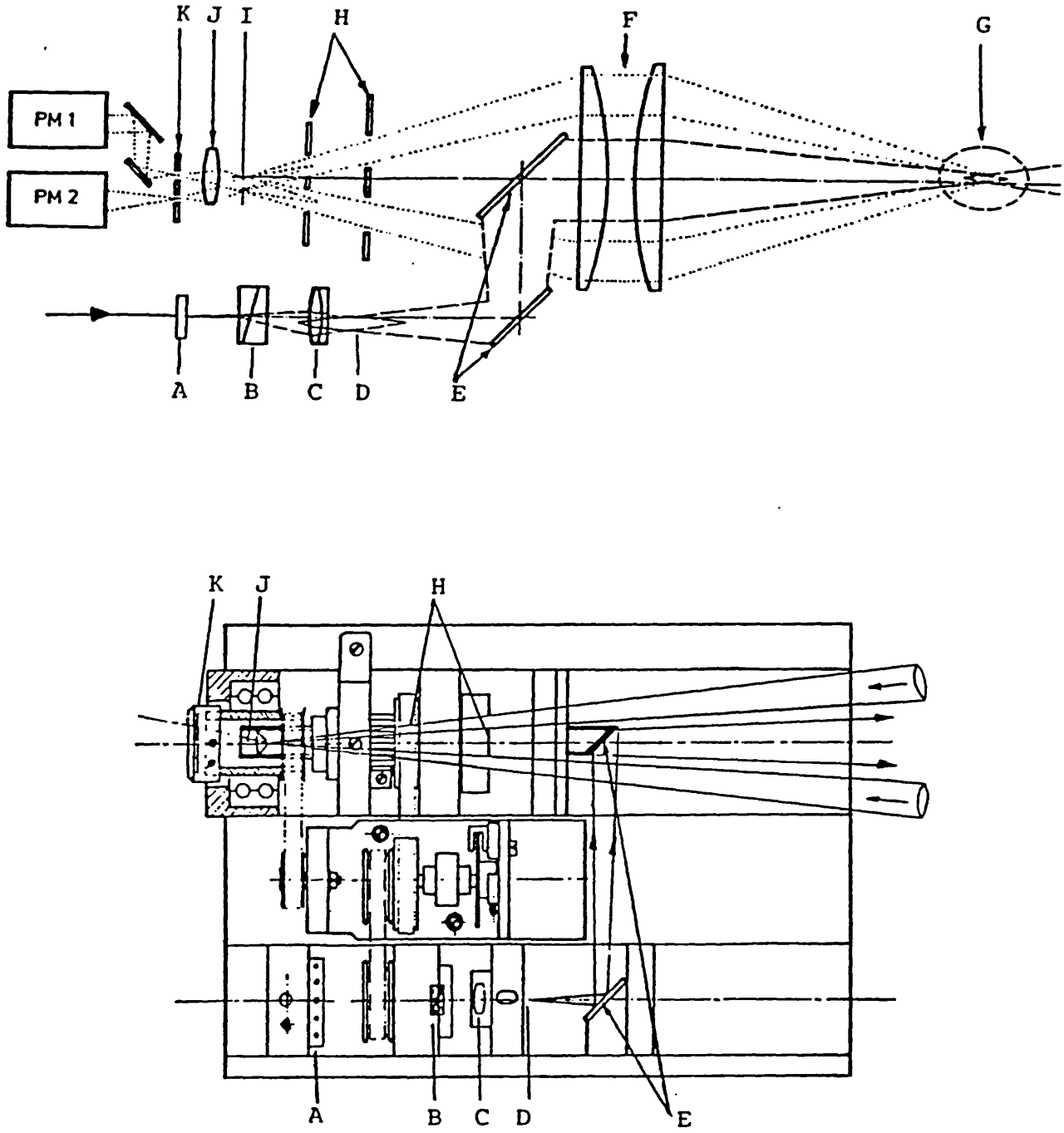


(c)



(d)

Fig 3.8 Typical Velocity and Angular data distributions during a test run with turbine rotor



Optical arrangement of the L2F Velocimeter

Fig. 3.9

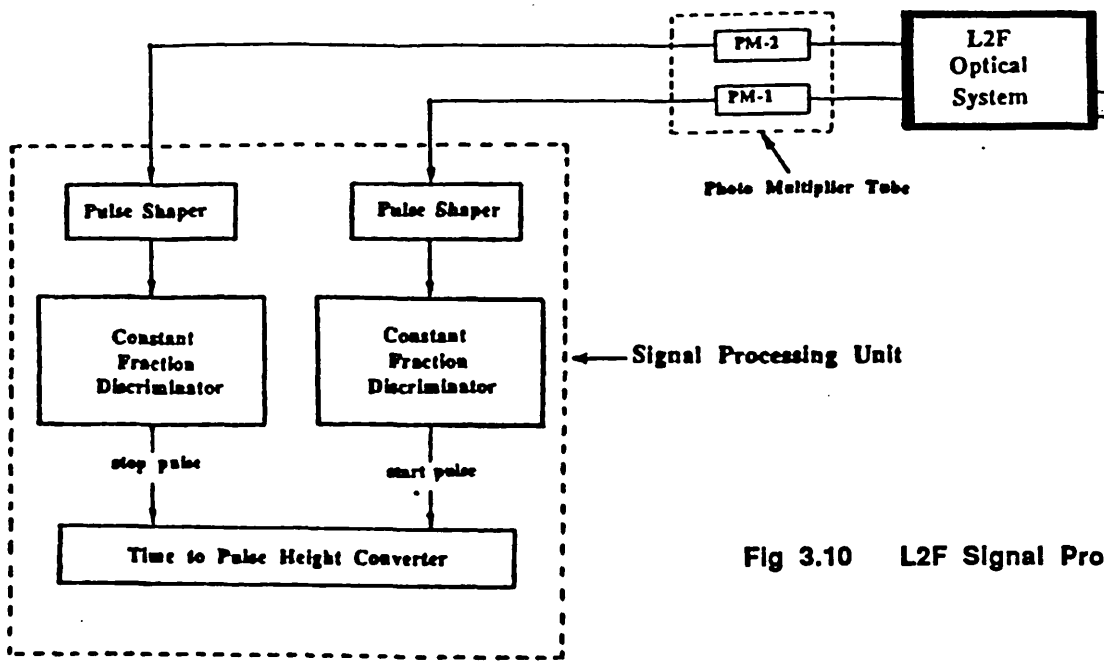


Fig 3.10 L2F Signal Processing

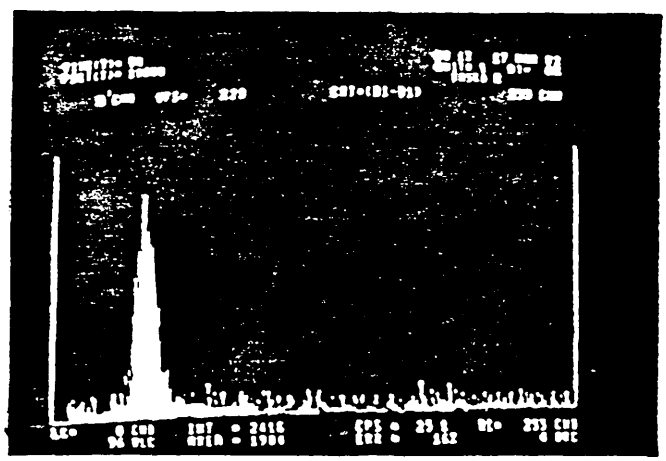


Fig. 3.11

Spectrum of time of flight

Single Window Operation

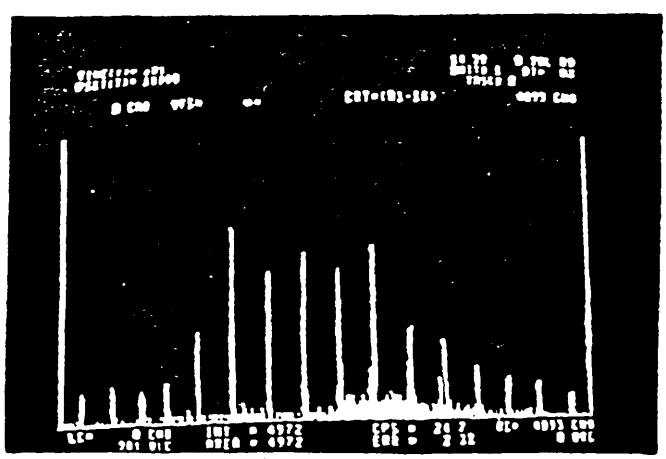


Fig. 3.12

Spectrum of time of flight

Multi-Window Operation with 16 time windows

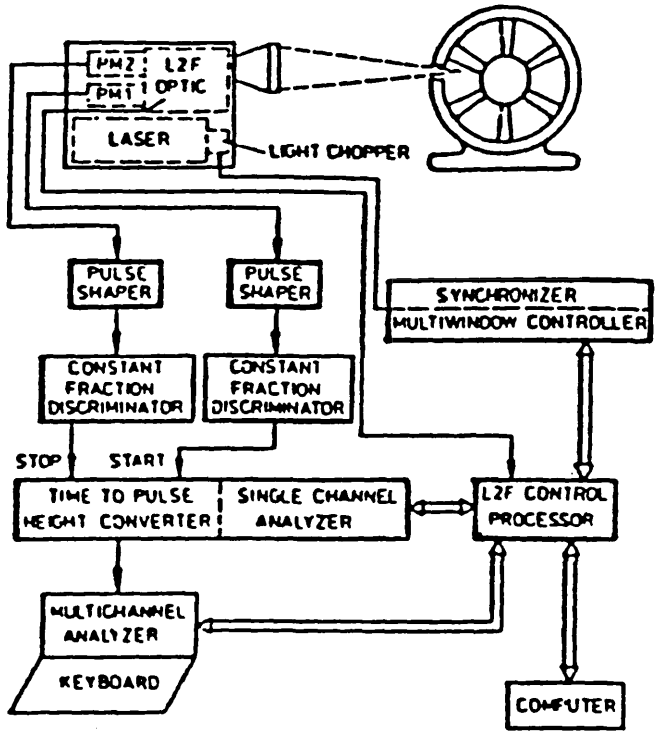


Fig. 3.13

L2F Velocimeter with Synchronizer for Periodic Flow Mapping

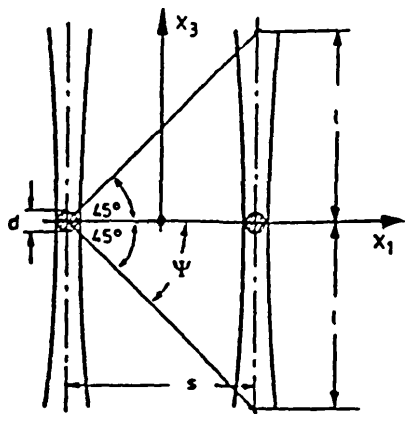


Fig. 3.14a

L2F Probe Volume

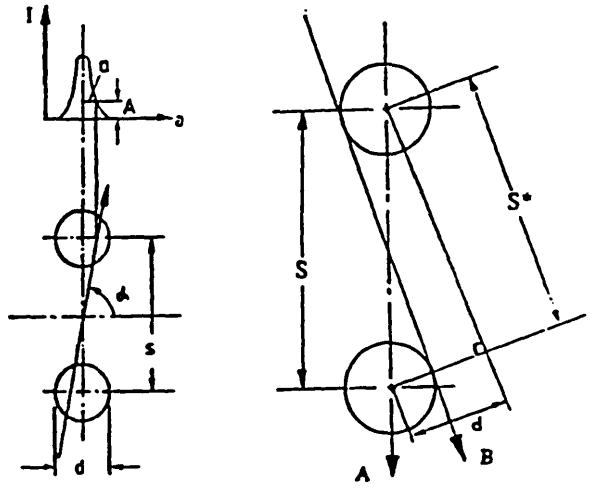


Fig. 3.14b

Error of beam distribution and intensity within an L2F probe volume

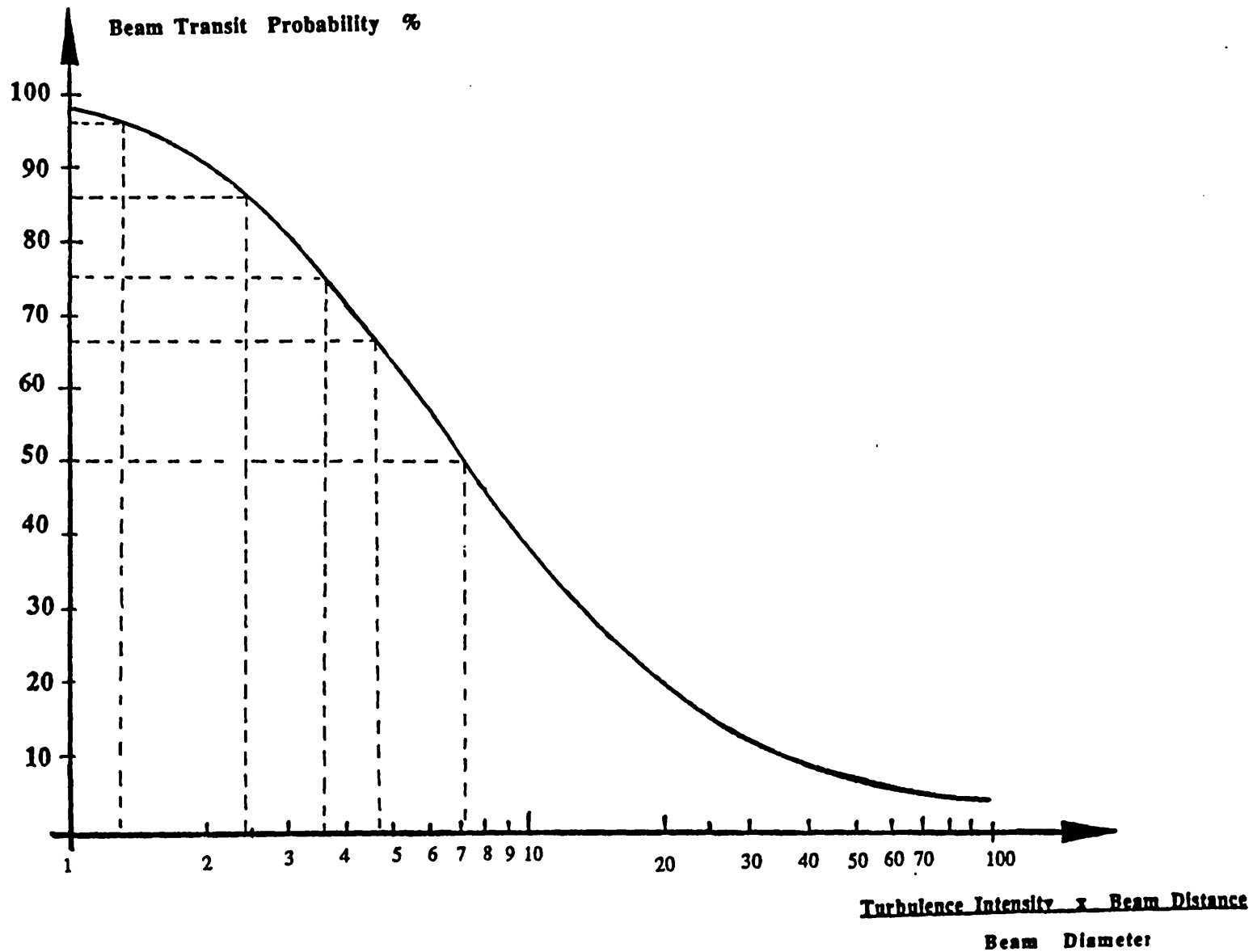


Fig 3.15 Variation of successful dual peak events with turbulence intensity and s/d variation.

CHAPTER 4

EXPERIMENTAL FACILITIES

This chapter describes the experimental test facilities, automatic data logging of steady flow, instrumented turbine housing and measuring concept.
The same test facility is used as described by Dale (38,39). Modifications were made to accommodate L2F seeding injection at a section immediately after the rotary pulse generator. All data acquisition facilities remain unchanged except for the automatic data logging system for steady state testing. The same equations for data reduction to efficiency, blade speed ratio and non dimensional flow were applied (38,39).
In the test, an exit duct was also installed to guide the flow leaving the rotor so that measurements of gas flow characteristics at the rotor exit could be made.

4.1 Test Rig Facility

A schematic diagram of the test rig facility is illustrated in Fig.4.1. The system is capable of supplying hot air to a twin entry turbocharger turbine for steady and unsteady flow, and partial and equal admission. The test rig was designed to supply air to the twin entry turbine inlet via two separate limbs. The mass flow in the two limbs can be varied through individual regulating valves. This facilitates partial mass flow conditions to the turbine. A 4" pipe supplies the two limbs through a plenum. The speed of the rotor, the load on the dynamometer and the pulse frequency can be controlled to achieve the desired operating conditions. A data monitoring programme, which accepts temperature and pressure inputs,

further reduced it to desired parameters (mass flow, pressure ratio, non dimensional parameters etc) and displayed them on monitor screen. The running condition of the rig can then be updated regularly.

Compressed air is supplied by an electrically driven compressor capable of delivering 0.5 kg/s at 4 bar to the following stages:

Regulating Valve: The supplied air is delivered through a 4" pipe. The regulating valve provides a means of shutting the whole system completely. A safety feature is built into the system so that an activation to cut off the air supply to the rig is done through this 4" regulating valve. The total mass flow supplied to the turbine is also controlled by means of this valve.

3-Stage Filter : Air supplied from the source passes through a series of pipes which carry along with it rust particles from the pipe. Fine instrument probes are sensitive to particles. With the operation of the L2F system, these particle of varying sizes will have an undesirable effect. The air is passed through this 3-stage filter (coarse grid,cyclonic and paper element) to achieve clean air.

4" Orifice Plate : The flow measuring section is located along a straight pipe in compliance with BS 1042 practices for flow measurement. The total mass flow to the turbine is measured here.

Heater Stack : This is a 60 kw electical heater stack. The compressed air is heated sufficiently to avoid water vapour in the air condensing and freezing as it expands through the turbine. It is not possible to heat the air sufficiently to

reproduce typical turbocharger temperatures, so that turbine performance measurements must be scaled using the conventional non-dimensional groups. The present test were run at a turbine inlet air temperature of 400K for steady flow and 350K for unsteady flow test. The heater is thyristor controlled from the turbine inlet total temperature thermocouple and is capable of maintaining inlet temperature to ± 1° C.

Plenum : The heated mass of hot air is settled in the plenum before branching to two 3" pipes (the inner limb and the outer limb). From this section onwards the pipes are insulated for safety and heat conservation reasons.

Regulating Valves : Two 3" regulating valves provide control of the mass flow in each limb. The opening and closing of the valves can be done independently from the control panel.

3" Orifice Plates : Individual mass flows in each limb are monitored through these flow measuring sections. The total mass flow measured from the two 3" pipes should match the intial delivery monitored at the 4" pipe section.

Pulse Generator : This consists essentially of a pair of rotating plates driven by a variable speed D.C motor. Fig.4.2 shows the sectional view of the pulse generator. As a steady stream of air passes the pulse generator, the rotating plate breaks down the flow allowing it to pass intermittently. The pressure pulse shape generated depends on the profile of the rotating plate and the pulse frequency is fixed by the speed of rotation of the disks. The pressure pulse shape produced is intended to be representative of an engine exhaust pressure profile. Fig.4.3 shows a disk profile producing a pressure pulse shape as monitored at the turbine inlet. The rotating

plate can be positioned to produce either in-phase or out-of-phase pressure pulses. In the pulsating flow tests this is set to produce a 180° out-of-phase pulse shape. For steady flow tests, the openings of the two rotating plates are aligned with the pipes. Without rotating the plate a steady flow can be passed with no obstruction from the rotating plate.
After the pulse generator the 3" pipes gradually converge to the instrument volume section, keeping the two flows separated right up to the turbine volute. This section was fabricated so that the cross sectional area changes from semi-circular to rectangular to suit the turbine inlet. Fig.4.4 shows a perspective view of one half of this pipe section.

Seeding Injection : Seeding is injected into each individual limb downstream of the pulse generator. The injection point is located at the mid section of each pipe, injecting in the direction of the flow. The point of injection is about 1.2m from the turbine inlet. Each individual injection inlet each has a valve so that during test with one limb fully closed the respective valve can be closed.

Emergency Stop Valve : A twin-passage rotary emergency stop valve is fitted just before the turbine. This is normally held open magnetically and does not obstruct the flow. It closes automatically when an over speed, high vibration, high dynamometer temperature or high dynamometer bearing temperature is detected. It can also be activated by the operator.
A very short section separates the stop valve from the turbine housing. This is the instrumented section where the total temperatures, instantaneous pressures and mass flows are monitored before the turbine inlet.

Dynamometer : The dynamometer is a high speed eddy current type, with ball bearings, designed for speeds up to 70000 rpm

and a power absorption of 12 kw. The turbine rotor is fixed on the dynamometer through a collet of high machining tolerance. The turbine shaft is reduced in length and diameter to fit the collet. A full descrption of the dynamometer and its operation is given by Dale (39).

L2F Unit : The L2F unit rested on a traverse table having horizontal, axial and vertical motions. It has been located squarely with the turbine housing and checked using the laser beam.

4.2 Automatic Data Logging for Steady State

In the experiments conducted by Dale (38,39), all the steady flow test data logging were done by manual recording. In each test run, there are about 16 temperature and pressure readings to be recorded. This process is not only time consuming but also requires the rotor to be maintained at a desired speed until all the data had been recorded. This holding time (to maintain a constant speed whilst data logging is in progress) causes the dynamometer bearing temperature to creep up especially when testing at high speed. Thus a data logging program was developed to do away with manual recording and hence reduce testing time. With the time taken to data log reduced, the steady flow speed error could be substantially reduced improving the steady flow efficiency error at low blade speed ratio.

Fig.4.5 shows the data logging system and Fig.4.6 shows a simplified flow chart of the program. With the data logging program, all temperatures and pressures are scanned and displayed on the monitor. The program also calculates the mass flow rates in the 3" and 4" pipes and the mass flow ratio between the two limbs. Now the operator can decide whether to

save this operating condition or to change the operating condition and scan all the pressures and temperatures again. If the operating condition is set, inputs of speed and dynamometer load are required. The program will then proceed to calculate the turbine performance data and print out a hardcopy. A typical printout of the steady state flow test is in Fig.4.7. The equations used for data reduction to the required parameter of efficiency, blade speed ratio and non dimensional flow are given by Dale (38,39).

4.3 Instrumented Turbine Housing

The turbocharger turbine housing was a standard Garrett AiResearch type TO4B, A/R = 1.00, E-trim component.

Fig.4.8 shows a side view of the scroll with locations of the optical windows at the rotor inlet. Fig.4.9 shows a sectional view of the scroll.
Measurements were made primarily at the rotor inlet and outlet. Optical windows were mounted on the turbine scroll and the exit duct to allow the L2F beam access to the measuring locations.
At the rotor inlet, measurements were made at four azimuth angles, 20°, 90°, 180° and 270°. At each azimuth angle there are 3 optical accesses. One is in the axial direction which allows the L2F beam to pass directly into the measuring area. The other two optical windows allow the L2F beam to be directed from the top (at an angle) by deflection through a mirror.
Two mirrors were used in the measurement. Fig.4.10 shows the location of the mirrors and the measuring points. The front mirror was used to measure points 5,6 and 7mm, while the rear mirror picked up measurements at points 2,3 and 4mm. Measurements were made with reference to the inner wall along the axial direction, 2mm to 8mm at 1mm interval. The axial

distance between the walls at the volute exit is about 9mm; constant around the scroll. The axis of measurement is 3mm above the rotor tip and 5mm below the tip of the dividing wall. At the rotor exit, measurements were made across the exit duct diameter, 30mm downstream of the rotor. Fig.4.10 shows the exit duct fitted onto the turbine. The diameter of the duct is 60mm. Measurements were made along the diameter at 5mm intervals with reference to the top of the duct. The duct is designed in compliance to the SAE Recommended Practice J 1826 for the testing of turbocharger turbines. The length of the duct is approximately 2 times the duct diameter. Towards the end of the duct, a short section is slightly bent to divert the flow, thus avoiding the exhaust from directing onto the L2F optical head. The duct is designed so that its internal diameter is flush with the exit diameter at the turbine exit. Initially, it was decided that the most likely region for achieving good measurable flow downstream of the rotor exit was some distance away from the rotor exit so as to avoid any problems of blade wake or flow separation immediately after the rotor. Consequently the measuring axis was located 30mm from rotor blade. Measurement along this axis was successful and another turbine housing was instrumented to allow measurement closer to the exit blade. Fig.4.11 shows another instrumented turbine housing capable of allowing measurement as close as 3mm to the rotor exit plane.

The turbine used for the basic experiments was the standard Garrett component. In order to investigate the effect of housing geometry on turbine performance under partial admission and pulsating flow conditions, the housing was redesigned so that the diameter of the separating wall, or divider, between the two entries could be varied. For this purpose, the turbine housing is split into two halves, Fig.4.12. The separating wall plate was carefully machined to take the shape of each half of

the split housing. The thickness of the plate was chosen so that it matched the thickness of metal that had been removed from each half of the housing. Locking these 3 components together then produced the original turbine housing, except for the different separating wall diameters. More than one separating wall plate with different diameters have been fabricated to fit the split turbine housing. This method of modification to study the effect of divider depth was also applied by Lymbero poulos (18). However there the separating wall plate was machined flat with sharp corners especially at the tip of the divider, Fig.4.13, which do not reproduce the geometry of the original housing. For a more realistic modification, the edges of the separating wall were rounded. The contours of the divider depth were finished by hand-filing so that any section of it shows a tapering edge, (instead of a flat face) which is similar to the original design.
Fig.4.14 shows an exploded view of the split housing assembly The split housing and the separating wall plate is assembled with the aid of two locating pins. High temperature sealant is applied to ensure good seals around the split housing. The assembly is finally secured with 5 locking screws.

4.4 Measuring Concept

4.4.1 Measuring the same point within a flow from two directions.

Since the L2F velocimeter measures the magnitude and direction of the flow vector component in the plane perpendicular to the beam axis, it is considered to be a 2D-measuring system. When two 2D-velocimeters, separated from each other by an angle Φ as in Fig.4.15, are used to measurure at the same point within a flow, two 2D velocities can be obtained, from which all 3

components of the total velocity vector can be calculated. To get sufficient resolution the angle Φ between the two devices should not be much smaller than 30° [52]. However, if the third component is comparatively small, the angle Φ has to be larger than 30° in order to have a good indication of the result.
In planning the experiment, it was expected that the third component (the axial component) would be be much smaller than the radial and tangential components and may not exist under equal admission flow conditions. The angle Φ was carefully chosen to be 60°. Ideally this should be 90°, but it is not possible because of the existence of the divider wall. The L2F beam was deflected via a mirror focusing on the same point through another optical access (see Fig.4.9). The important point here is the focusing of the L2F measuring volume on the same point in the flow. This has created a formidable task in the designing and instrumenting of the volute and also a reference gauge to assist the setting up. Details of the measuring technique and the use of the reference gauge are given in Appendix A. When the same point in the flow has been measured, the results can also be used for cross-checking because of a total of four velocity components are measured. In practice the tangential component predominates and this should match.

4.4.2 Measurements made with L2F beam directed in axial direction

At the rotor inlet, measurements were made with the L2F beam directed (a) in the axial direction and (b) via a mirror.When measurements were made with the L2F beam directed in the axial direction, the radial and the tangential components of velocity can be derived. Fig.4.16 shows the velocity components as measured in the axial direction.

In Fig.4.16, the flow is assumed to consist of tangential, radial and axial components. When measurement is made with L2F beam directed in the axial direction, the absolute velocity V_1 is measured in a plane perpendicular to the L2F beam. In this case, the L2F is insensitive to the axial component. From V_1 and α_1 the tangential and radial components is derived as follows :

V_1	=	Absolute Flow Velocity	m/s
α_1	=	Absolute Flow Angle	deg
$V_1.\cos\ \alpha_1$	=	Tangential Velocity	m/s
$V_1.\sin\ \alpha_1$	=	Radial Velocity	m/s

4.4.3 Measurements made with L2F beam directed via the mirror

Measurements at the rotor inlet were also made via the mirror.Thus the radial, tangential and axial components of velocity can be derived. Fig.4.17 shows that the absolute flow velocity and angle were measured on a plane perpendicular to the beam axis. The velocity components are derived as follows :

V_{11}	=	Absolute Flow Velocity	m/s
α_{11}	=	Absolute Flow Angle	deg
$V_{11}.\cos\ \alpha_{11}$	=	Tangential Velocity	m/s
$V_{11}.\cos 30.\sin\ \alpha_{11}$	=	Axial Velocity	m/s

4.4.4 Flow Angle Orientation

The mean flow angle output by the L2F can be confusing when measuring at different azimuth angles and measuring through the mirrors. The position of the L2F unit is such that its angular

orientation as defined by the L2F velocimeter operating system is as follows:

Flow Direction	Mean Flow Angle
Vertically upwards	0°
Vertically downwards	180°
Horizontal towards LHS	90°
Horizontal towards RHS	270°

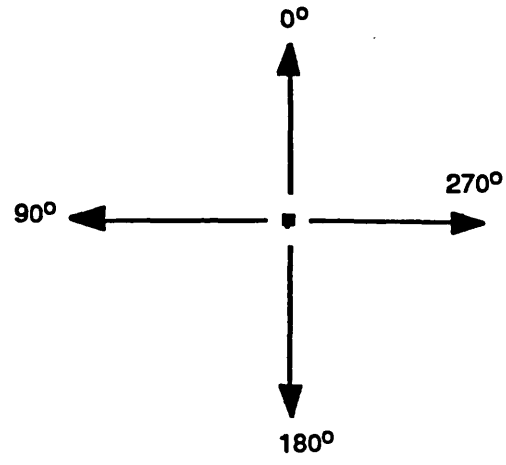


Fig.4.18 shows the orientation of the flow angle at different azimuthm angles. The absolute flow angle has to be deduced from the mean flow angle output from the L2F processor, with respect to the azimuth angle. For example, suppose the mean flow angle at 180° azimuth angle is measured to be 115°. Referring to Fig.4.18, the absolute flow angle is 115° - 90° = 25°.

Similarly for the remaining azimuth angles, the mean flow angle has to be subtracted accordingly to obtain the absolute flow angle. For easy understanding all the flow angles displayed in the graphs and tables are absolute values with respect to the local tangential direction.

Figs.4.19(a-d) present 3D views of the general flow directions at different azimuth angles. The figures indicate only tangential and radial components. Axial components will be indicated as inclinations towards the inner limb or the outer limb (deviation from the radial plane).

When measuring via the mirror, the tangential component is still predominant. Any axial component will be indicated as a shift towards the inner limb or outer limb. Fig.4.20 shows the

L2F beam deflected via the front and rear mirrors at 180° azimuth angle. The L2F focal volume is rotating on a plane inclined at 30° to the axis. The figure indicates that when the mean flow angle measured is 90°, the axial component of velocity is zero. The following mean flow angle at a 180° azimuth angle section will have an axial component given by :

Example :

Mean Flow Angle		
80°	indicates	axial aomponent towards outer limb
90°	indicates	zero axial component
110°	indicates	axial component towards inner limb

At different azimuth angles, the direction is indicated by other sets of mean flow angles. Fig.4.21 shows diagrammatically how the mean flow angle is worked out to indicate the direction at different azimuth angles. The problem is complicated by the fact that flow angle is flipped by 180° when viewed through the mirror.

The above will only indicated the direction to which the axial component will take. Its mean flow angle will have to be further reduced to obtain its magnitude.
Referring to Fig.4.17,

V_{11} = Absolute Flow Velocity on a 30° plane
α_{11} = Absolute Flow Angle on a 30° plane

$$V_{axial} = V_{11}.\sin \alpha_{11}.\cos 30$$

$$\alpha_3 = \tan^{-1}\left[\frac{V_{11}.\sin \alpha_{11}.\cos.30}{V_{11}.\cos \alpha_{11}}\right]$$

$$\alpha_3 = \tan^{-1} (\tan \alpha_{11} . \cos.30)$$

For simplicity, the flow angles presented are the absolute flow angles, α_{11} and α_3, as in the graphs and tables.

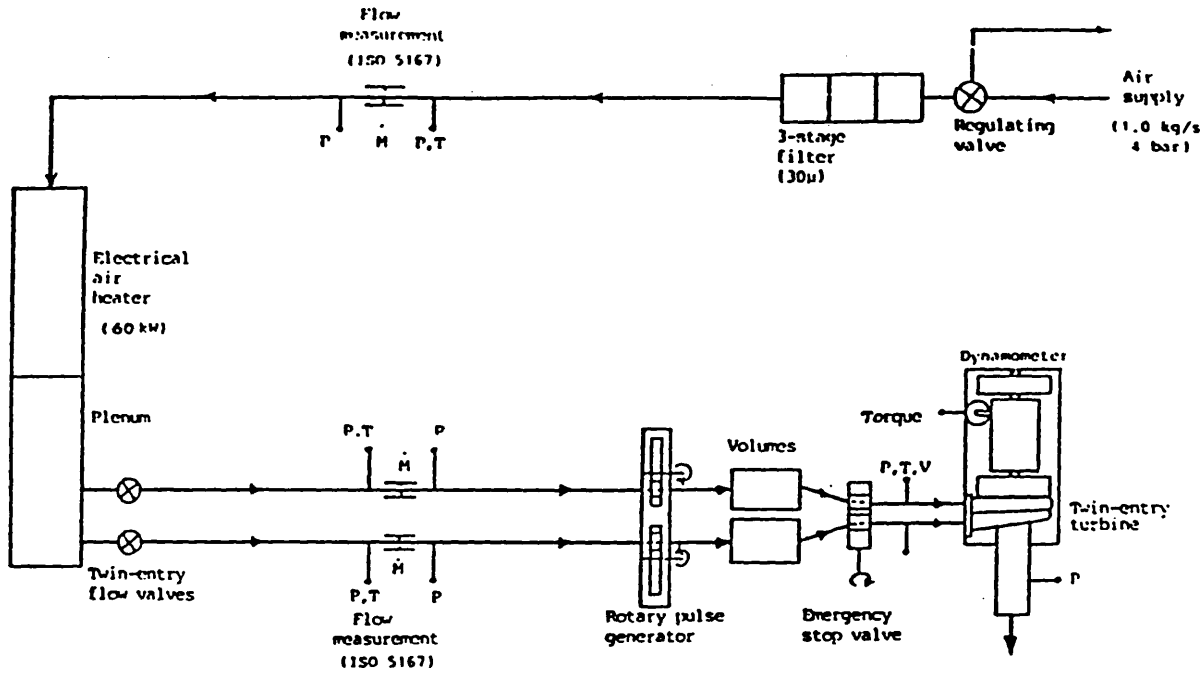


Fig 4.1 Schematic layout of test rig facility

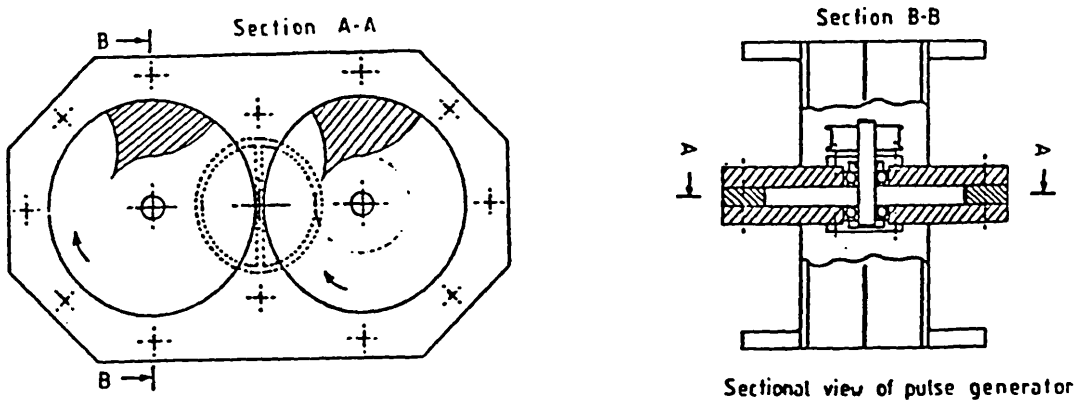


Fig. 4.2 Pulse generator

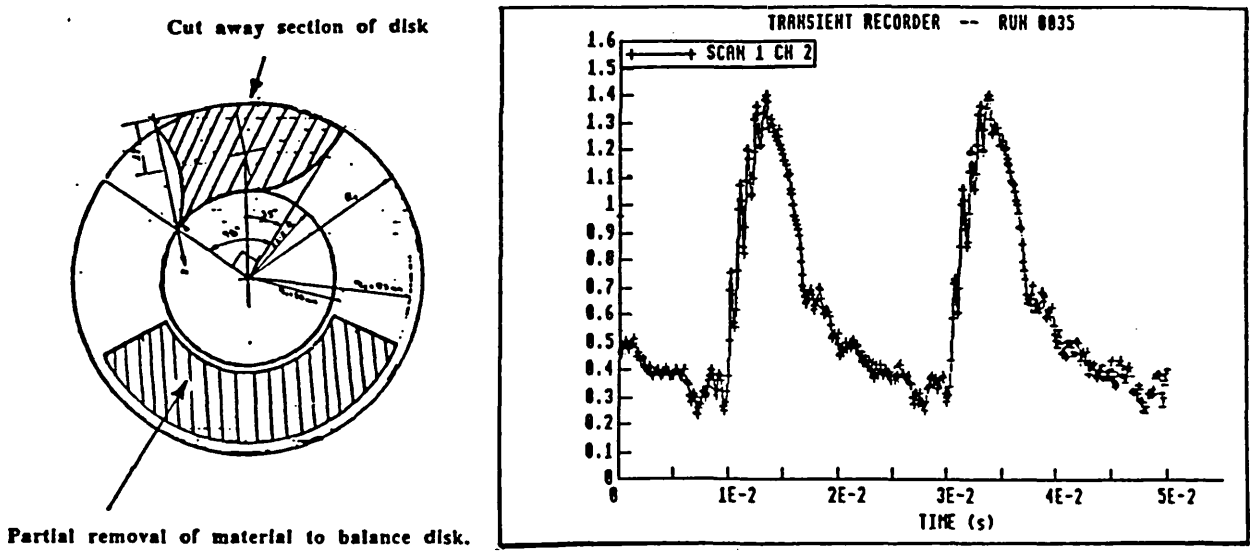


Fig. 4.3 Typical pressure pulse shape

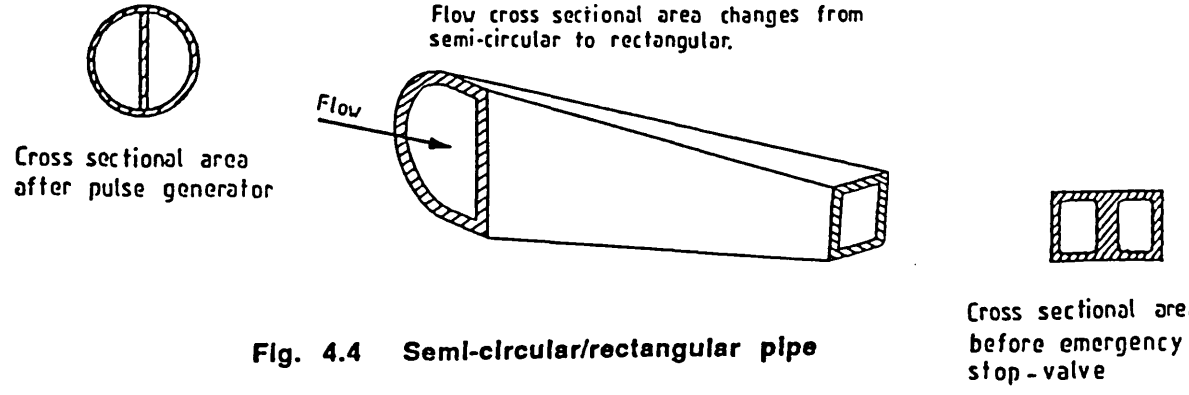


Fig. 4.4 Semi-circular/rectangular pipe

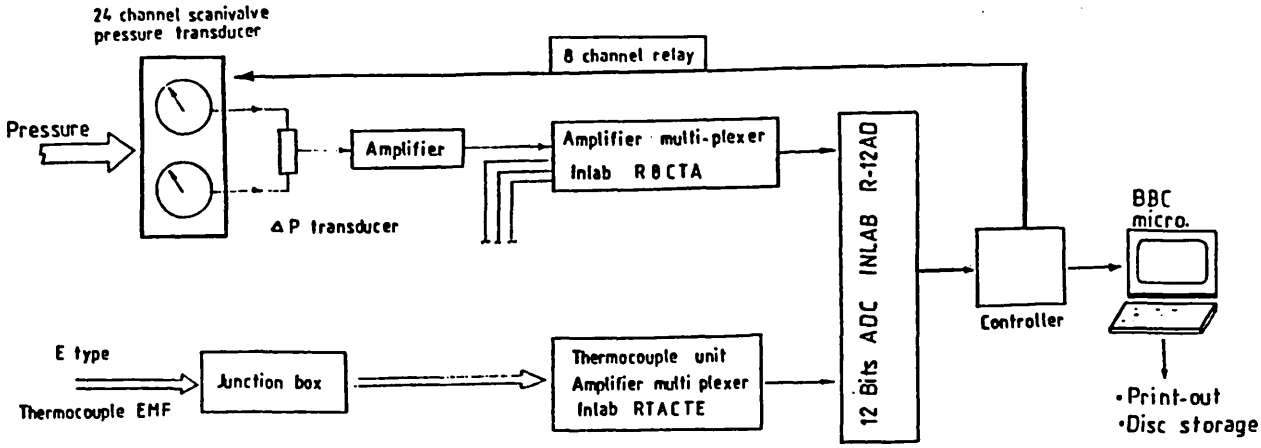


Fig. 4.5 Steady state data logging system

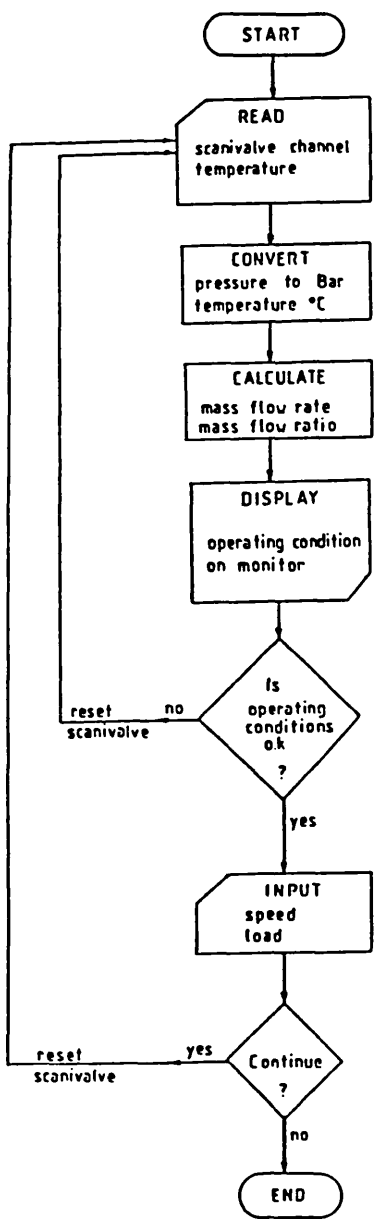


Fig. 4.6 Flow chart of data logging program

```
 SPEED  =  34000.00
 A/R    =      1.00
 TEST   = EQUAL ADMISSION
 DATE   = 5 APRIL 89


TEST NO = _____

TEMPERATURE    ( DEG - C )                  GAUGE PRESSURE ( N/M2  )
==========                                  ==========
INLET TEMPERATURE          = 20.9       4 INS PIPE   STATIC   = 23845.8
36 KW  OUTLET              = 82.9       4 INS PRESS DIFF      = 2272.6
3 INS PIPE ORIFIC (INNER)  = 79.8       3 INS STATIC P (INNER)= 21437.4
3 INS PIPE ORIFIC (OUTER)  = 80.9       3 INS STATIC P (OUTER)= 21267.8
3 INS TURBINE INLET  (IN)  = 75.2       3 INS P.DIFF. (INNER) = 1390.7
3 INS TURBINE INLET  (OUT) = 76.6       3 INS P.DIFF. (OUTER) = 1322.9
DYNA WATER TEMPERATURE     = 25.1        3 INS TOTAL P.(OUTER) = 20725.1
                                         3 INS TOTAL P.(INNER) = 20623.4

SPEED   ( RPM )          = 34000.0
AMBP    ( mm-Hg )        = 750.0000
AMBP    ( BAR )          = 0.9998

=================================================================

MASS FLOW RATIO ( O/I )= 0.9734
MASS FLOW RATIO ( I/O )= 1.0273
                                        MASS FLOW
TOTAL MASS FLOW  KG/S  = 0.1491         ERROR  %.= 0.0424
INNER LIMB FLOW  KG/S  = 0.0755
OUTER LIMB FLOW  KG/S  = 0.0735

UC BASE ON TMA         = 0.6972     EFFICIENCY (T-S)    = 0.6698
UC BASE ON OUTER       = 0.6965
UC BASE ON INNER       = 0.6980
PRESS RATIO (MASS AVG) = 1.2068     N.D.F  TOTAL  = 2.3073
PRESS RATIO  OUTER     = 1.2073     N.D.F  OUTER  = 1.1376
PRESS RATIO  INNER     = 1.2063     N.D.F  INNER  = 1.1697

ISENTROPIC POWER  (KW) = 2.7332     DENSITY outer = 1.1849
ACTUAL     POWER  (KW) = 1.8309     DENSITY inner = 1.1879

NON DIM SPEED          = 1819.9
TEMP MASS AVG  ( K )   = 349.0
CP - VALUE ( J/KG.K )  = 1023.0

TORQUE ( mV )          = 182.0
TORQUE ( NM )          = 0.5141

GAMMA                  = 1.3899
mV-NM CONVERSION       = 0.002825
```

Fig. 4.7 A typical steady state test printout

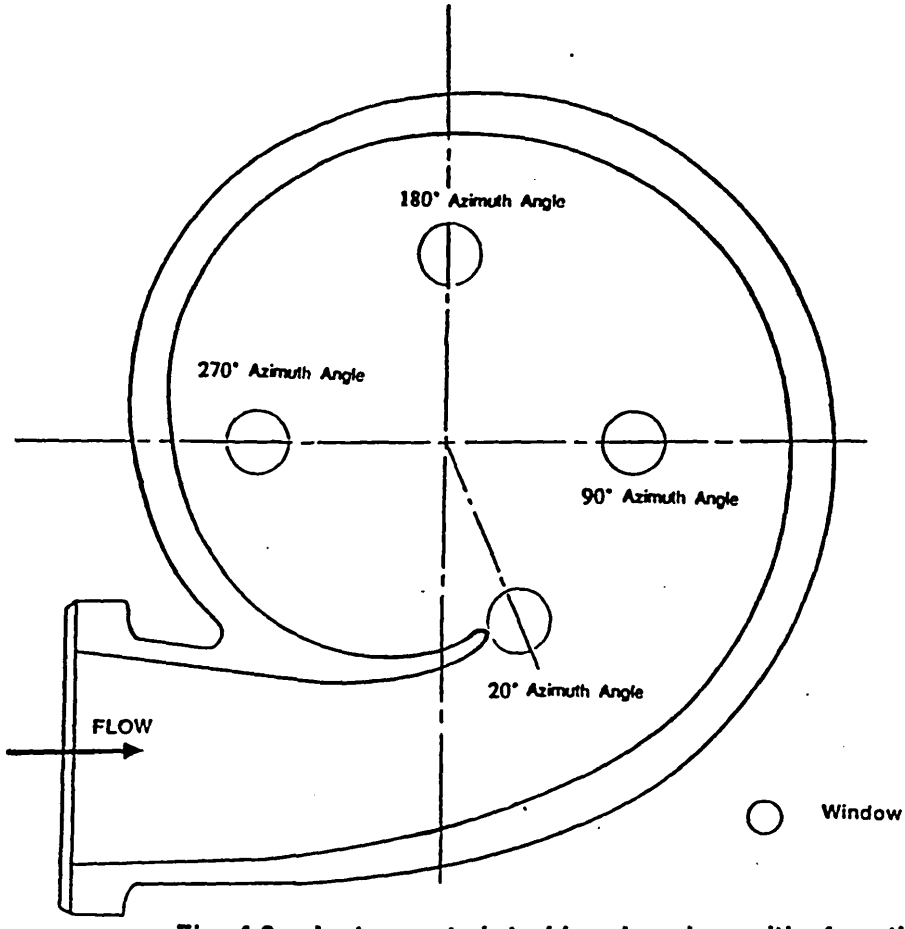


Fig 4.8 Instrumented turbine housing with 4 optical windows at different azimuth angles

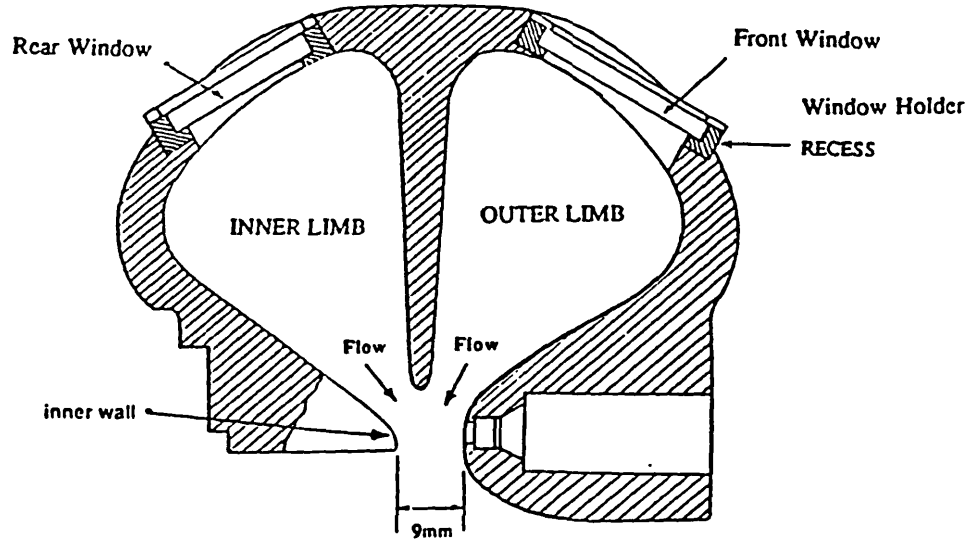


Fig 4.9 Sectional view showing different optical windows at one azimuth angle

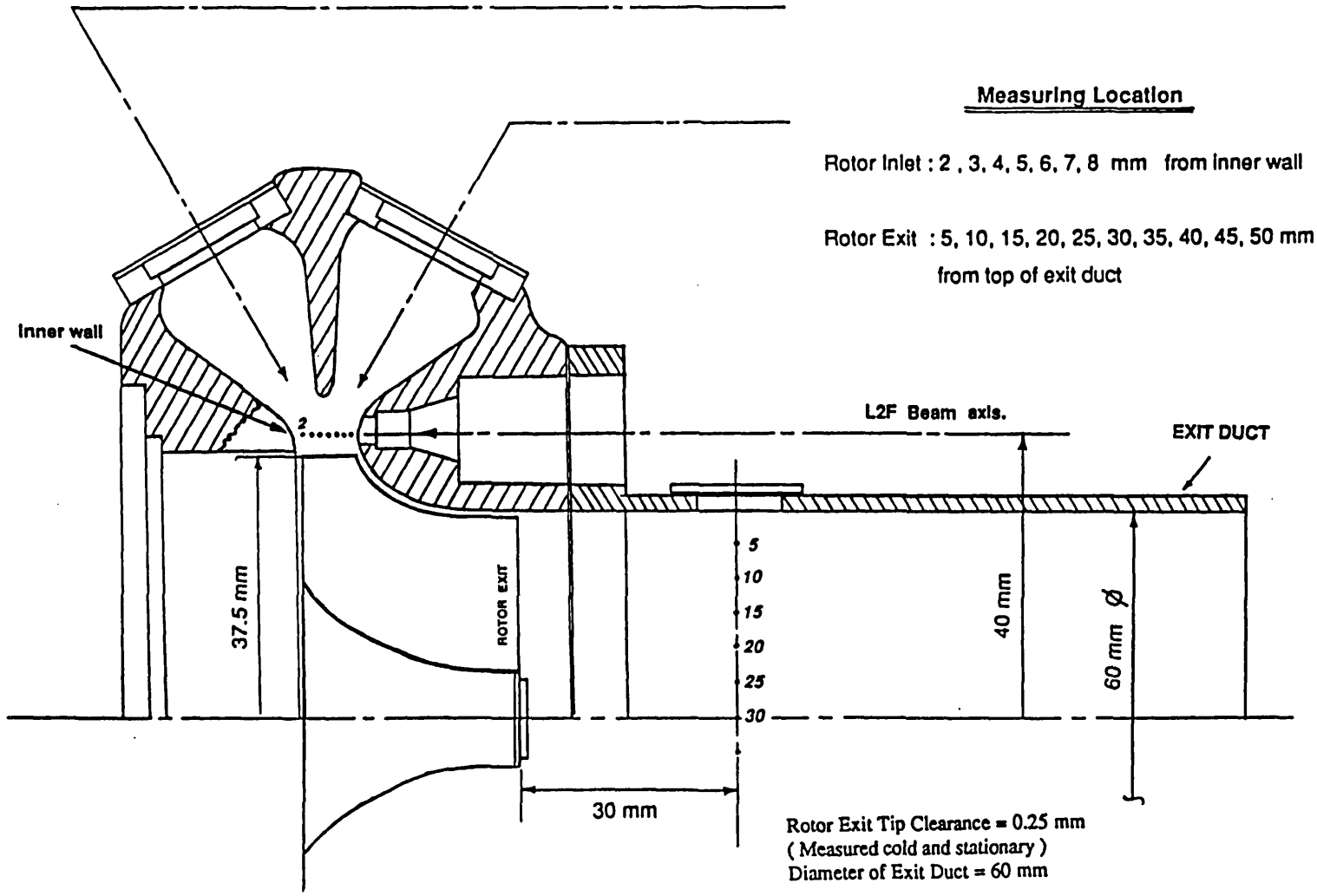


Fig. 4.10 Measuring points at rotor inlet and exit

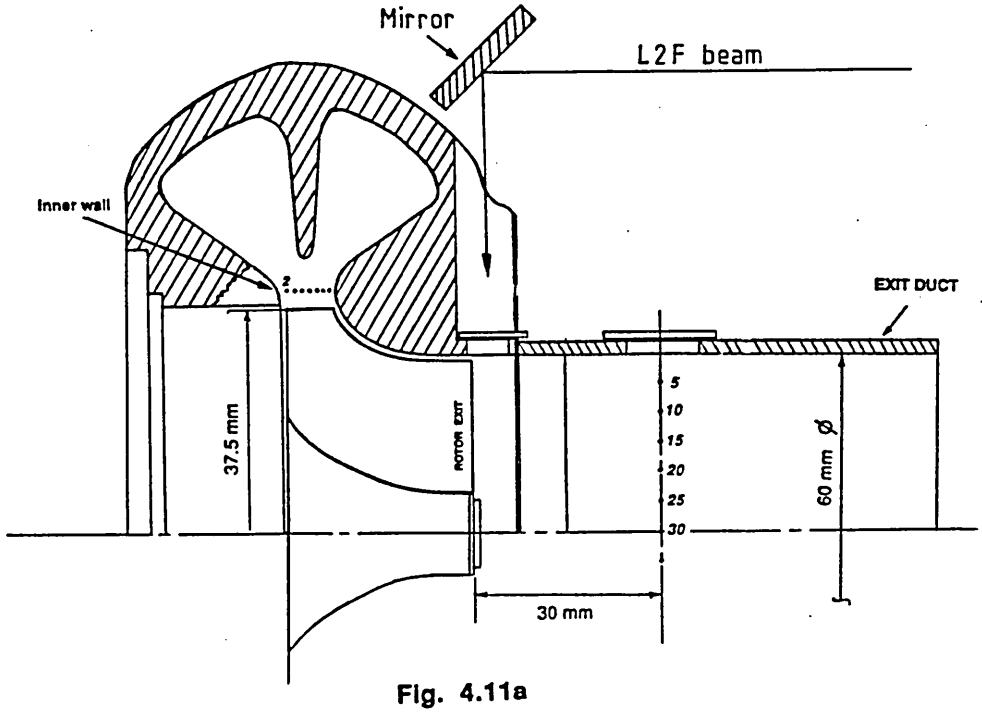


Fig. 4.11a

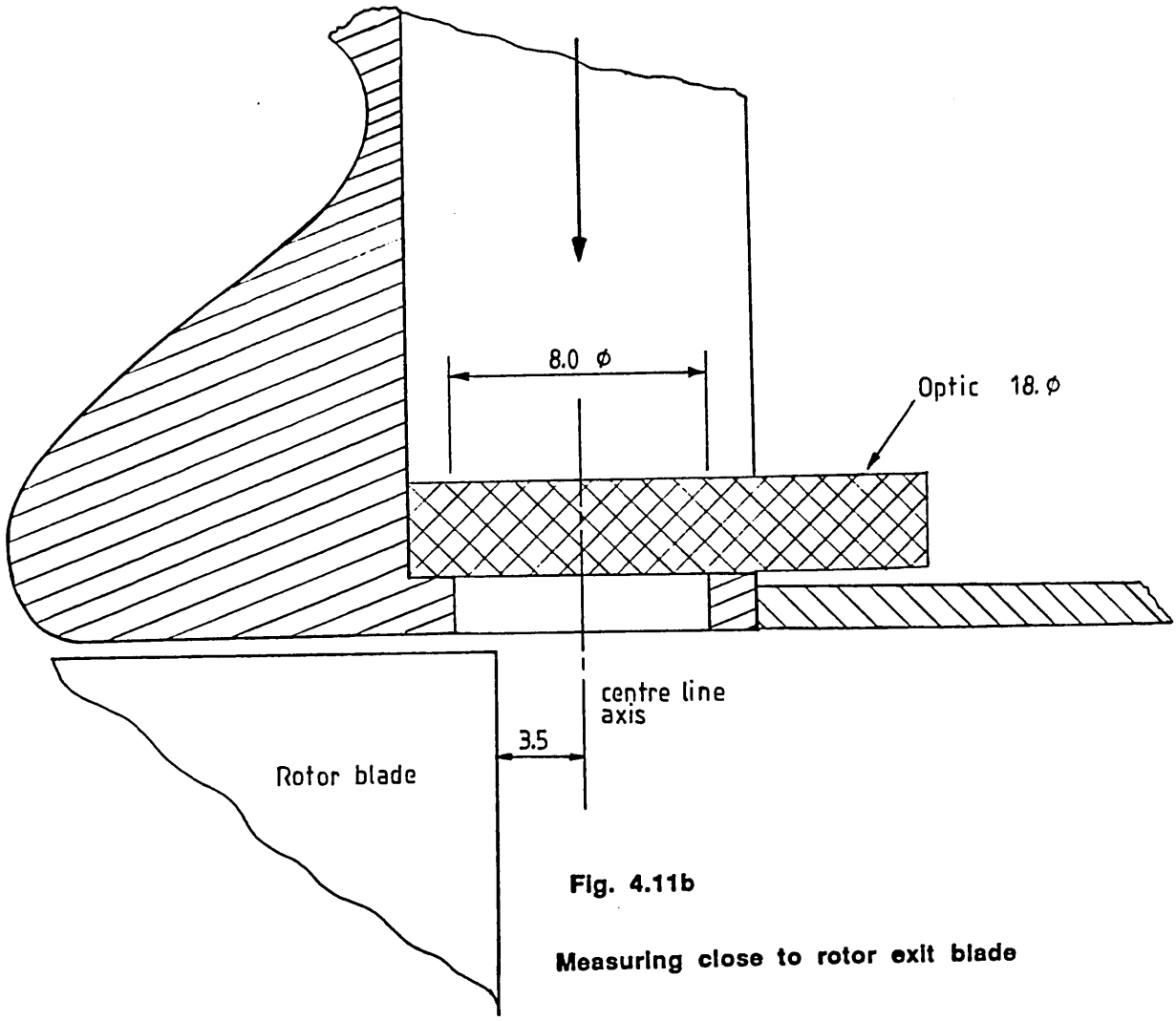


Fig. 4.11b

Measuring close to rotor exit blade

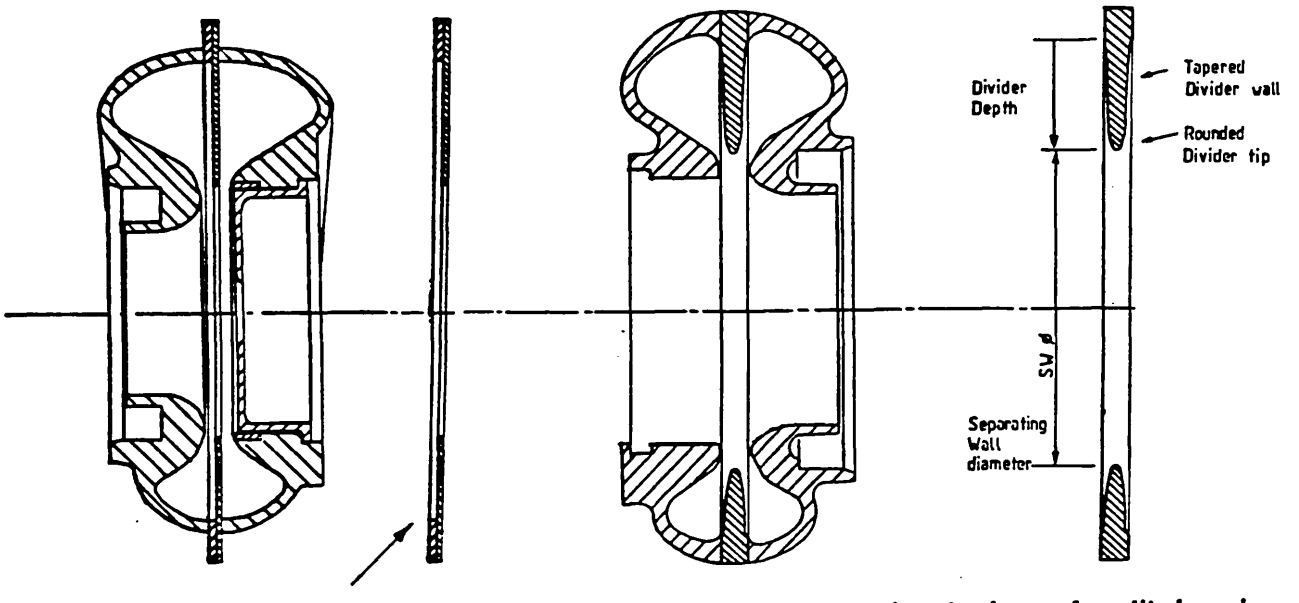
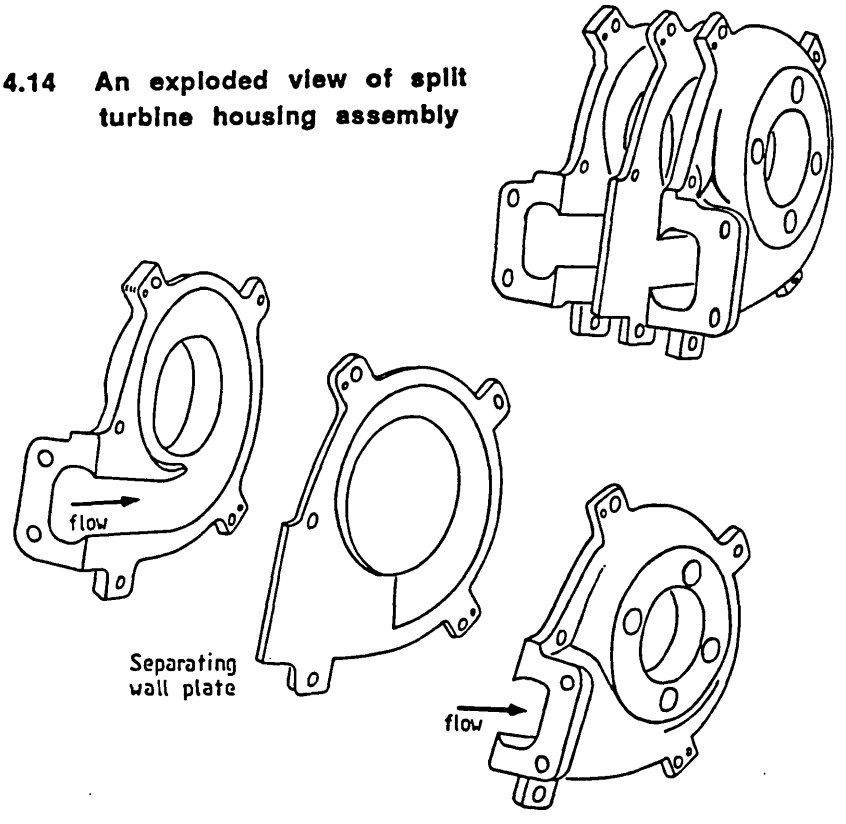


Fig. 4.12 Sectional view of split housing

Fig. 4.13 Split housing with flat separating wall plate

Fig. 4.14 An exploded view of split turbine housing assembly



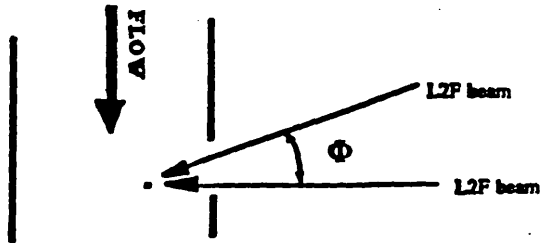
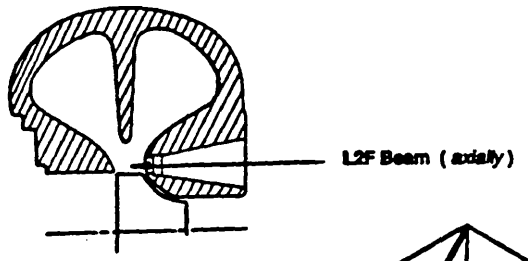


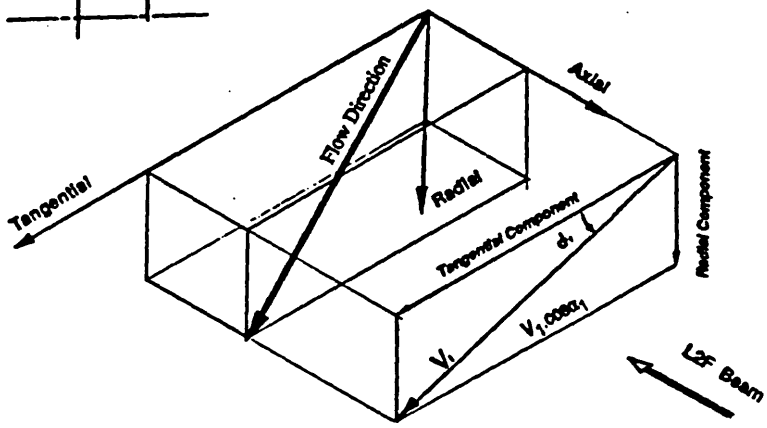
Fig. 4.15

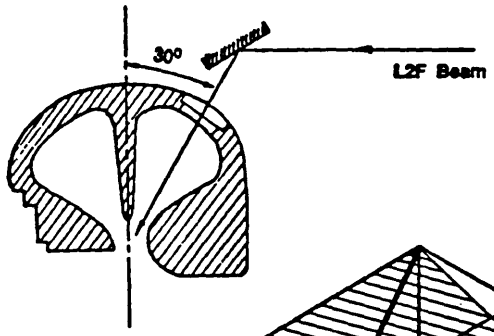
Measuring the same point within the flow.



Measured velocity component with L2F beam directed in axial direction

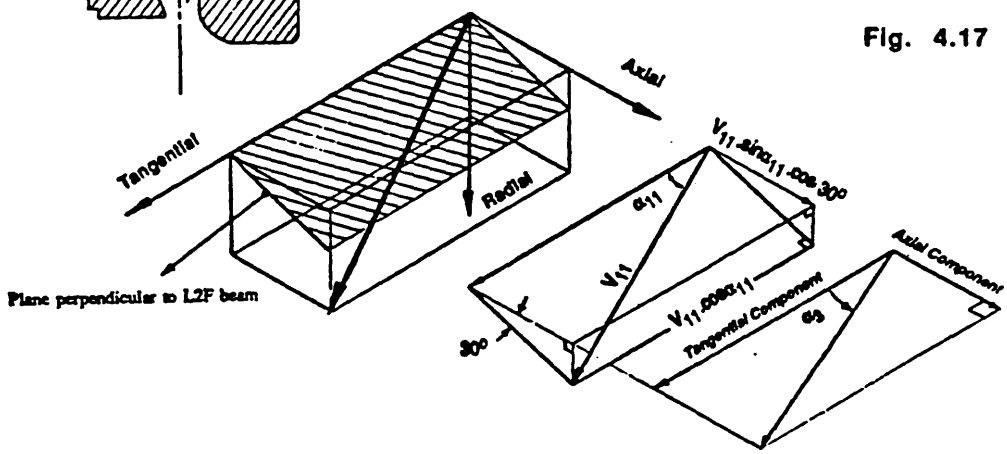
Fig. 4.16

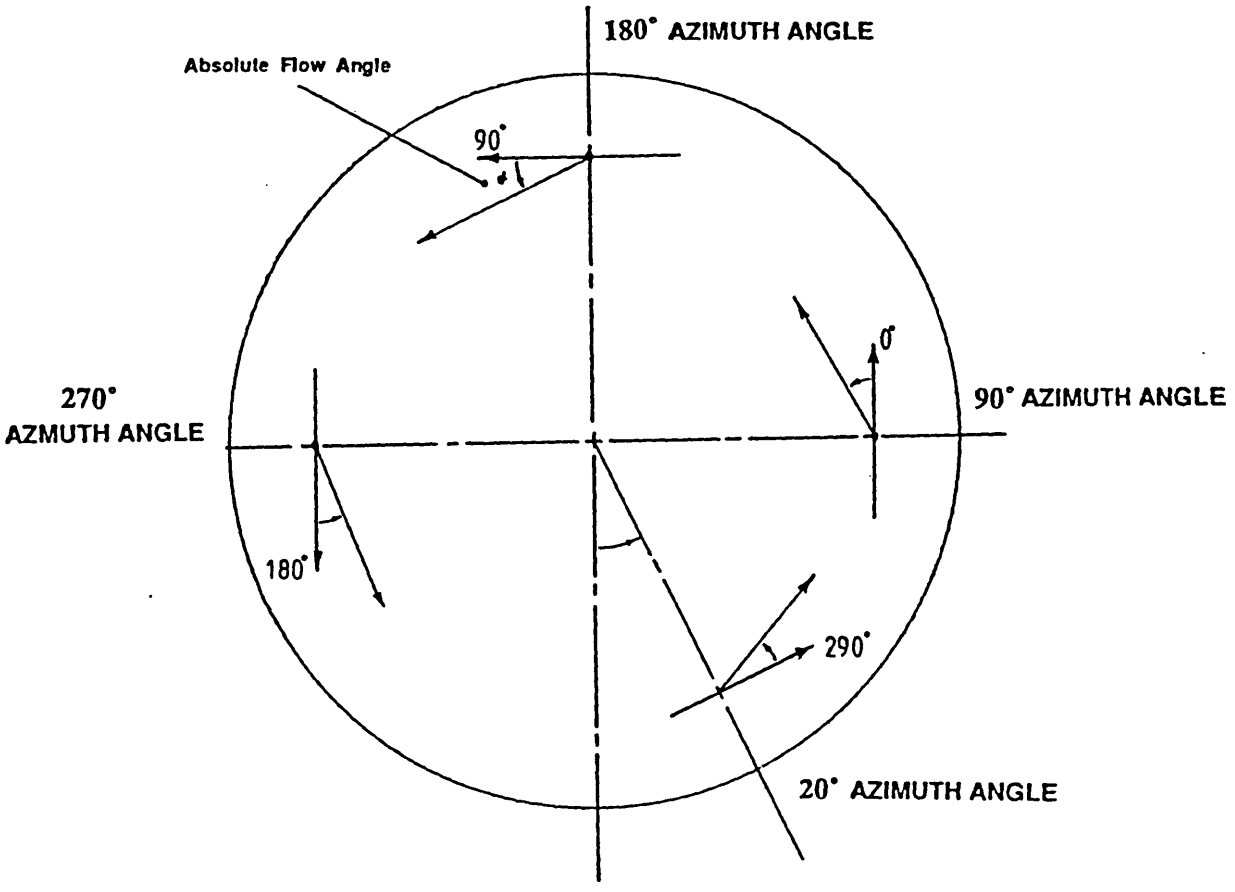




Measured velocity component with L2F beam directed via the mirror

Fig. 4.17





At different azimuth angles, the mean flow angle produced by the L2F processor changes with respect to its orientation. The mean flow angle has to be subtracted accordingly to provide the correct absolute flow angle.

Fig.4.18 Orientation of L2F velocimeter flow angle

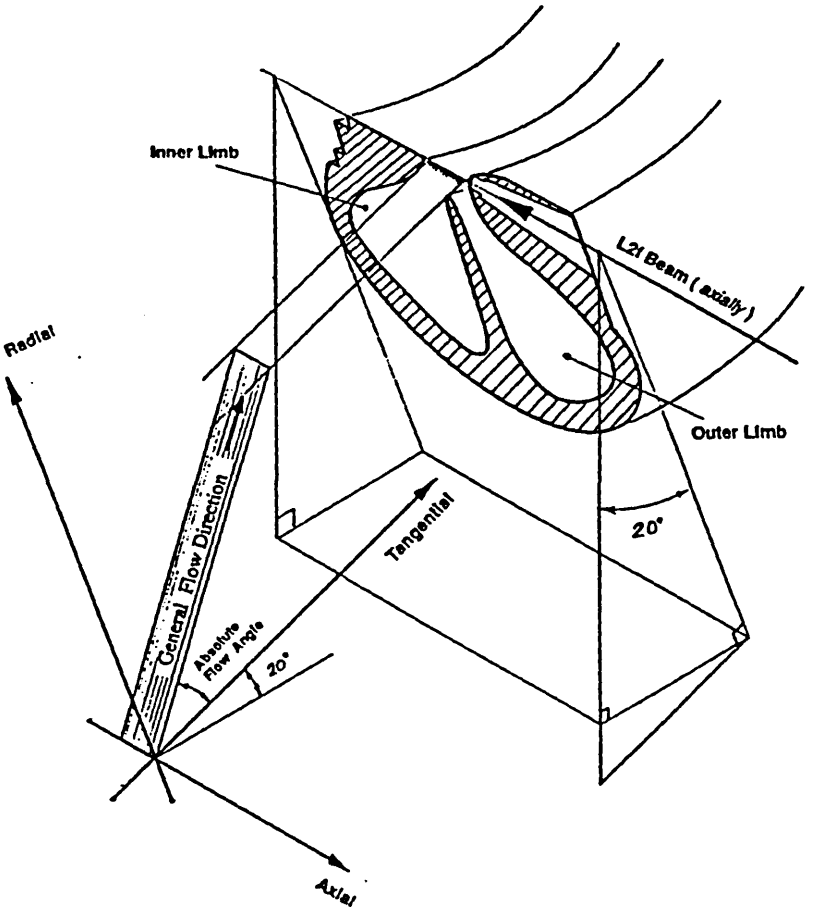


Fig. 4.19a

20° AZIMUTH ANGLE

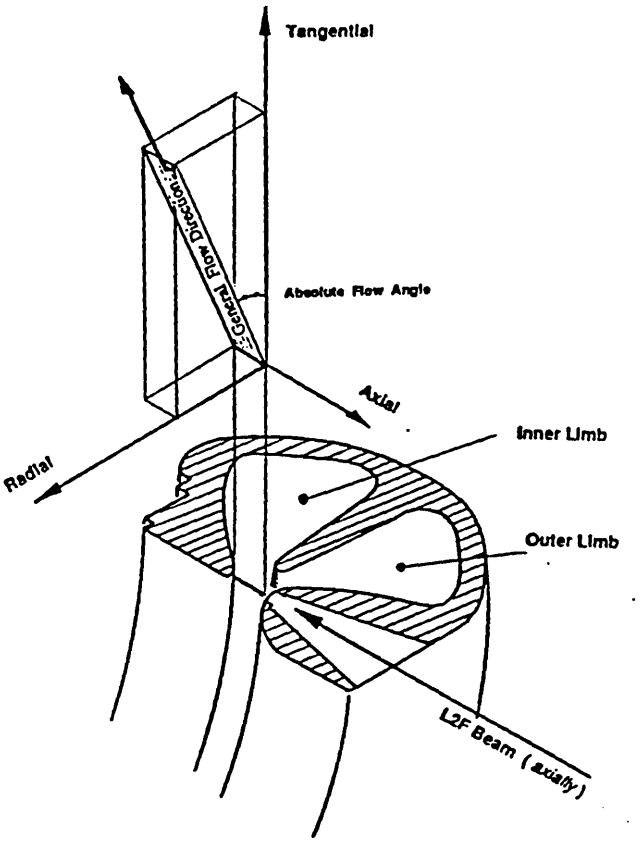


Fig. 4.19b

90° AZIMUTH ANGLE

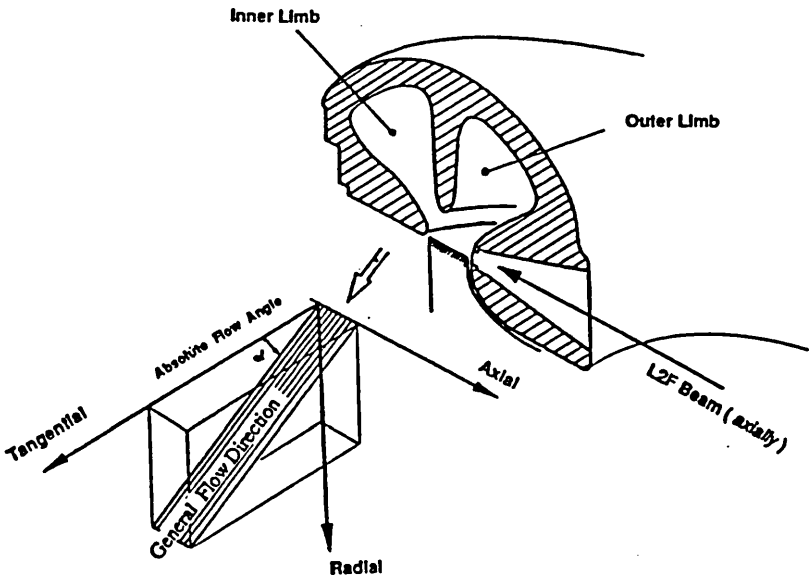


Fig. 4.19c

180° AZIMUTH ANGLE

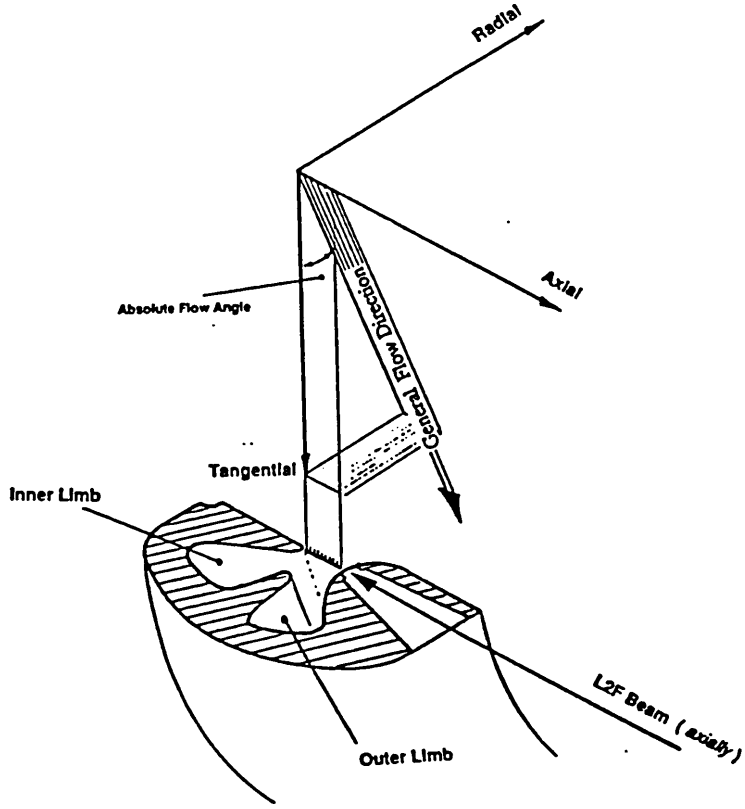


Fig. 4.19d

270° AZMUTH ANGLE

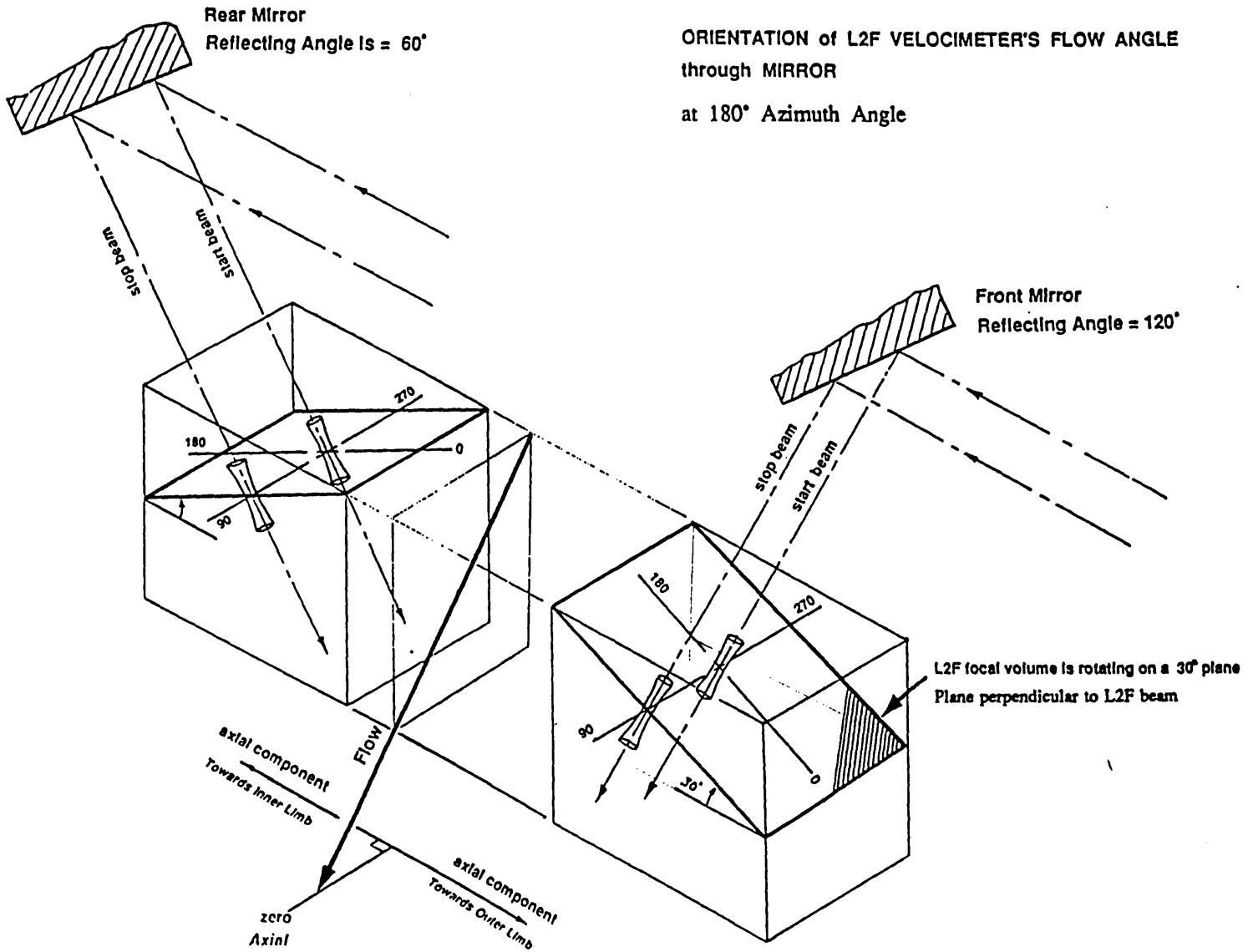
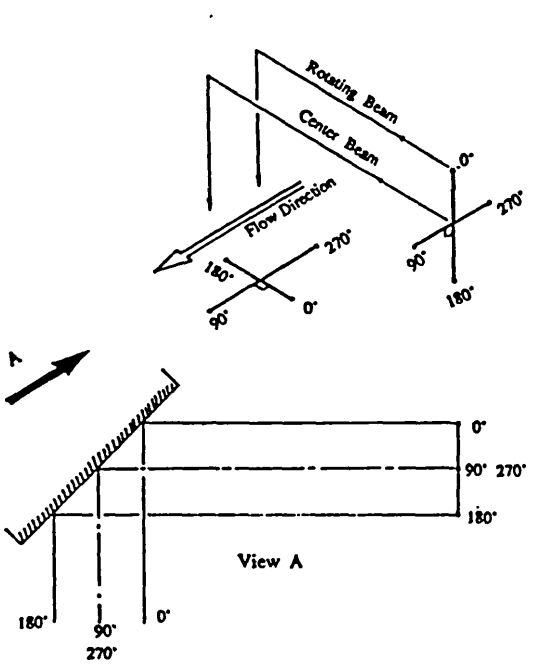
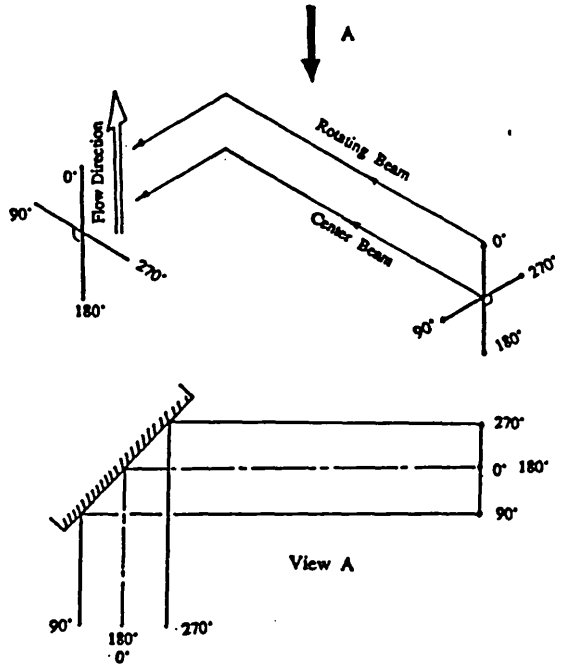

Rear Mirror
Reflecting Angle is = 60°
ORIENTATION of L2F VELOCIMETER'S FLOW ANGLE
through MIRROR
at 180° Azimuth Angle
stop beam
start beam
Front Mirror
Reflecting Angle = 120°
270
180
0
90
stop beam
start beam
180
270
L2F focal volume is rotating on a 30° plane
Plane perpendicular to L2F beam
90
30°
0
Flow
axial component
Towards Inner Limb
axial component
Towards Outer Limb
zero
Axial

Fig. 4.20



Greater than 90° ------ towards inner limb
Less than 90° ------ towards outer limb

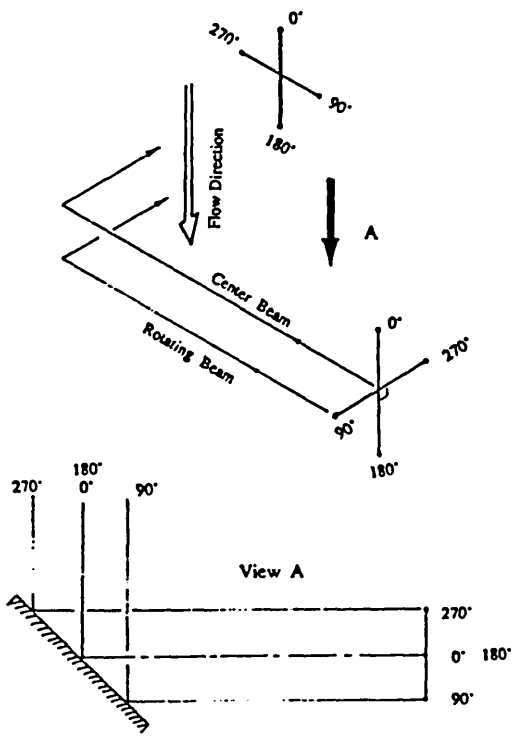
180° AZIMUTH ANGLE



Greater than 0°,360° (eg. 20°) ------ towards inner limb
Less than 0°,360° (eg. 350) ------ towards outer limb

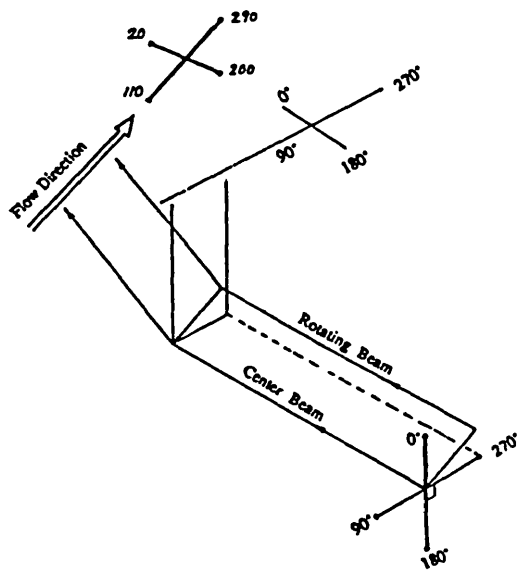
90° AZIMUTH ANGLE

270° AZIMUTH ANGLE



Greater than 180° ----- towards inner limb
Less than 180° ------ towards outer limb

20° AZIMUTH ANGLE



Greater than 290° ------ towards inner limb
Less than 290° ------ towards outer limb

Fig. 4.21

Chapter 5

Steady Flow Test Results and Discussion

5.1 Introduction

In pulse turbocharging when the exhaust gas is delivered to the turbine by two separate manifolds, the turbine operates under time-varying partial admission conditions. This partial admission varies from zero flow in one limb with full admission in the other, through to equal flow in both limbs. Therefore a knowledge of the real flow characteristics under these various conditions is a basic requirement to a better understanding of the pulse flow behaviour in the turbine.

This chapter contains the turbine performance gas flow characteristics under steady flow for equal and partial admission flow conditions. Separating wall plates of different diameters (see Fig.4.12) were also introduced in to the turbine housing to study the effects of the meridional divider depth. The steady flow tests were carried out in two phases.

In phase one, three different flow conditions were applied to study the effect on the gas flow characteristics. The through-flow velocity and axial velocity components just upstream of the rotor inlet were measured. With the laser beam in the axial direction (described in Chapter 4), velocities in the radial-tangential plane, i.e the through-flow velocity components were measured. The axial velocity component is obtained from measurements in the axial-tangential plane (measured via the mirror).

In phase two, a single flow condition (at the design point) is applied to a turbine housing with different divider depths in order to study the influence of the meridional divider depth on the gas flow at the rotor inlet for a series of partial

admission flow conditions. Only the through-flow velocity components were measured.

5.1.1 Phase One

The objective of the phase one work is to investigate the gas flow characteristics at the rotor inlet and exit for three different flow conditions.

In the investigation three different flow conditions were applied to study the flow field at different mass flow conditions. The rotor speed was maintained at 34000 rpm. The load applied at the eddy current dynamometer was varied to keep the speed constant when the total mass flow in the system is changed. Total pressure, temperature, speed, mass flows and load applied at the dynamometer were monitored, and from these the following parameters were deduced : turbine efficiency, pressure ratio, u/c ratio, and $(m\sqrt{T})/p$. The table below shows these parameters at varying mass flow conditions.

TABLE 5.1

	Total Mass Flow to Turbine		
	0.13 Kg/s	0.17 Kg/s	0.24 Kg/s
u/c ratio	0.67	0.57	0.44
Efficiency t-s	67 %	62 %	53 %
Pressure Ratio	1.2	1.27	1.52
$\frac{m\sqrt{T}}{p}$ $\left[\frac{(K)^{0.5}}{m.s^2}\right]$	2.17	2.6	3.27

The lowest mass flow condition is very close to the design point of the turbine, the other two correspond to underspeed (low u/c) conditions. Mechanical limitations of the dynamometer meant that it was not possible to run for extended periods at

higher speeds, so that it was not possible to make measurements at overspeed conditions. At the rotor inlet, flow measurements were made at four different azimuth angles, 20°, 90°, 180° and 270° measuring from the tip of the tongue, under both full and partial admission conditions.
The flow characteristics at the rotor exit were also measured along an axis 30mm downstream of the rotor trailing edge, again under full and partial admission conditions. The results in phase one work are presented in the following sections:

5.2 Rotor inlet, equal admission flow, 3 flow conditions, azimuth angle = 20°, 90°, 180° and 270°.

5.3 Rotor inlet, equal and partial admission flow conditions.

5.4 Rotor exit, equal and partial admission flow conditions

5.1.2 Phase Two

The objective of the phase two work is to investigate the gas flow characteristics by applying different meridional divider depths, with emphasis on more detailed partial admission flows. Unlike the phase one work, a series of partial admission flow tests were carried out. Partial admission was achieved by varying the mass flow in each limb whilst keeping the total mass flow supply to the turbine constant. A total of nine different mass flow ratios were applied to study their effect on the gas flow in the rotor inlet region. The variation of mass flow ratio starts with the outer limb fully closed. This is opened gradually through equal admission to closing the inner limb fully.
For each partial admission condition, the turbine performance was monitored so that correlations could be made between the gas flow characteristics and the turbine performance. This investigation was extended to different separating wall plate diameters to study the effect of different meridional divider

depths on the flow characteristics and turbine performance. Due to a large amount of experimental work, no axial velocity components were measured during this phase.
Flow measurements were also made at the rotor exit. Measurements were made 4mm downstream of the rotor trailing edge for comparison with measurements made 30mm downstream in phase one.
The results of the phase two work are presented in the following sections:

5.5 Rotor inlet, equal admission flow, different divider depth

5.6 Rotor inlet, series of partial admission flow, different divider depth.

5.7 Rotor exit, 4mm and 30mm from rotor trailing edge

In the discussion to follow, the inner limb region refers to measuring point 2,3 and 4mm, whilst outer limb region refers 5,6,7 and 8mm, see Figs.4.9 and 4.10. These measuring points are approximately below the inner and outer limb through-flow area respectively.
The terms separating wall diameter and divider depth basically refer to the same component, Fig.4.13. As the separating wall diameter gets larger, the divider depth becomes small, thus the interspace is increased. Both terms had been used in the past and will also be applied in the discussion.
In the following discussion, it is evident that there were difficulties in measuring the flow at certain points under different flow conditions. This occurs in regions where the flow is highly mixed or disturbed, and the L2F velocimeter did will not yield results due to insufficient quality data to produce a distribution. In a situation like this, there are also other possiblities that can cause insufficient quality data such as poor seeding, dirty optics and incorrect setting of the L2F units. These were always checked first and a

measurement at previous point was repeated to confirm that the seeding, optics and L2F units setting were correct. Thus subsequent measurements at points that do not yield results indicate a problem associated with the flow rather than with the instrumentation in that region.

5.2 Rotor Inlet,Equal Admission Flow,3 Flow Conditions, Azimuth Angle = 20°,90°,180°, and 270°.

5.2.1 Through-flow velocity

The flow characteristics for three different flow conditions at equal admission are presented in this section. Results derived from the velocity triangles are also presented.
Measurements were made at four azimuth angles for the above 3 flow conditions. Figs.5.1,5.2,5.3 and 5.4 show the variation of the absolute flow velocity and flow angle for azimuth angles 20°,90°,180° and 270° respectively. In each figure,the variation of tangential and radial velocity, relative velocity and incidence angle (blade angle - relative flow angle) across the volute exit are also presented.
The absolute velocity and flow angle profiles are consistent for the three flow condition measured at each of the 4 azimuth angles. Higher mass flow yields higher velocity and this is evident from the plots. Both radial and tangential components are similarly affected; radial component directly via increased mass flow, and tangential via increased tangential momentum. Hence the flow angle is hardly affected. Figs.5.2,5.3,5.4 show also the effect of the divider at 4mm and 5mm measuring point, where the absolute velocity decreases by about 12%. This effect is also manifested in the flow angle profile, where the absolute flow angle increases near the tip of the divider. This causes the flow to turn radially inwards, thus reducing the

tangential component of velcity. The radial component is also reduced somewhat, indicating, a low-momentum wake flow downstream of the divider. From equ. 2 (chapter 1) this also represents a drop in specific work at that region. Flow investigation by Miller (17) and Lymberopoulos (18) in a twin entry turbine also show similar effects of the divider.

A peculiarity of the flow is noted at 20° azimuth angle, where the effect of the divider is not apparent and there is a marked change in absolute flow angle across the passage. This is presumably because the measuring point is close enough to the tongue region to experience this disturbance. Higher pressure ratios produce similar patterns for the flow angle plots. The velocity profile appears to shift so that the wake effect of the divider is apparent around the 3mm measuring point. Its magnitude increases with pressure ratio. It is not obvious why the flow decreases from about 40° at the inner wall to 15° at point 8mm.

Figs.5.5,5.6, and 5.7 show how the flow changes as it travels around the scroll at the three different conditions. The variations in the measured data with azimuth angle (with the exception of 20°) do not appear to be as great as the variations with flow conditions, especially at higher pressure ratio which is further away from design point. In all cases, the highest absolute flow angle is consistently measured at 180° azimuth angle followed by 90° azimuth angle. The velocity is lowest at the 20° azimuth angle, where the effects of the tongue are felt. It is also noteworthy that the turbulence intensity levels measured at 20° section are consistently high which is attributed to the mixing of two streams of unequal flow, see Fig.5.7b.
Earlier investigations by Bhinder (8) and Scrimshaw (10) also indicated the large variation in flow angle at the tongue

region (340° to 30° azimuth angle). This is also noted by Miller (17) who made detailed flow studies in single and twin-entry turbines.

In a rotor high incidence angle between the gas and the rotor blade may cause the flow to separate from the blades and there will be a subsequent mixing loss within the rotor. The incidence angle derived from the measured velocity and the blade speed changes significantly with the flow conditions. At near design condition (u/c = 0.67), the incidence angle varies from 20° to 45° across the volute exit, Fig.5.5. The higher incidence angle occurs at the divider tip where the flow angle is comparatively high.
As the operating condition departs from the design point, the incidence angle becomes more negative (negative incidence is here defined in the direction of rotation, Fig.1.7). The following table shows typical values of incidence angle with flow conditions (except at 20° azimuth angle)

Flow condition	Incidence Angle	Averaged across volute exit at 180° azimuth angle
u/c = 0.67	20° to 45°	30° (20.3° to 38°)
u/c = 0.57	30° to -10°	16.5° (6.3° to 29°)
u/c = 0.44	10° to -40°	-11.3° (-1.5° to 24°)

5.2.2 Axial velocity component

The presence of axial component of velocity is investigated by directing the L2F beam via a mirror to measure the same point in the flow , see Fig. 4.17. The axial component of velocity is generally low. Fig.5.8a gives an indication of the flow direction of the axial component, and Fig.5.8b summarizes the

the angular deviation, α_3 from the radial plane. The flow direction is indicated by an arrow either towards the inner wall or away from it. In terms of angular deviation from the radial plane, this value, α_3 is between 2° to 8°. The axial component of velocity in the direction indicates clearly the divider effect, with the following results :

At 2,3,4mm measuring point, the axial component is directed towards the inner limb.
At 5,6,7 mm measuring point , the axial component is directed towards the outer limb.

However at 20° azimuth angle, the axial component points in the direction of the inner limb, suggesting that the pressure in the outer limb is somewhat higher, causing the flow to incline towards the inner limb, see Fig.5.8c. This is consistent with higher radial component of velocity in inner limb, Fig.5.1.

The only other axial velocity component measurements in a twin-entry turbine known to be available have been published by Miller (17). Theses results also showed deviation of flow from the radial plane, Fig.5.9. From the velocity diagram, -ve δ_2 refers to flow towards the bearing side (inner wall). The result shows that the flow is almost radial (δ_2 close to zero deviation) for the shroud side. Towards the bearing side, the flow is biassed towards the shroud region (+ve δ_2) by about 8° from radial plane. At 30° azimuth angle, Miller (17) showed that the flow is biassed towards the bearing side (inner limb) as δ_2 is -ve throughout. This observation is consistent with present investigation at 20° azimuth angle, thus supporting the deduction that around the tongue region the pressure from the outer limb (shroud side) is somewhat greater, causing the flow to move towards the inner limb (bearing side).

5.2.3 Conclusion from equal admission flow characteristics

The deduction so far from the above investigation shows the wake effect under the divider tip. Flow investigations in a twin-entry turbine by Miller (17) and Lymberopoulos (18) also showed similar effects of the divider. The incidence angle varied radially and circumferentially across the volute exit by up to 40°. At the divider tip where two streams of flow mix, the flow turns more radially and higher incidence angles are noted.

The flow characteristics change with operating conditions of the turbine. At low u/c the velocities are higher because of the mass flow rate, but the flow angles do not vary significantly. Close to the design point condition, the incidence angle varies between about 20° to 60° (higher value is noted near divider tip). This value is increasing more negative at off-design conditions.

The deviation of flow from the radial plane (i.e axial component of velocity) is generally small. The effect of the divider is also indicated from the way flow is directed axially. In the inner wall region flow is biassed towards the inner wall and vice versa.

At 20° azimuth angle, the greater pressure from the outer limb caused the flow to be biassed toward inner wall right across the section.

5.3 Rotor Inlet, Equal and Partial Admission Flow

This section compares the flow characteristics for equal admission and partial admission flow conditions. The results presented here will be amplified in section 5.6 where measurements made for a series of partial admission flows are discussed. The through-flow velocity and axial velocity

components were measured. This section highlights the axial velocity component under partial admission flow. Partial admission flow tests were carried out at the following conditions.

Test Conditions	Total Mass Flow Kg/s
Inner Limb Fully Closed	0.125
Outer Limb Fully Closed	0.125
Mass Flow Ratio (inner / outer) = 0.5	0.148 & 0.24
Mass Flow Ratio (inner / outer) = 0.67	0.148 & 0.24
Mass Flow Ratio (inner / outer) = 1.5	0.148 & 0.24
Mass Flow Ratio (inner / outer) = 2.0	0.148 & 0.24

The flows at different azimuth angles were measured for equal admission conditions. Due to the large number of flow conditions to be investigated under partial admission, measurements were made only at 180° azimuth angle throughout. Partial admission flow results are presents in the following sub-sections :

5.3.1 One Limb Fully Closed
5.3.2 Mass Flow Ratio ($^{inner}/_{outer}$) = 1.5 and 2.0
5.3.3 Mass Flow Ratio ($^{inner}/_{outer}$) = 0.5 and 0.67

5.3.1 One Limb Fully Closed

5.3.1.1 Through-flow velocity

Fig.5.10 presents the flow behaviour at rotor inlet, when one of the limbs is fully closed. Flow into the rotor is fed by either inner or outer limb.

Inner Limb Fully Closed

With the inner limb fully closed, flow predominates in the outer limb. Fig.5.11a gives an indication of the flow with respect to the limbs. The measuring points below the outer limb are 5,6,7 and 8mm while points 2,3 and 4mm are below the inner limb. Flow was measured at all the points. Fig.5.10 also shows that the flow angle measured was highest on the outer limb side, and decreases consistently towards the inner limb side (from 30° to 7°). The absolute flow velocity decreases sharply across the divider towards the inner side. Thus about half the width of the rotor inlet will experience a lower absolute velocity. The flow also becomes more tangential in this region. The flow appears to move across the inlet from the outer to the inner region, adjusting itself gradually into the rotor inlet. Away from the inner wall, the flow turns more towards the radial direction. The incidence angle varies between -18° to -50° across the volute exit. The is roughly the range obtained under equal admission flow at off-design condition ($u/_c$=0.44), see Fig.5.3. Thus with one limb fully closed, the operating condition is comparable to off-design condition.

Outer Limb Fully Closed

With the outer limb fully closed, a similar but spatially reversed effect is noted in both velocity and flow angle profiles. Refer to Fig.5.11b for the flow indication. The velocity drops significantly across the divider towards the outer limb. The flow angle decreases away from the inner wall. Therefore around the inner wall region where the flow predominates, the flow turns more radially.
No measurements were possible at points 7 and 8mm due to poor signal quality. This is most likely to be caused by poor seeding quality or seeding deposited on the optical window.

However measurements under similar conditions at point 7mm and 8mm made subsequently (section 5.6) yield good quality signals.

5.3.1.2 Axial velocity component

Under this extreme condition, the axial component of velocity is most pronounced. Fig.5.11c shows the shift from the radial plane under these conditions.
With the outer limb closed, there is a significant velocity in the outward axial direction. A maximum of 20° axial shift (α_3) is noted and this reduces gradually from point 5mm towards 7mm. The tangential components of velocity measured in the tangential-radial and tangential-axial planes are comparable.
With the inner limb fully closed, the axial shift still points outwards for points 5,6, and 7mm, but the magnitude is much reduced. Clearly the flow is not symmetrical. It might be expected that the flow here should to incline towards the inner limb since it is a lower pressure region, but this was not observed in the result. The divider and the curvature of the outer wall may contribute to this effect.
The results obtained at 3mm and 4mm, cannot be used to draw any logical conclusion because the tangential components measured from the two directions are not comparable. This may have been caused by inaccuracies in the measuring point due to the complicated traverse setting required.

5.3.2 Mass Flow Ratio ($^{inner}/_{outer}$) = 1.5 and 2.0

Through-flow velocity

Partial admission flow is achieved either by closing the inner or outer limb partially to obtain the required mass flow ratio.

Figs.5.12 and 5.13 show the flow behaviour when the outer limb is partially closed and the inner limb is kept fully open. Both test conditions show unusual behaviour of the flow as no measurements were possible at 2mm and 3mm when the outer limb is partially closed. In the earlier tests when the outer limb was fully closed, measurements were possible (see Fig.5.10). This flow characteristic for partial admission was consistent throughout the investigation. The pattern of the results at the two different total mass flow rates is very similar (Fig.5.12 and 5.13).

In Fig.5.13 the flow characteristics for partial and equal admission flow are compared for the same total mass flow to the turbine. The flow angles remains similar across the passage except at point 8mm. At partial admission conditions, the incidence angle appears to be closer to the optimum value (20° to 40° at design condition; section 5.2) than at equal admission conditions. However this applies only to half the rotor inlet (point 5mm to 8mm). The flow condition at the remaining points is not clear from this investigation as no measurement was possible here.

Axial velocity component:

The axial component of velocity under partial admission condition is presented in Fig.5.16. The axial component is always outwards. This is similar in magnitude to the case when the outer limb is fully closed. The effect of the axial component is still significant as in the case when the outer limb is fully closed. Deviation of flow from the radial plane is between α_3 = 3° to 18°.

5.3.3 Mass Flow Ratio ($^{inner}/_{outer}$) = 0.5 and 0.67

Through-flow velocity

For the same total mass flow conditions as in Section 5.3.1 the mass flow ratio is now set by partially closing the inner limb and maintaining the outer limb fully open.
Figs.5.14 and 5.15 show the flow variations for these partial admission conditions. Again, the unusual behaviour of the flow is observed as in the previous mass flow ratio condition. No measurements were possible at 7mm and 8mm points at a ratio of 0.5. When the inner limb is fully closed measurements were possible at these points. Thus the inner limb partially open appears to cause a mixing of the two flows which results in a highly disturbed flow at these points.
At the higher mass flow (away from design point), Fig.5.15 the flow angle is more nearly constant, compared with the equal admission flow condition. Partial admission flow has not affected the turning of the flow radially. Fig.5.15 shows once again that the incidence angle is more favourable than the equal admission flow condition, at least over the inner region of the passage. Similar results were noted in Section 5.3.2. Dale (39) found from experiment that partial admission with mass flow ratio $^{inner}/_{outer}$ = 0.5 and 0.67 produces higher turbine efficiencies than at equal admission flow. No clear explanation has been possible up till now, but this finding appears to be consistent with the more nearly optimum incidence at partial admission conditions. Here it has been found that the through-flow velocity for all but the extreme partial admission conditions ($^{inner}/_{outer}$ = 0.5,0.67,1.5 and 2.0) indicates that the incidence angle is more favourable than the equal admission flow condition, for about half the volute exit. Therefore a study of the axial velocity under these flow conditions is necessary to better understand the flow characteristics.

Axial velocity component

The axial component of velocity can be studied from Fig.5.16 in terms of deviation from radial plane. The flow deviation from the radial plane towards the inner limb is small; α_3 is between 3° to 7°. The effect of the divider wall is noted at points 4mm and 5mm, when the axial flow direction swings towards the outer limb. The axial component becomes greater, from 10° to 15°.
Referring back to the inner limb fully closed case, the axial flow angle towards the outer limb is only 4° to 6°. When the inner limb is partially opened, the flow from the inner limb moves towards the outer limb causing the axial component at points 5mm and 6mm to increase.
Fig. 5.16 summarizes the axial shift and the direction of shift is indicated by the arrow pointing either towards inner or outer limb. With more mass flow from the outer limb. The flow at 2,3,4mm is biassed towards the inner wall region. Under these conditions higher turbine efficiencies were observed by Dale (38,39)

5.3.4 Conclusion from partial admission flow

The partial admission flow measurements presented here are, to the best of the author's knowledge, unique and it is therefore not possible to make comparisons with other test data.
The presence of an axial component of velocity is most significant when one limb is fully closed. Comparisons between these data at different partial admission flow conditions have been made. The conclusion so far is that under extreme partial admission, the presence of an axial component reduces the tangential component of velocity and hence the rotor specific work.
At partial admission, the flow shifts from the radial plane as

the mass flow ratio changes. At the more favourable partial admission $^{inner}/_{outer}$ = 0.67 and 0.5, the flow at 2,3,4mm points, is directed towards the inner wall. Further discussion on the flow characteristics at this partial admission is presented in section 5.5 together with turbine performance and axial velocity results.

5.4 Rotor Exit, Equal and Partial Admission Flow

Fig.4.10 shows the measuring locations at the rotor exit. The flow conditions applied when measuring the rotor inlet gas flow were repeated for measurements at the rotor exit. The flow conditions are as follows:

Test Conditions	Total Mass Flow Kg/s
Equal Admission Flow	0.13, 0.17 & 0.24
Inner Limb Fully Closed	0.17
Outer Limb Fully Closed	0.17
Mass Flow Ratio (inner / outer) = 0.67	0.24
Mass Flow Ratio (inner / outer) = 1.5	0.24

Measurements were mainly made along the vertical axis across the exit duct. Fig.5.17 presents a three dimensional view of the measuring direction and a typical set of results for equal admission at 0.24 Kg/s total mass flow. The vertical measuring axis is 30mm away from the rotor exit.

The flow angle measurement indicates the absolute flow value towards either the LHS or RHS. Starting from the top of the duct, the flow is directed towards the LHS. As measurements

were made gradually towards the bottom the flow direction changes towards the RHS, indicating a swirling flow about the axis of the duct.

Fig.5.18 presents the same view of the duct and the flow behaviour, but with the measuring axis in the horizontal direction. At the extreme RHS, the flow is directed upwards. As the measuring points moves towards the LHS, the flow changes its direction, gradually pointing downwards, confirming the swirling nature of the flow.

Figs.5.17 and 5.18 give a good visualization of the flow angle with respect to its measured point and orientation. This representation of flow behaviour is however less suitable for comparison purposes and subsequent results are presented in a different format.

5.4.1 Equal admission flow, three flow conditions

Rotor exit flow variation has been investigated under equal admission flow for three different flow conditions. Fig.5.19a illustrates the flow behaviour in the exit duct, for total mass flows of 0.13,0.17,0.24 Kg/s and equal admission flow at the turbine inlet. The axis of measurement is 30mm away from the rotor tip. The hub diameter of the rotor exit is about 22mm. The rotor exit tip diameter is 59.5mm. Thus exit blade height is 18.25mm.

At the lowest mass flow, which is closest to the design point, the flow velocity is almost constant across the duct. The flow angle deviation from the axial is a minimum and roughly symmetrical about the centre axis. The result shows minimum swirl near the design point conditions. As the mass flow increases, moving away from the design point, the deviation of the flow angle becomes more pronounced. The symmetry of the flow angle across the duct is still maintained. Increasing swirl at the rotor exit at off design points is evident from Fig.5.19a. Maximum swirl is indicated close to the wall region,

at point 15mm which is about 25% across the diameter axis. At off design points, the variation of the absolute velocity across the duct becomes larger. The velocity profile remains approximately symmetrical but contains a high velocity core in the centre of the duct, which falls rapidly towards the walls. In the very centre there is some small evidence of the wake from the solid centre of the hub.

For the same mass flow conditions, measurements were made along a horizontal axis across the duct. The results are presented in Fig.5.20. Similar results are obtained as in the case of measuring from the vertical axis. Symmetry is observed in both the velocity and flow angle profiles. Minimum swirl and roughly constant velocity profile across the duct remain the characteristics for near design point operation. These results show that the flow in the exit duct is roughly symmetrical about the centre axis of the duct.

Exit flow variations have also been studied by Milton (19,20,23) and Samuel (21,22). Fig.2.8 shows these results. Generally, the flow angle increases towards the shroud side (outer wall) indicating an increasing swirl. Milton (19) concluded that the variation of flow angle and absolute velocity across the duct indicated that there was a non-uniform work distribution from shroud to hub, with minimum work occuring at the outer wall (shroud). This may be due to the blade unloading which near the shroud because of tip leakage and from the centrifuging of low momentum fluid into this region. Low total pressure losses were measured at the hub region.

In the experiments conducted by Milton and Samuel, measurements at the rotor exit were made at a some unstated distance downstream of the rotor trailing edge. A centre-body was installed close to the rotor exit to obtain measurements of the static pressure at the hub. This centre-body will in fact guide

the flow from the rotor exit. In a practical turbocharger installation this is not likely to be in place, and it may influence the comparison with the present results. Although there is some agreement with measurement made at the shroud side, there are difference in the measurements at the hub region because of the presence of the centre-body.

A more detailed study of the flow at the rotor exit (without the centre-body) by Miller (17) showed some contrasting results. The rotor exit blade height was about 1.26" and test speed at 50000 RPM. The measuring axis was 0.506" away from the rotor trailing edge. Therefore the ratio of distance downstream to exit blade height 0.402.

Fig.5.21 shows the variation of exit flow angle and velocity, at the rotor exit. Although these results were taken at the design condition where the u/c = 0.70, the flow variation in the rotor exit shows comparatively large swirl. However the ratio of distance downstream to exit blade height is 0.402 compared to 0.222 in the present study. Along the axis of measurement the flow changes from α_3 = 20° at the shroud side to -15° at the hub side, see Fig.5.21. The flow actually turns from "in the direction of rotation" to "against the direction of rotation" from the shroud to the hub side. In the hub region, the flow is affected by the reducing flow area. Mizumachi (24) has shown that the measured rotor exit flow angle is affected by the blade angle. The minimum deviation appears to be in the mid section of the rotor exit where the flow has minimum swirl component.

The difference in flow characteristics between present investigation and that obtained by Miller (17) is likely to be due to the size effect rather than the test speed. In section 5.7 this effect will be highlighted when measurements made very close to the rotor exit are presented.

The flow fields presented here are confined to the core of the

duct. No measurements were possible for points close to the wall. Repeated attempts to measure close to the wall did not yield any results. The signal was weak and noise level was high. This could be caused by a fairly thick boundary layer or high swirl. Fig.5.19a shows, however, that high swirl indicated by absolute flow angles up to 40° was measured at off-design point. It is unlikely that near the design point such high absolute flow angles will be encountered close to the wall, so that high swirl is unlikely to be responsible. The other likely cause is the effects of overtip leakage propagating into this region causing a highly disturbed flow around the wall.
Fig.5.19a also shows that at off-design operation, the flow in the duct is basically swirling in nature. Fig.5.19b shows the turbulence intensity level for measurements at rotor exit. The overall results indicated a high turbulence intensities level of 17% to 25%. The maximum turbulence intensity is consistently noted at the centre of the duct.
It might be expected that the line of measurement is close enough to the rotor exit to be affected by the separation due to the solid hub. However the velocity measurements show very little of this effect but the high turbulence intensity measured at the centre may well indicate some residual wake.

5.4.2 Equal and Partial Admission Flow condition

The effect of partial admission on the flow behaviour is noticeable at the rotor inlet. Its effect at the rotor exit was also investigated and the results are presented in Figs.5.22 and 5.23. Fig.5.22 compares the flow variations for equal admission and mass flow ratio = 1.5 and 0.67. The results show very little variation in either the velocity or the flow angle. The symmetry of the flow across the duct remains unchanged.
Fig.5.23 compares the flow variations for equal admission and

one limb closed. Slight differences in both the flow angle and velocity profile are observed, but the overall trends and symmetry remains unchanged. The effect of partial admission flow on the flow field at the rotor exit appears to be very small.

5.5 Rotor Inlet, Equal Admission Flow, Different divider depth.

The effect of divider depth on the flow characteristics is presented in this section. Four different divider depths were used in a common turbine housing. The different divider is identified in terms of separating wall diameter (SWϕ).

SWϕ	R/R_{tip}	Divider tip
80mm	1.067	very close to rotor edge (2.5 mm)
86mm	1.147	
90mm	1.200	
96mm	1.280	furthest from rotor edge (10.5 mm)

The change in through-flow area in each limb and the interspace due to different divider depths is tabulated in Fig.5.24. With SWϕ = 80mm the through-flow area is the smallest and the interspace between divider tip and rotor inlet is a minimum. Therefore the flow from each limb will have the minimum interspace in which to mix before entering the rotor. For SWϕ = 96mm, the flow area is largest and the interspace between the divider tip and the rotor inlet is a maximum so that there is a greater volume in which the flows can mix before entering the rotor.

Measurements were made at the design condition (u/c = 0.69 to

0.70). The flow characteristics with different separating wall diameters is presented for 180° azimuth angle in Fig.5.25.
For SWϕ = 80mm, no measurements were possible at 2 and 3mm points. This was consistently the case for measurements at all azimuth angles.
Fig.5.24 shows that the flow area near the inner wall is small. This, together with the reduced interspace may cause the flow in this inner limb region to be highly disturbed or mixed. For this turbine geometry flow from the inner limb has not been able to mix well with the outer limb with the reduced interspace. The inability to measure velocity in the inner region of the inlet under these conditions (Fig.5.25a) is evidence of the highly disturbed flow in this region. It is likely that there is a high axial velocity component due to the curvature of the inner wall and this effect is amplified by the narrow through-area of the inner limb. If there is a large axial component of velocity, experience suggests that measurement in the tangential-radial plane is not likely to be possible.
A high axial velocity component will tend to reduce the absolute velocity measured in the tangential-radial plane. This may also explain a drop in absolute velocity at point 4mm.

Under equal admission condition, there is no very significant change in flow characteristics with different dividers. The flow tends to be affected more on the outer limb region only. The inner limb region remains much the same. As the divider is extended close to the rotor it is suggested that, a highly disturbed flow resulted in the inner limb region. There is probably a high axial velocity component in this region.

5.6 Rotor Inlet, Series of Partial Admission Flow, Different divider depth.

5.6.1 Introduction

The flow characteristics under equal and partial admission conditions have been shown earlier. The following presentation shows how the flow characteristics vary in stages as the flow condition changes from one limb fully closed, through equal admission to the other limb fully closed. The partial admission tests were carried out by first setting the operating conditions under equal admission flow so that the u/c is in the range 0.69 to 0.70. With the total mass flow to the turbine fixed, the test was carried out by varying the control valves in each limb, and applying the necessary load on the eddy current dynamometer to maintain a constant rotor speed. For each value of the total mass flow, nine separate partial admission conditions covering the entire range of mass flow ratios were tested. This was repeated for each of the four separating wall diameters. The flow characteristics and turbine performance are presented in the following figures :

Fig. 5.26 SWϕ = 80mm
Fig. 5.27 SWϕ = 86mm
Fig. 5.28 SWϕ = 90mm
Fig. 5.29 SWϕ = 96mm

5.6.2 Flow characteristics with different dividers

A comparison of the velocity is shown in Figs. 5.26a to 5.29a, and a comparison of the mean flow angle is presented in Figs5.26b to 5.29b. As the flow in one limb is restricted, the flow in the other limb becomes slightly more tangential and the absolute velocity (Figs.5.26a to 5.29a) decreases consistently.

This characteristic is common for all the different dividers. With SWϕ = 80 and 86mm, some flow reversal is noted when one limb is fully closed, Figs.5.26b, 5.27b. This is not observed as the SWϕ gets larger, Figs.5.28b to 5.29b. This presumably because the mixing of the flow from both limbs can occur at a higher radius. Therefore this flow has been able to settle before entering the rotor. Although under one limb fully closed conditions there is no mixing, the flow will nevertheless move across the volute exit before entering the rotor.

This observation was also noted by Lymberopoulos (18) when he measured the flow at the volute exit using two different separating wall diameters. He concluded that the flow properties are more uniform across the volute throat for the larger SWϕ since the mixing of the two streams has taken place at a higher radius. As his measurements were made with a bladeless hub, they are not directly comparable to results in present investigation.

At equal admission conditions, the average incidence angles at 180° azimuth angle measured across the volute exit are 22°, 28°, 29° and 33° for SWϕ = 80, 86, 90 and 96mm respectively. This shows an upward trend for the optimum incidence angle as the separating wall diameter increases.

Under a typical pulsating flow condition, the rotor will be experiencing partial admission conditions most of the time. The range of incidence angles under these conditions (when flow condition in turbine vary from zero flow in one limb to equal admission flow) is as follows :

68° to -50°	for SWϕ = 80mm
60° to -34°	for SWϕ = 86mm
50° to -60°	for SWϕ = 90mm
46° to -78°	for SWϕ = 96mm

The turbine efficiency under partial admission condition is

presented in Fig.5.30. The turbine efficiency is a minimum at the extremes of partial admission and increases towards equal admission. In all cases, however, the maximum efficiency occurs, not at equal admission, but at a mass flow ratio $_{inner/outer}$ = 0.67 to 0.50. This observation has been consistent with Dale's results (39) in which the same turbine (A:R = 1.0 SWϕ = 86mm) was tested. His investigation showed that the variation of turbine efficiency with mass flow ratio was asymmetric i.e the effect of throttling one turbine entry did not produce the same efficiency as throttling the other to the same extent. This effect occurred at all rotational speeds tested by Dale (39). A full discussion of turbine efficiency characteristics is now possible with an understanding of the flow characteristics under similar conditions.

The flow characteristics under which partial admission ($^{inner}/_{outer}$ = o.67 and 0.50) yielded higher turbine efficiency is here compared with equal admission flow results. Fig.5.31 compares the flow characteristics across the volute exit for the equal and partial admission conditions for SWϕ = 86, 90 and 96mm.

At equal flow conditions, the flow shows the influence of the divider but is otherwise reasonably uniform across the passage. As the flow in the outer limb increases, the absoute velocity dominates in this region. The flow also becomes more tangential (Fig.5.31a). Over the inner region the absolute velocity decreases below the equal admission flow value. It is still not clear up to here why the flow characteristics at partial admission compares more favourably than the equal admission condition. The flow under partial admission displays a greater variation across the volute exit while under equal admission the flow is only influence by the divider.

The axial velocity component was not measured under these conditions. However it was measured under similar flow condition as presented in Figs.5.8b and 5.16. The axial

velocity component is abstracted and presented in tabular form in Fig.5.31c. This compares the flow deviation from the radial plane for partial and equal conditions. A plan view of the rotor also in Fig.5.31c shows the curvature of the rotor inlet blade.

Fig.5.31c shows that under equal admission, the flow in the inner limb region is almost in the tangential-radial plane i.e zero axial velocity component. This is favourable and it is commonly assumed that axial velocity is zero.

Under partial admission, the flow at point 2 and 3mm, has an increased deviation towards the inner wall while the remaining point in the outer limb region shows also an increase in deviation away from the inner wall. This also means that the flow in the outer limb will have less turning in the meridional plane of rotor.

This flow shift from radial plane with respect to the curvature at the rotor inlet appears to have a positive effect on the specific work in the rotor.

5.7 Gas flow characteristics and turbine performance with partial and equal admission flow.

Fig.5.32 shows the flow characteristics at a fixed measuring point 7mm from the inner wall, as the flow conditions are varied. The turbine efficiency is plotted for direct comparison with the flow characteristics at different stages of the partial admission conditions. The variation of mass flow ratio starts with the outer limb fully closed (X). This is opened gradually through equal admission (Y) to closing the inner limb fully (Z). The variation in both flow characteristics and turbine performance are shown in Fig.5.32. The incidence angles varied from 63° to -38° between the two extreme partial admission condition.

The performance of the radial inflow turbine is strongly dependant on the gas angle at the entry to the turbine rotor. The blades are designed to match these angles in such a way that a correct match will occur only for specific combinations of mass flow rate, rotor speed and pressure ratio. Away from this design point, the gas angle will not match the blade angle and an incidence loss will occur. This loss increases as the flow departs further from the optimum incidence angle. It was shown earlier that the average incidence angle is about 28° at equal admission flow with $u/c = 0.70$. The greater the incidence loss the lower the turbine efficiency.

In Fig.5.32 u/c and efficiency at X is the lowest, where the outer limb is fully closed. Under this condition, about half the rotor is experiencing low velocity flow, Fig.5.26a . The incidence angle at this stage is about 60° causing large incidence losses. As the outer limb is opened gradually to equal admission, the incidence angle decrease to about 25° while the turbine efficiency increases to about 67%. Closing the inner limb gradually to fully closed at Z causes the u/c and turbine efficiency to decrease to approximately the same value as when the outer limb is fully closed. The incidence angle decreases to -28°.

The lowest turbine efficiency is associated with the most adverse incidence angle. In addition the earlier results show that the maximum axial component is noted under these condition Figs.5.10 and 5.11. These are factors contributing to the poor rotor specific work and hence lower turbine efficieny.

The efficiency path XYZ (Figs.5.32 and 5.30) forms a loop which is consistent with the instantaneous efficiencies observed by Dale (38,39).

The swallowing capacity curve for the turbine is also mapped under steady flow condition with equal admission flow and one limb fully closed. In Fig.5.32, closing one limb causes the mean pressure ratio to rise significantly. This is related to

the minimum turbine efficiency and extreme incidence angle.

Fig.5.33a shows the turbine efficiency under equal admission and one limb fully closed condition at constant speed. Fig.5.33b shows the variation of u/c values with the total mass flow to the turbine. At $u/c = 0.70$ for equal admission the total mass flow to the turbine is 0.10 Kg/s. For this same total mass flow to the turbine when one of the limb is fully closed, the u/c drops to 0.46. Closing one limb reduces the effective area of the turbine, therefore turbine inlet pressure must be increased to maintain same mass flow, so "c" rises and u/c falls. This value ($u/c = 0.46$) is plotted on the efficiency curve for one limb fully closed to obtain its respective operating point. Fig.5.33a shows that the operating point between A and A' as the flow condition in the turbine changes fron equal admission to condition when one of the limb is fully closed for the total mass flow held constant. Although this is not a realistic circumstance it does support the earlier investigation using series of partial admission (with total masss flow held constant) which shows the variation of turbine efficiency with u/c.

Fig.5.34 elaborates this changing of operating points of the turbine for a number of flow conditions. These results do not in any way represents a typical turbocharger operation but they show the limits between which the turbine will operate under pulse flow conditions. These results can be compared with the instantaneous efficiency obtained by Dale's experiment (39). Fig.5.35 contains a series of instantaneous efficiency plots for a range of rotor speeds at pulse frequencies of 40 and 60 Hz. The variation of u/c and efficiency are marked with dotted lines and the range of these variations is compared with Fig.5.32. These variations are fairly consistent with those noted using the steady flow results.

The above investigation shows how the turbine efficiency (under

steady flow conditions) will decay as the flow condition in the turbine changes from equal admission to one limb fully closed. The extent of decay in efficiency is fairly consistent with that noted for instantaneous efficiency measurements.

5.8 Measurement close to rotor exit

The flow measurements at the rotor exit so far described have been made along an axis 30mm downstream of the rotor trailing edge. This section presents the results of flow characteristics made at 4mm away from the rotor and compares them with that taken 30mm away under the same flow conditions. All measurements were made at the design point, $u/c = 0.70$.

Fig.5.36 shows the measuring points at the rotor exit. The flow characteristics for measurements made at 4mm and 30mm are presented in Fig.5.37. Flow at 30mm is very nearly symmetrical across the duct (see Fig.5.19) and the results are presented for half the exit duct only.

Close to the rotor edge, measurements were made around the top half of the rotor, from 1mm to 11mm. From 12mm onwards no measurements has been possible indicating that the flow near the hub region of the rotor is highly disturbed.

Comparing the measurements made at 4mm and 30mm downstream (Fig.5.37) there is a notable decrease in axial velocity downstream of the rotor. This is expected due to the increased flow area in the duct after the hub. The degree of swirl is indicated by the magnitude of the rotor exit absolute flow angle. Fig.5.37 shows that neither the flow angle nor the tangential velocity are affected anything like as much as the axial velocity, although the mean tangential velocity is roughly halved.

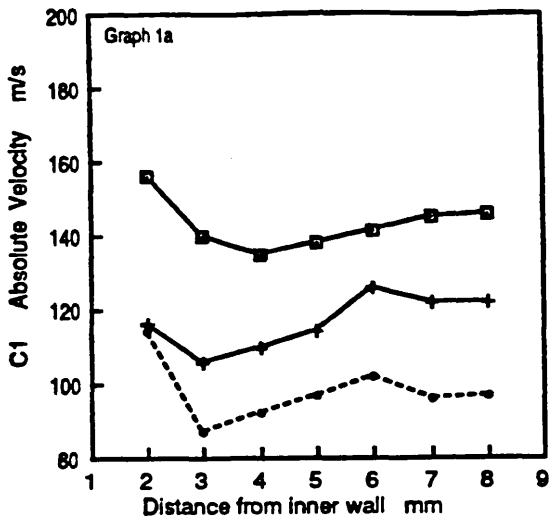
Miller (17) and Mizumachi (24) measured flow characteristics very close to the rotor using a probe. There was no mention of difficulties regarding measurement around the hub region. The main reason for this difference is probably due to measuring technique. On the measurement, a probe will produce a reading in highly turbulent flow (particularly with a lot of pnuematic damping) where the L2F velocimeter may not, but one must question (a) the interpretation of mean velocity and flow angle in highly turbulent time varying flow, and (b) the blockage of the probe itself. The problem with measuring near the hub is probably the large blade wakes shedded. This may be overcome by phase-locking the measurements with the blade frequency.
Rotor exit measurements by Miller (17) show that the absolute velocity peaks around the shroud side (top of duct) and decreases towards the hub, Fig.5.38. The corresponding absolute flow angle in Fig.5.21 indicates that greater swirl exists around the shroud side. These rotor exit characteristics were measured under optimum flow conditions, $u/c = 0.70$. The rotor exit flow survey by Miller (17) shows comparatively larger swirl component at optimum flow condition.

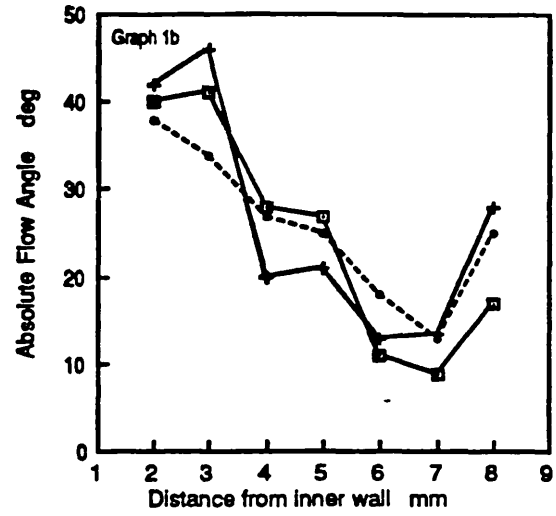
While it was not possible to measure the flow around the lower half of the rotor exit (at 4mm from rotor) it is possible to make a simple one dimensional analysis (mass conservation, free vortex assumption and angular momentum equation) to estimate the flow characteristics immediately after the rotor exit from the measured values 30mm downstream (see Appendix C for description of method).
The calculated values are compared with the flow measured at 4mm from rotor exit. Fig.5.39 compares absolute velocity and flow angle, and axial and tangential velocity components. The measured absolute and axial velocities in Fig.5.39 are fairly constant up to the mid section of the rotor exit blade. The calculated value shows the absolute and axial velocity to peak

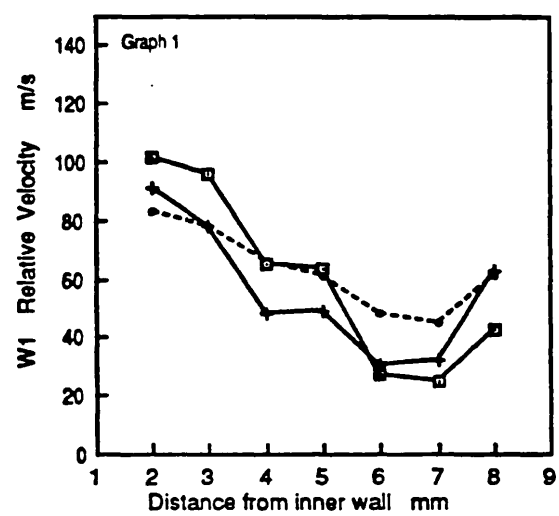
around the shroud side (2 to 6mm) and decreases consistently to a minimum at the hub. This is due to the annulus area at 30mm downsteam which tends towards zero at centre axis and thus the corresponding annulus area at the hub becomes greater. From mass flow conservation, the axial velocity near the hub will tends to zero.

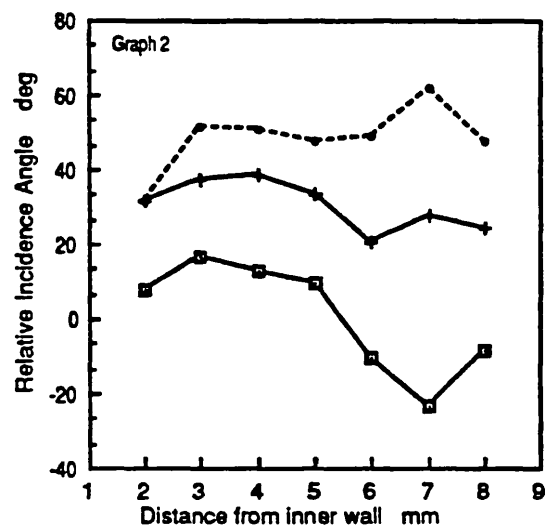
After 11mm point where no measurements were made, the calculated value shows the absolute velocity to decrease toward the hub. The absolute flow angle shows increasing value towards the hub because the calculated tangential component increases while the axial component decreases.

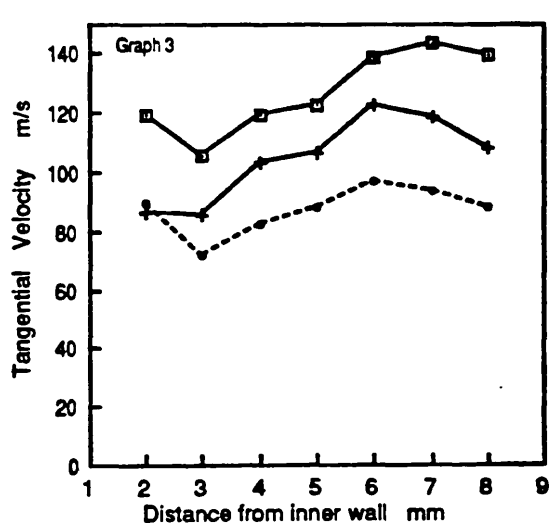
The conclusion from the above comparison shows that the trends in angle and tangential velocity in the outer region are right. The magnitude of axial velocity in the outer region are reasonably close although measured values show a rather flat velocity profile. This is probably due to its simplicity in the analysis and the assumption made. The flow in the exit duct is three dimensional and this is not considered. However the calculated values present an indication of the flow characteristics immediately after the rotor exit in particular at the lower half of the rotor exit where measurement has not been possible.

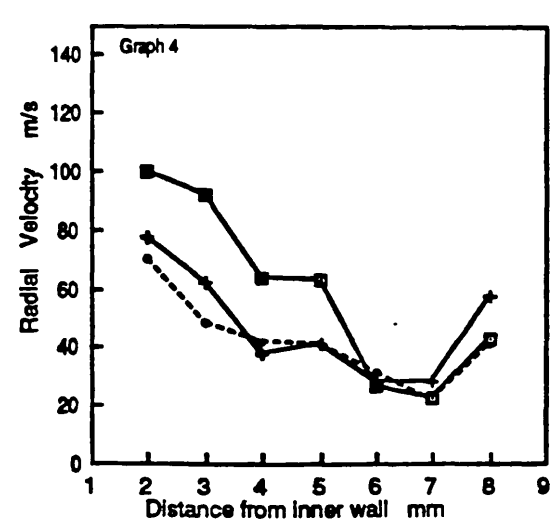












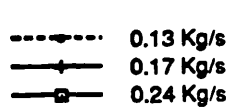
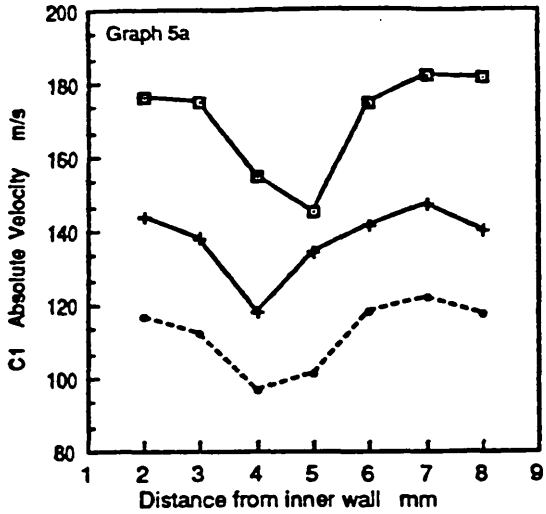
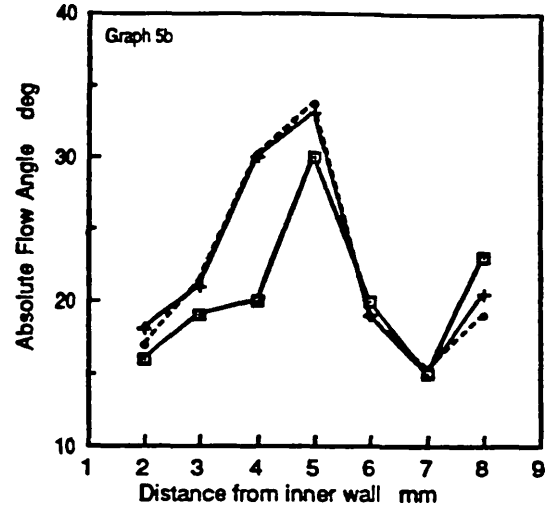


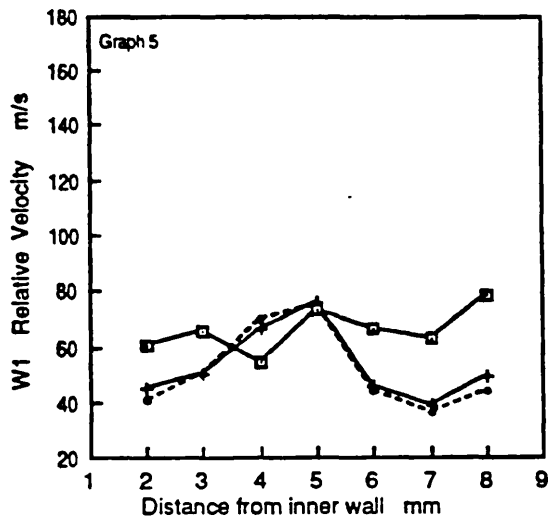
Figure 5.1

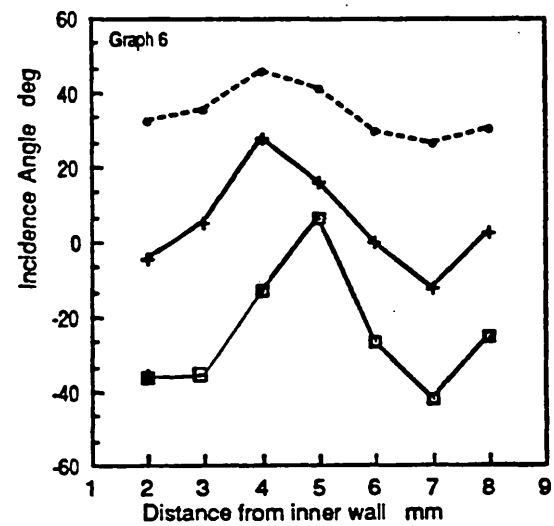
20° Azimuth Angle

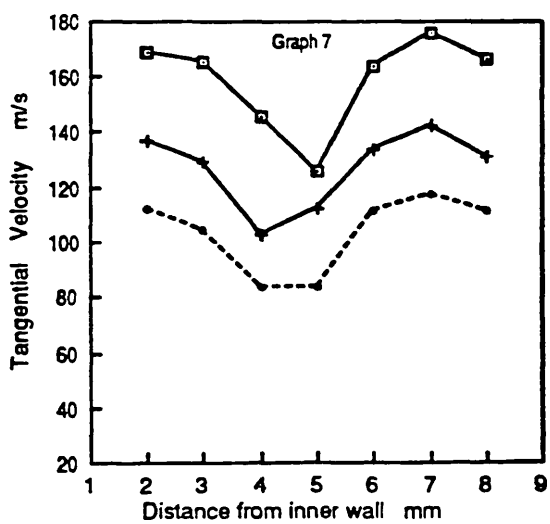
Equal Admission Flow
ROTOR INLET
34000 RPM

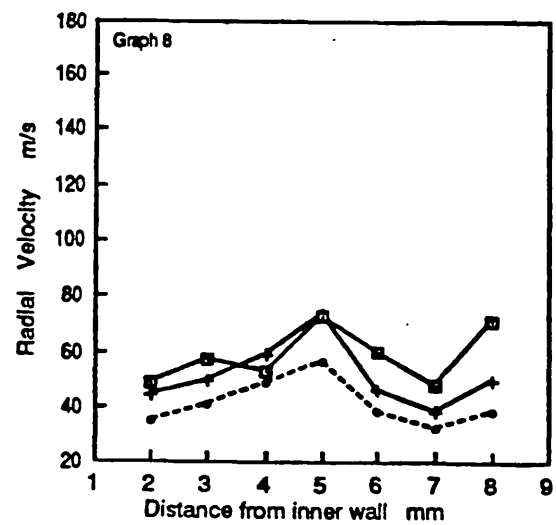










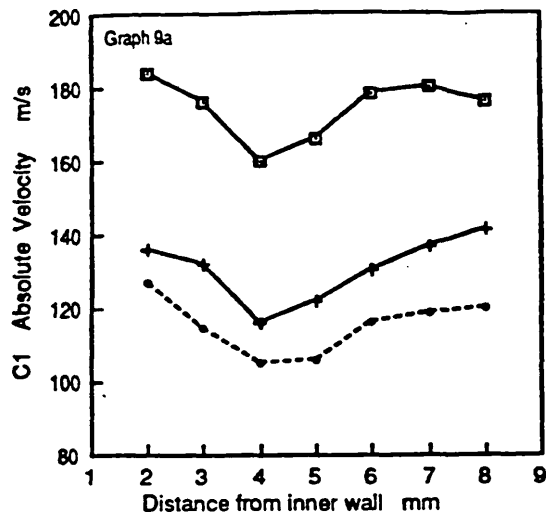


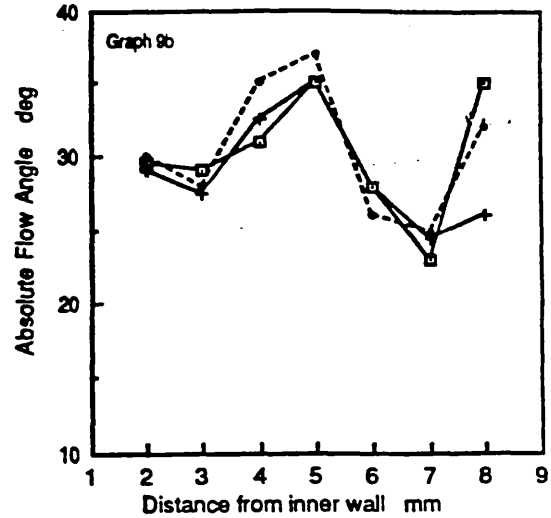
0.13 Kg/s
0.17 Kg/s
o.24 Kg/s

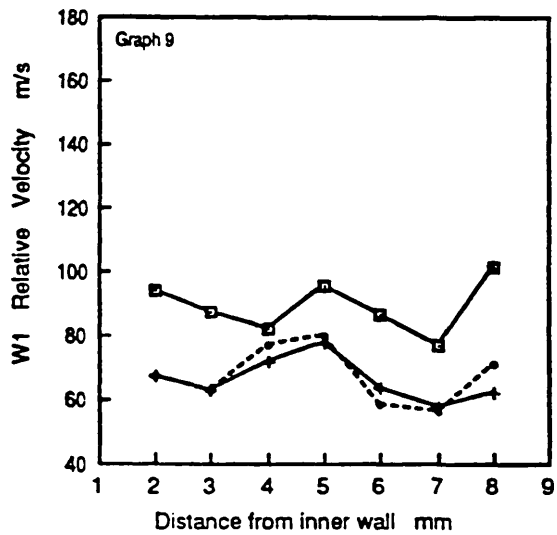
Figure 5.2

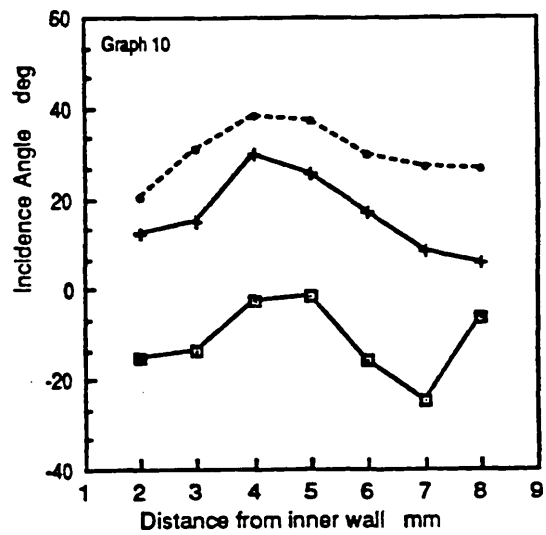
90° Azimuth Angle

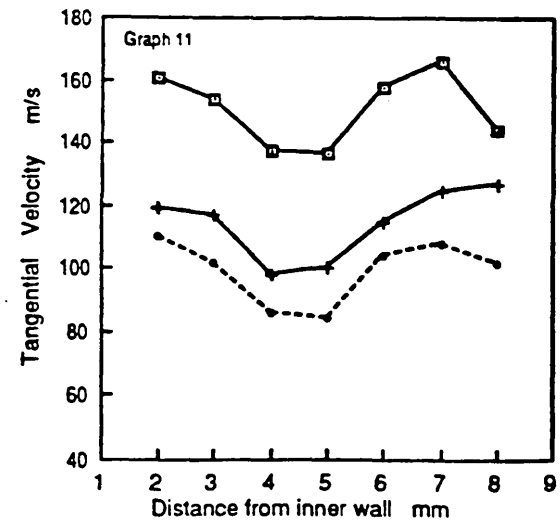
Equal Admission Flow
ROTOR INLET
34000 RPM

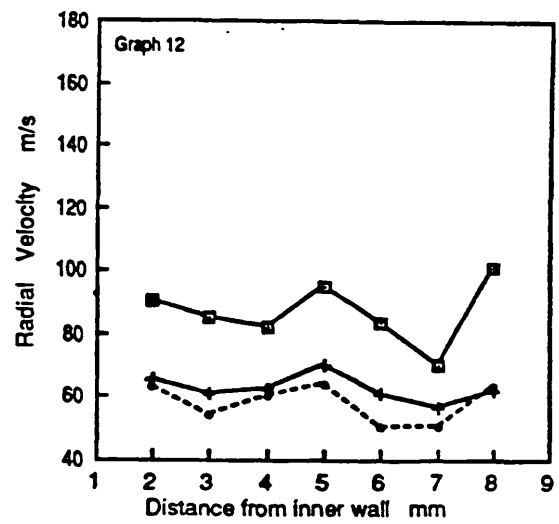










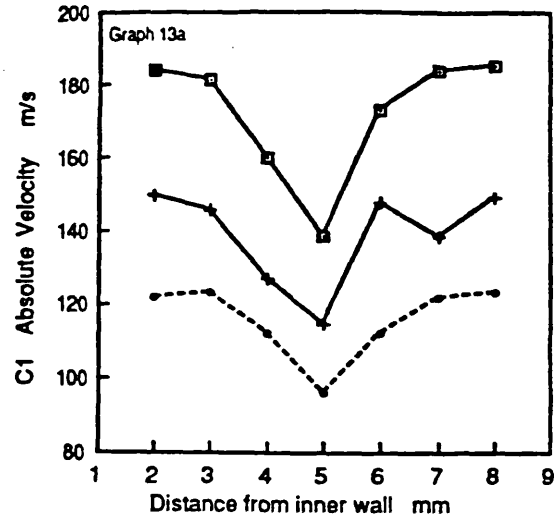


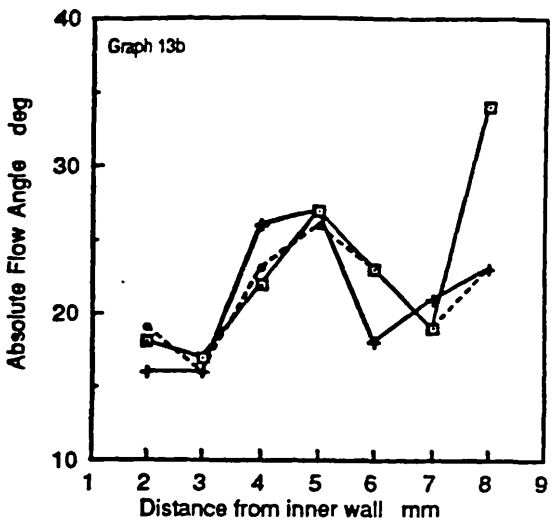
0.13 Kg/s
0.17 Kg/s
0.24 Kg/s

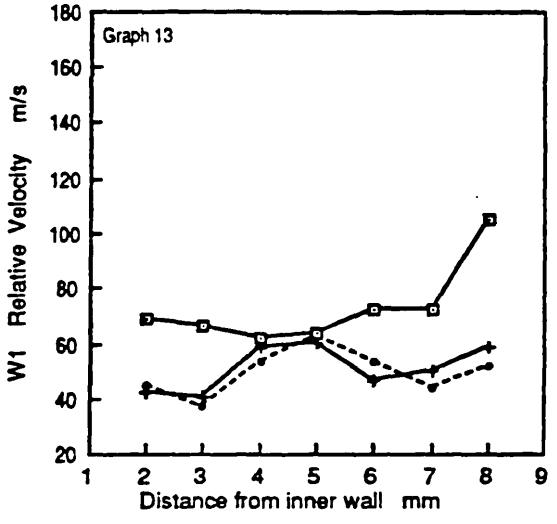
Figure 5.3

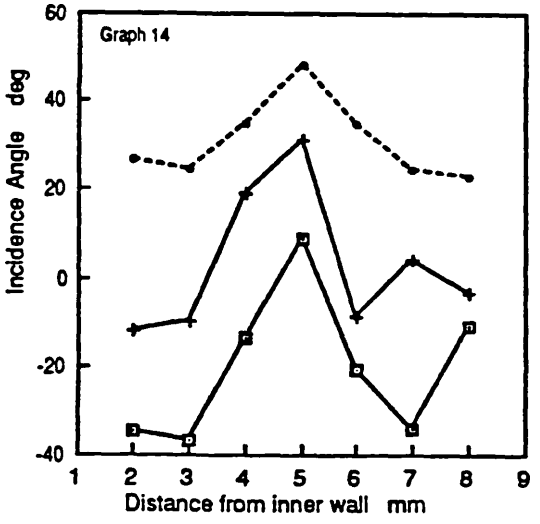
180° Azimuth Angle

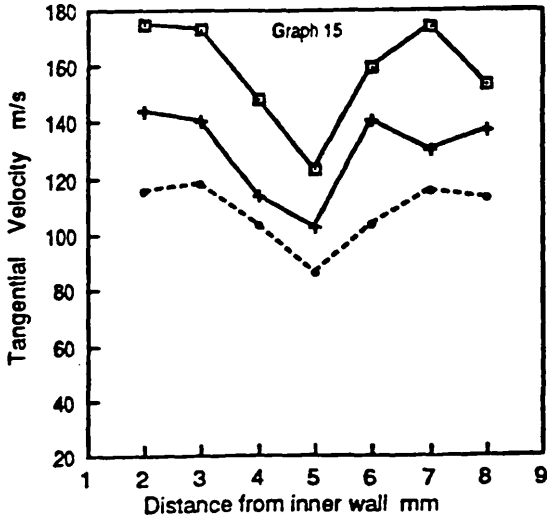
Equal Admission Flow
ROTOR INLET
34000 RPM

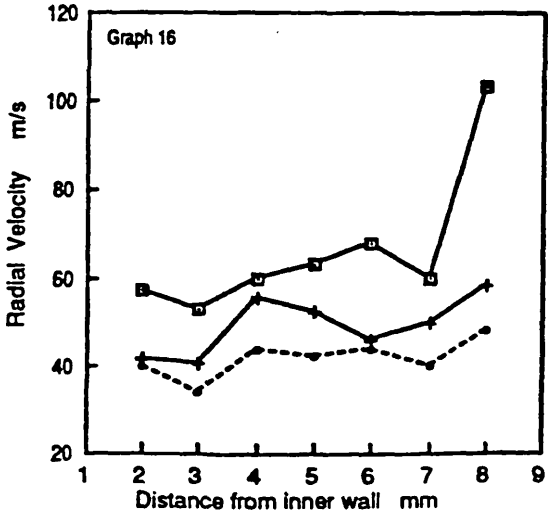










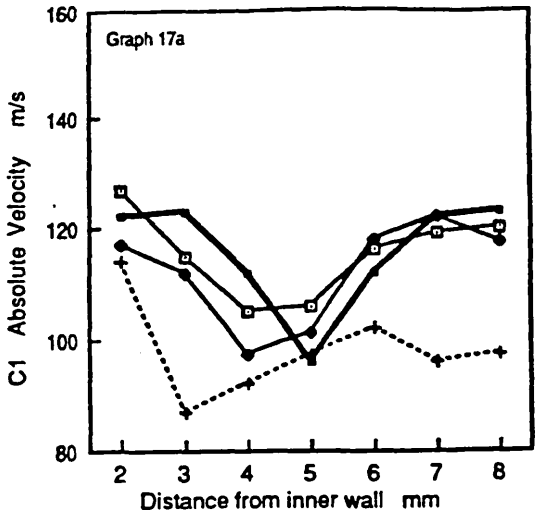


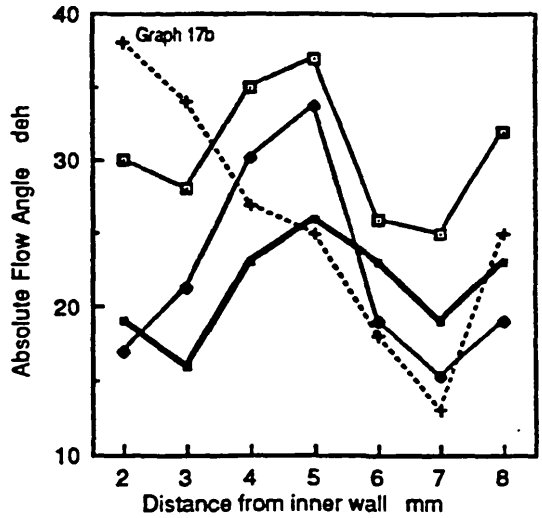
0.13 kg/s
0.17 kg/s
0.24 kg/s

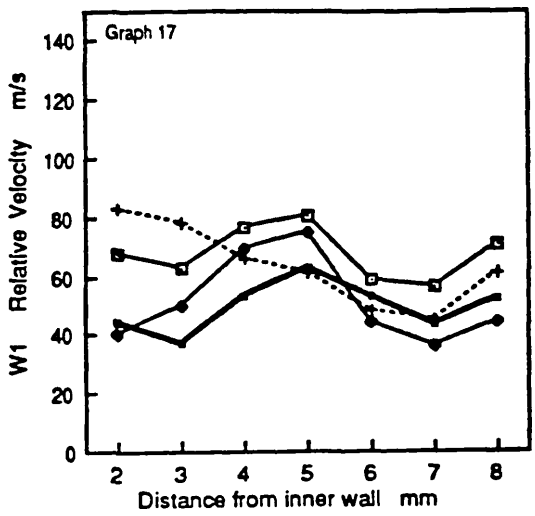
Figure 5.4

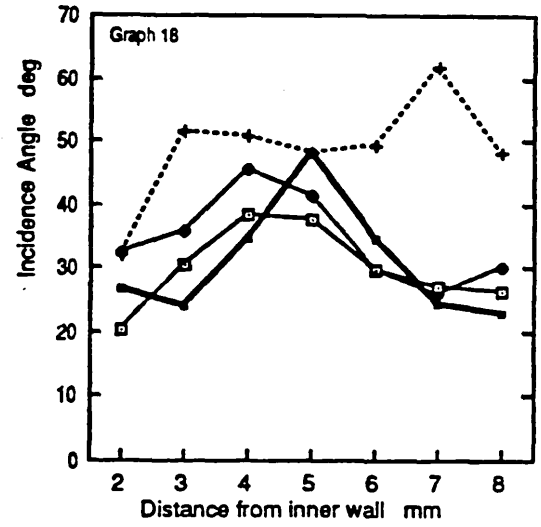
270° Azimuth Angle

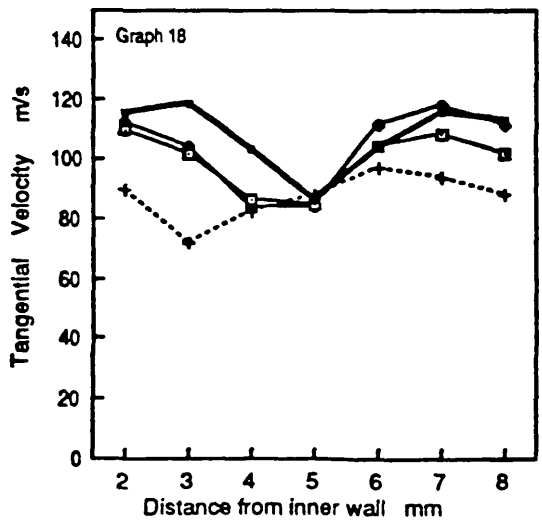
Equal Admission Flow
ROTOR INLET
34000 RPM

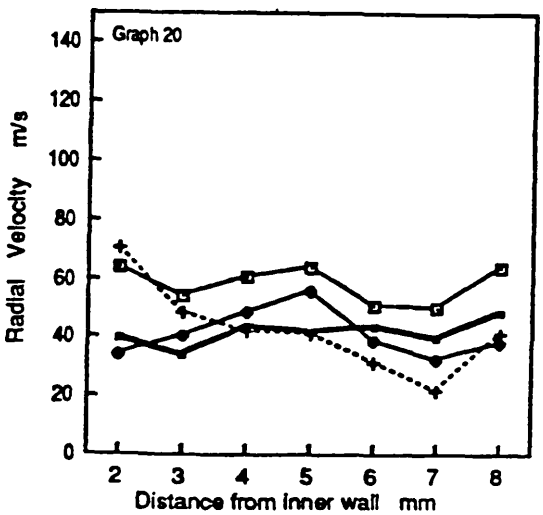












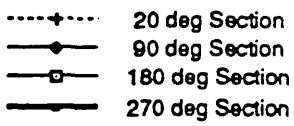
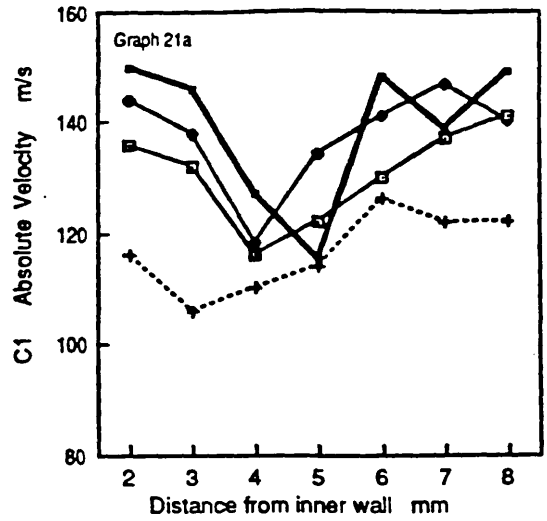
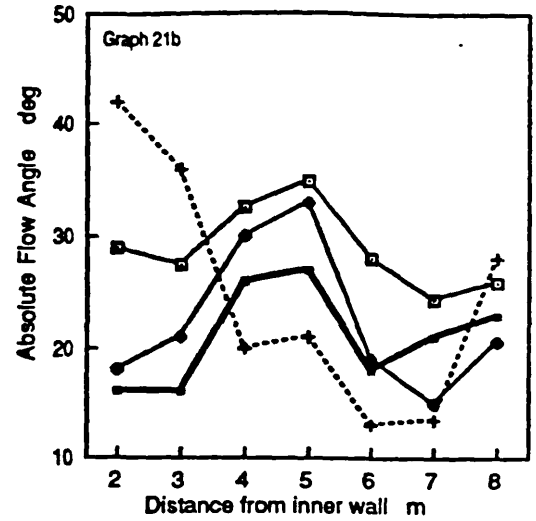


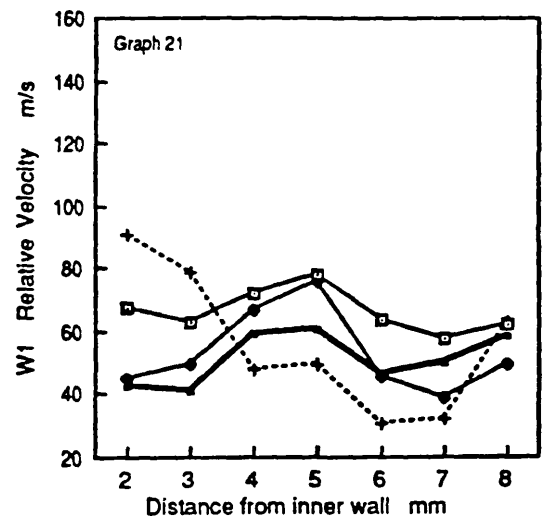
Figure 5.5

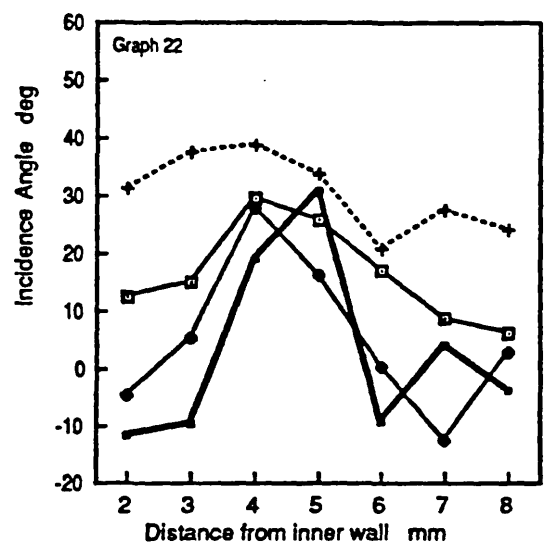
Total Mass Flow = 0.13 Kg/s

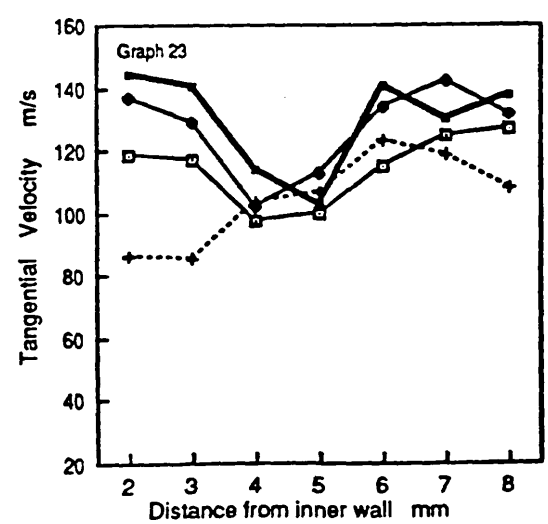
Equal Admission Flow
ROTOR INLET
34000 RPM

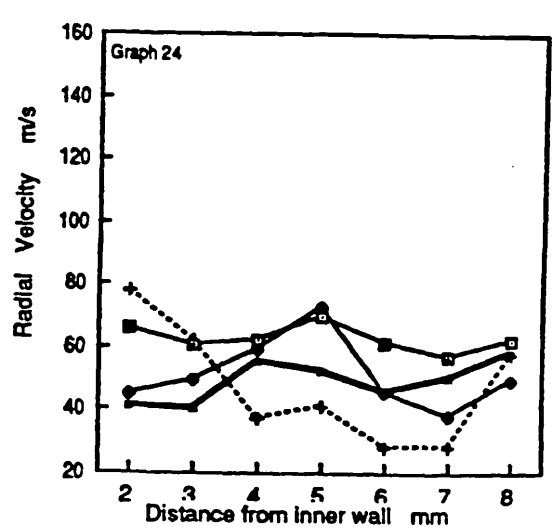












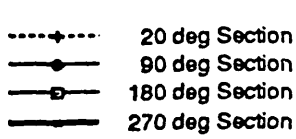
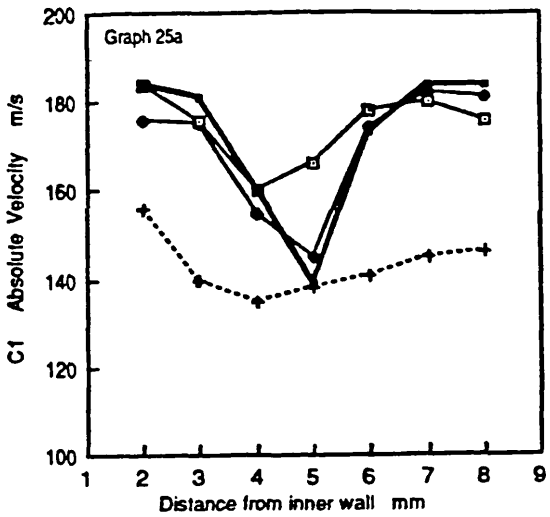
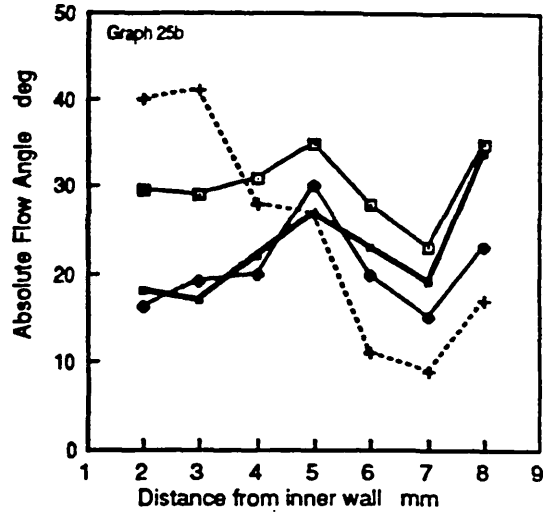


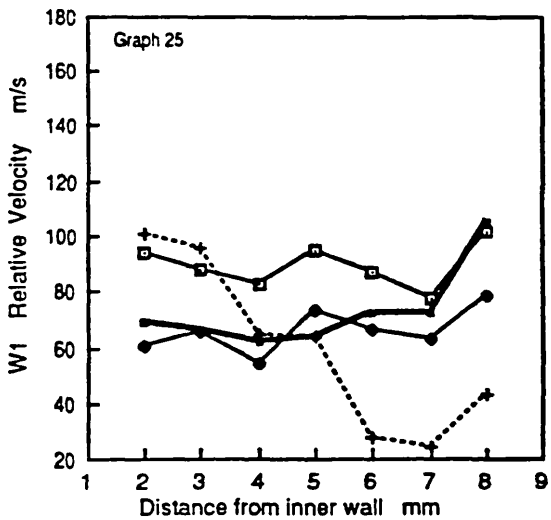
Figure 5.6

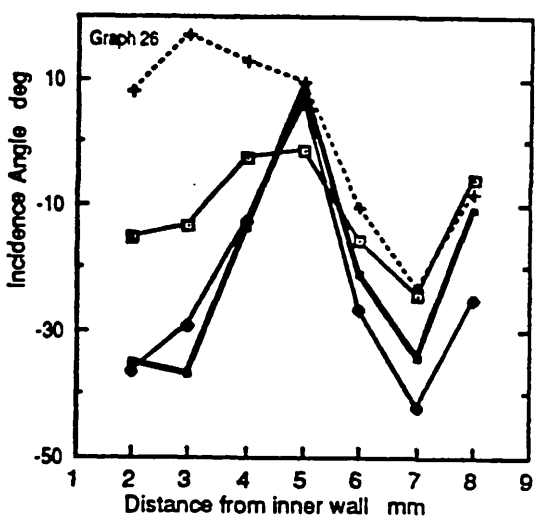
Total Mass Flow = 0.17 Kg/s

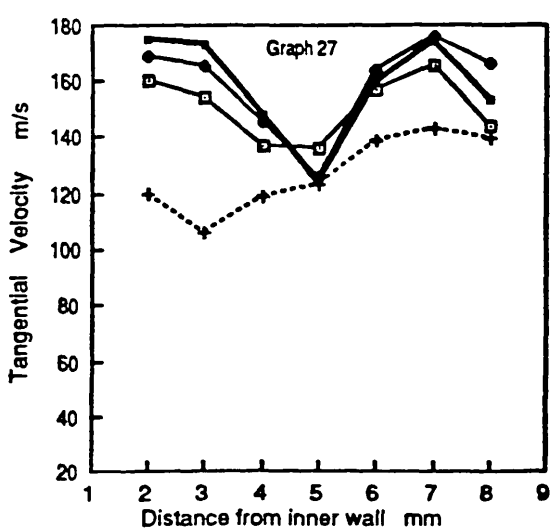
Equal Admission Flow
ROTOR INLET
34000 RPM

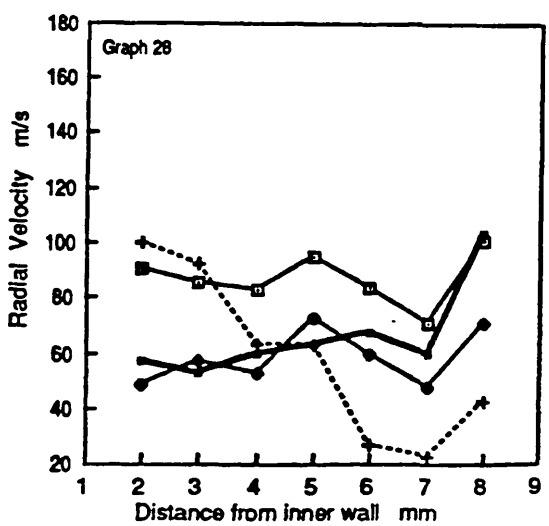












20 deg Section
90 deg Section
180 deg Section
270 deg Section

Figure 5.7

Total Mass Flow = 0.24 Kg/s

Equal Admission Flow
ROTOR INLET
34000 RPM

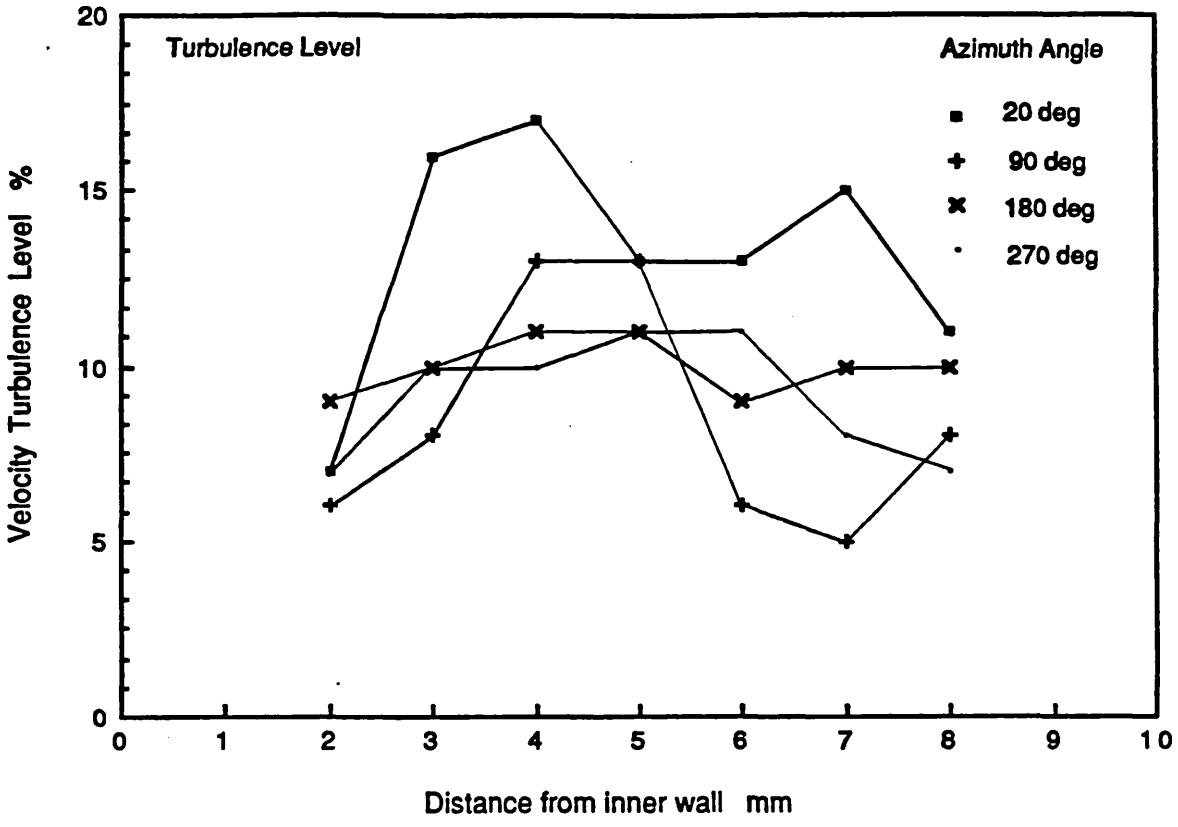


Fig 5.7b Velocity turbulence level% at different azimuth angles

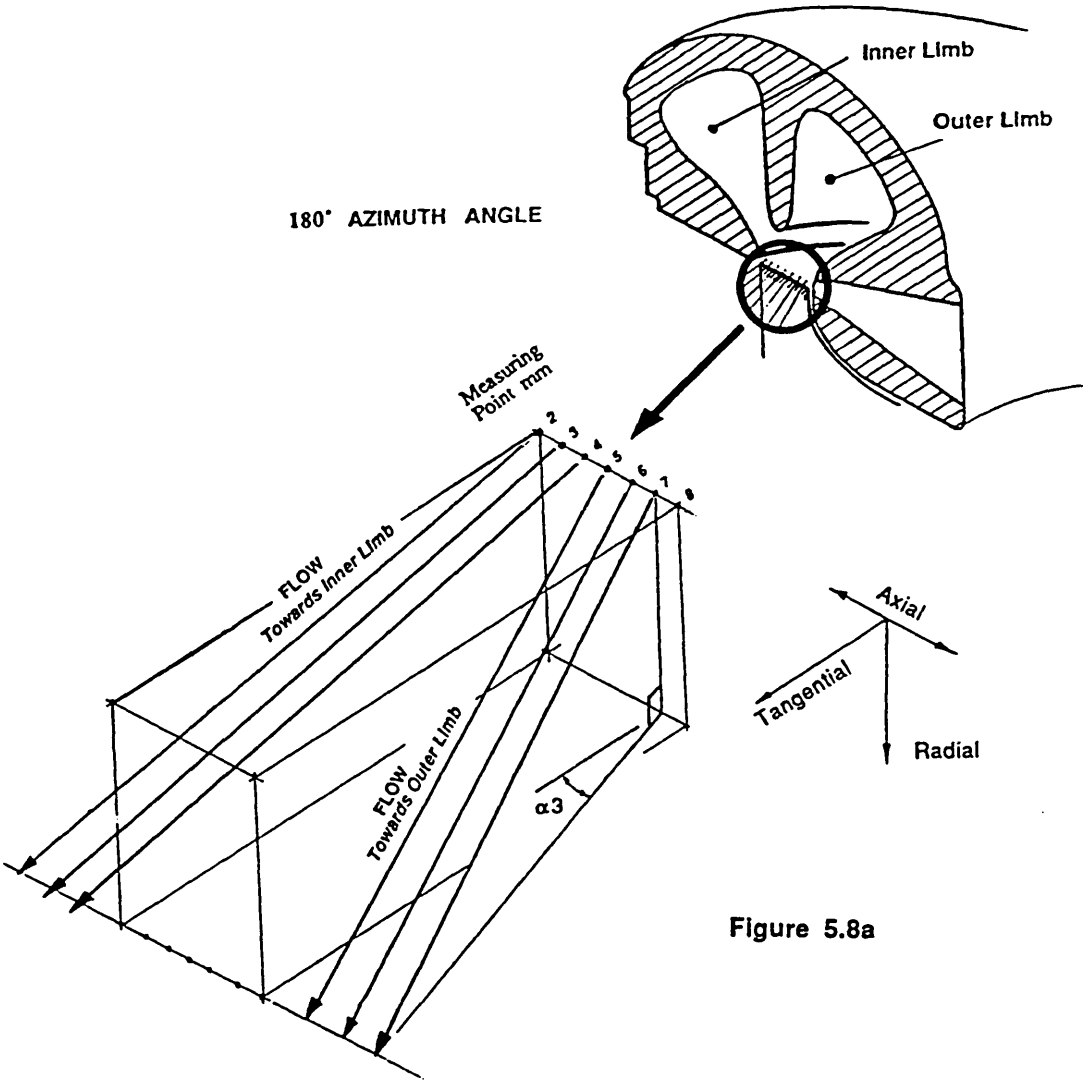
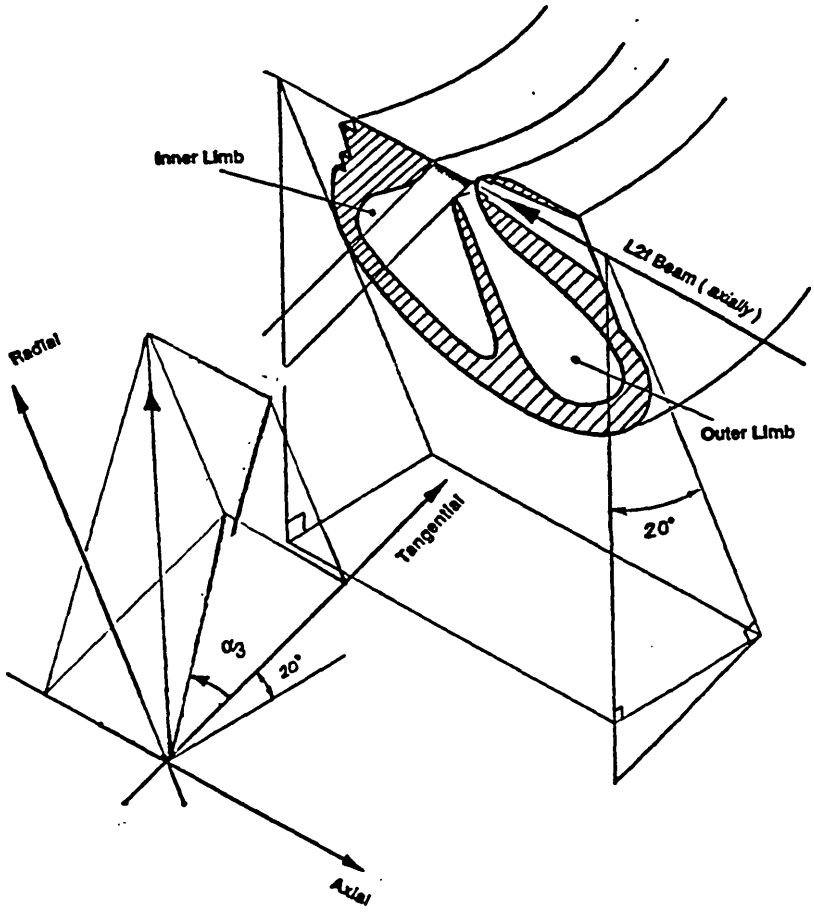


Figure 5.8a

Deviation of flow from radial plane, α_3 (deg)						
Distance from inner wall	2 mm	3 mm	4 mm	5 mm	6 mm	7 mm
U/C = 0.67	0.9° ↙	1.7° ↙	1.3° ↙	3.5° ↘	3.5° ↘	4.3° ↘
U/C = 0.57	2.6° ↙	4.3° ↙	5.2° ↙	8° ↘	7° ↘	6° ↘
U/C = 0.44	2.6° ↙	3.4° ↙	2.2° ↙	5.2° ↘	7° ↘	3.4° ↘

↘ Towards outer limb
↙ Towards inner limb

Figure 5.8b



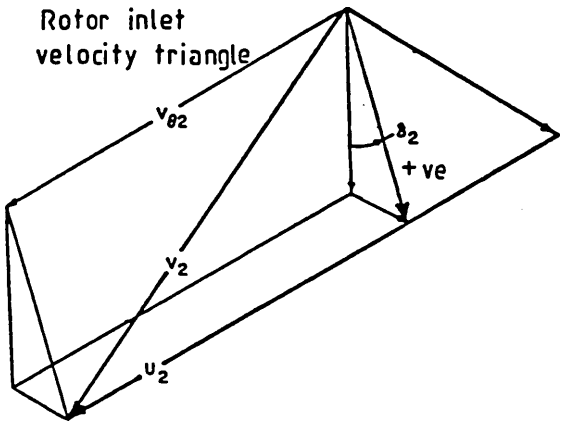
20° AZIMUTH ANGLE

Deviation of flow from radial plane, α_3 (deg)						
Distance from inner wall	2 mm	3 mm	4 mm	5 mm	6 mm	7 mm
0.13 kg/s	7 ↙	13 ↙	26 ↙	1.7 ↘	2.6 ↙	2.6 ↙
0.17 kg/s	5.2 ↙	8.7 ↙	26.7 ↙	4.7 ↙	—	1.6 ↙
0.24 kg/s	4.3 ↙	8.7 ↙	4.3 ↙	5 ↙	3.4 ↙	—

↘ Towards outer limb
↙ Towards inner limb

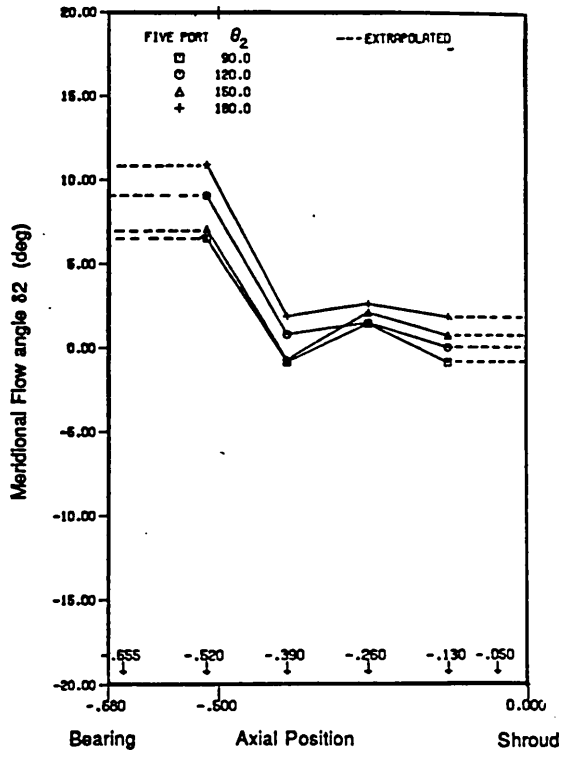
Figure 5.8c

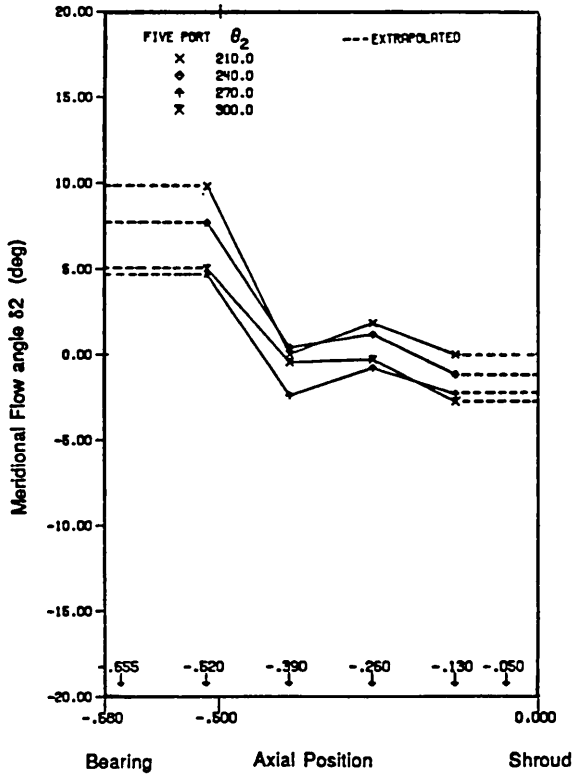
Flow deviation from radial plane at 20° azimuth angle.

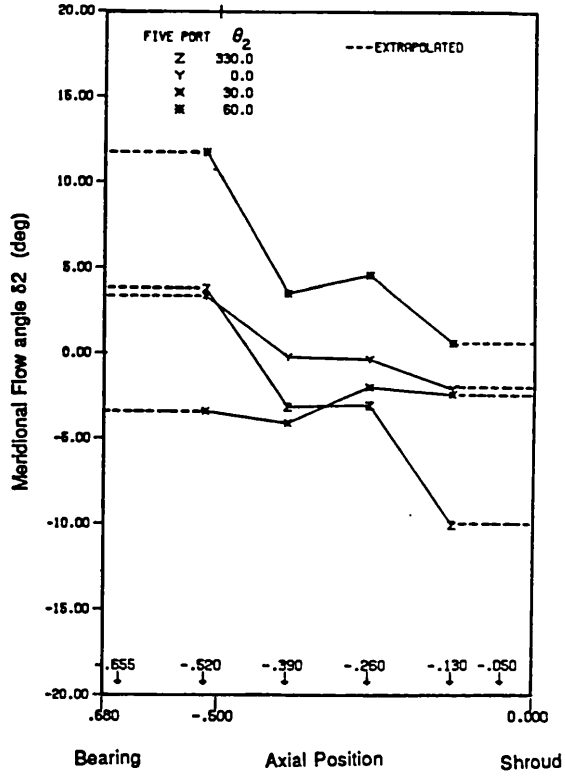


From velocity diagram

-Ve δ2 means flow towards bearing side (inner wall)

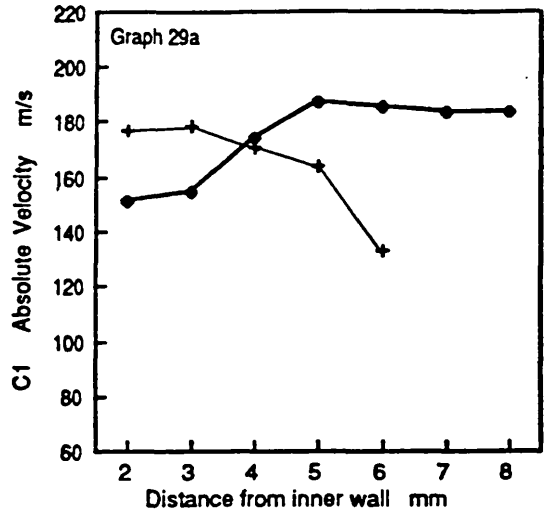


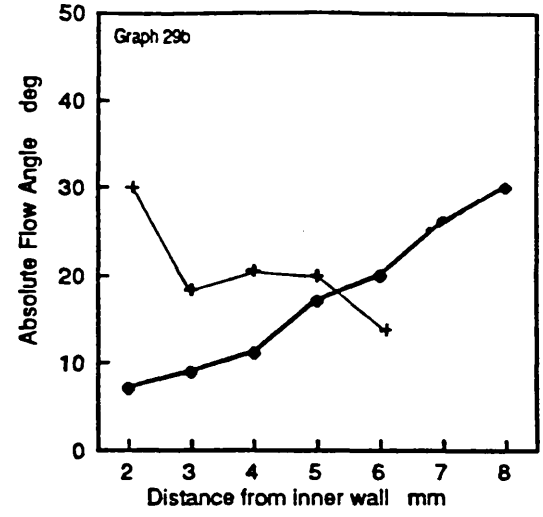


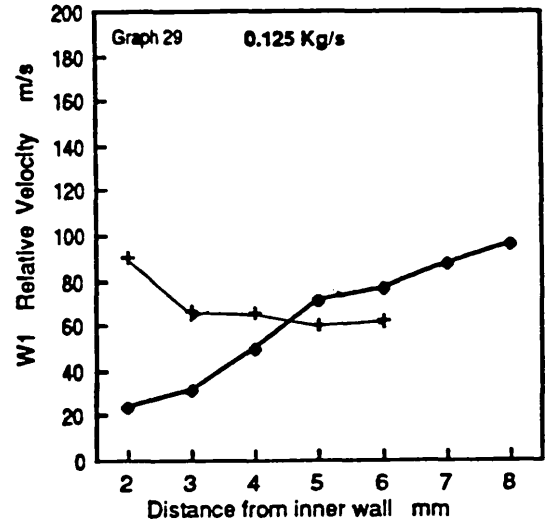


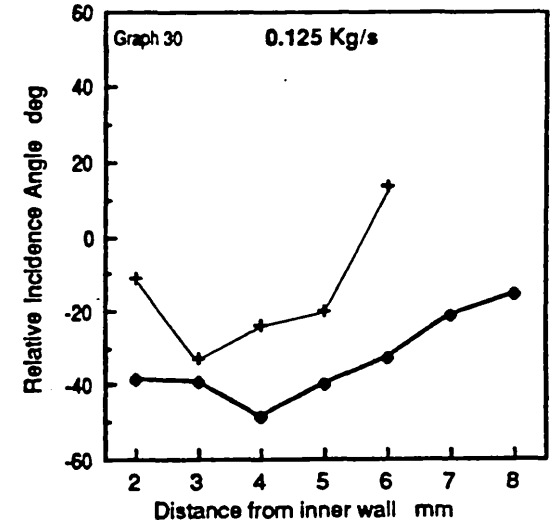
Axial Distribution of Twin Flow Housing Rotor Inlet Meridional Flow Angle by Miller (17)

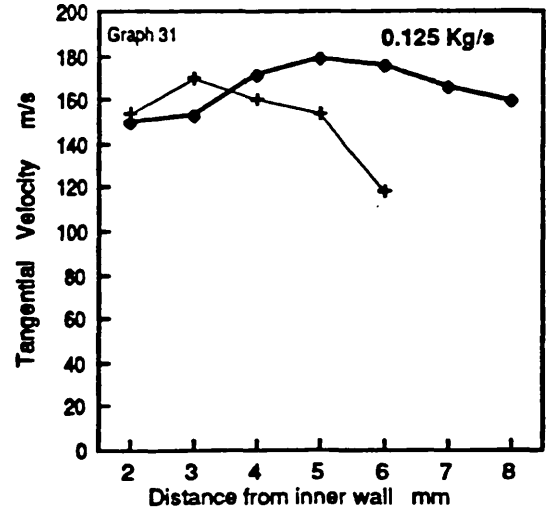
Figure 5.9

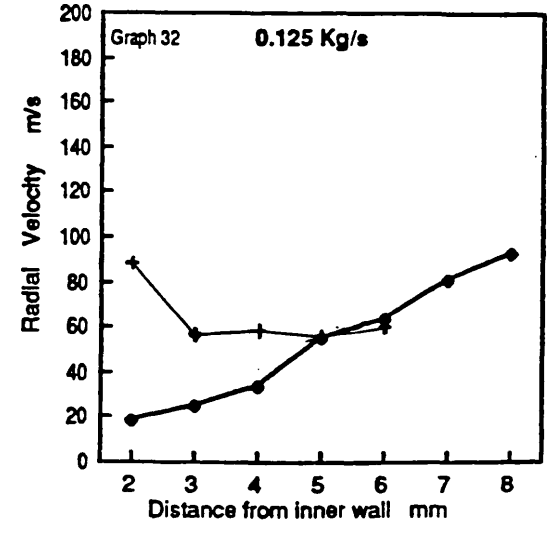










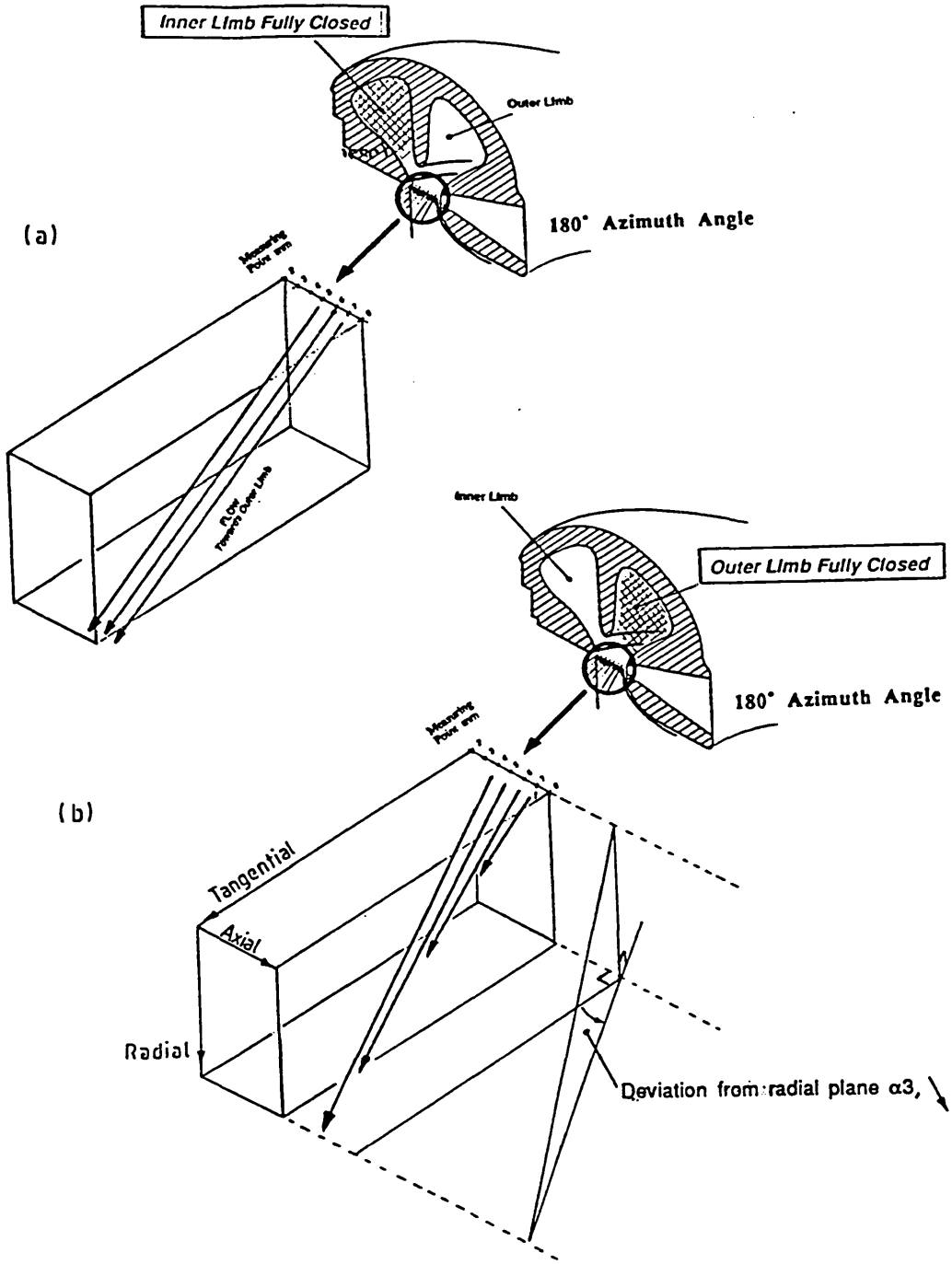


Inner Limb Closed
Outer Limb Closed

Figure 5.10

Total Mass Flow = 0.125 Kg/s

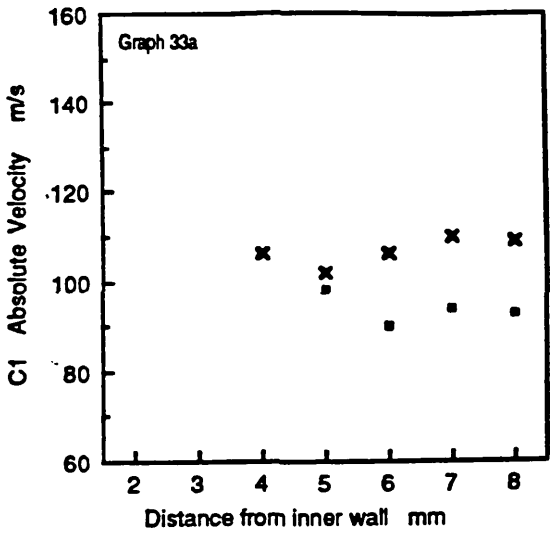
Partial Admission Flow
ROTOR INLET
34000 RPM
180° Azimuth Angle

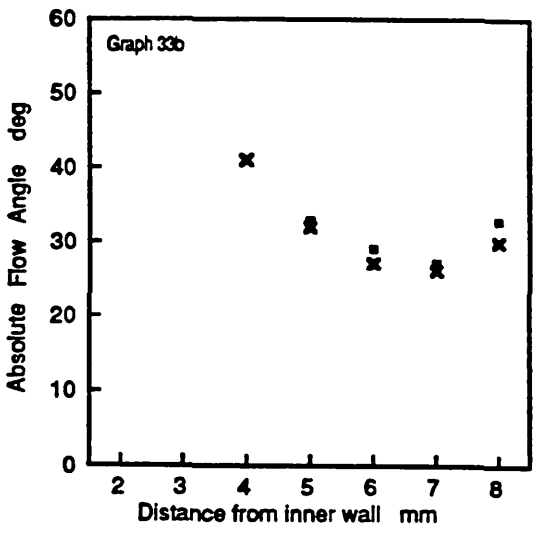


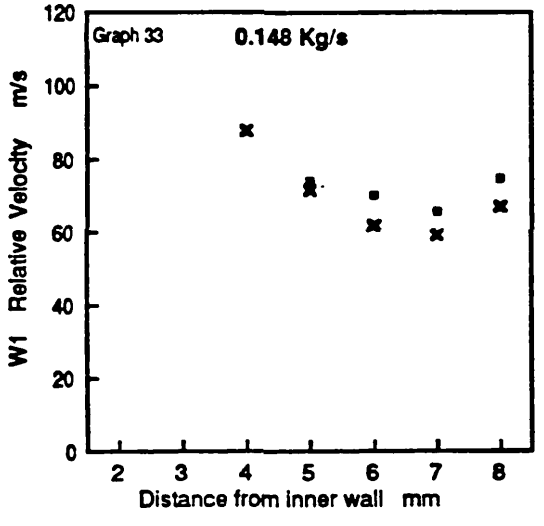
Deviation of flow from radial plane, α_3 (deg)						
Distance from inner wall	2 mm	3 mm	4 mm	5 mm	6 mm	7 mm
Outer limb fully closed	0° ↓	0° ↓	20° ↘	16° ↘	12° ↘	5° ↘
Inner limb fully closed		2.6° ↘	1.6° ↘	4.3° ↘	6° ↘	4° ↘

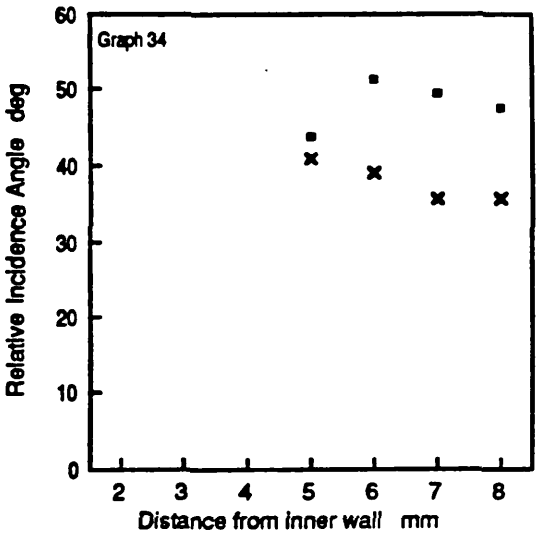
(c)

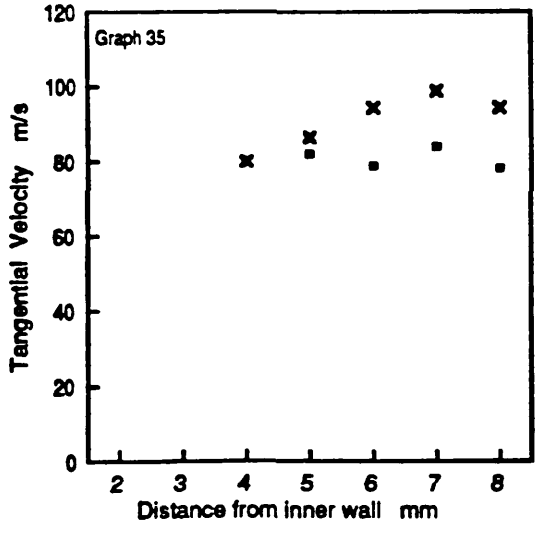
Figure 5.11











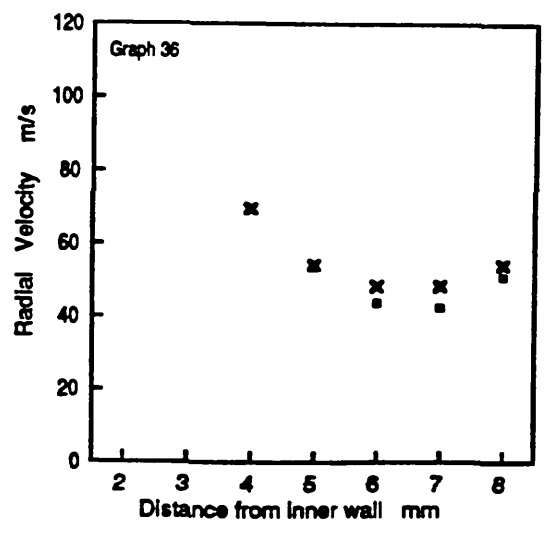


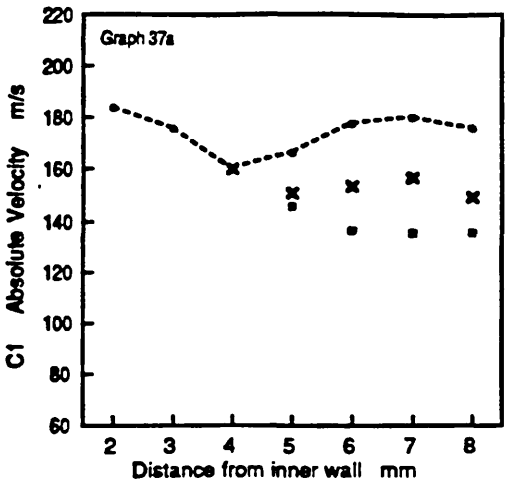
Figure 5.12

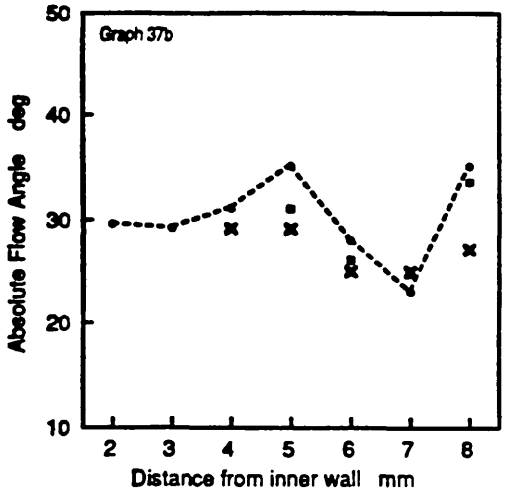
Mass Flow Ratio

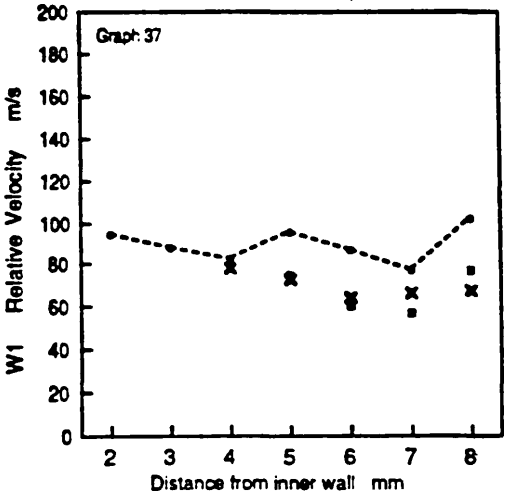
- inner limb / outer limb = 1.5
- inner limb / outer limb = 2.0

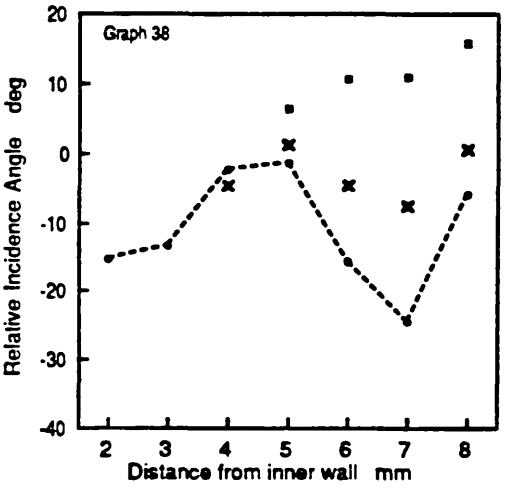
Total Mass Flow = 0.148 Kg/s

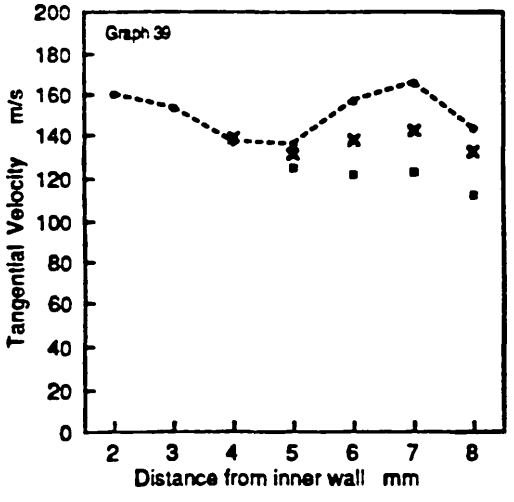
Partial Admission Flow
ROTOR INLET
34000 RPM
180° Azimuth Angle

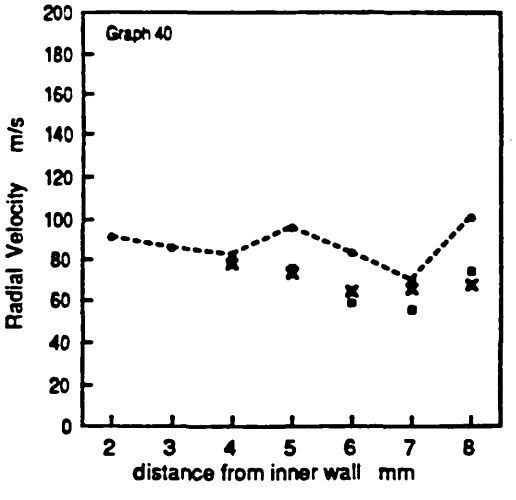












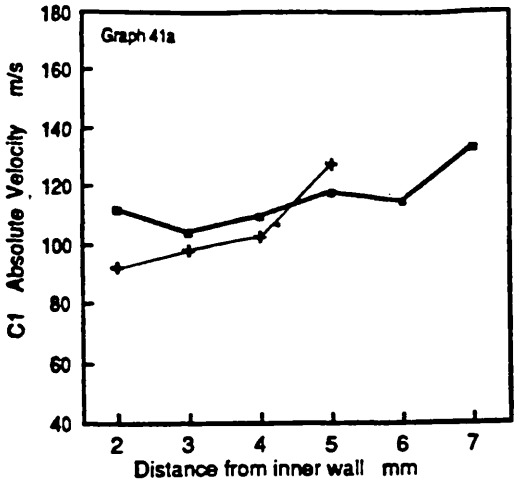
Mass Flow Ratio

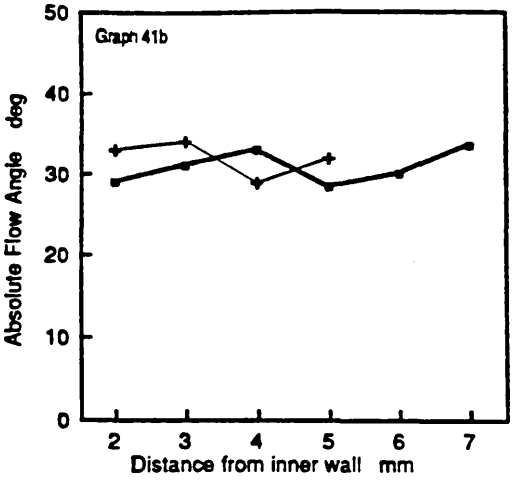
- Equal Admission
- Inner Limb / Outer Limb = 1.5
- Inner Limb / Outer Limb = 2.0

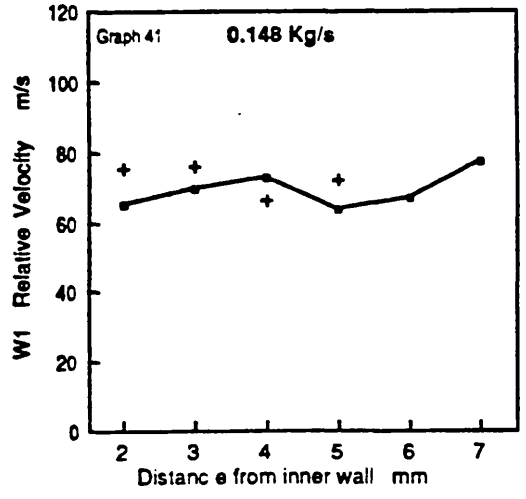
Figure 5.13

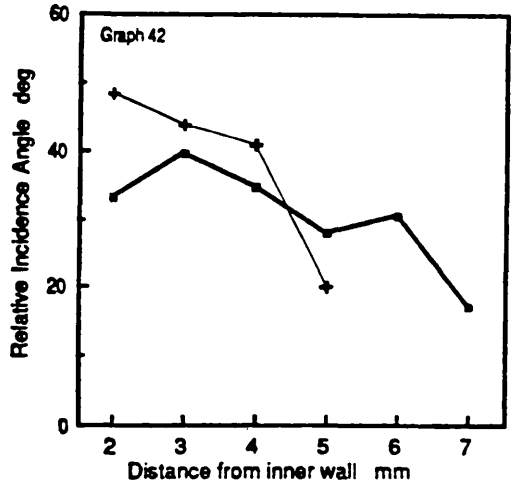
Total Mass Flow = 0.24 Kg/s

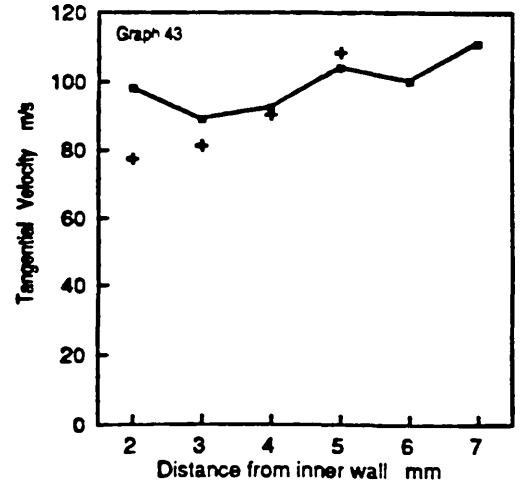
Partial Amission Flow
ROTOR INLET
34000 RPM
180° Azimuth Angle

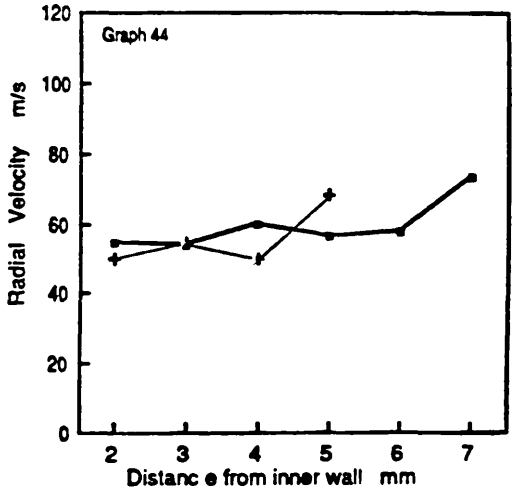












Mass Flow Ratio

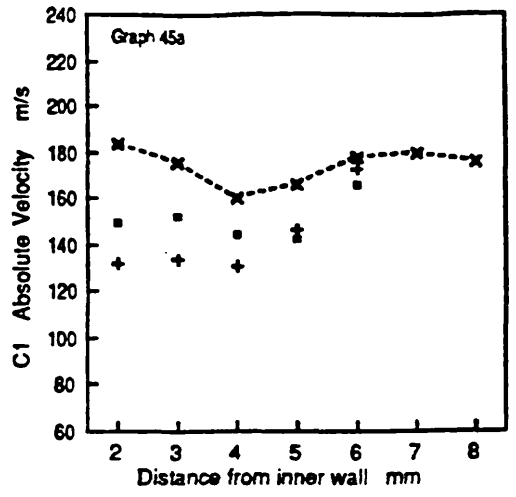
Inner Limb / Outer Limb = 0.67

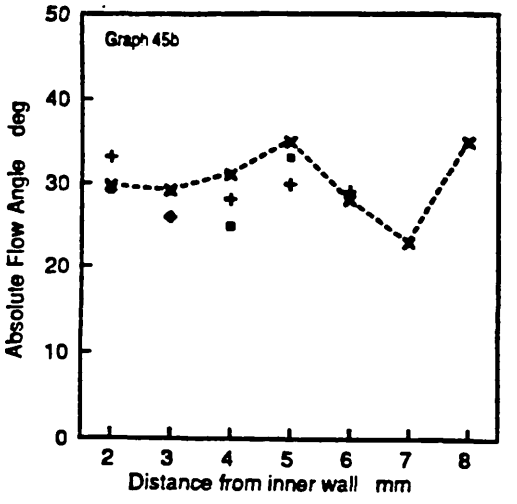
Inner Limb / Outer Limb = 0.5

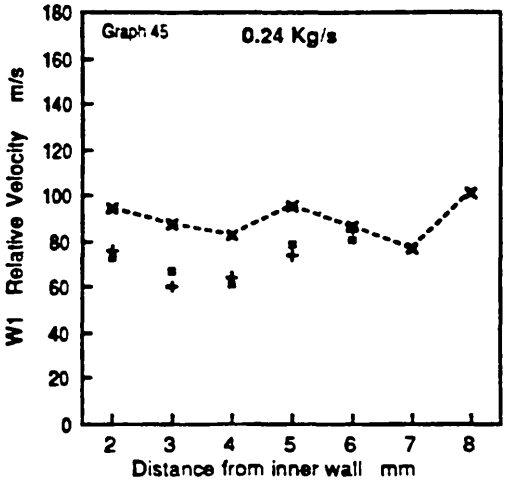
Figure 5.14

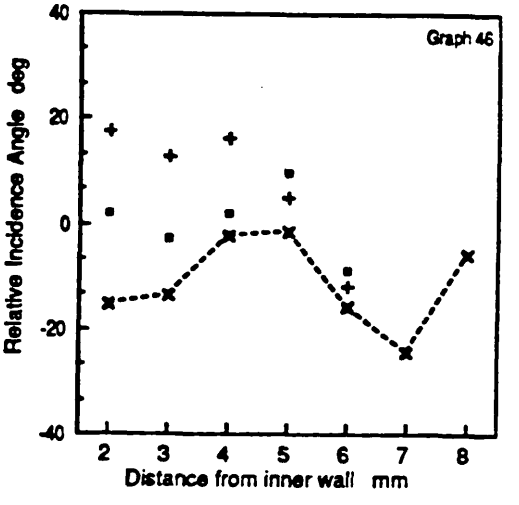
Total Mass Flow = 0.148 Kg/s

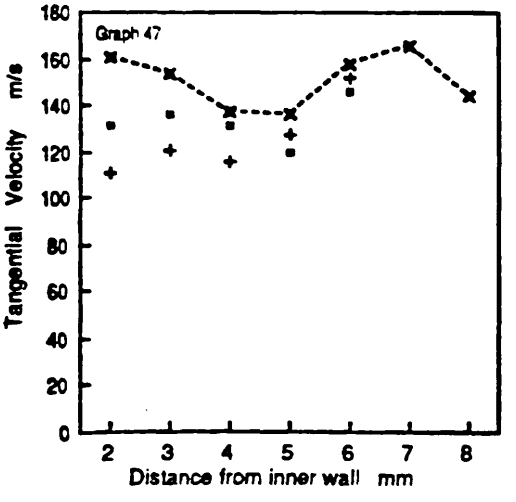
Partial Amission Flow
ROTOR INLET
34000 RPM
180° Azimuth Angle

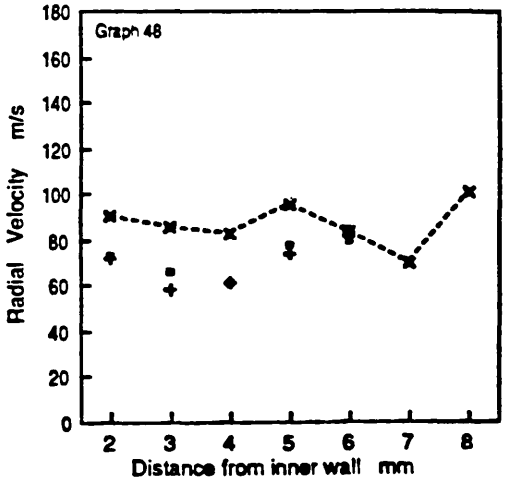












Equal Admission
Inner Limb / Outer Limb = 0.67
Inner Limb / Outer limb = 0.5

Figure 5.15

Total Mass Flow = 0.24 Kg/s

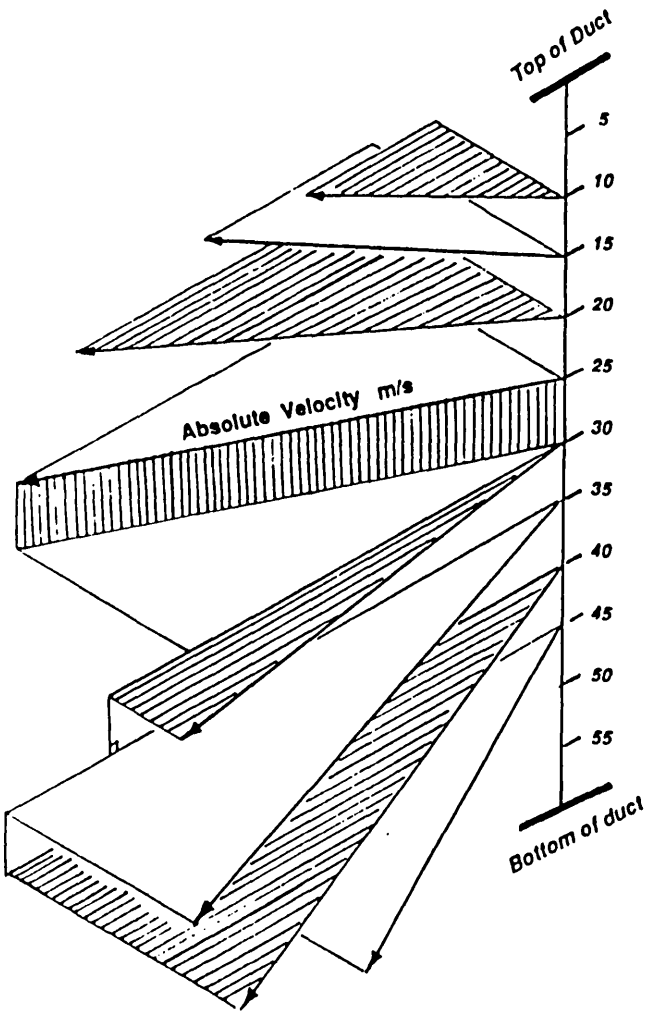
Partial Admission Flow
ROTOR INLET
34000 RPM
180° Azimuth Angle

Total Mass Flow = 0.24 Kg/s						
Distance from inner wall	2 mm	3 mm	4 mm	5 mm	6 mm	7 mm
$inner/outer = 2.0$				12° ↘	9° ↘	11° ↘
$inner/outer = 1.5$			17° ↙	12° ↘	10° ↘	7.7° ↘
Equal Admission	2.6° ↓	3.4° ↓	2.2° ↓	5.2° ↘	7° ↘	3.4° ↘
$inner/outer = 0.67$	5° ↙	7° ↙	4° ↙	16° ↘		
$inner/outer = 0.5$	3° ↙	3° ↙	15° ↘	18° ↘		

Total Mass Flow = 0.148 Kg/s						
Distance from inner wall	2 mm	3 mm	4 mm	5 mm	6 mm	7 mm
$inner/outer = 2.0$			18° ↘	16° ↘	5° ↙	2° ↙
$inner/outer = 1.5$				16° ↘	12° ↘	12° ↘
$inner/outer = 0.5$	4° ↙	5° ↙	10° ↘	9.5° ↘	8.7° ↘	
$inner/outer = 0.67$	4.3° ↓	5° ↙	14° ↘	12° ↘	16° ↘	

Deviation of flow from radial plane, α_3

Figure 5.16



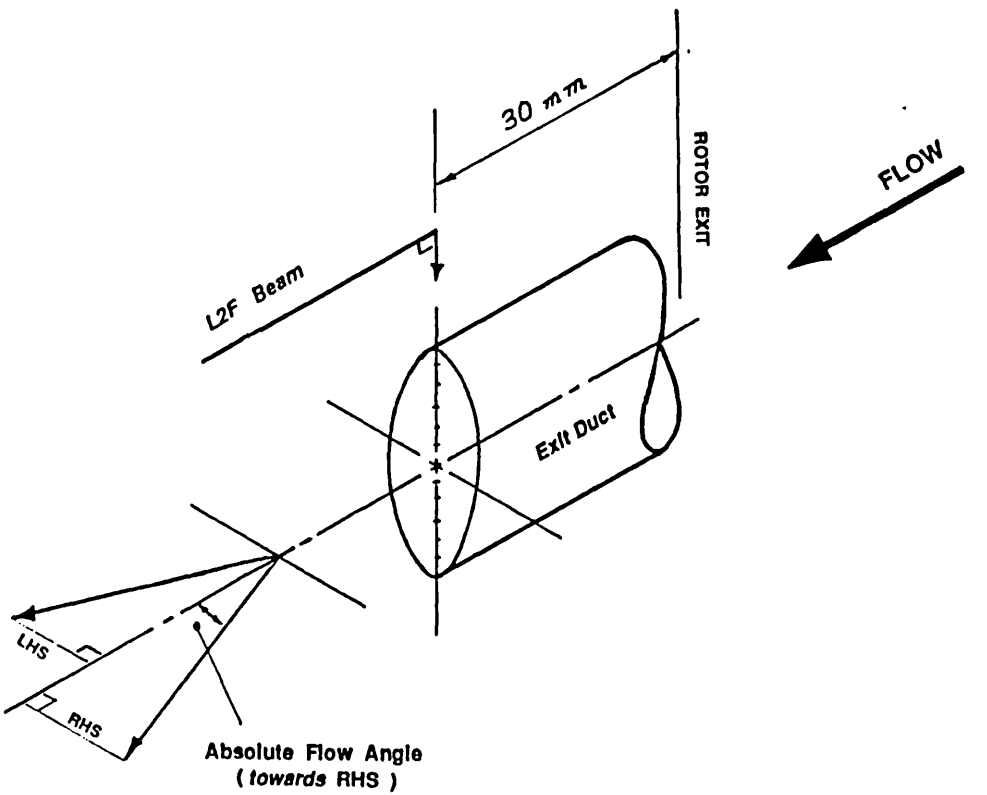


Figure 5.17

Note

L2F beam is directed into the exit duct via a mirror

Measurements are made along a vertical axis

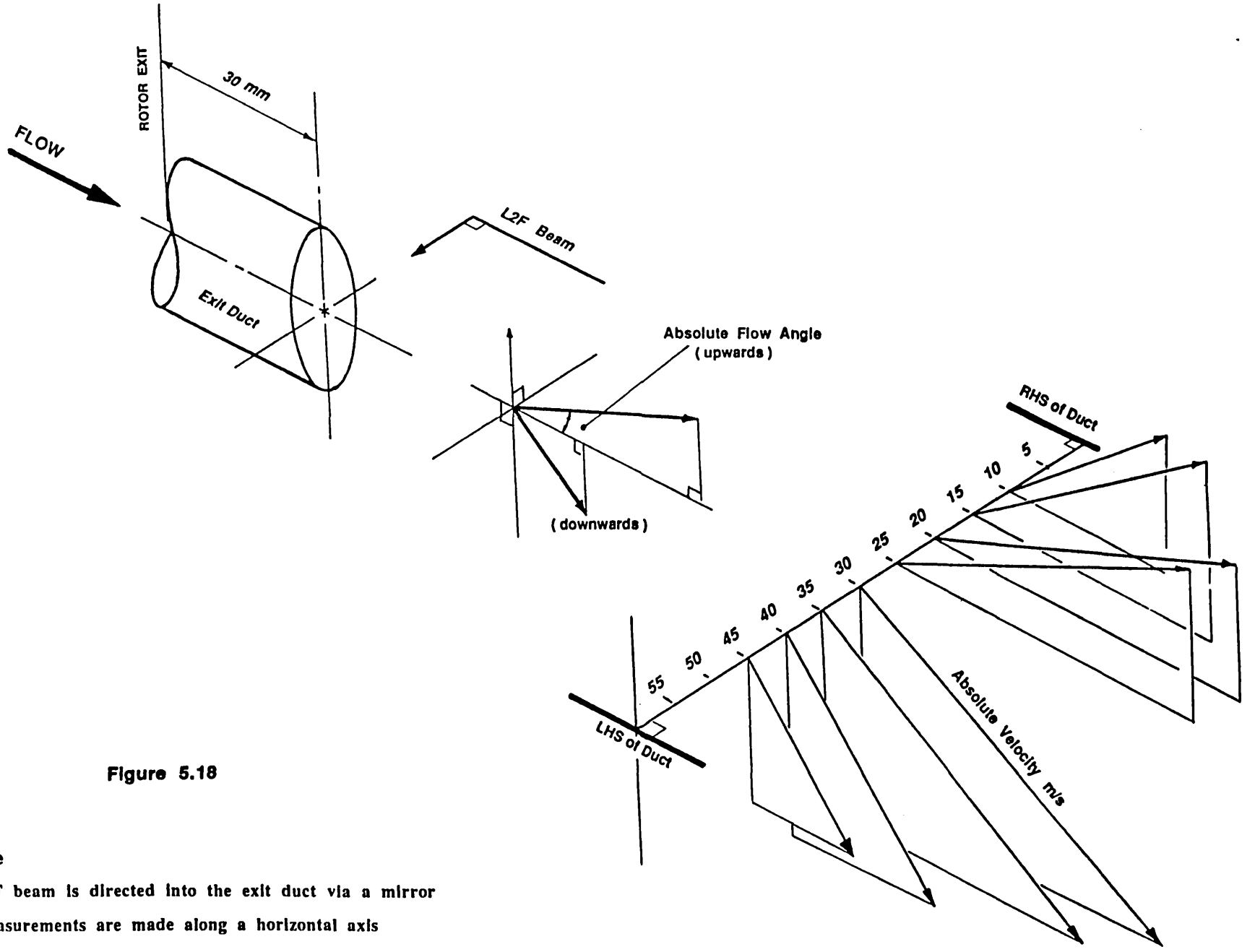
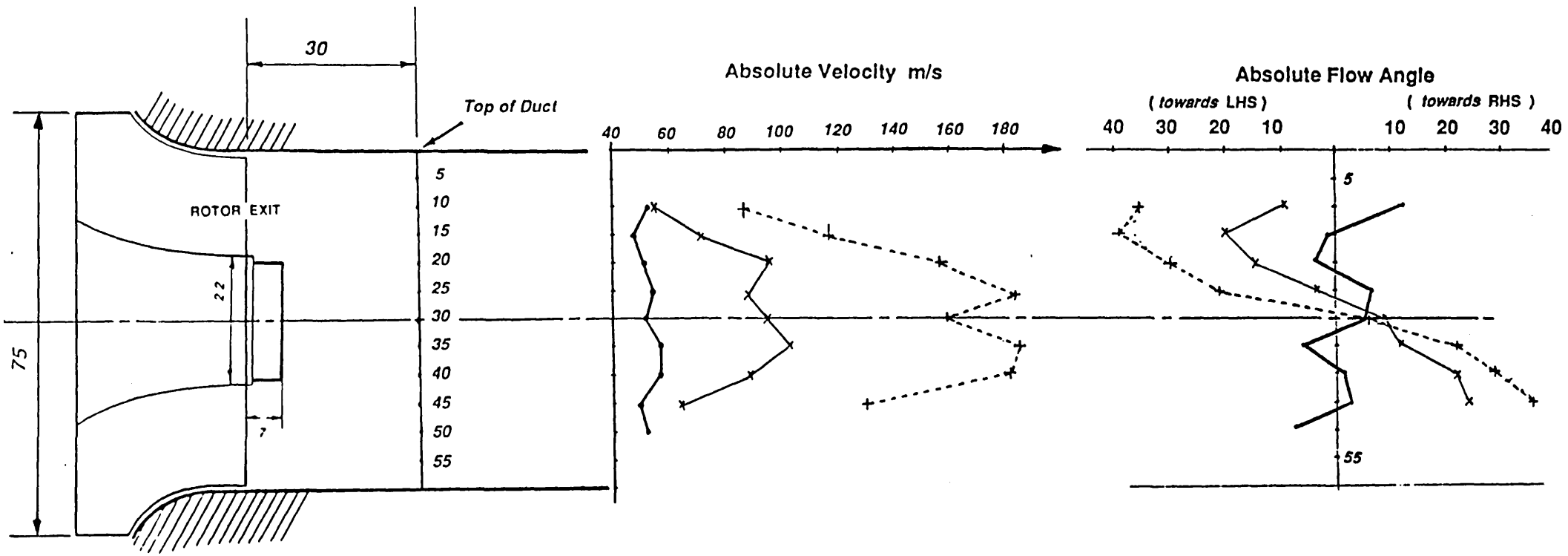


Figure 5.18

Note

L2F beam is directed into the exit duct via a mirror

Measurements are made along a horizontal axis



Rotor Exit Tip Clearance = 0.25 mm
(measured cold and stationary)
Diameter of Exit Duct = 60 mm

Figure 5.19a

Note

Axis of measurement is *Vertical*

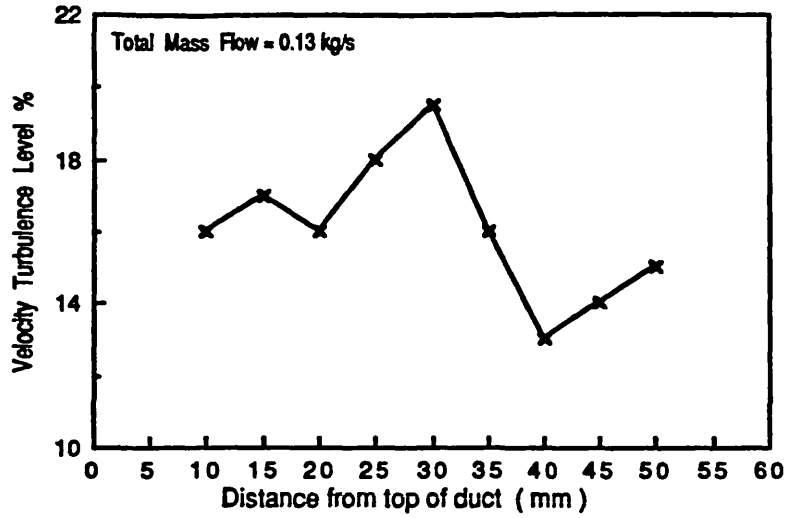
Total Mass Flow : 0.24 Kg/s

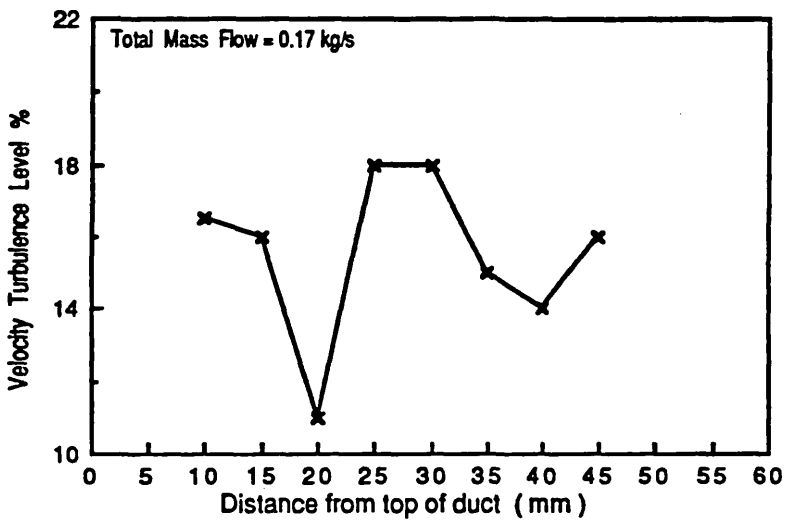
Total Mass Flow : 0.17 Kg/s

Total Mass Flow : 0.13 Kg/s

EQUAL ADMISSION FLOW

ROTOR EXIT





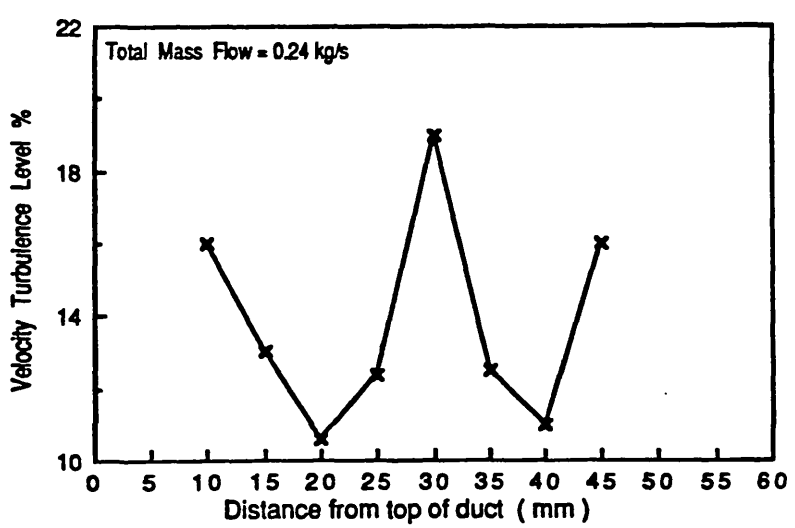
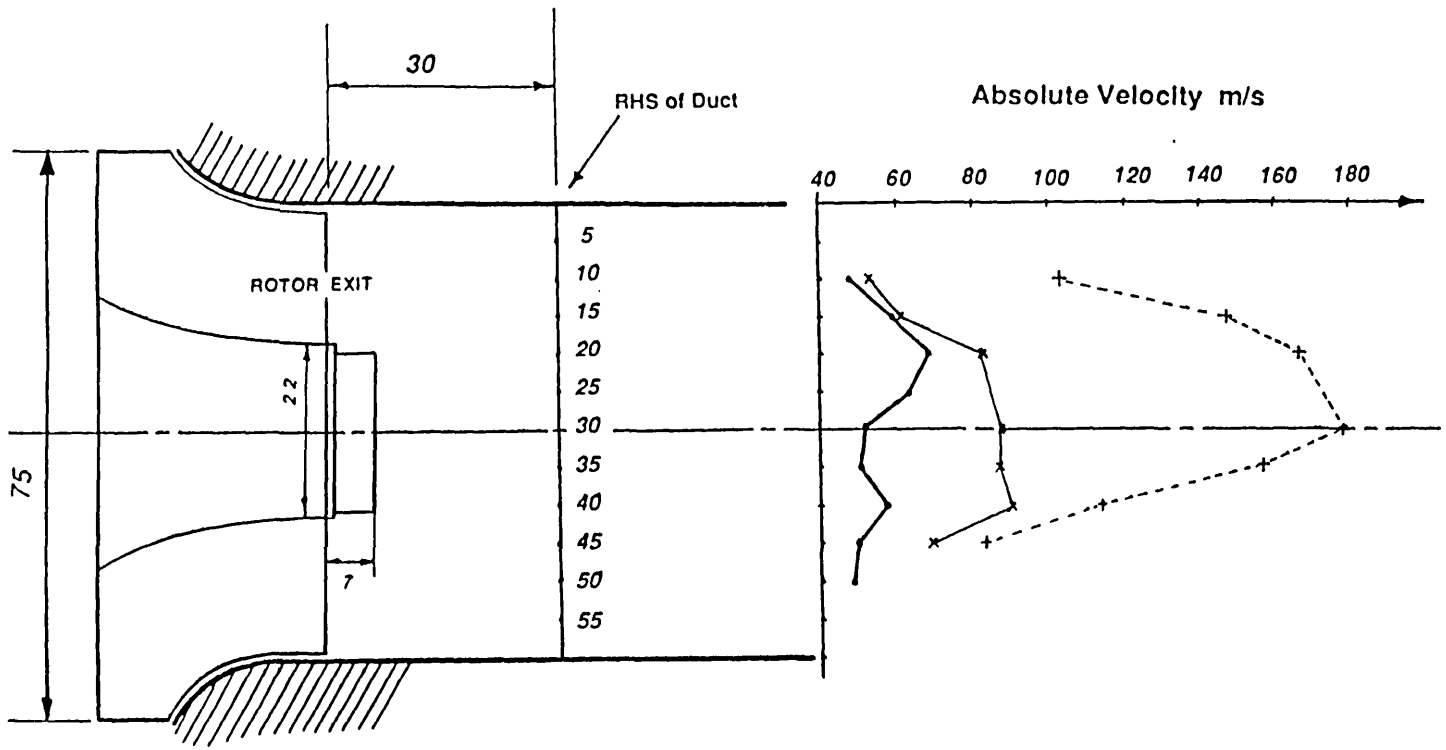
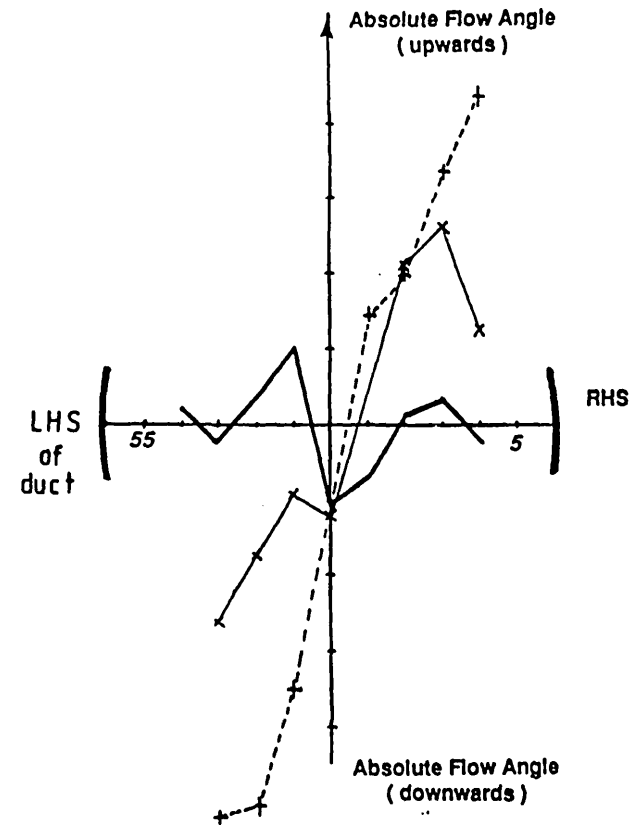


Figure 5.19b Turbulence Level at Rotor Exit



Rotor Exit Tip Clearance = 0.25 mm
(Measured cold and stationary)
Diameter of Exit Duct = 60 mm



Note
Axis of measurement is *Horizontal*

Figure 5.20

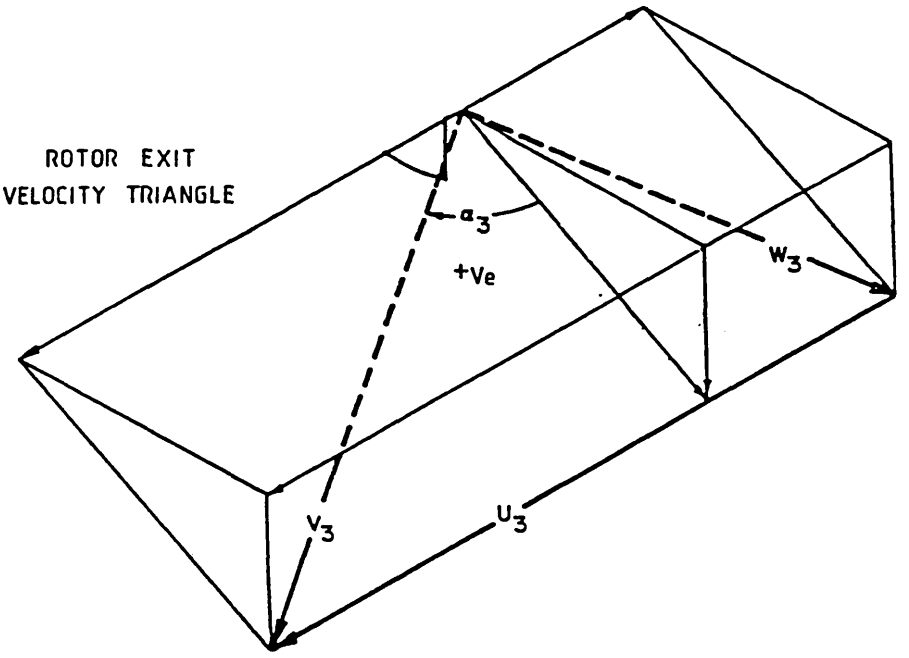
+------+ Total Mass Flow : 0.24 Kg/s

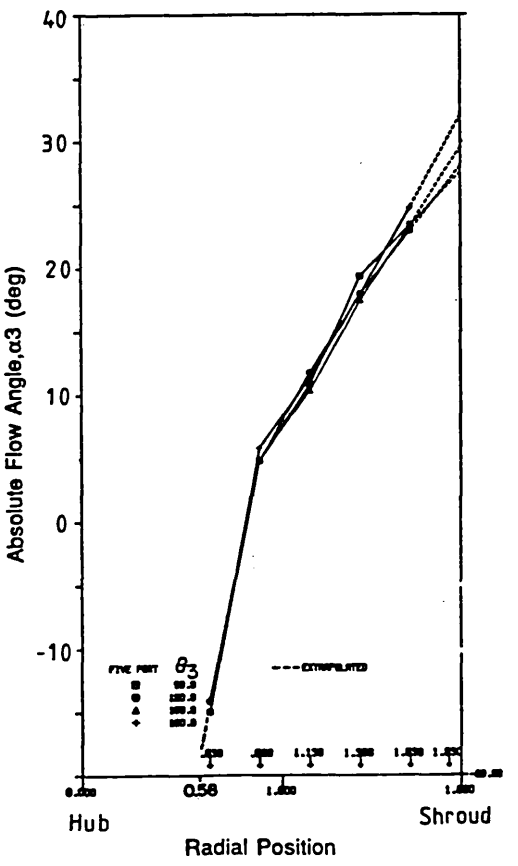
×------× Total Mass Flow : 0.17 Kg/s

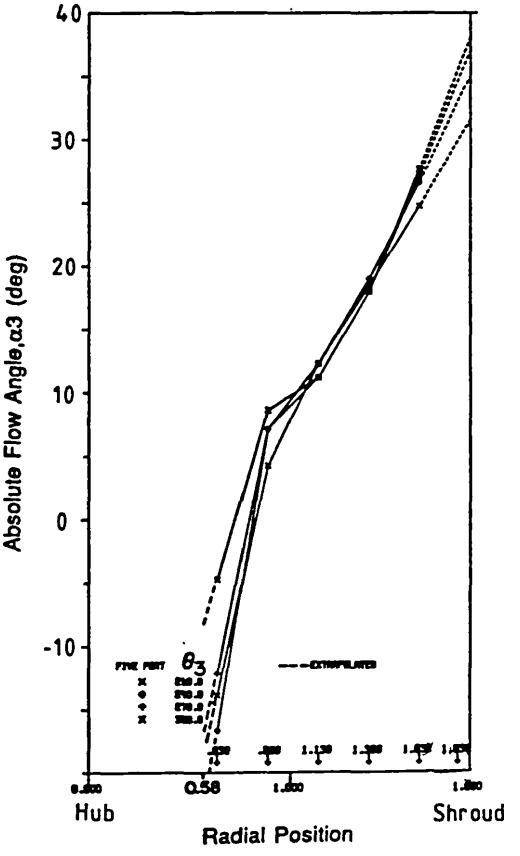
●——● Total Mass Flow : 0.13 Kg/s

EQUAL ADMISSION FLOW

ROTOR EXIT

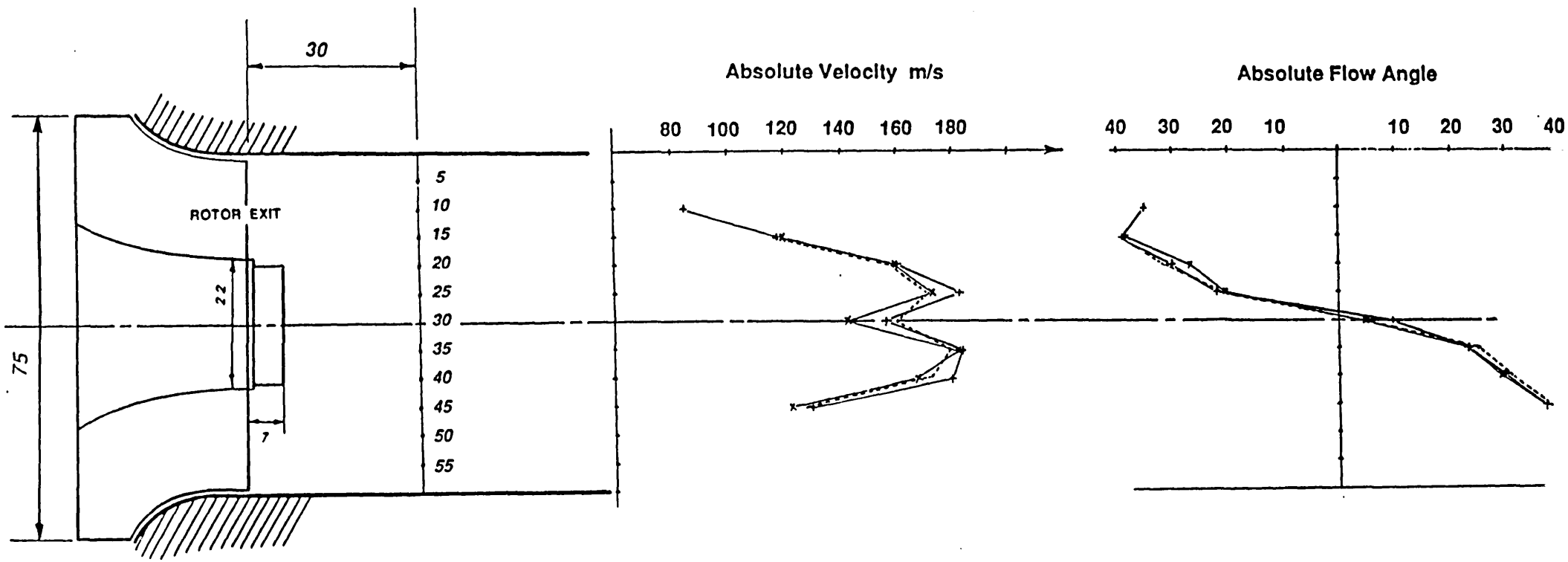






Radial Distribution of Rotor Exit Absolute Flow Angle by Miller (17)

Figure 5.21



Rotor Exit Tip Clearance = 0.25mm
(measured cold and stationary)
Diameter of Exit Duct = 60 mm

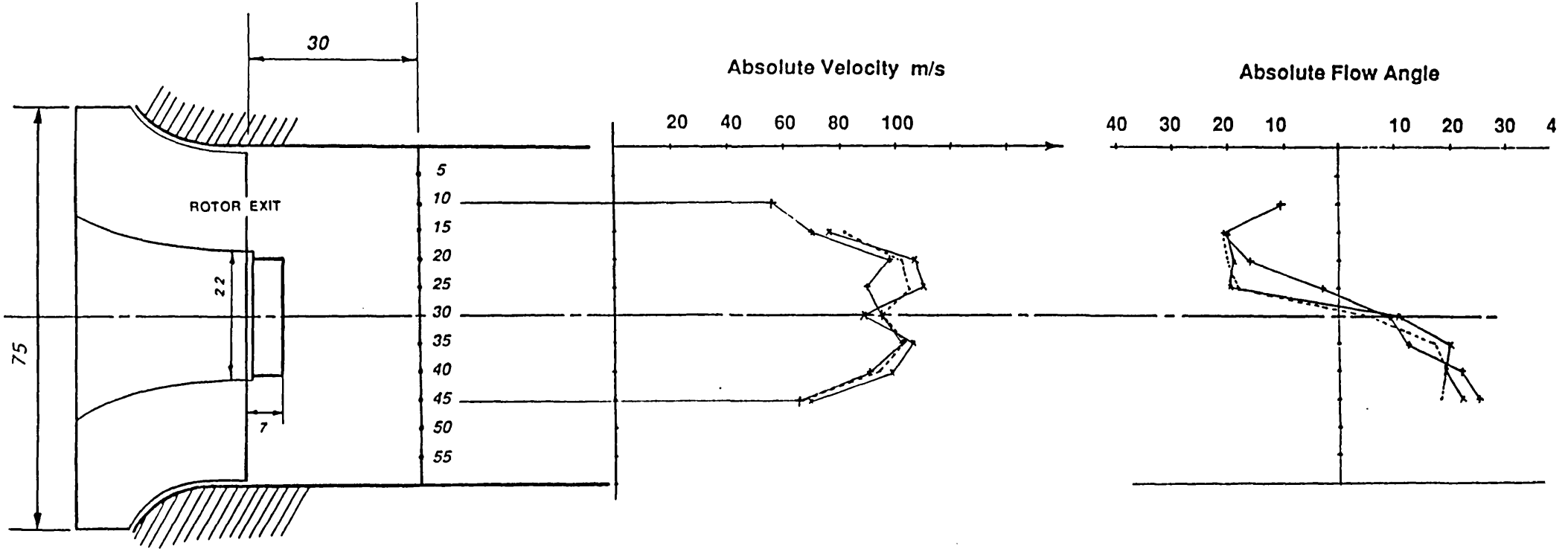
Figure 5.22

Axis of measurement is vertical

—+— Equal Admission Flow
—x— Mass Flow Ratio (inner / outer) = 0.667
- - - - - - Mass Flow Ratio (inner / outer) = 1.5

ROTOR EXIT

Total Mass Flow : 0.24 Kg/s



Rotor Exit Tip Clearance = 0.25 mm
(measured cold and stationary)
Diameter of Exit Duct = 60 mm

Figure 5.23

Axis of measurement is vertical

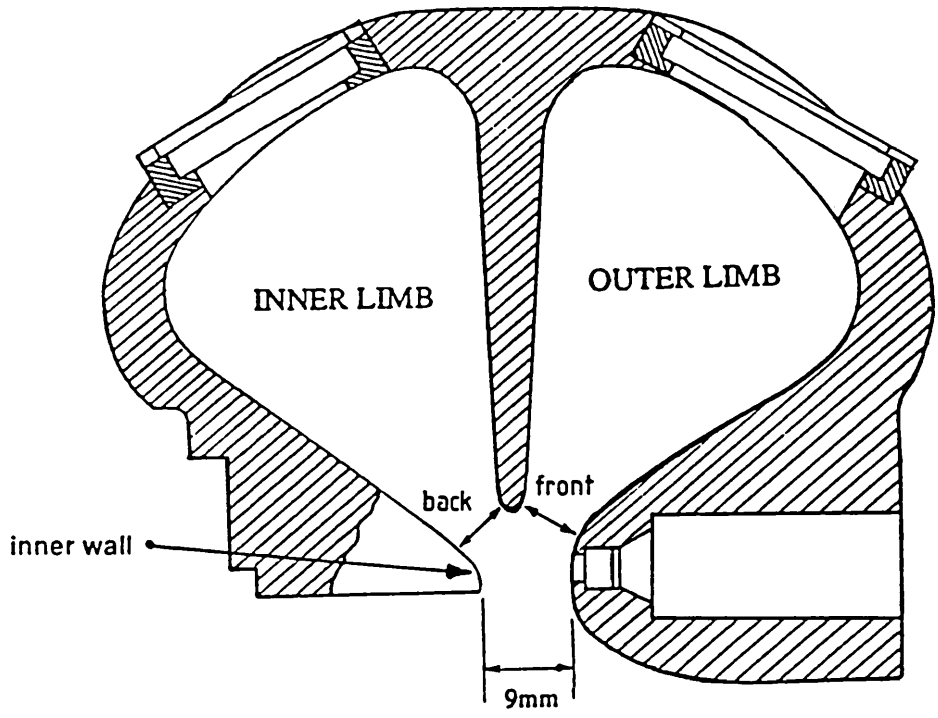
† EQUAL ADMISSION FLOW

x *Inner Limb Fully Closed*

..... *Outer Limb Fully Closed*

ROTOR EXIT

Total Mass Flow : 0.17 Kg/s



Minimum distance from divider tip to wall

	Azimuth Angle / SW ϕ mm	20°	90°	180°	270°
Back	80	4.00	3.98	3.63	3.53
	86	5.36	5.40	4.80	4.78
	90	6.80	6.55	6.10	6.26
	96	9.10	8.81	8.46	8.57
Front	80	5.33	5.25	4.70	4.70
	86	6.38	5.88	5.22	5.31
	90	7.95	7.91	7.40	7.45
	96	9.02	8.71	8.50	8.65

Figure 5.24

Equal Admission Flow 20° Azimuth Angle

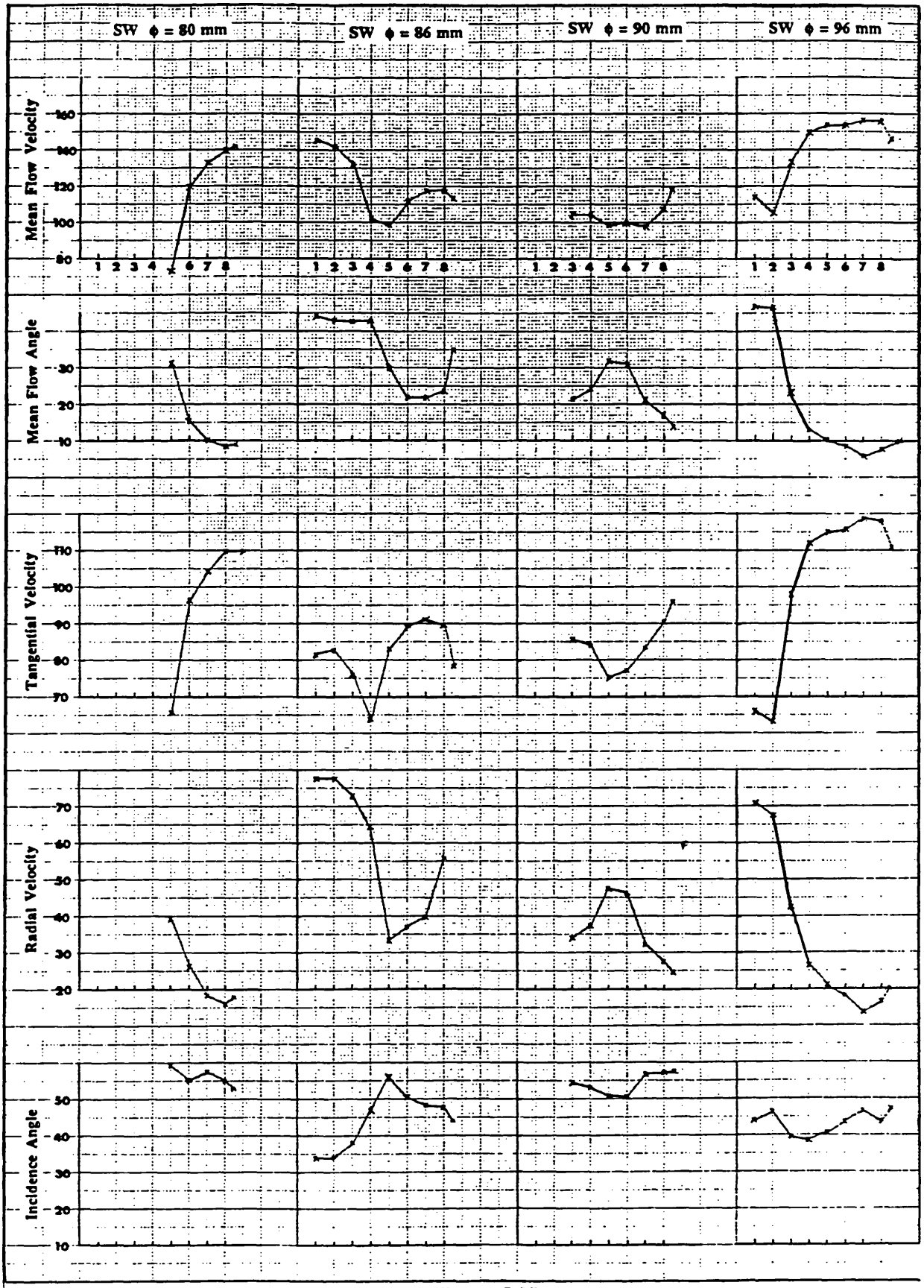


Figure 5.25a

Equal Admission Flow 90° Azimuth Angle

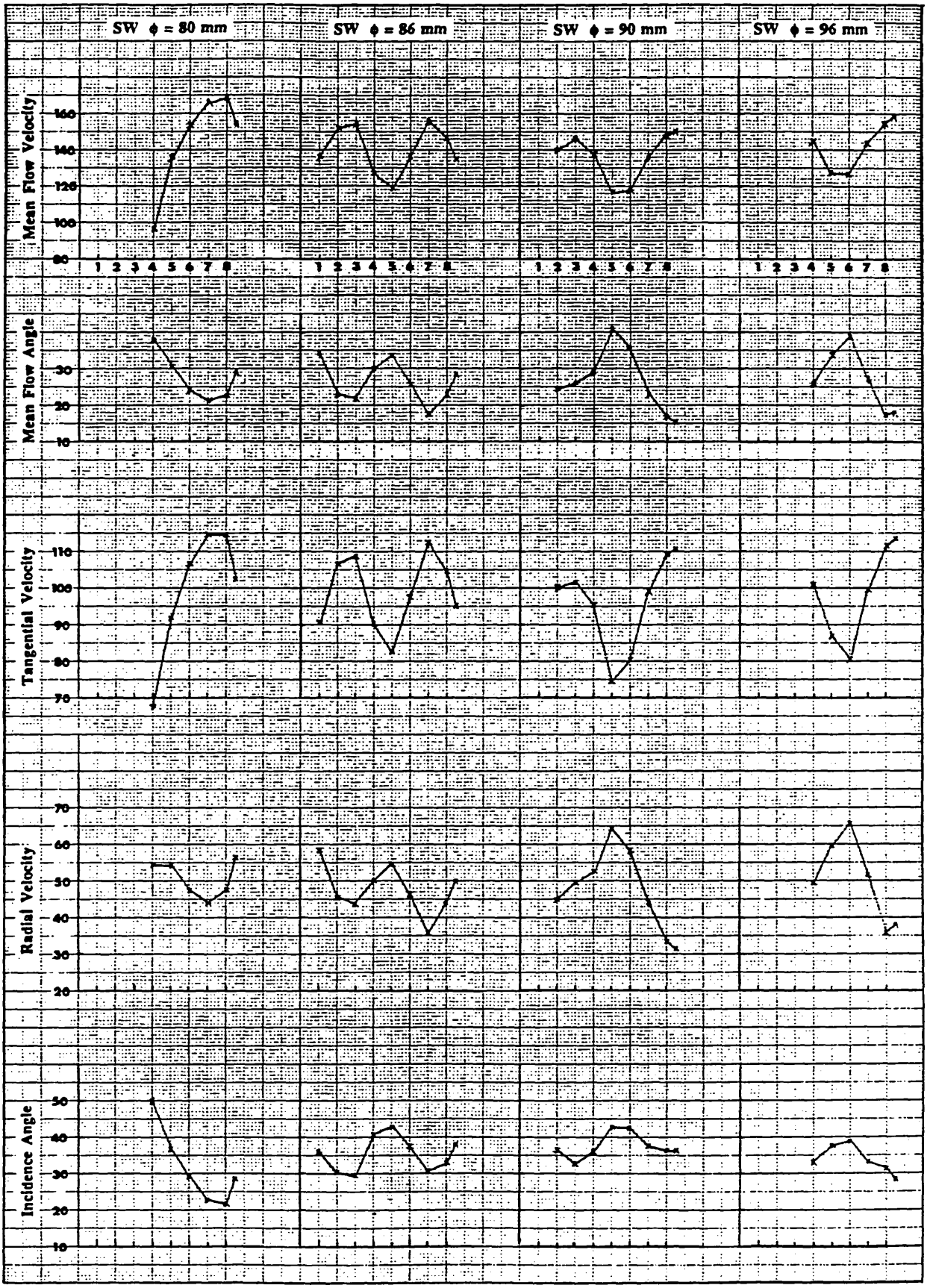


Figure 5.25b

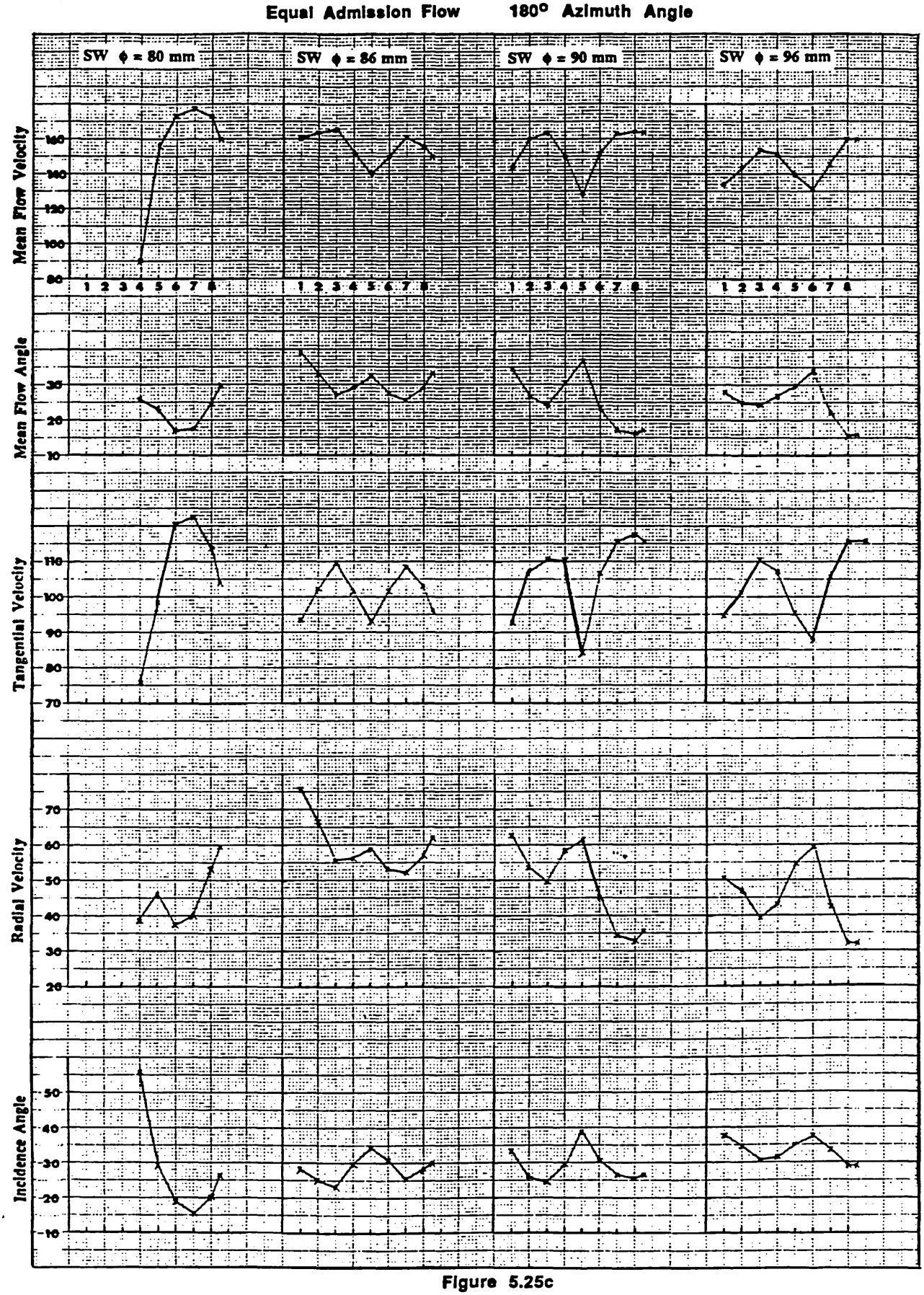

Equal Admission Flow 180° Azimuth Angle
SW ϕ = 80 mm
SW ϕ = 86 mm
SW ϕ = 90 mm
SW ϕ = 96 mm
Mean Flow Velocity
Mean Flow Angle
Tangential Velocity
Radial Velocity
Incidence Angle

Figure 5.25c

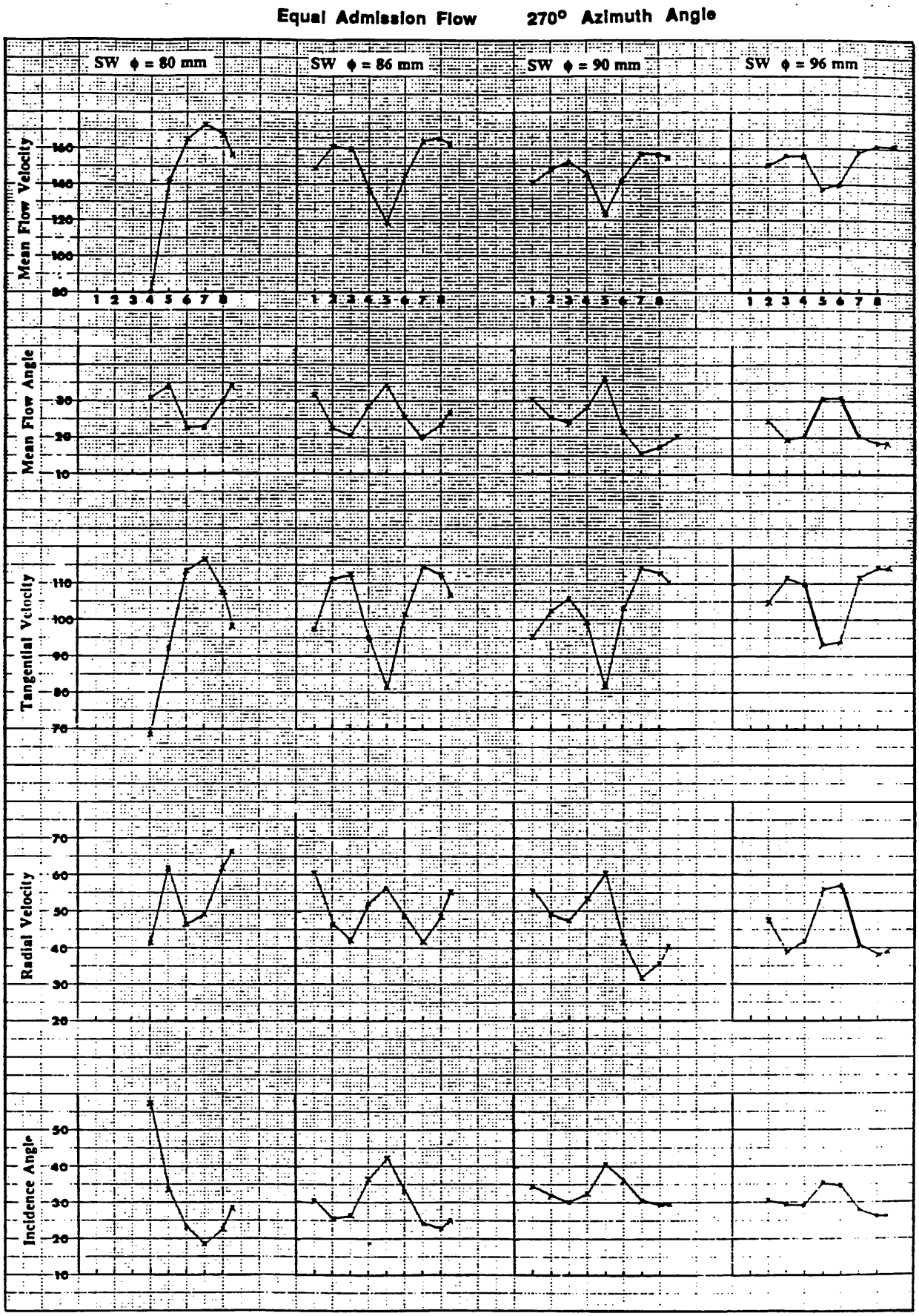
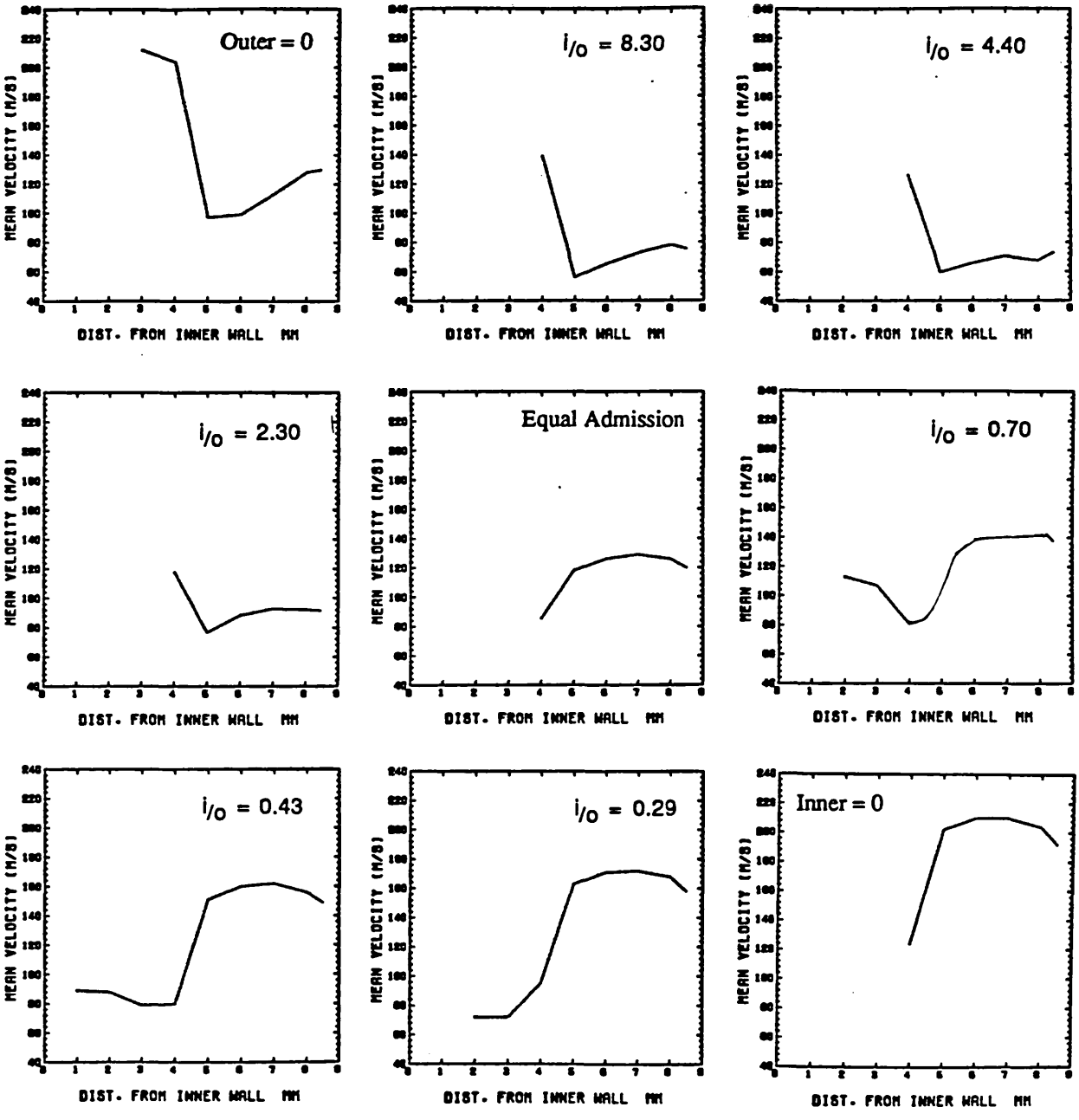

Equal Admission Flow 270° Azimuth Angle
SW ϕ = 80 mm
SW ϕ = 86 mm
SW ϕ = 90 mm
SW ϕ = 96 mm
Mean Flow Velocity
Mean Flow Angle
Tangential Velocity
Radial Velocity
Incidence Angle

Figure 5.25d

Flow Velocity

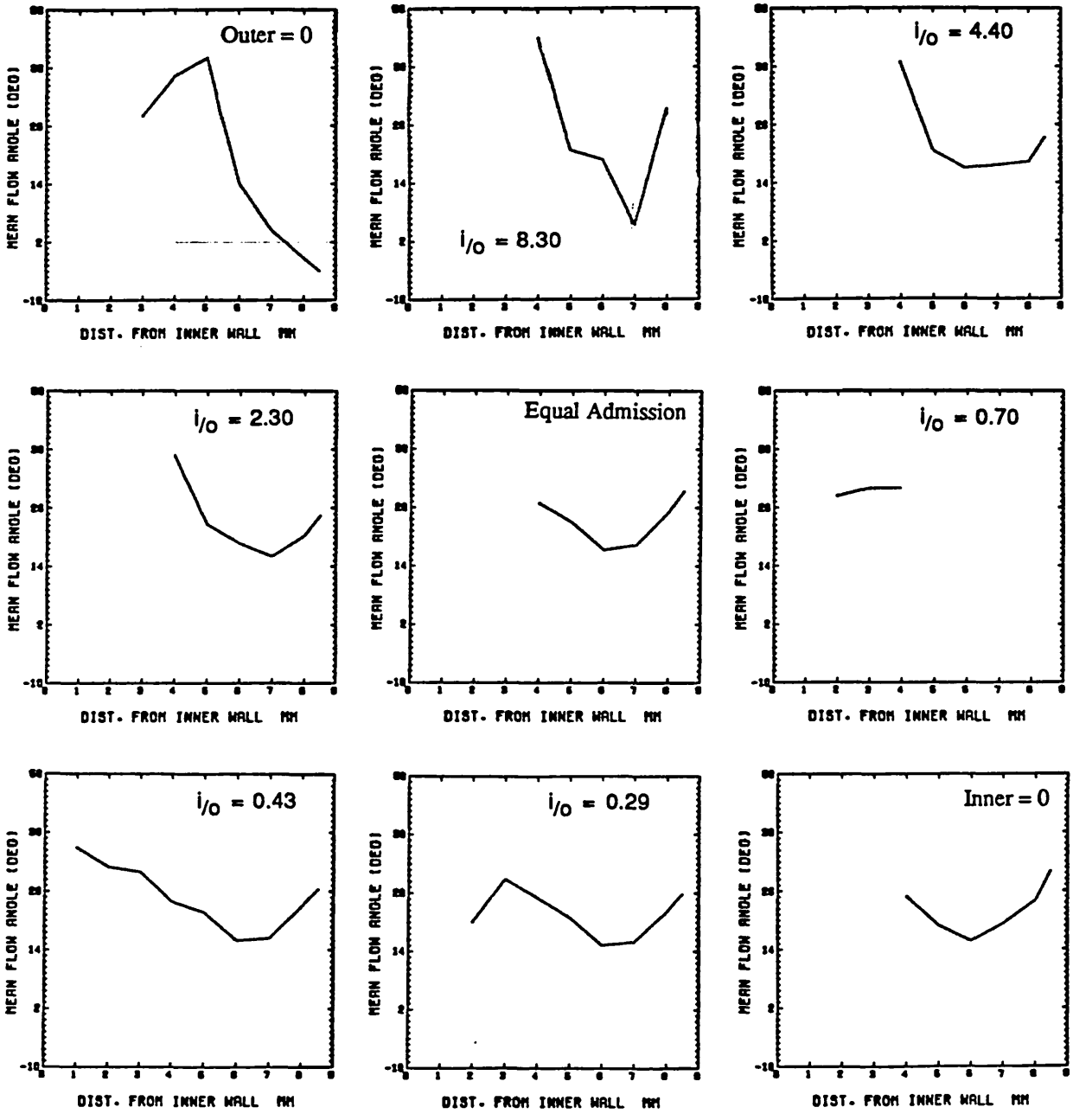


Equal Admission : Equal admission flow in each limb
Inner = 0 : Inner limb is fully closed
Outer = 0 : Outer limb is fully closed
i/o : Mass flow ratio of $\frac{\text{innerlimb}}{\text{outer limb}}$

SW ϕ = 80 mm

Figure 5.26a

Flow Angle

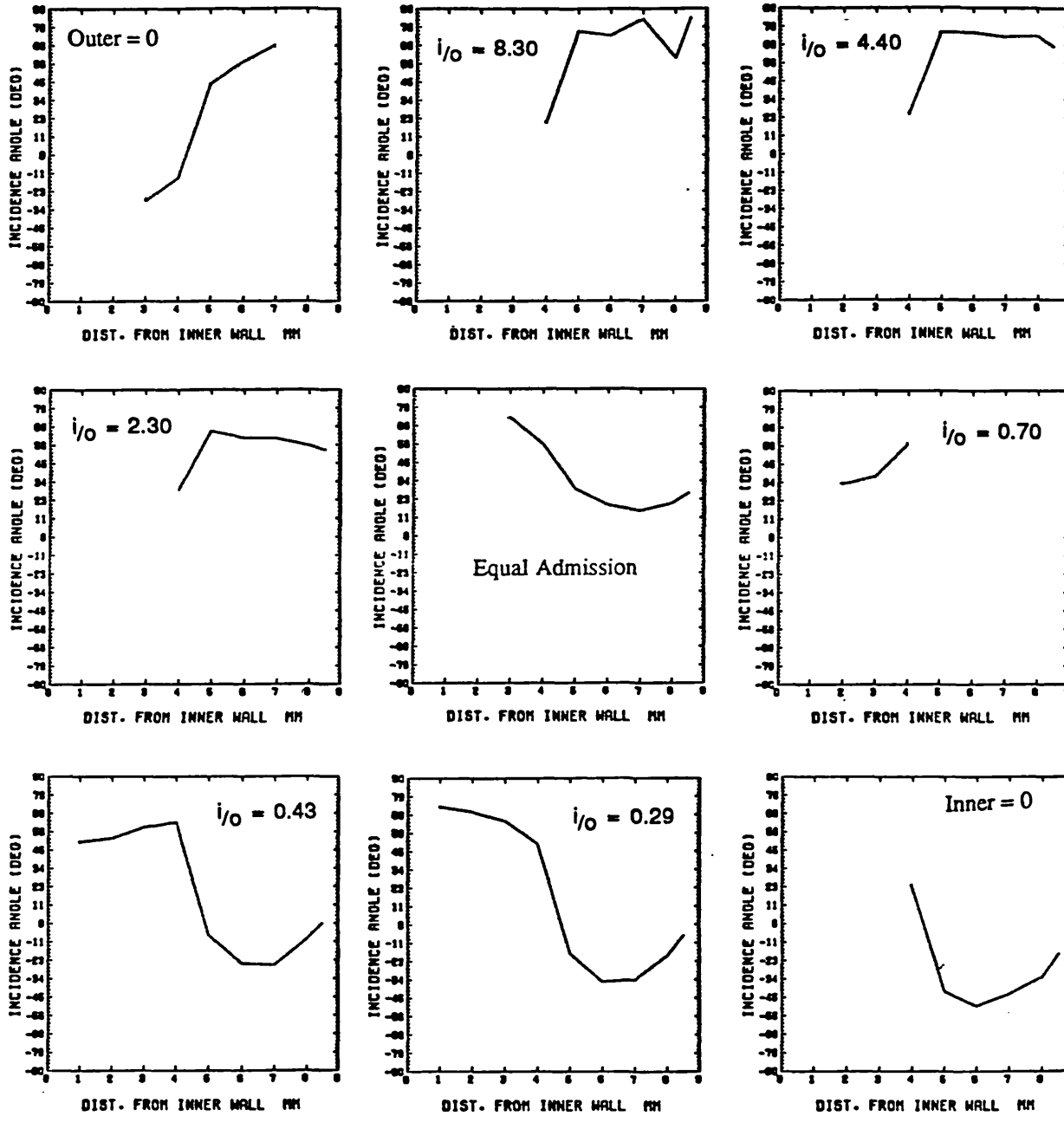


Equal Admission : Equal admission flow in each limb
Inner = 0 : Inner limb is fully closed
Outer = 0 : Outer limb is fully closed
i_o : Mass flow ratio of $\text{innerlimb}_{/\text{outer limb}}$

SW ϕ = 80 mm

Figure 5.26b

Incidence Angle

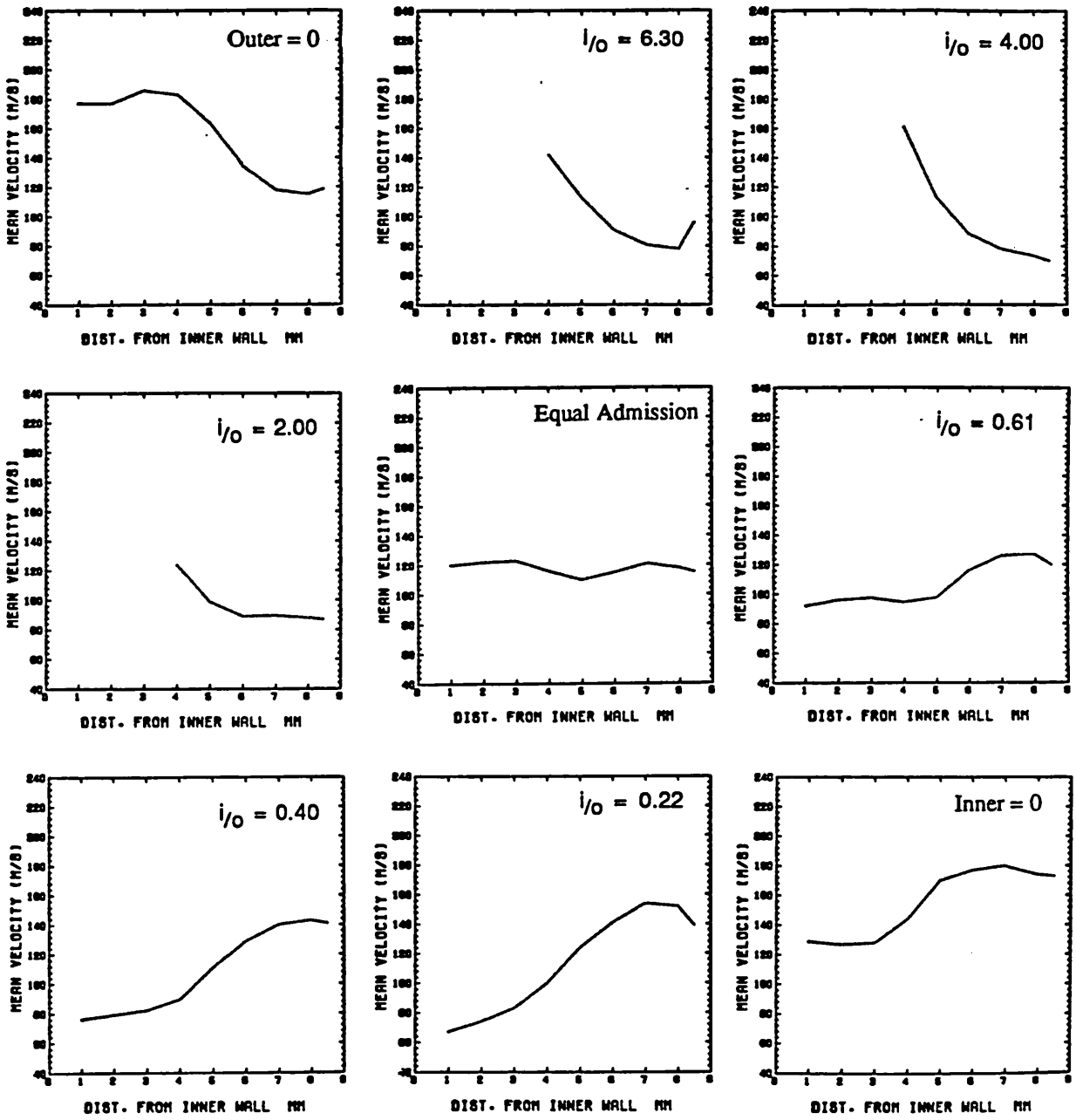


Equal Admission : Equal admission flow in each limb
Inner = 0 : Inner limb is fully closed
Outer = 0 : Outer limb is fully closed
i/o : Mass flow ratio of innerlimb/outer limb

SW ϕ = 80 mm

Figure 5.26c

Flow Velocity

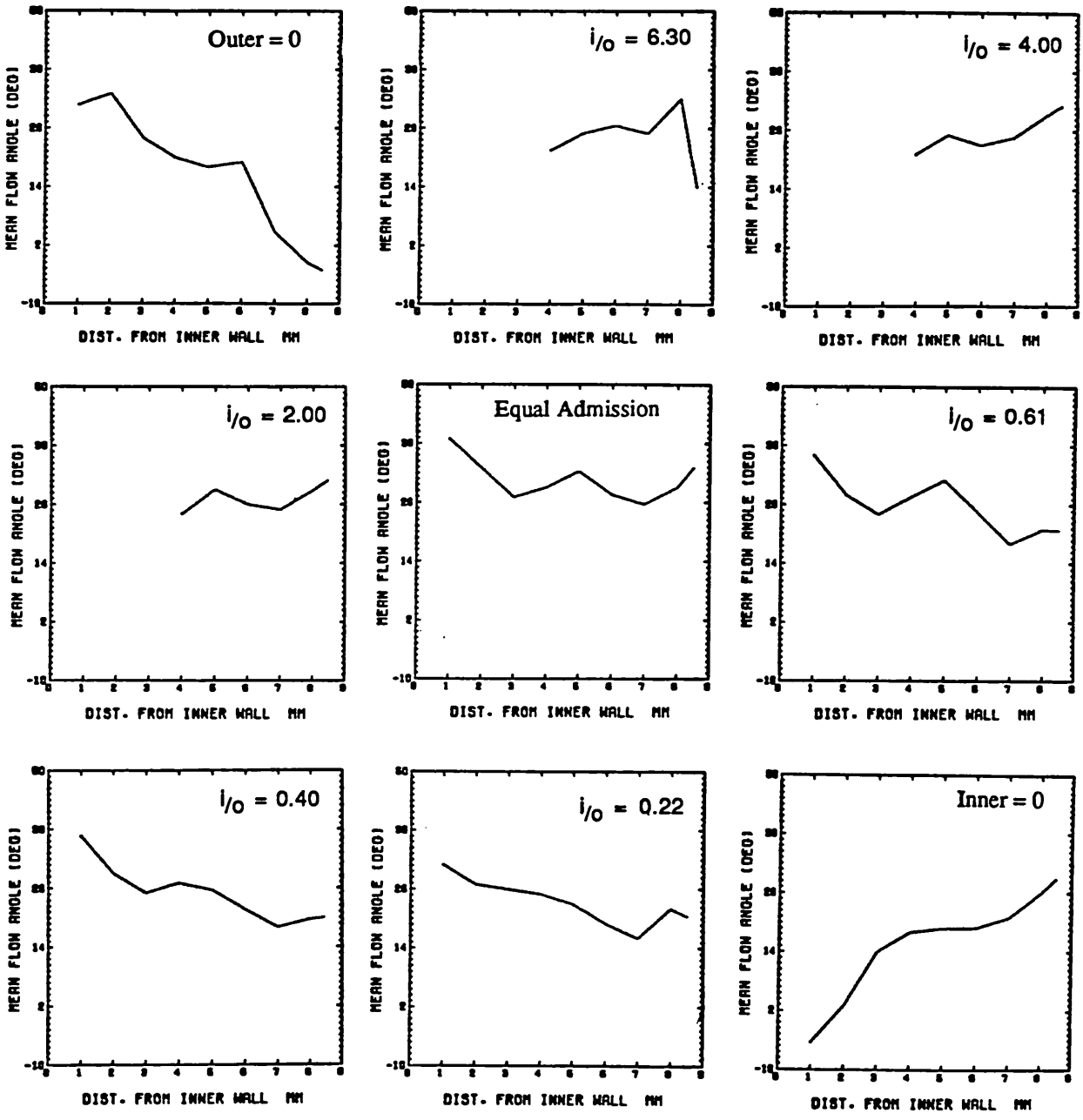


Equal Admission : Equal admission flow in each limb
Inner = 0 : Inner limb is fully closed
Outer = 0 : Outer limb is fully closed
i_o : Mass flow ratio of $\text{innerlimb}_{/\text{outer limb}}$

SW ϕ = 86 mm

Figure 5.27a

Flow Angle

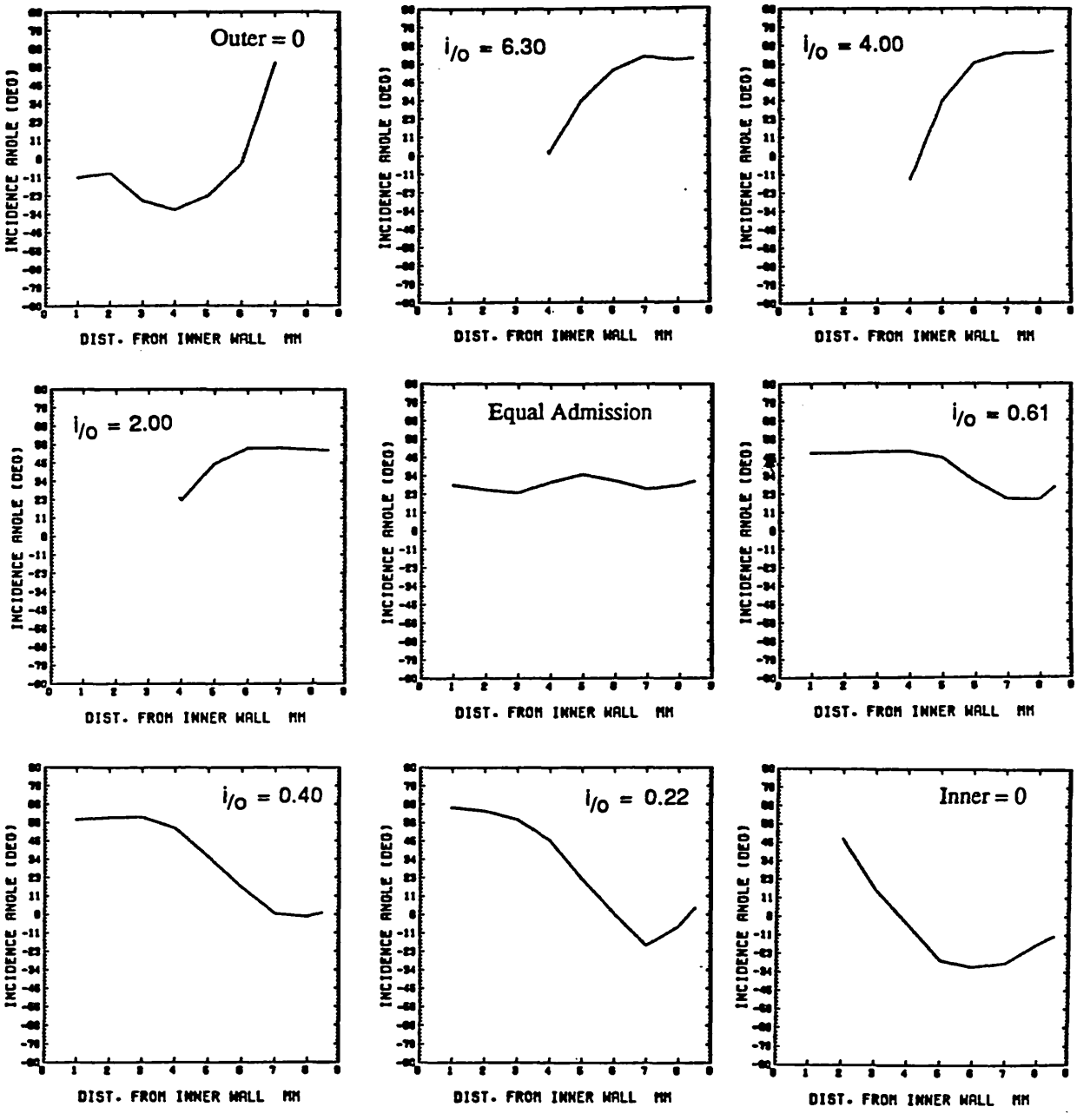


Equal Admission	: Equal admission flow in each limb
Inner = 0	: Inner limb is fully closed
Outer = 0	: Outer limb is fully closed
i_o	: Mass flow ratio of innerlimb/outer limb

SW ϕ = 86 mm

Figure 5.27b

Incidence Angle

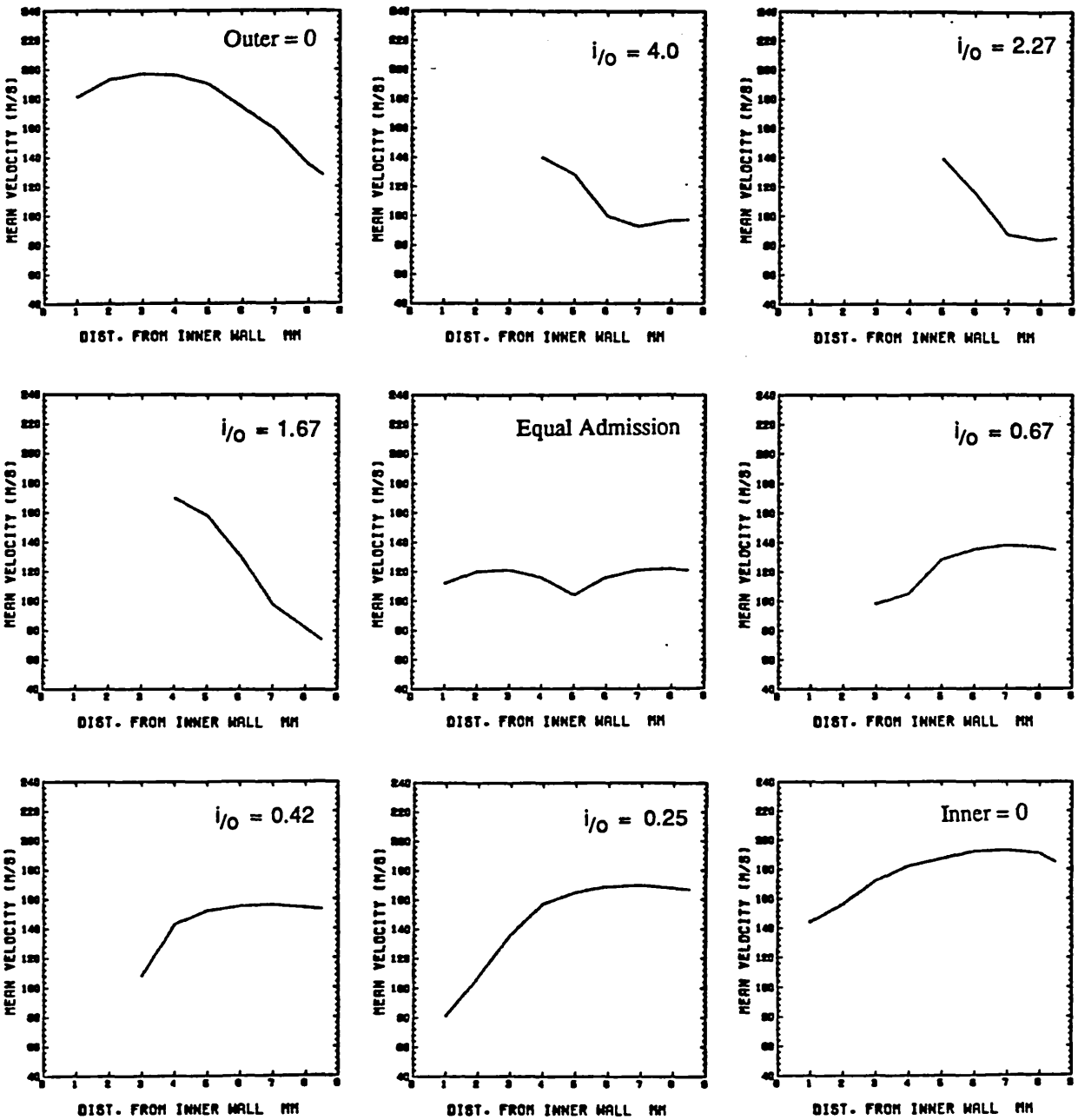


Equal Admission : Equal admission flow in each limb
Inner = 0 : Inner limb is fully closed
Outer = 0 : Outer limb is fully closed
$i_{/o}$: Mass flow ratio of $inner limb_{/outer\ limb}$

SW ϕ = 86 mm

Figure 5.27c

Flow Velocity

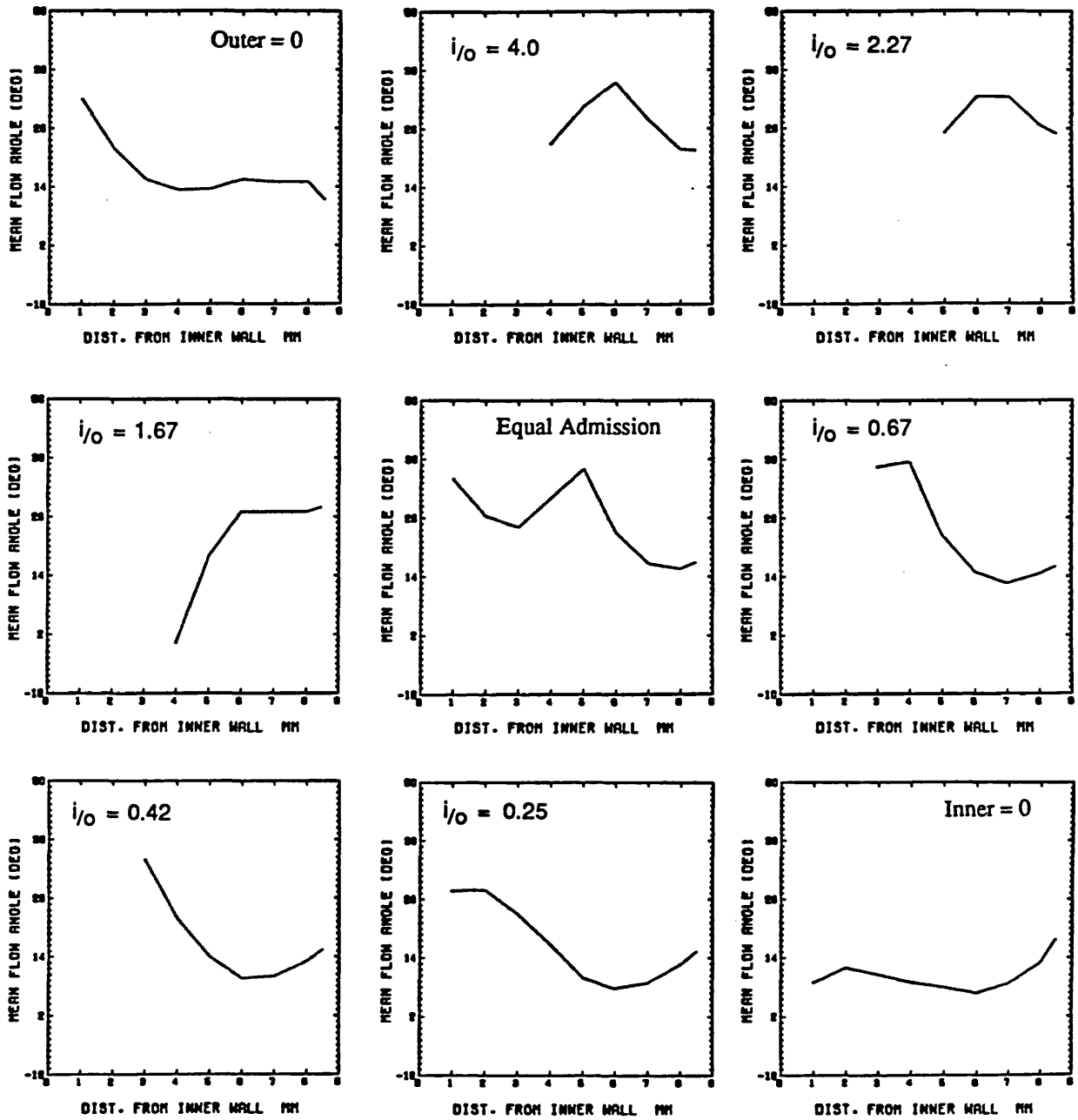


Equal Admission : Equal admission flow in each limb
Inner = 0 : Inner limb is fully closed
Outer = 0 : Outer limb is fully closed
$i_{/o}$: Mass flow ratio of innerlimb/outer limb

SW ϕ = 90 mm

Figure 5.28a

Flow Angle

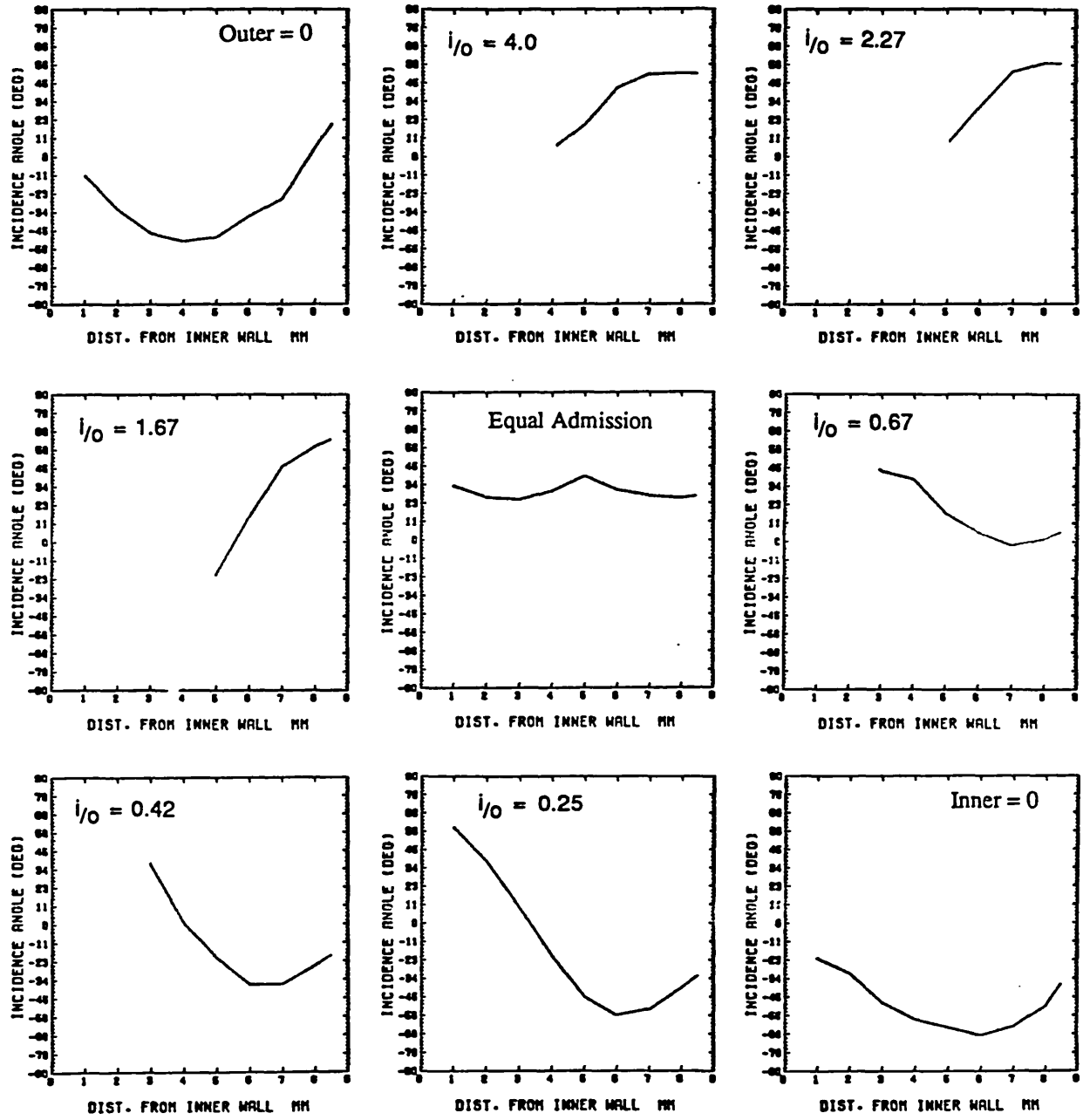


Equal Admission : Equal admission flow in each limb
Inner = 0 : Inner limb is fully closed
Outer = 0 : Outer limb is fully closed
i_o : Mass flow ratio of innerlimb/outer limb

SW ϕ = 90 mm

Figure 5.28b

Incidence Angle

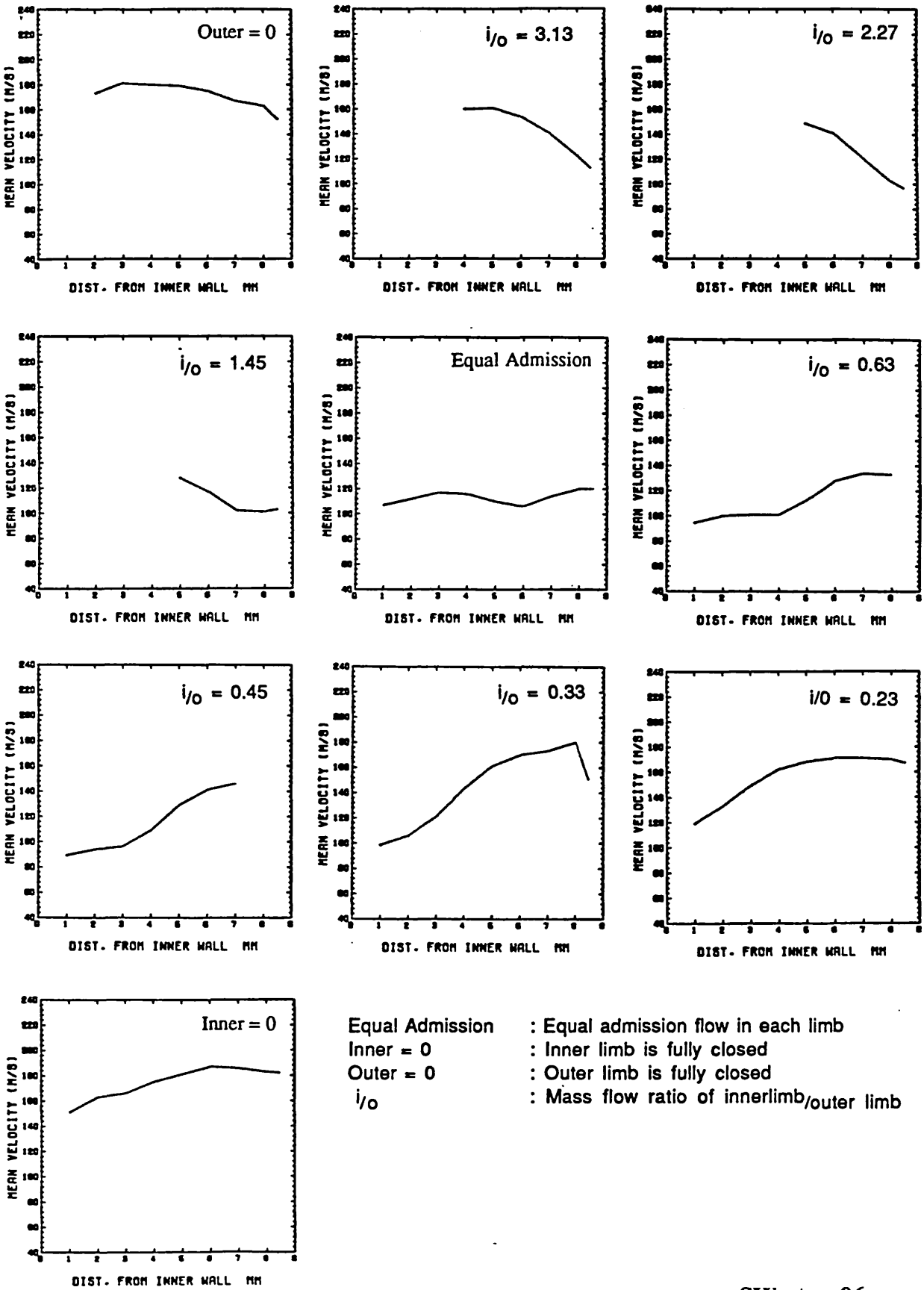


Equal Admission : Equal admission flow in each limb
Inner = 0 : Inner limb is fully closed
Outer = 0 : Outer limb is fully closed
i/o : Mass flow ratio of $\text{innerlimb}_{/\text{outer limb}}$

Figure 5.28c

SW ϕ = 90 mm

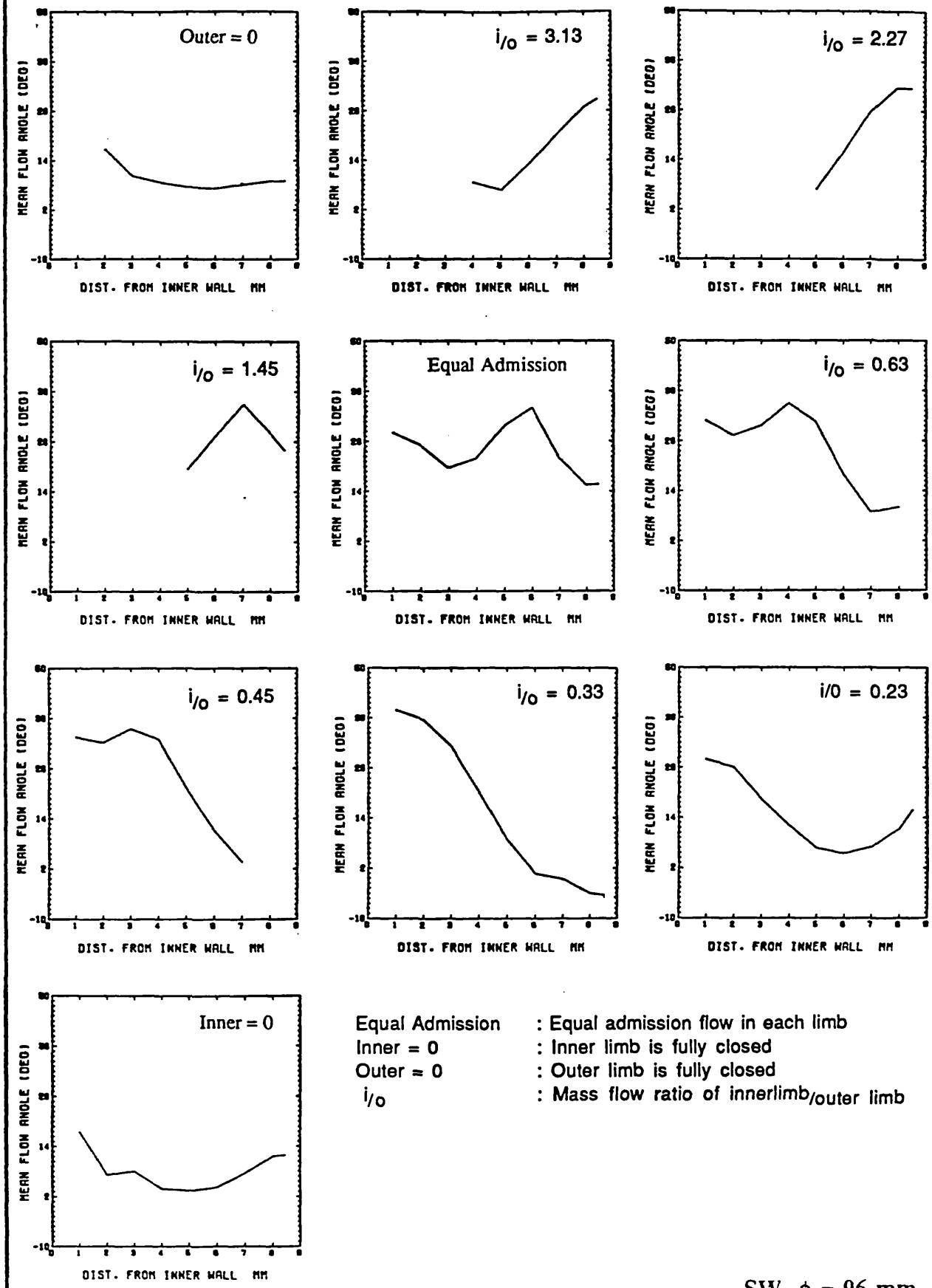
Flow Velocity



Equal Admission	: Equal admission flow in each limb
Inner = 0	: Inner limb is fully closed
Outer = 0	: Outer limb is fully closed
i_o	: Mass flow ratio of $\text{innerlimb}_{/\text{outer limb}}$

SW ϕ = 96 mm

Figure 5.29a

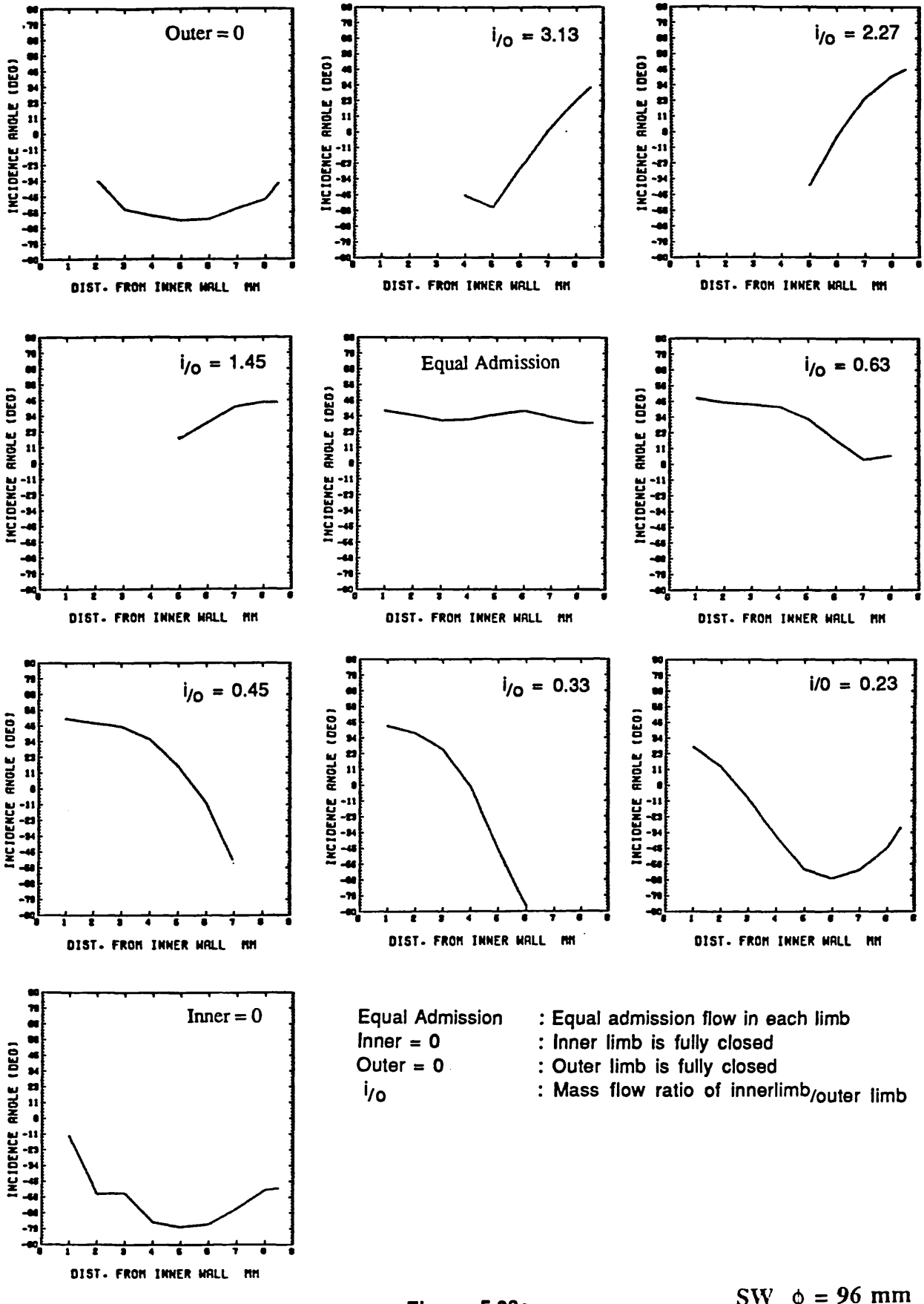


Equal Admission : Equal admission flow in each limb
Inner = 0 : Inner limb is fully closed
Outer = 0 : Outer limb is fully closed
i/o : Mass flow ratio of innerlimb/outer limb

SW ϕ = 96 mm

Figure 5.29b

Incidence Angle



Equal Admission	: Equal admission flow in each limb
Inner = 0	: Inner limb is fully closed
Outer = 0	: Outer limb is fully closed
i/o	: Mass flow ratio of $\text{innerlimb}_{/\text{outer limb}}$

Figure 5.29c

SW ϕ = 96 mm

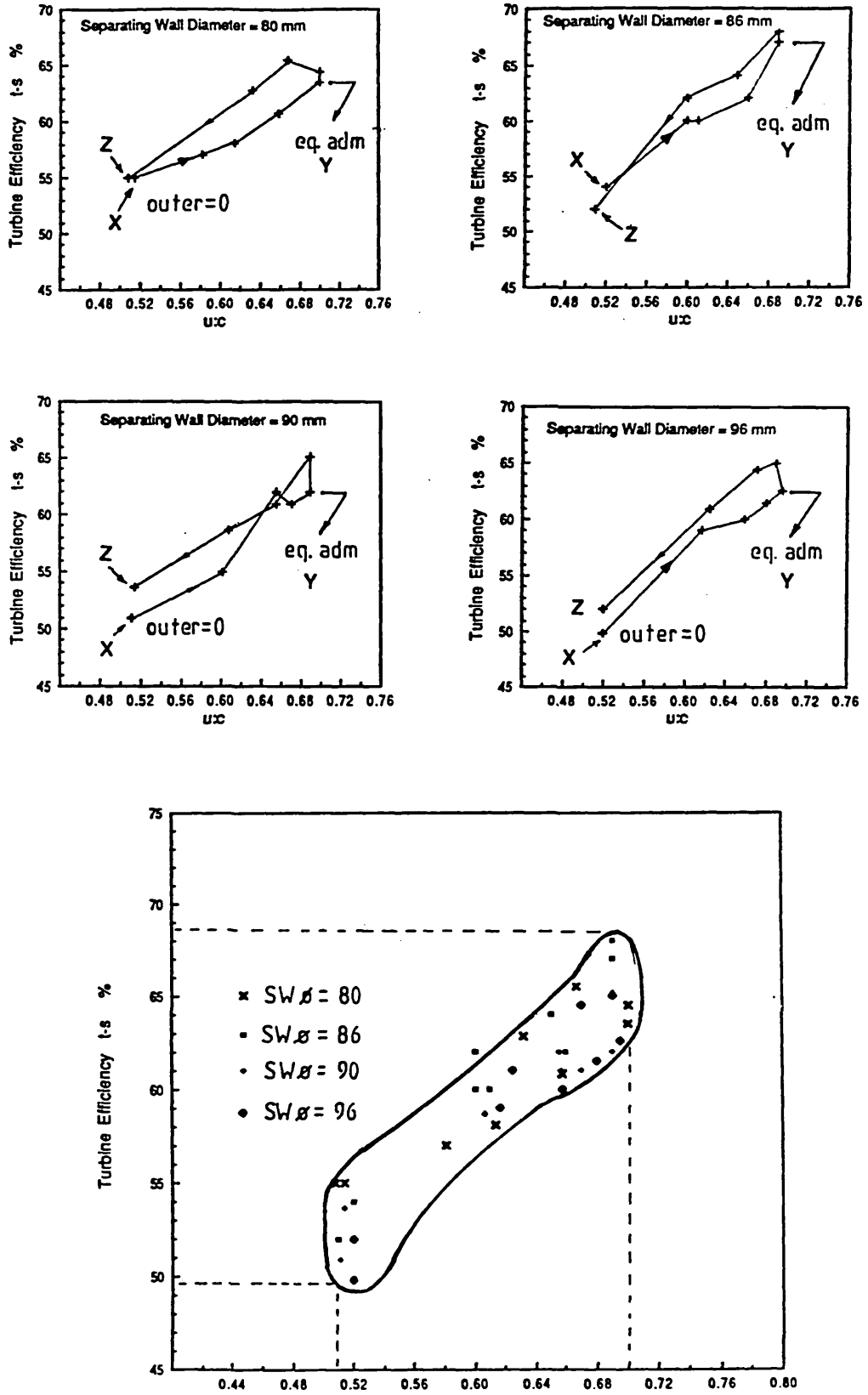
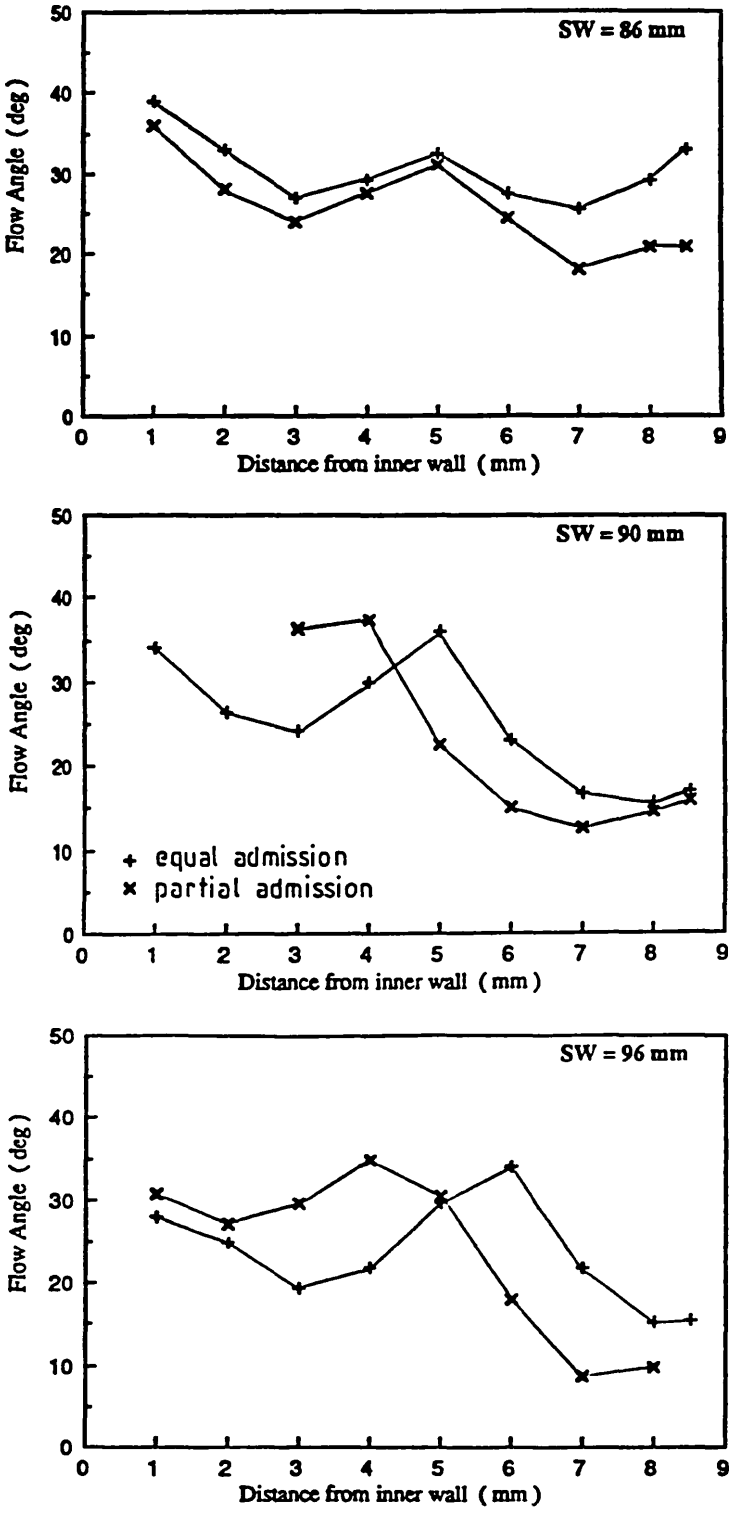


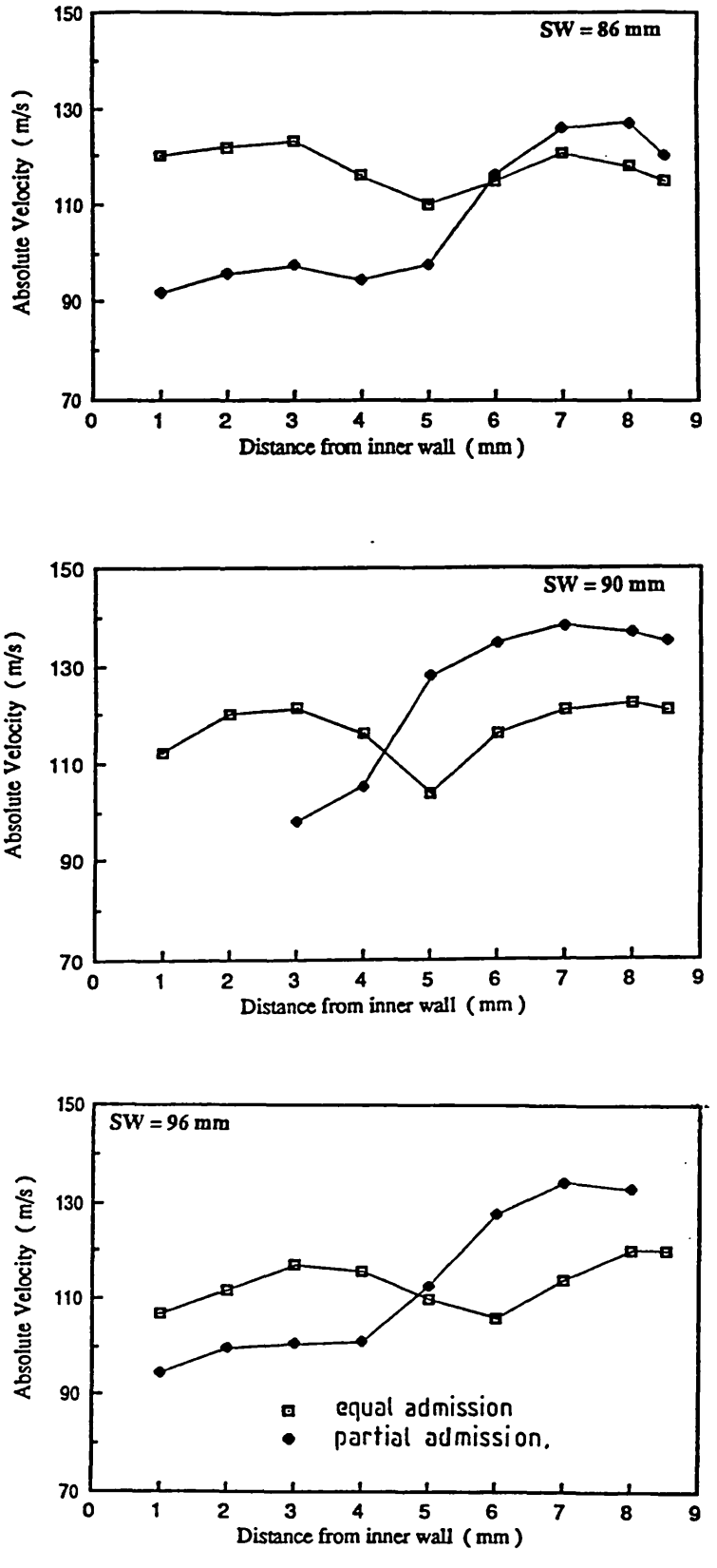
Figure 5.30 Turbine Efficiency under Partial Admission

Flow Angle



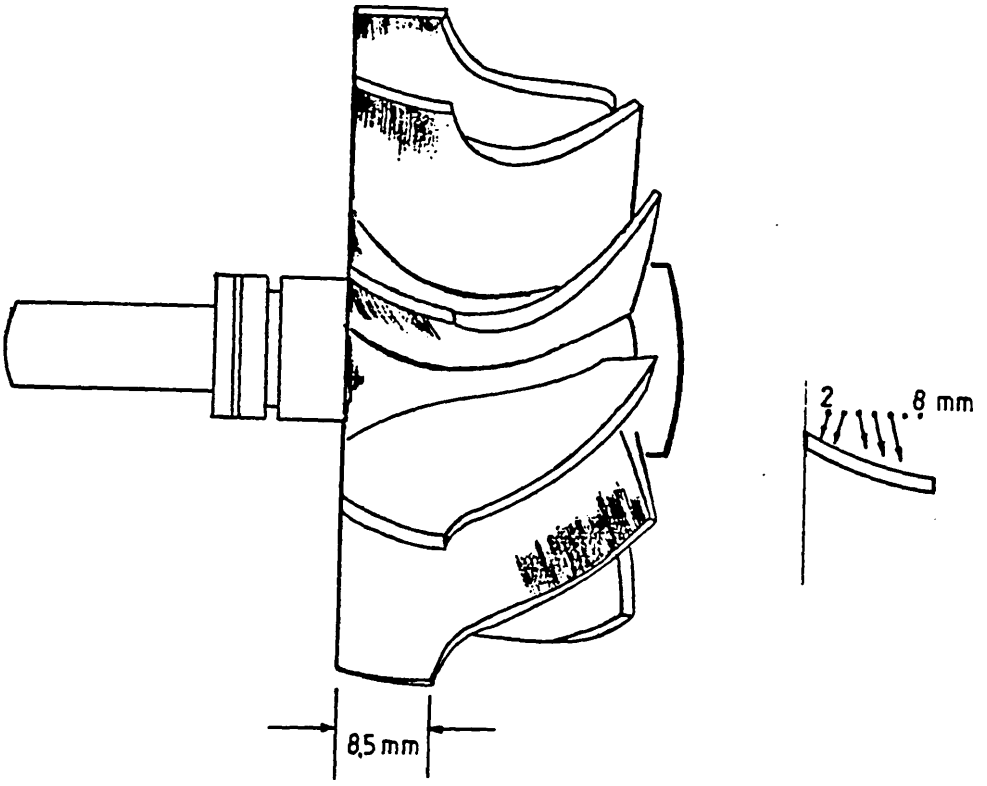
Comparison of Equal and Partial Admission ($inner/outer$ = 0.625) Flow

Figure 5.31a



Comparison of Equal and Partial Admission ($inner/outer$ = 0.625) Flow

Figure 5.31b



Deviation of flow from radial plane, α_3						
Diatance from inner wall	2 mm	3 mm	4 mm	5 mm	6 mm	7 mm
Equal Admission	0.9° ↙	1.7° ↙	1.3° ↙	3.5° ↘	3.5° ↘	4.3° ↘
Partial Admission $\frac{\text{outer}}{\text{inner}} = 1.5$	4.0° ↙	5.0° ↙	10° ↘	9.5° ↘	8.7° ↘	

Deviation of Flow from Radial Plane, α3

Figure 5.31c

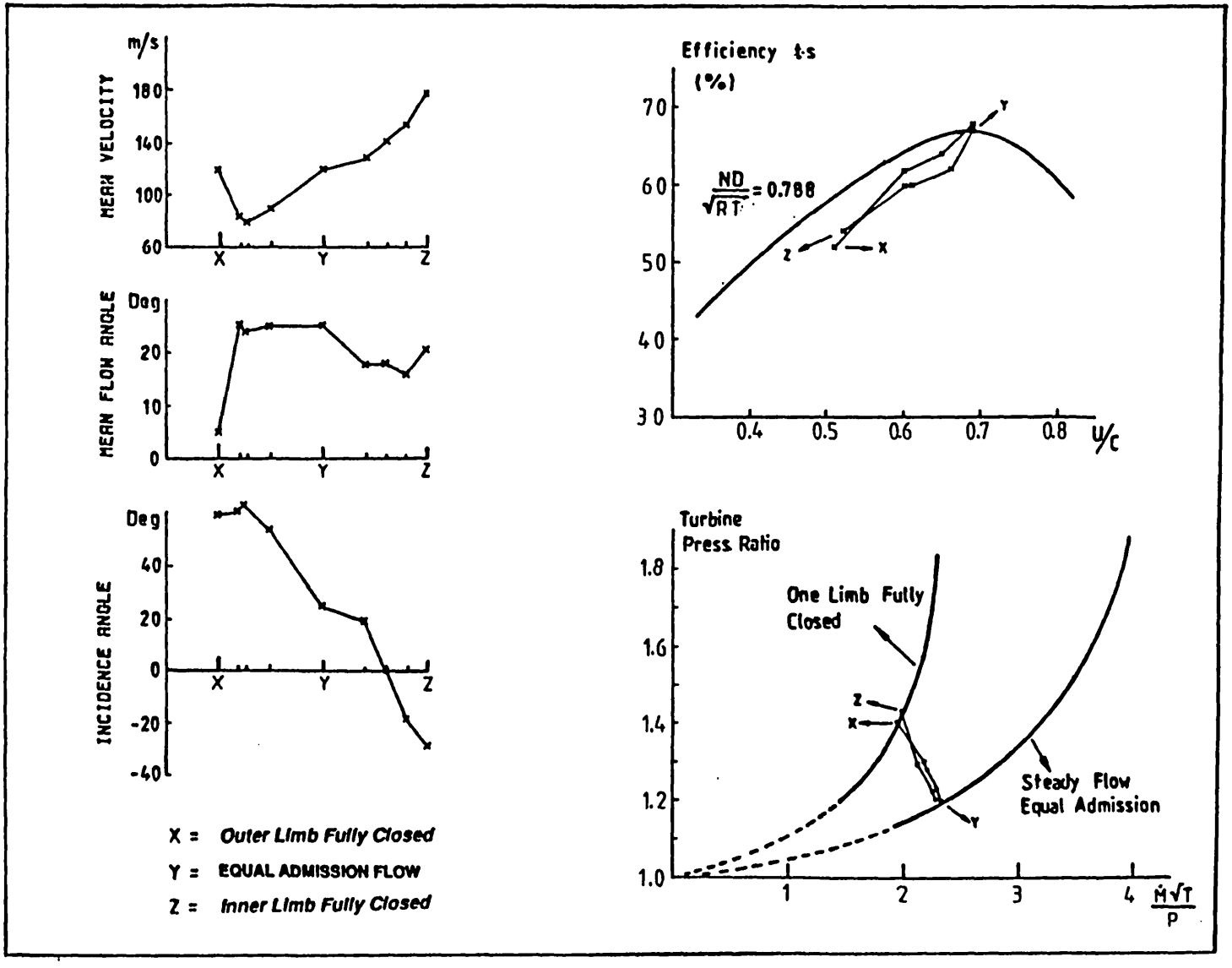
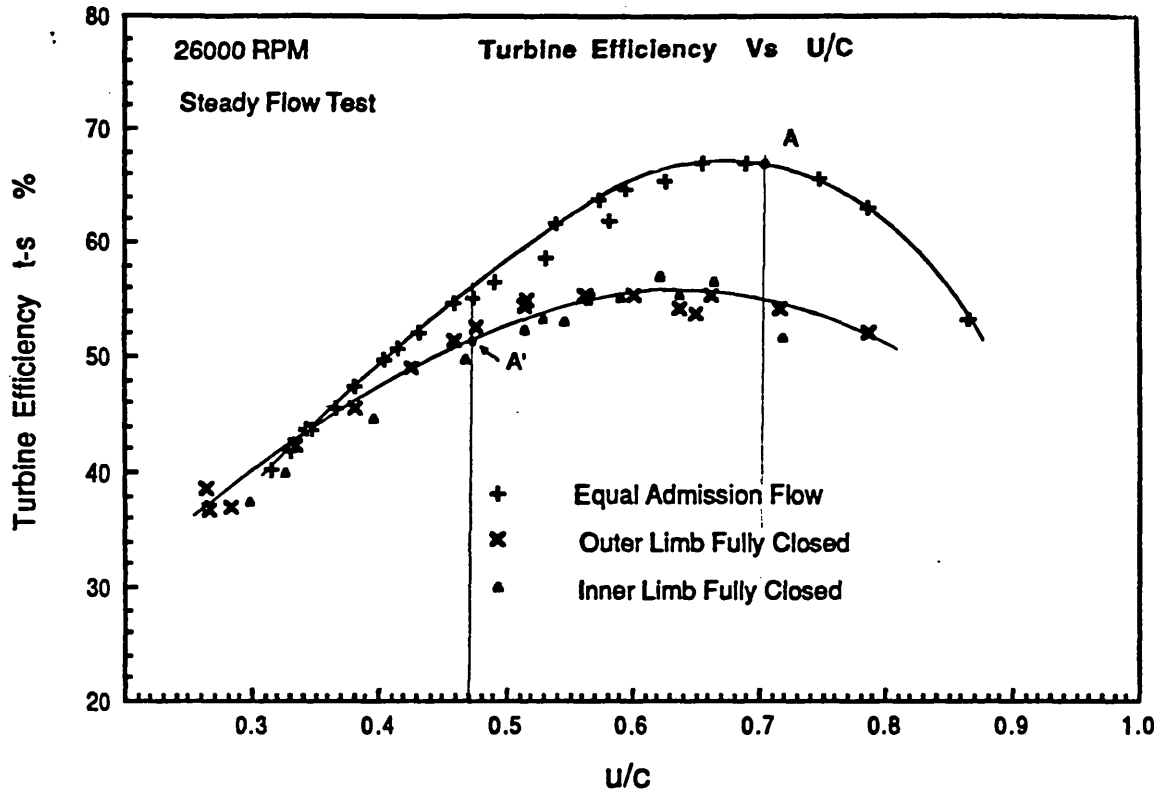
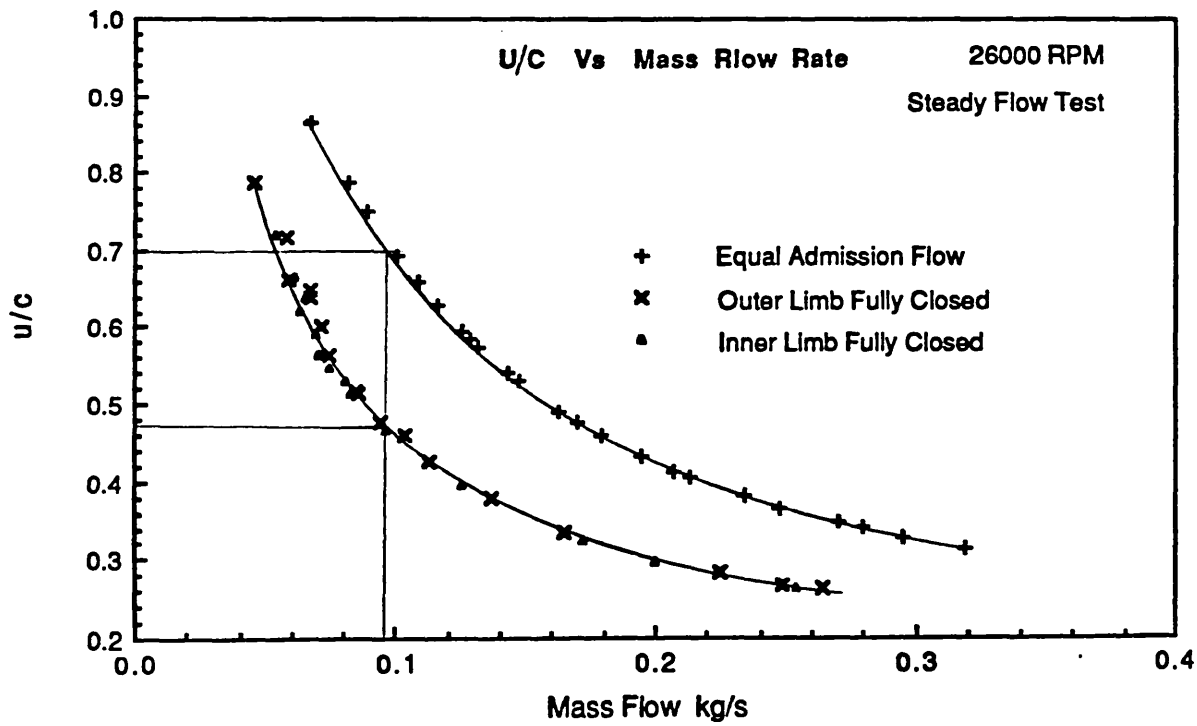

m/s
MEAN VELOCITY
180
140
100
60
X
Y
Z
Deg
MEAN FLOW ANGLE
20
10
0
Deg
INCIDENCE ANGLE
40
20
0
-20
-40
X = Outer Limb Fully Closed
Y = EQUAL ADMISSION FLOW
Z = Inner Limb Fully Closed
Efficiency t-s
(%)
70
60
50
40
30
ND/√RT = 0.788
0.4
0.5
0.6
0.7
0.8
U/C
Turbine
Press Ratio
1.8
1.6
1.4
1.2
1.0
One Limb Fully
Closed
Steady Flow
Equal Admission
1
2
3
4
ṁ√T/P

Figure 5.32

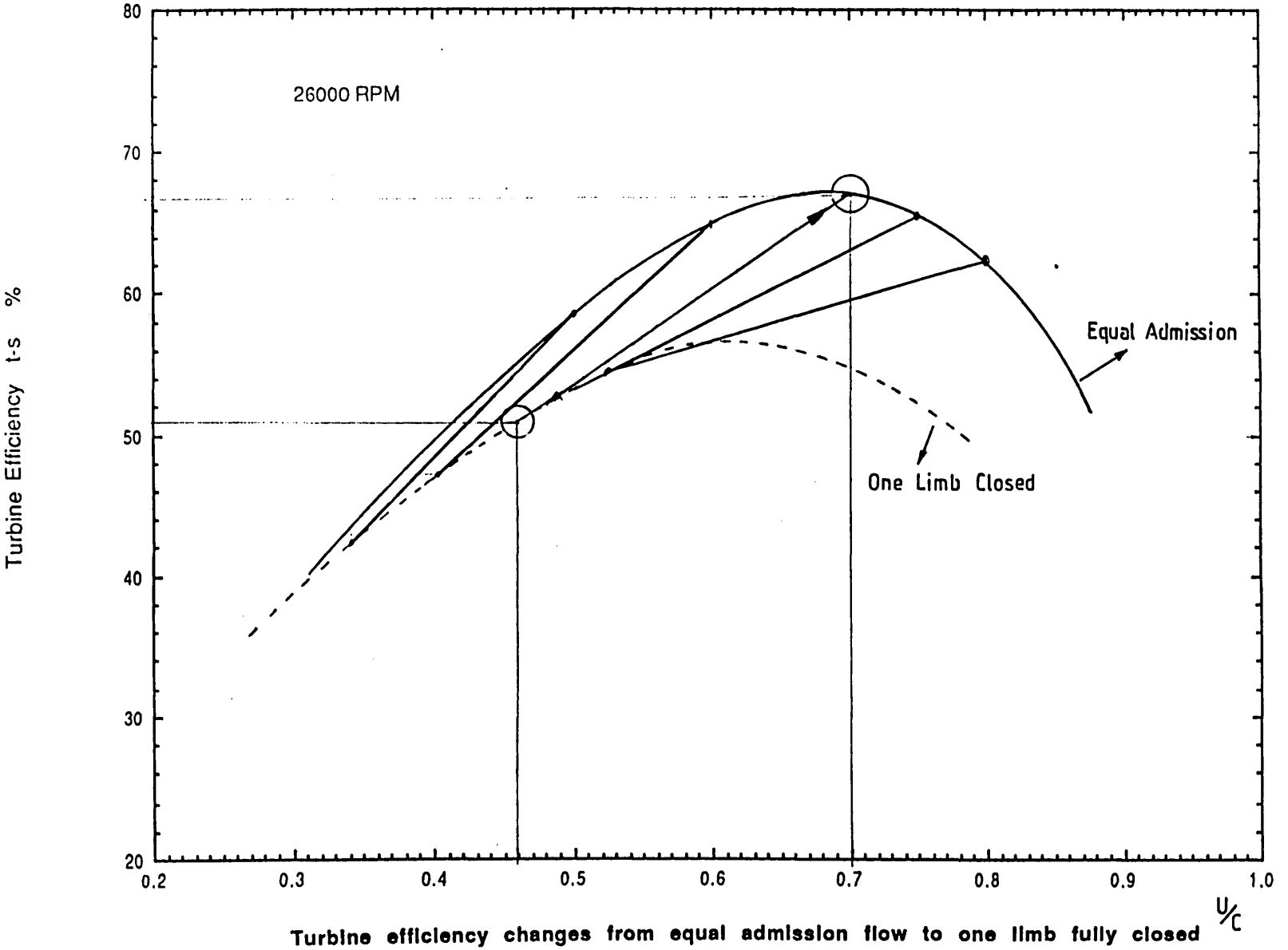


(a)



(b)

Figure 5.33



Turbine efficiency changes from equal admission flow to one limb fully closed

Figure 5.34

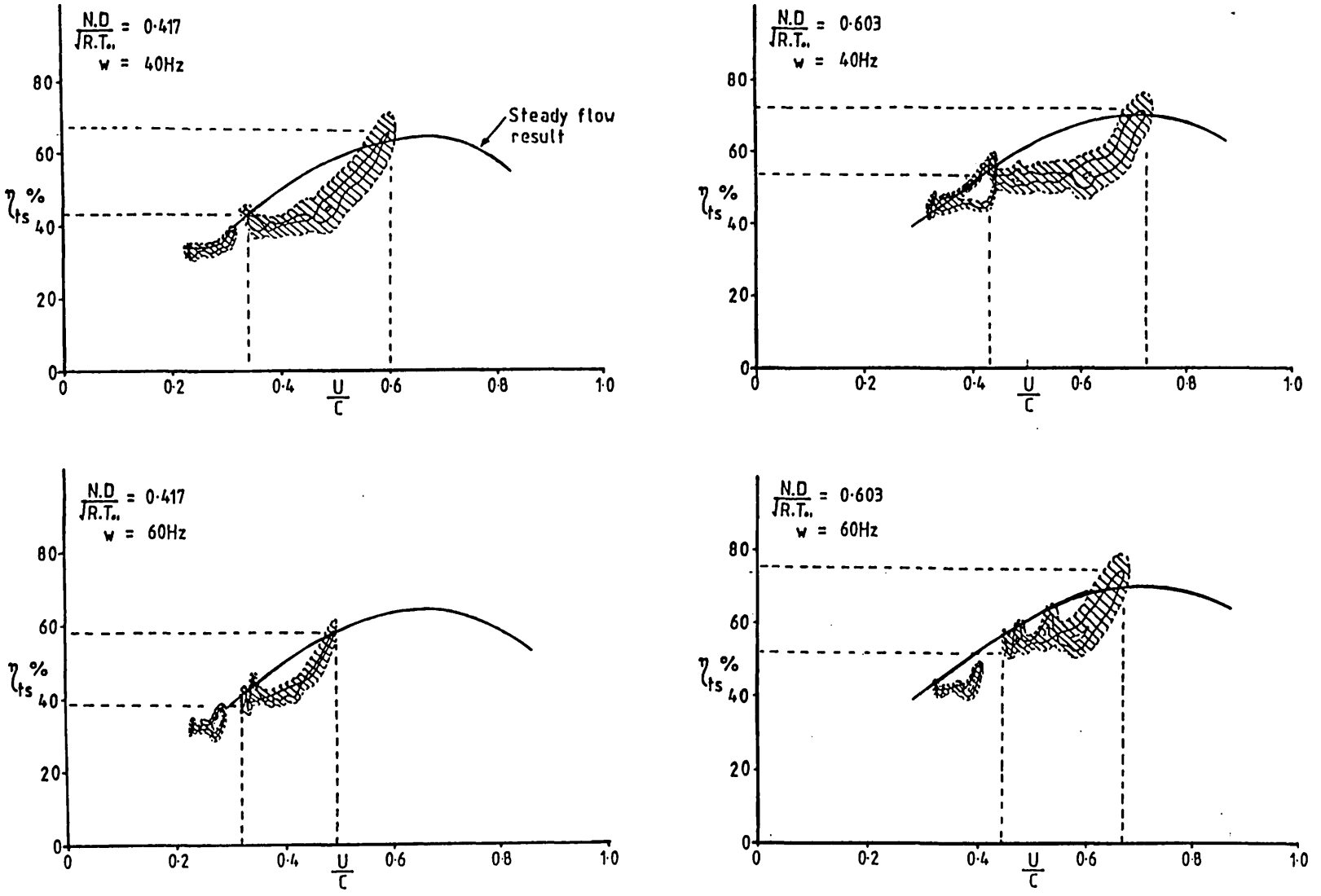
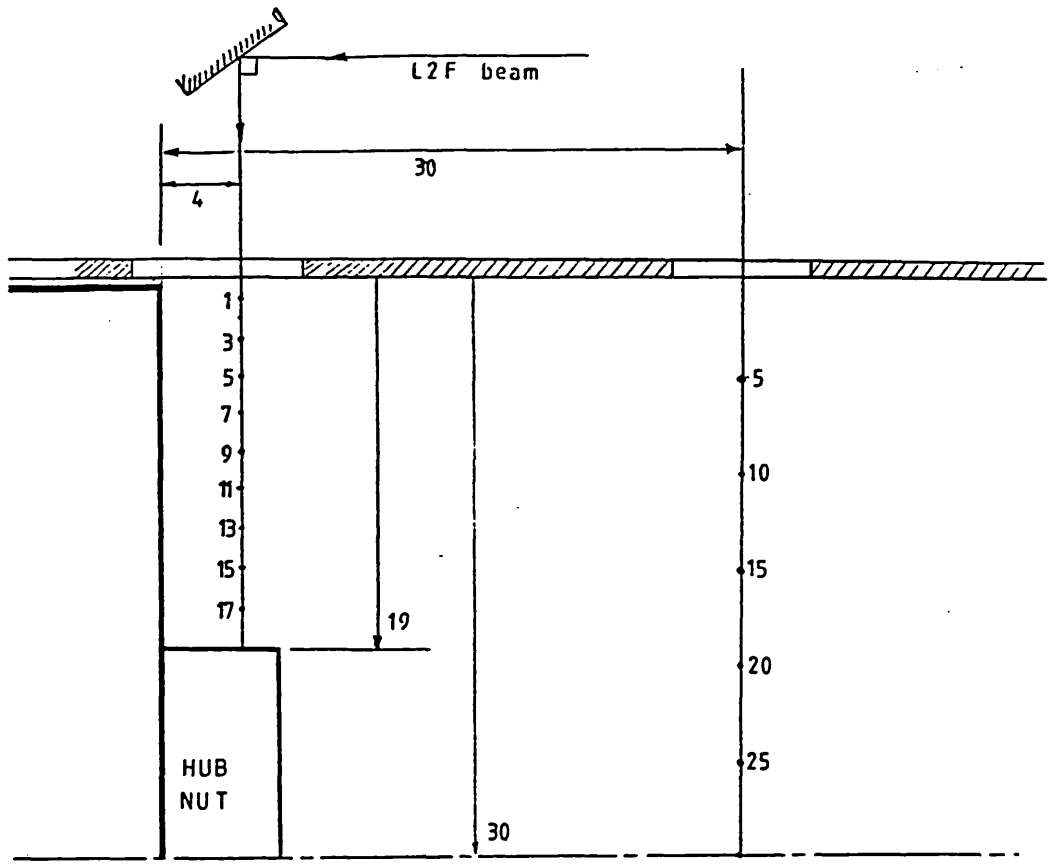


Figure 5.35 Instantaneous Efficiency by Dale (39)

The locus of instantaneous operation is shown as a solid line bounded by two dashed lines indicationg the limits of the error band (shaded)



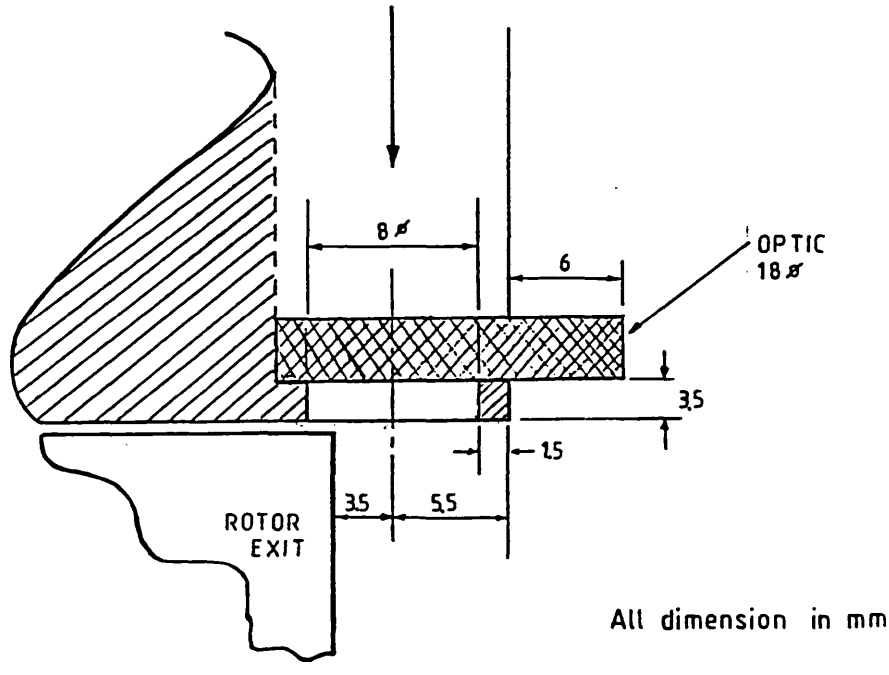
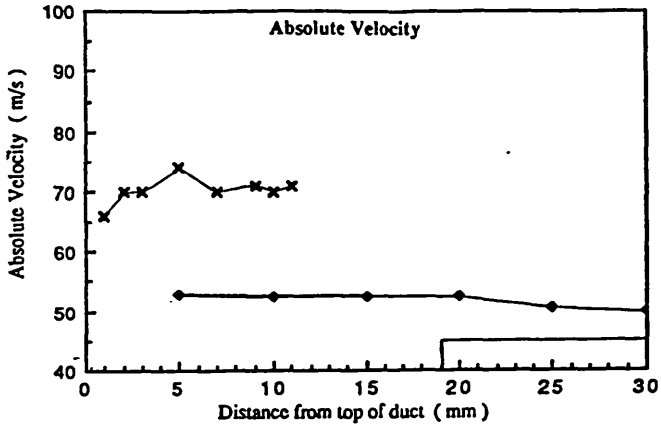
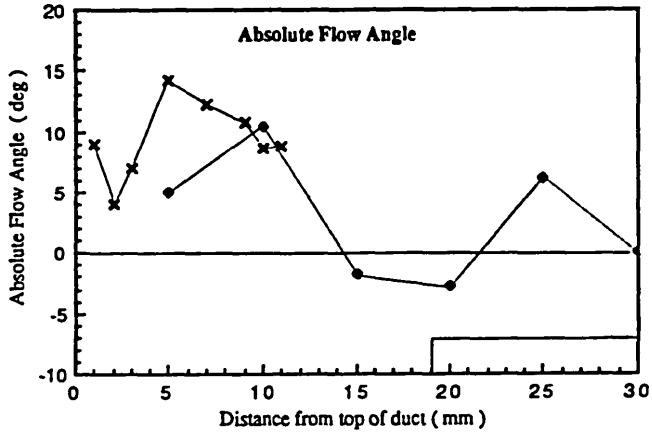
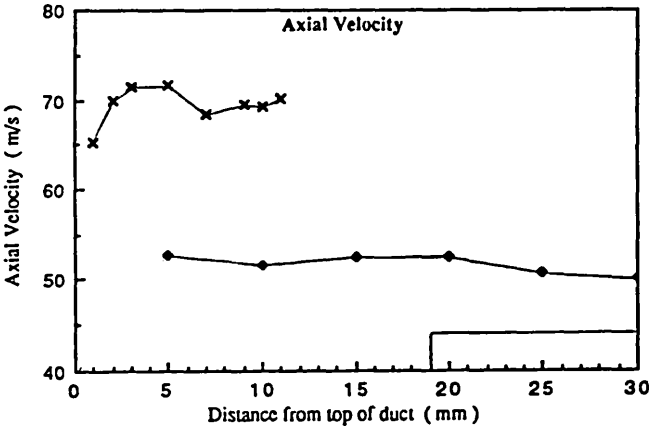
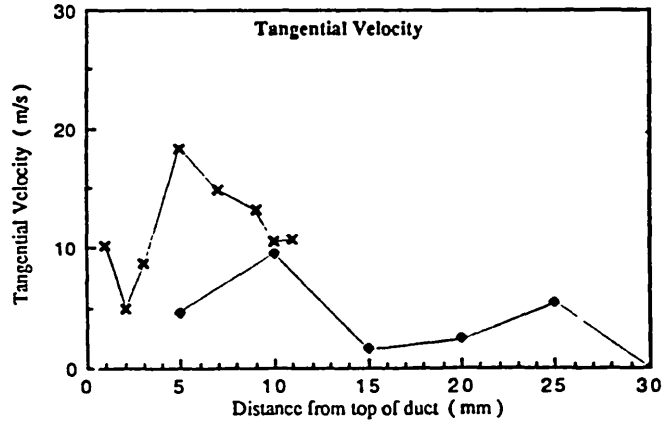


Figure 5.36 Measuring location close to rotor exit







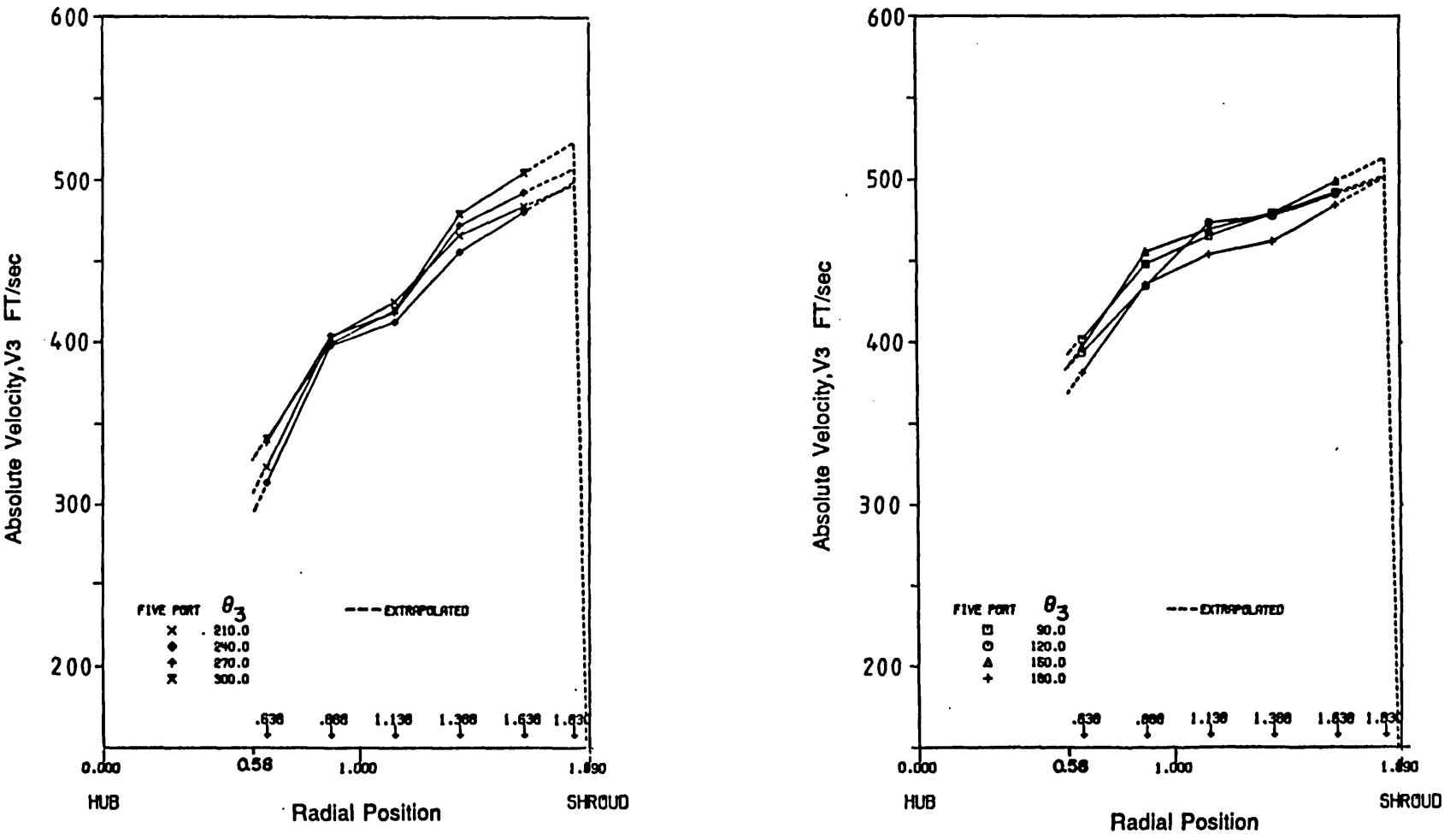


x 4 mm from rotor trailing edge

◆ 30 mm from rotor trailing edge

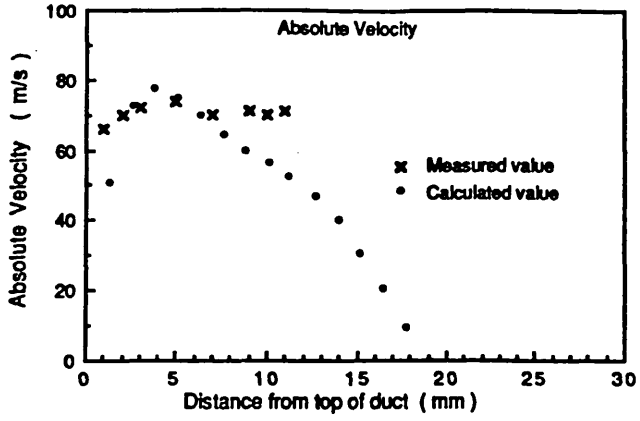
Flow measurements at 4mm and 30mm from rotor exit

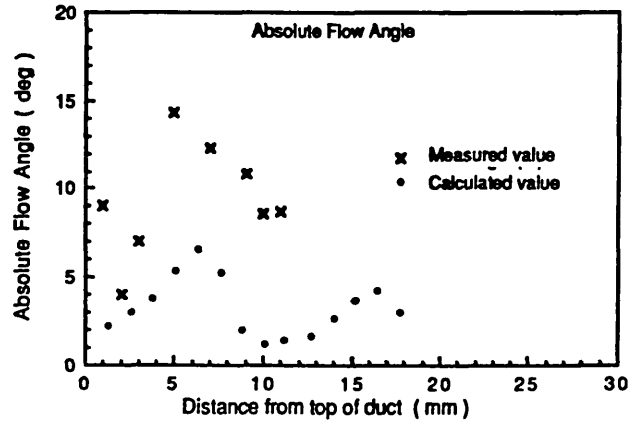
Figure 5.37

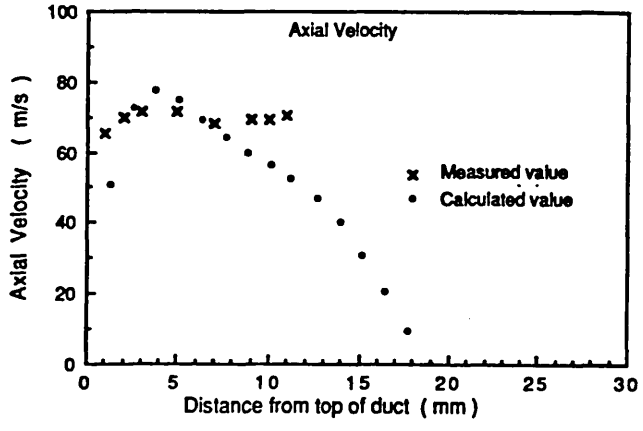


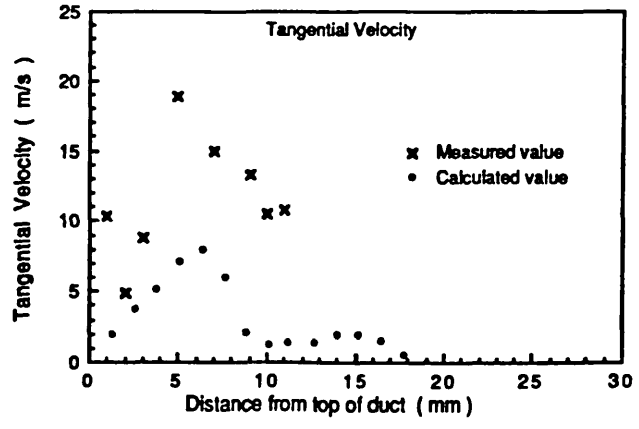
Radial Distribution of Rotor Exit Absolute Velocity by Miller (17)

Figure 5.38









Flow characteristics at rotor exit from measured and calculated values

Fig 5.39

Chapter 6

Unsteady Flow Test Results and Discussion

6.1 Introduction

This chapter contains the results of the gas flow characteristic measurements under unsteady flow conditions. The tests were carried out at a pulse frequency of 50 Hz. The total time-averaged mass flow to the turbine was monitored at a distance of approximately 15m upstream of the rotary pulse generator. The pressure pulse in each of the two limbs is set at 180° out of phase. This reproduces the flow conditions in many common turbochargers, such as a twin-entry turbine fed from a multi-cylinder engine with divided manifold. Measurements were made at rotor inlet and exit at the same points as for the steady flow tests described in Chapter 5.
Different separating wall plate diameters were also introduced to the turbine housing to study the effects of the meridional divider depth under unsteady flow conditions. The unsteady flow tests were carried out in two phases. In phase one, three different operating conditions were applied. In phase two, a single operating condition (whose total mass flow under steady flow gives the optimum operating point, $u/c = 0.70$) was applied to study the flow characteristics using different separating wall diameters. All these tests were done at a time-averaged speed of 34000 RPM and an inlet total temperature of 350K.
The unsteady flow tests carried in the two phases are as follows :

Phase One

The objective of the work in phase one was to investigate the gas flow characteristics at the rotor inlet and exit for three different total time averaged mass flow conditions.
High frequency pressure transducers in each limb positioned before the inlet to the turbine measured the instantaneous static pressure. The pressure pulse shapes for the three different total mass flow conditions are shown in Fig.6.1. The pulse generator was developed so that these pressure pulses are similar in form to automotive exhaust pressure pulses.
The turbine steady state performance points corresponding to these mass flows are listed in Table 5.1. The lowest mass flow condition is closest to the design point, and the others correspond to underspeed (low u/c) conditions.
At the rotor inlet, because of a shortage of time flow measurements were made only at 180° azimuth angle. The through-flow velocity and axial velocity components of velocity were measured.
At the rotor exit, measurements were made along an axis 30mm away from the rotor trailing edge, at 5mm intervals from the top of the exit duct.
The results in phase one work are presented in the following sections

6.2 Rotor inlet, 3 flow conditions, through-flow velocity
6.3 Rotor inlet, axial component of velocity
6.4 Rotor exit, 3 flow conditions

Phase Two

The objective of the phase two work was to investigate the unsteady gas flow characteristics at the rotor inlet with different separating wall plate diameters. A single mass flow

condition (under steady flow condition, $u/c = 0.69$) was applied throughout the investigation. Measurements at the rotor inlet were extended to different azimuth angles. The axial component of velocity was not, however, investigated in this phase.
Flow measurements at the rotor exit were made closer to the rotor trailing edge, than in phase one, at 4mm downstream. These results are compared with measurements made at 30mm away, for the same flow conditions. The results of the phase two work are presented in section 6.5.
For periodic flow mapping, the L2F processor divides a cycle pulse or a blade passage into a number of time windows, either 2,4,8,16, which are phase locked to the pulse or blade passing frequency. Fig.6.2 shows a typical unsteady flow characteristics with different numbers of time windows for a fixed flow condition.
In the present experiments the synchronizer was triggered from the rotary pulse generator so that each cycle of the pulse generator is divided into equal number of parts depending on the number of time windows applied. The two pulses of pressure (Fig.6.1) are clearly visible as velocity pulses in Fig.6.2. For best resolution, all tests were carried out with 16 time windows selected. Subsequent presentations of unsteady flow characteristics are plotted on a time base instead of window number.
The overall performance of the turbine under unsteady flow conditions was not measured. However, the measurements at rotor inlet and exit were sufficiently comprehensive that they could be used to estimate the turbine power output using the Euler turbomachine equation, and hence the time-varying efficiency.

6.2 Rotor Inlet,3 Flow Conditions,Through-flow velocity

Figs.6.3, 6.4 and 6.5 show the pressure pulse flow, velocity and angle profiles measured under unsteady flow for 3 different

conditions. These measurements were made at a point 3mm from the inner wall. In Fig.6.3 the time-averaged total mass flow to the turbine produces near design operating condition (Table 5.1). Figs.6.4 and 6.5 show the gas flow characteristics at operating conditions which are further away from design point. Figs. 6.3 and 6.4 show clearly that absolute velocity and flow angle vary with the pressure pulse. As the mass flow increases, the pressure pulse becomes greater in magnitude. At the highest mass flow rate there are missing data points in the flow characteristics. The L2F velocimeter is sensitive to flow condition and where insufficient quality data is received, no measurements can be possible.

One likely cause for the missing data is the sudden rise in pressure, causing an instantaneously highly disturbed flow. Fig.6.5 shows that data were collected around the peak pressure and the falling pressure regions. The missing data appears to fall around a transition zone where one pressure pulse is decaying and the pressure pulse in the other limb is rapidly rising. This problem does not occur near to the design point (Figs.6.3 and 6.4). But at off-design conditions, the higher pressure pulse appears to cause a momentarily highly disturbed flow as two streams of highly unequal pressure meet.

Figs.6.3 to 6.5 show clearly the two velocity pulses in a cycle. It is also clear that one pulse is greater in magnitude than the other. This effect is observed in each of the three different flow conditions. One pulse is greater than the other by approximately 15 to 25% (by estimating from the peak of the pulse). The unequal velocity pulses are due to measurements made at different points in the volute exit.

Figs.6.6, 6.7 and 6.8 show the variation of absolute velocity for 3 different unsteady flow conditions. In each flow condition, measurements were made across the volute exit. Two

velocity pulses, one corresponding to the pressure pulse in each limb are noted in each case. The magnitudes of the velocity pulses are observed to change at different measurement points. For example, one of the peak velocities at the 3mm position for a flow condition of 0.17 kg/s is 215 m/s (Fig.6.4b). This peak velocity at a time of 17ms. corresponds to the pressure pulse from inner limb. The second peak velocity caused by the pressure pulse from the outer limb is 173 m/s at a time of 7ms. As the measuring point moves to 7mm, the peak velocity caused by the inner limb decreases to about 160 m/s, Fig.6.7.

To see this effect more clearly only the peak velocities corresponding to each pressure pulse are plotted along the measured points in Fig.6.9. The curve at the lowest total mass flow (Fig.6.9a) shows how the higher peak velocity (corresponding to inner limb) of 229 m/s at the 2mm position decreases gradually to 160 m/s at the 7mm position. The other curve in this figure shows the second peak velocity (corresponding to outer limb) of 173 m/s at the 2mm position increasing gradually to 220 m/s at the 7mm position. The intersection point between the two loci of peak velocity is around 4mm which is approximately the centre of the volute exit.

This change in magnitude of the velocity pulses follows a similar trend to steady flow test results in which one limb is fully opened or closed. The flow characteristics in these figures are comparable to that in Fig.5.10 where a difference in velocity is noted across the measured point, for these two operating conditions. The intersection point of the two peak velocity loci is again around 4mm.

From the results of the above analysis of this phenomenon it is apparent that the most likely cause of the unequal velocity pulses is linked to its measuring location. This information becomes very useful at a later stage when it can be used as a

guide to construct a time-varying representation of pulse flow characteristics across the volute exit, where there are missing data points.

At some point in the pulsating flow there exists conditions where one limb is not flowing, where both flow equally, and between these, where the conditions are those of partial admission. This comparison (Figs.5.10 and 6.9) suggests that the unsteady gas flow characteristics are instantaneously very similar to the steady flow at corresponding partial admission conditions. A more important conclusion from this analysis is that under pulsating flow the fluid is in dynamic equilibrium i.e the turbine is "quasi-steady".

Flow Angle and Incidence Angle

Figs.6.3c to 6.5c show the variation of the absolute flow angles within a cycle pulse. At near the design point condition (Fig.6.3c) the flow angle profile shows two pulses corresponding to the velocity pulses. The peak velocities correspond to the lowest flow angles and vice versa. The flow varies from about 5° to 34°. This represents a large variation which is generally not perceived in the designing of turbocharger turbines. All previous flow investigations (8,10) carried out so far reveal a minimum variation of flow angle except around the tongue region. The results here show that under unsteady flow conditions, the flow angle at the rotor inlet varies considerably near the design and less so, but still significantly, off-design (Figs.6.4c and 6.5c).

The inertia of the rotating assembly is sufficiently high that the rotor speed is effectively constant during pulsating flow, so that the blade speed can be calculated. With this and the measured absolute velocity and flow angle, the velocity triangle can be constructed and hence the tangential and radial components of velocity and incidence angle can be calculated,

Figs.6.10 to 6.12. The variation of flow angle has a greater effect on the radial velocity ($Cr = C.\sin(\alpha)$) than the tangential velocity. It follows that the variation of radial velocity in Figs.6.10 to 6.12 is similar to absolute flow angle while the tangential velocity variation is similar to the absolute velocity.

In Fig.6.10 where the flow condition is close to design point, very large changes in incidence angle is observed with a cycle. At higher mass flow rates smaller variations are observed. This variation is between 60° to -65°. This large variation of incidence angle means that the rotor is operating over a wide range of off-design conditions, and implies large incidence losses. This probably contributes to the large variation of turbine efficiency noted by Dale (39). Dale's unsteady flow test reveals a consistent efficiency loop under all flow conditions. In Fig.5.35 it shows that this variation of turbine efficiency is of significant magnitude.

Figs.6.10 to 6.12 shows the variation of incidence angle for different flow conditions. Large variation of incidence is noted even at near design point operation.

The typical results previously noted that low absolute velocity corresponds approximately with high flow angles and vice versa is responsible for the magnitude of the variation in incidence angle. Fig.6.13 shows an example of how the incidence angle can be affected by the gas angle whilst keeping the absolute velocity and blade speed constant. Fig.6.13a shows that when the tangential velocity exceeds the blade speed, a decrease in absolute flow angle (from 30° to 20°) changes the incidence angle from -18.4° to -35°. This causes the flow to depart further from design point. Fig.6.13b shows that for the same decrease in absolute flow angle, with tangential velocity less than blade speed, the change in incidence angle is small. But the unsteady flow results show the case of large variation of

absolute velocity so that the incidence angle changes significantly from +ve to -ve.

Conclusion from unsteady gas flow characteristics

This section shows the variation of gas flow characteristics at inlet to the rotor with respect to inlet pressure pulse. The following conclusions can be made :

. The absolute velocity and flow angle show large variations with the pressure pulse.
. From these measurements, it is possible to construct the time-varying rotor inlet velocity triangle, thus showing the variations of tangential and radial components of velocity, incidence angle and relative velocity.
. Very large variation of incidence angle is noted even at near design operation, indicating a large range of incidence losses.
. The magnitude of the velocity pulses varies with the measuring point across the volute exit.
. Under pulsating flow the fluid is in dynamic equilibrium i.e the turbine is "quasi-steady".

6.3 Rotor Inlet, Axial Velocity of Component.

Measurements were also made via the mirror to investigate the presence of tangential, axial and radial components of velocity under pulsating flow. Refer to Fig.4.17 the flow velocity V_{11} and flow angle α_{11} were measured on a plane perpendicular to the laser beam. This plane is 30° to the tangent. Figs.6.14 and 6.15 show the variation in flow velocity and flow angle (measured on the 30° plane; 90° represents zero axial component of velocity) this under pulsating condition for points 3mm and 7mm from the inner wall respectively. At each point only one

pulse was measured completely. A second pulse appears partially at the higher total mass flow condition. There is less good data available from these measurements than those measured in the tangential-radial plane in which two complete pulses were measured. There is no straight forward explanation for the missing second pulse when measurements were made on the tangential-axial plane.

Appendix B explains the effects of the L2F focal volume rotating of a 30° plane. As the flow deviates more from the radial plane, it becomes increasingly difficult to take measurements.

When measuring on a tangential-axial plane, if the flow angle on this plane is greater the 45°, the same seeding particle is not likely to trigger both the start and stop beams of the L2F focal volume, (Fig.3.14) so that no measurement is possible by the L2F. In this case however the absolute flow angle varies from 5° to 34° (for near design point operation) which is less than this limit. Therefore this is not likely to be the cause to the missing data for the second pulse.

However, due to the presence of the divider wall it is not possible to measure on a purely tangential-axial plane. The laser beam was reflected so that the focal volume is rotating on a 30° plane (Fig.4.20) causing the angle ψ (see Fig.B2) to vary as the focal volume rotates on this plane. Appendix B details this variation of ψ as the focal volume rotates (ie scans over a possible range of flow angle). As ψ gets smaller, it becomes more likely that no measurement can be made when the absolute flow angle (measured in tangential-radial plane) becomes closer to ψ. The front and rear mirrors will affect the measurement as follows:

. To measure point 7mm, the front mirror was used. As the angular scan is greater than 90°, ψ decreases (Appendix B). Greater than 90° scan refers to flow deviation (or axial

velocity) in the direction towards inner limb. Thus when measuring this point from the tangential-axial plane, the smaller value of ψ implies that there is a greater possibility of missing out flow towards the inner limb.

. To measure point 3mm the rear mirror was used. For the angular scan less than 90°, ψ decreases. Less than 90° scan refers to flow deviation in the direction towards outer limb. Thus when measuring point 3mm from tangential-axial plane, there is a greater possibility to miss out flow towards the outer limb due to reduced angle ψ.

Figs.6.14 and 6.15 both show only one pulse, but each pulse is due to different limb however. From Figs.6.3 to 6.5, it is clear that the one pulse shown in Fig.6.14 is due to pressure pulse from inner limb while that shown in Fig.6.15 the single pulse is due to the outer limb. But measuring from tangential-radial at point 7mm reveals two pulses (Figs.6.6 to 6.8). This indicates that the missing pulse (while measuring from tangential-axial plane) is not likely due to a highly disturbed or mixed flow.

From the analysis of the above findings, it is most probable that the missing pulse has a rather high axial component of velocity and because with the effect of rotating the L2F focal volume on a 30° plane insufficient seeding particles were able to trigger both the start and stop beams to produce a quality distribution. The measured pulse is in the direction towards the inner limb region. The measured data in Fig.6.15 is due to the pressure pulse from outer limb, in which the flow is directed toward the outer limb with a deviation of approximately 7° from radial plane.
The same conclusion can be drawn about conditions at the 3mm measuring points.

Conclusion from measurements on the tangential-axial plane.

Measuring on the tangential-radial plane clearly demonstrates two pulses, one from each pressure pulse. Measuring the same point in the flow on a tangential-axial plane reveals a missing pulse. Analysis of the results suggest that the missing pulse probably has a high axial component of velocity. This together with the effect of the L2F focal volume rotating on a 30° plane, resulted in insufficient quality data to produce the second pulse.

6.4 Rotor Exit, 3 Flow Conditions

Fig.6.16 shows the flow velocity and angle profiles at the rotor exit, 20mm from the top of the duct for 3 different flow conditions. The two pulses within a cycle are well defined in both the flow velocity and angle profiles. Unlike the measurements made at the rotor inlet these velocity pulses have approximately the same magnitude. The flow angle pulses increase in magnitude at higher total mass flow conditions (away from the design point). From the steady test results it may be possible to understand why these pulses are approximately of equal magnitude instead of the unequal pulse, seen at the rotor inlet.

Figs.5.22 and 5.23 show that the effect of partial admission flow the effect on the flow velocity and angle is minimum. For example, when one of the limbs is fully closed the flow velocity and angle is almost the same as in partial and equal admission conditions (this is not the case at rotor inlet). Since the pulse flow condition is instantaneously similar to steady partial admission flow, similar effects on the flow velocity and angle are likely to result at the rotor exit under pulse flow conditions.

Fig.5.19 shows that at off design points the swirl in the duct

becomes more severe. This effect is also seen in pulsating flow where the flow angle, apart from increasing, also has a large fluctuation within the cycle. Fig.6.16 shows the variation of flow angles to be up to 12°, 5° to 23° and 12° to 36° as the flow condition moves away from design point.

Fig.6.17 shows the variation of flow velocity as pulse measurements were made across the duct for one off-design condition. The two velocity pulses of approximately equal magnitude are observed. The figure also show that the magnitude changes as the measurement point is moved across the duct. Fig.6.18 shows this variation more clearly by plotting only the peak velocity across the duct. This velocity profile is very similar to those obtained in the steady flow test as shown in Fig.5.22.

Fig.6.19 shows the variation of flow angle across the duct for the same condition. The two angular pulses are still pronounced in the flow angle profile. At the centre of the duct the flow angle is low indicating a minimum swirl. The flow angle variation is 12° to 30° at 25mm and 9° to 30° at 35mm. Closer to the wall (at 15mm and 45mm) this flow angle variation is between 18° to 50°, indicating high swirl. At the centre of the duct (30mm) most of the results were not processed due to the lack of sufficient quality data collect. This indicates a difficulty in measurement possibly due to the wake shed by the solid hub.

Conclusion from measurement at rotor exit

In the steady flow tests, rotor exit measurements showed that swirl increases as the flow condition departs from design point. When the flow condition is near the design point, a minimum swirl is noted. Under unsteady flow conditions, the extent of the swirl varies within a pulse. The pulses are well defined in terms of absolute velocity and flow angle. For flow

conditions away from the design point, it is clear that the swirl is more severe and the variation is greater.
By plotting the peak velocity of the flow characteristics across the exit duct, the result shows variation that is similar to those obtained under steady flow test. This is some indication that the fluid flow remains in dynamic equilibrium whilst the flow is unsteady.
Unlike the flow characteristics at the rotor inlet, both velocity pulses measured are of equal magnitude. This observation is also noted for different flow conditions and measuring points.

6.5 Rotor Inlet, Azimuth angle = 20°, 90°, 180° and 270° Different Divider Depth,

This section compares the unsteady gas flow characteristics for different separating divider wall plates. Measurements at different azimuth angles are also be compared.

Fig.6.20 shows measurements made with SWϕ = 80mm at different azimuth angles. Measurements at 1,2 and 3mm (measuring point) were not possible. Measurements at 4mm to 8mm reveal only one velocity pulse. The second pulse due to the pressure pulse coming from the inner limb is not measured around the outer limb region. It is probable that this pulse from the inner limb develops into a flow with a high axial component of velocity (as it arrives at the outer limb region) so that it cannot be detected whilst measuring in the tangential-radial plane. It could also be the result of a momentarily highly disturbed flow. This may leave very little space between it and the rotor for flow from the two limb to mix. With the extended divider, the space between the divider tip and the rotor tip is a minimum, so that the flow from each limb has very little

interspace in which to mix before arriving at the rotor inlet.

Fig.6.21 shows the flow characteristics measured at azimuth angle = 270° for SWϕ = 86 and 96mm. These are compared with the flow characteristics obtained at the same azimuth angle and with SWϕ = 80mm, Fig.6.20c. The measurements at SWϕ of 80mm show only one velocity pulse (consistently due to a pressure pulse coming from outer limb) for measurements from 4mm to 8mm. With SWϕ = 86mm, Fig.6.21a also shows one velocity pulse for measurements made from 3mm to 8mm. Unlike the flow characteristics with SWϕ = 80mm, these measurements show that the single velocity pulse is due to the pressure pulse from either the outer or inner limb depending on the measuring point. At measuring point 3mm and 4mm (which is around the inner limb region) the velocity pulse is due to pressure pulse arising from inner limb. At measuring points 6mm to 8mm, (which are around the outer limb region) the velocity pulse is due to pressure pulse arising from the outer limb. At the 5mm point which is approximately the centre of the volute exit, two velocity pulses are noted. This indicates that the flow from both limbs has been able to mix well at the mid section of the volute exit. With a larger separating wall diameter (from SWϕ = 80mm to 86mm) the larger interspace allows the flow from both limbs to mix at higher radius. This observation is note in steady gas flow characteristics.

Fig.6.21b shows the familiar two velocity pulses with SWϕ = 96mm. It also shows characteristically the varying magnitudes of the velocity pulses with the measuring point across the volute exit.

The comparison shows that with the larger separating wall diameter plates, the flow due to the pressure pulses in the two limbs have been able to mix better before arriving at the rotor. As the separating wall diameter becomes smaller, there is apparently little room for the flow in each limb to mix.

Fig.6.21c to 6.21e show the absolute flow angle for SWϕ = 80,86, and 96mm measured at 270° azimuth angle. The variation of the flow angle is significant in all cases. For SWϕ = 80mm and 86mm this is from 5° to 45°, depending on measuring point. Fig.6.21e shows some flow reversal with SWϕ = 96mm. This characteristic is not observed at 90° and 180° azimuth angle.

Fig.6.22 compares the velocities at volute exit with different separating wall diameters at 180° azimuth angle. The flow characteristics obtained with different separating wall diameter reveals very little difference, except for SWϕ = 80mm. This is also the observation made under steady flow condition.

Conclusions from the measurements with different separating wall diameters.

1. With a small separating wall diameter, SWϕ = 80mm, the flow from the pressure pulse in the inner limb does not mix well with flow from outer limb as it crosses to the outer limb region. This results in what is consistently observed as a single velocity pulse arising from the pressure pulse in outer limb. This observation is made at 270° azimuth angle only.

2. With SWϕ = 86mm the flow characteristics change noticeably from 180° to 270° azimuth angle. Two velocity pulses are observed at 180° azimuth angle. As the flow moves to 270° azimuth angle mainly one velocity pulse is observed. The single velocity pulse in this case arise from a pressure pulse in either the outer or the inner limb, depending on measuring point.

3. From the analysis of the results, applying different separating wall diameters does not significantly change the flow characteristics except for SWϕ = 80mm

6.6 Turbine performance under unsteady flow conditions.

6.6.1 Power developed by rotor

The unsteady gas flow characteristics at the rotor inlet and exit demonstrate large variations of absolute flow velocity and angle. Measurements of unsteady turbine performance by Dale (39) have shown large variations in turbine efficiency with blade speed ratio. Similar overall turbine performance measurements were not made during the present flow investigations. However, it is possible to combine the unsteady flow characteristics measured at both rotor inlet and exit to estimate the power developed by the rotor and from this the time-varying efficiency.

At the inlet flow velocities were measured just upstream of the rotor tip ($R/_{Rtip}$= 1.147, SWϕ = 86mm). The tangential and axial components of velocity required just downstream of the rotor exit can be estimated from the results obtained 30mm downstream of rotor trailing edge using method described in Appendix C. The method used to derive the power developed, isentropic power, blade speed ratio and turbine efficiency is described in Appendix D.

Fig.6.23 shows the variation of incidence angle for 3 different flow conditions. The instantaneous incidence angle is an averaged value obtained from measurements across the volute exit. This will be related to the turbine performance. Fig.6.24 shows the variation of power developed by the rotor for different flow conditions. In each case, it is apparent that the maximum power developed is associated with the maximum inlet pressure during the pulse. The pressure pulse and power variations are roughly in phase. With a high absolute velocity so that the tangential component of velocity exceeds the blade speed, an extreme negative incidence angle results. Thus the

maximum power is developed around the peak of the pressure pulse, where the incidence angle is in the negative region and away from the optimum value (from the steady flow results this is between 20° and 40° see Fig.5.3). Hence it follows that maximum incidence losses occur when the maximum power is developed in the rotor.

Fig.6.25 shows the development of instantaneous u/c under different flow conditions. At close to design point, Fig.6.25a shows variation of u/c between 0.44 to 0.67. It is also clear that the lower u/c values occur around high pressure pulse region where the absolute velocity is maximum.

The variation of u/c decreases as the flow condition departs from design point. At 0.17 kg/s and 0.24 kg/s flow conditions, the u/c variations are between 0.39 to 0.55 and 0.33 to 0.44 respectively. The general trend of instantaneous u/c values decreases as the flow condition departs from the design point. Comparing the instantaneous power developed by the rotor (Fig. 6.24) and u/c, it becomes clear that the maximum power occurs at about the low u/c region.

At the furthest off-design condition (Fig.6.24c) the power developed increases substantially and this corresponds to a marked decrease in u/c values. Because maximum power occurs at low u/c, it is advantageous to design the turbocharger turbine so that higher turbine efficiency can be realized at low u/c values.

Fig.6.26 shows the development of instantaneous turbine efficiency (total-static) for different flow conditions. At close to the design point, Fig.6.26a shows large variations of turbine efficiency between 30% to 70%. This is due the large variations of power developed by the rotor and incidence angle (and hence incidence losses). High efficiency occurs around a region where the pressure begins to fall. Low efficiency occurs when the pressure is rising. Relating this observation with

power developed it follows that high efficiency region occurs as the maximum exhaust pulse energy is declining. Low efficiency occurs when the bulk of exhaust pulse energy is building up.
As the flow departs from design point, the variation of turbine efficiency decreases. At the 0.17 kg/s and 0.24 kg/s flow conditions, the turbine efficiency varies between 26% and 61% and 26% and 45% respectively. The general trend of instantaneous turbine efficiency decreases significantly as the flow condition moves away from the design point (Fig. 6.26).

Fig.6.27 shows the instantaneous turbine efficiency plotted against the corresponding u/c values. The steady flow turbine efficiency curve obtained at the same rotor speed is superimposed. This comparison shows clearly that under unsteady flow conditions the turbine efficiency departs from the steady curve, and forms in what appears to be a loop (this will be refered to as an efficiency loop, Fig.6.27). This efficiency loop is similar to that which was observed in Dale's investigation (38,39). In addition similar variations of this efficiency loop are noted at different flow conditions. For example at near the design point condition (Fig.6.27a) the efficiency loop is broader. This efficiency loop is also similar to that which was obtained earlier (section 5.4) under steady flows condition using a series of partial admission flows with the total mass flow to turbine held constant.
At close to the design point, Fig 6.27a shows that the efficiency loop varies around but predominantly below the steady efficiency curve. This broad efficiency loop is a combination of large variations of instantaneous u/c and turbine efficiency at close to design flow conditions. The turbine efficiency varies from as high as 70% down to around 30%. This is a very large variation. It is associated with very large variation of incidence angle at rotor inlet (55° to -40°

see Fig.6.23). At the rotor exit there is a minimum swirl (instantaneously). The observation from steady flow tests (with a series of partial admissions) is that the turbine efficiency varies by about 16%.

As the flow departs from the design condition, the efficiency loop gradually falls below the steady efficiency curve. The loops also become narrower and extend over the lower end of the u/c and turbine efficiency range. Fig.6.27c shows that turbine efficiency decreases from 44% with u/c at 0.44 to 25% with u/c at 0.32. At this off-design flow condition, low turbine performance is linked to a negative incidence angle between -14° to -52° (Fig.6.23). Compared with near design flow conditions, this incidence angle variation is smaller but it becomes more negative. Similar results have been observed in steady flow tests in which the incidence angle becomes more negative as flow condition departs but only in one direction from design condition. At the rotor exit, the off-design flow condition is associated with a maximum variation of swirl (from 12° to 37° in Fig 6.16).

While Figs.6.27b,c outline only the efficiency loop, Fig.6.27a actually traces two distinct efficiency loops resulting from the two pressure pulses. Dale's (38,39) experiments were carried out with the pressure pulses from the outer and inner limbs aligned in phase, and this resulted in a single efficiency loop. The present investigation was carried out with the two pressure pulses aligned at 180° out of phase, resulting in these two efficiency loops. Fig.6.28 shows the breakdown of the efficiency loop and identifies them as efficiency loops 1 and 2, resulting from pressure pulses in the outer and inner limbs respectively. These figures show more clearly the variation of turbine performance under unsteady flow conditions. The turbine efficiency loop generally varies from high turbine efficiency and high u/c to low efficiency with low u/c values. Both efficiency loops are very similar at off-

design conditions.

6.6.2 Fixed absolute flow angle

Although a turbine with inlet nozzles usually achieves a higher peak efficiency than one with nozzleless casing (due to better and more uniform flow distribution and guidance around the rotor tip), the latter is better equipped to cope with off design condition, Watson (51). Regardless of mass flow rate, the use of inlet nozzles will constrain the flow angle at entry to the rotor. As the flow rate moves away from the design conditions, the inlet velocity will change in magnitude, not direction. The relative velocity approaching the impeller tip will depart from the radial direction, creating an incidence loss. If a nozzleless casing is used, the flow angle will change with the flow rate. An incidence loss will still result, but the incidence angle (and hence the loss) will be less. Thus the nozzleless turbine has a wider range of efficient working and is commonly used on turbochargers for engines working over wide speed and load ranges.

The information from Watson (51) on flow in nozzled and nozzleless turbine is based on steady flow knowledge. While the flow characteristics under steady flow conditions allow the gas angle in a nozzleless turbine to adapt itself when flow condition changes, the same may not be true when the flow condition is unsteady.

The unsteady flow measurements show that the flow angle varies significantly both within a cycle and around the rotor periphery. This, together with the variation of absolute velocity, results in large variations of incidence angle and turbine efficiency. Though the present investigation is not extended to unsteady flow measurements in a nozzled turbine, the results obtained with the nozzleless turbine can be used estimate how incidence angles and turbine performance under

pulsating flow conditions may be affected by the presence of a nozzle. This is done by applying a constant absolute flow angle (instead of the measured values) together with the varying absolute velocity to deduce the incidence angle and turbine efficiency. Results were obtained for constant absolute angles from 5° to 35° at 5° intervals with the unsteady flow characteristics for three flow conditions.

The incidence angle under these conditions together with conditions when the flow angle is allowed to vary are presented from Figs.6.29 to 6.35. At 5°, a greater variation of incidence angle (than when the flow angles vary) occurs for the three flow conditions. As the angle increases, this variation of incidence angle decreases. When this angle is greater than 20° the variation becomes less than when the flow angle is allowed to fluctuate.

Figs.6.36 to 6.42 show the turbine efficiency versus blade speed ratio (u/c) with different fixed angles applied. For the 5° angle a large variation of turbine efficiency is observed. Near the design point flow condition, the peak efficiency is higher than when the flow angle is allow to fluctuate (Fig.6.29), but for the off-design condition, fixing the flow angle at 5° resulted in a lower turbine efficiency (the low end of the efficiency loop is around 11%-12% which is very low compared to that in nozzleless turbine under similar conditions).

As the angle increases the variation of incidence angle reduces and with it, the turbine efficiency. However, the maximum efficiency also falls. The optimum angle appears to be from 10° to 15° where at off-design conditions the efficiency is maximised. At off-design conditions the efficiency values increase appreciably from what is noted with a 5° angle. The lower end of the turbine efficiency improves to 24% and the higher end to 50%. Also under this condition the efficiency

loop for near the design condition does not decrease appreciably (from the 5° fix-flow angle).

The above analysis shows that by increasing the stator exit angle, the variation of incidence angle may be reduced, thus bringing the incidence angle closer to the optimum value of about +28° noted in the steady flow tests presented in section 5.2. This ideally would be an advantage as it reduces incidence losses. But increasing the stator angle also causes the instantaneous mass flow to the rotor to increase. This increases the power output by the rotor and the isentropic power. Overall, the turbine efficiency decreases quite appreciably at higher angles. However it must be stressed that this analysis is based on applying a fixed stator angle to the unsteady gas flow characteristics obtained in a nozzleless turbine. The actual variation of absolute velocity in a nozzled turbine may be different from that obtained in nozzleless turbine. In addition with a nozzled turbine, whether the flow angle will remain constant after the nozzle under pulsating flow conditions requires experimental results to verify.

While there is still virtually no unsteady gas flow information in either nozzled or nozzleless turbines available in the open literature, this analysis offers some ideas on how the incidence angle and turbine performance can be affected by nozzle setting under pulsating conditions.

Conclusions from the turbine performance under unsteady flow conditions.

A method to derive the turbine performance using the unsteady flow characteristics measured at the rotor inlet and exit has yielded some useful deductions. There is certainly room for improvement in the method used to estimate the flow characteristics immediately after the rotor exit. However this method does provide some indication of the unsteady flow

turbine characteristics and these are comparable to results obtained by Dale's investigation (38,39).

1. The power developed by the rotor varies with the pressure pulse. Higher power is developed due to increased mass flow and this occurs around the low u/c region.

2. At off-design conditions, the variation of power is greater than near the design condition but u/c variation is greater near the design point.

3. Large variations of incidence angle are noted particularly at the design point condition. This, together with the variation in power developed, probably contributes to the large variation of turbine efficiency. This variation is a maximum near the design point condition. It is reduced as the flow departs from this condition but the general efficiency trend decreases as well.

4. Combining the instantaneous turbine efficiency with the corresponding u/c values produces efficiency loops. At near the design point condition, this loop is comparatively broad. At this point the turbine operates both above and below the steady efficiency curve.

5. As the flow departs from design point, the efficiency loops gradually fall below the steady efficiency curve. The loops also become narrower and extend over the lower end of the u/c and turbine efficiency ranges.

6. The variation of turbine efficiency versus u/c can be identified as two efficiency loops, each resulting from the pressure pulse arising from one limb. These loops are similar in particular at off-design conditions.

7. At off-design flow conditions the lower turbine efficiency is associated with a negative incidence angle between 14° to 52°. At the rotor exit, a higher swirl is observed.

8. By applying a constant flow angle to the unsteady flow characteristics, it is possible to model a nozzled turbine under pulsating flow conditions. As this angle increases, the incidence angle becomes more positive. This brings the incidence angle closer to optimum value (as in steady flow result). However, at angles greater than about 20° the trend is for turbine efficiency to decrease appreciably after 20° angle setting. The optimum angle appears to be 10° to 15°.

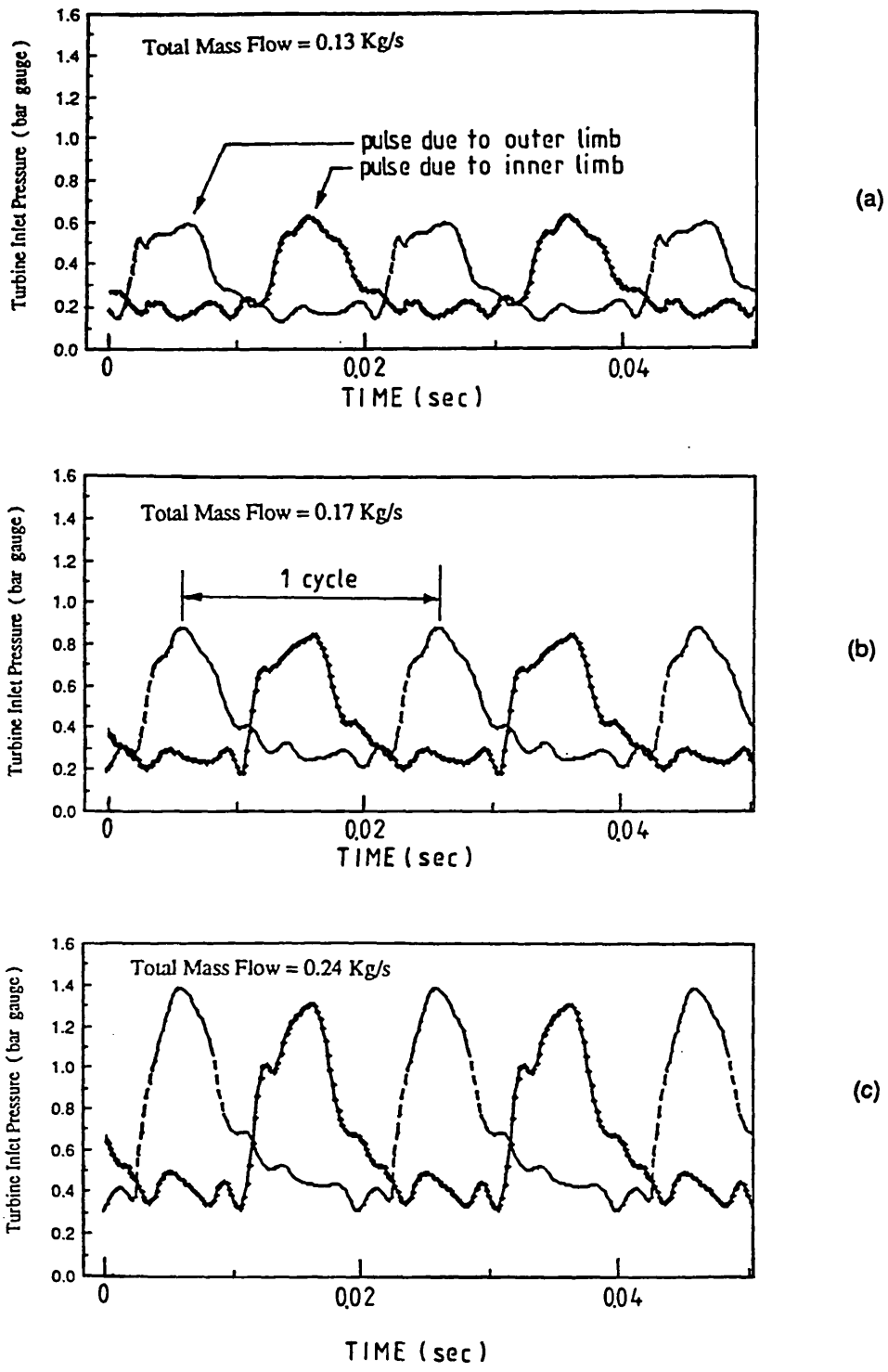


Fig. 6.1 Instantaneous Pressure

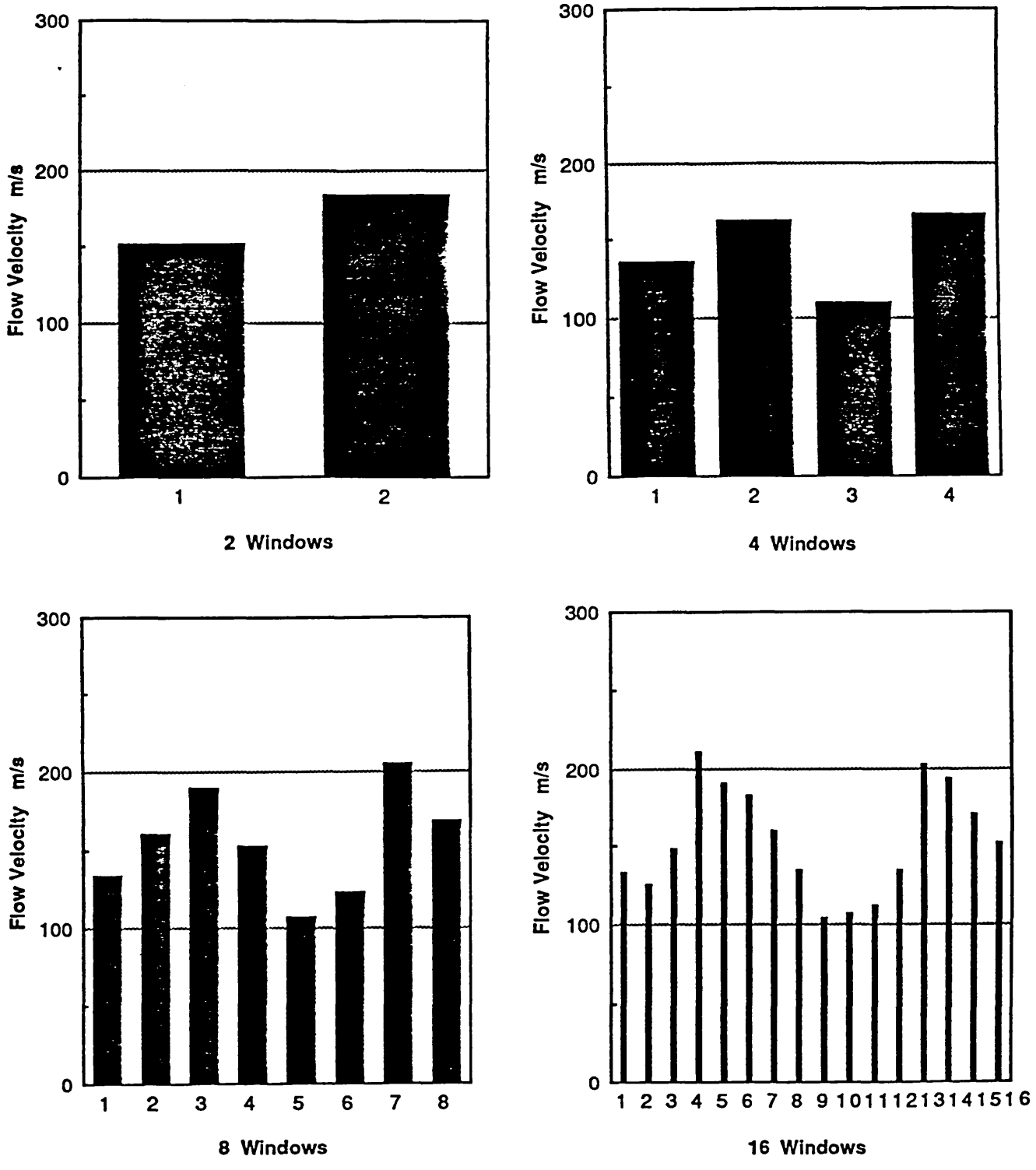
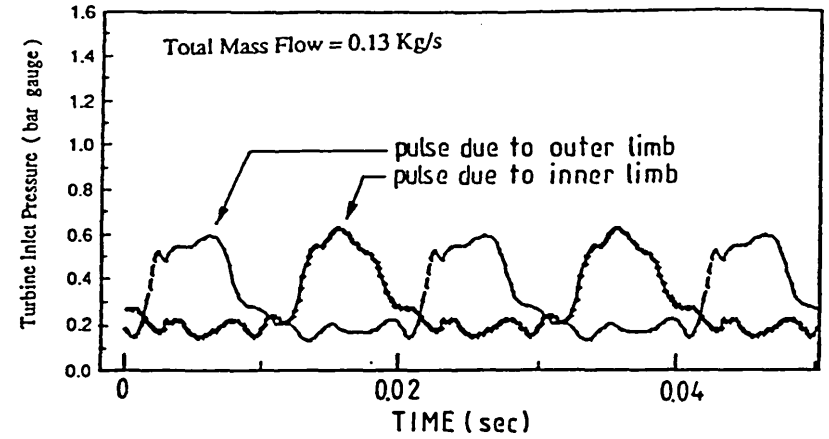
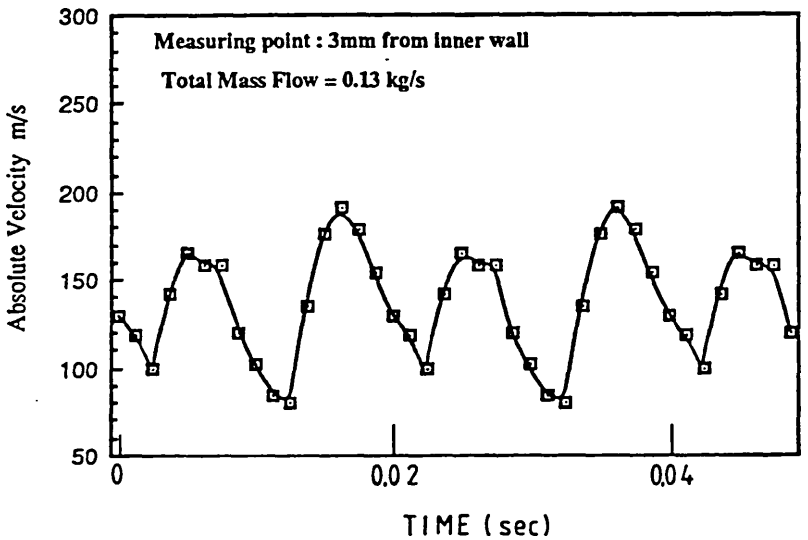


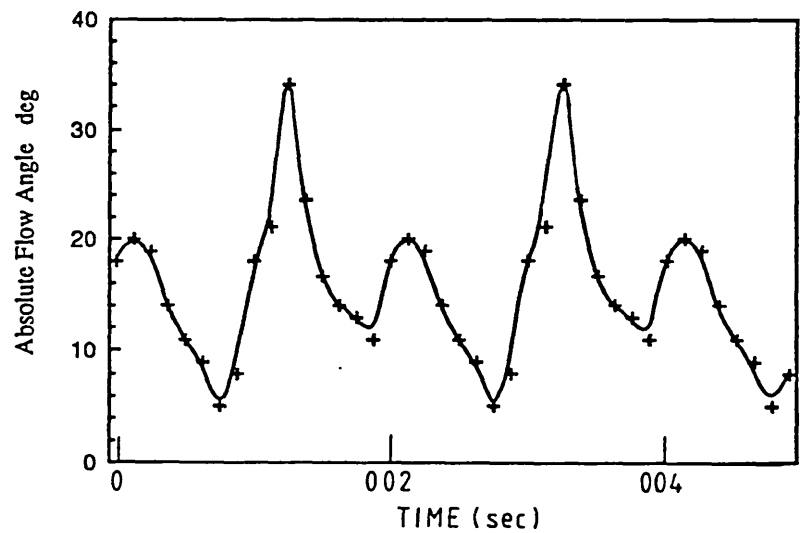
Fig. 6.2 Instantaneous Flow Velocity



(a)



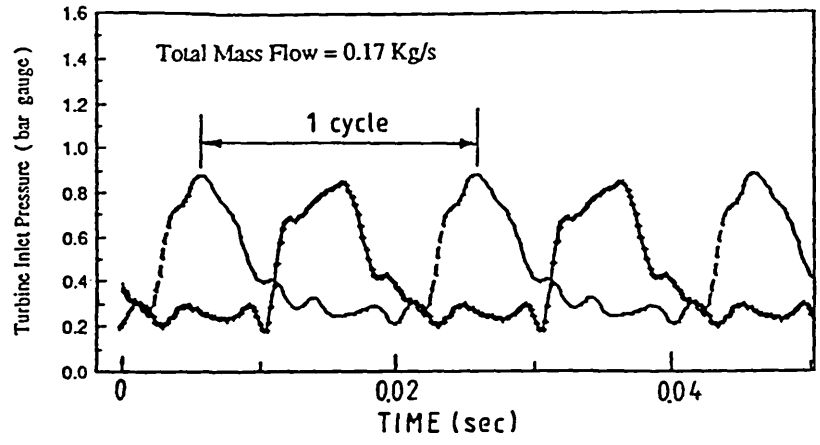
(b)



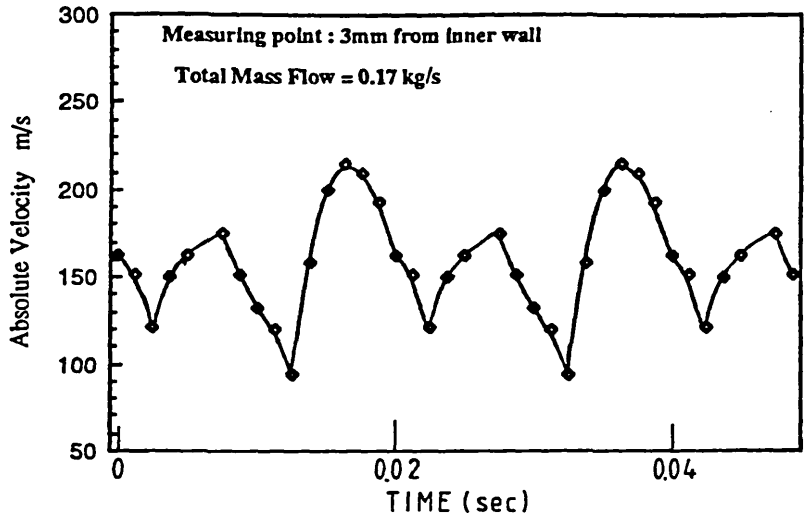
(c)

Unsteady flow characteristics at rotor inlet

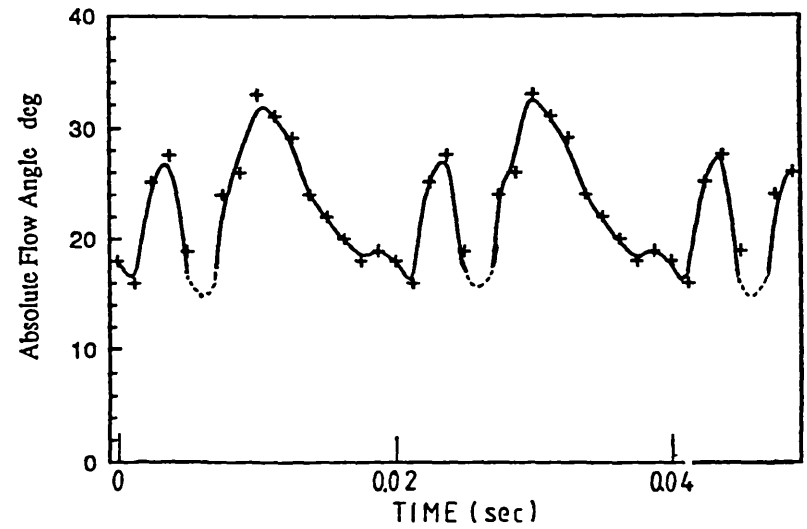
Fig. 6.3



(a)



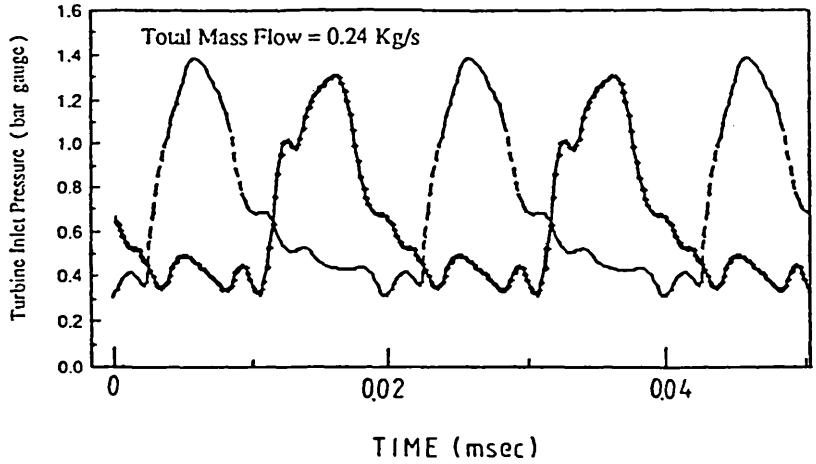
(b)



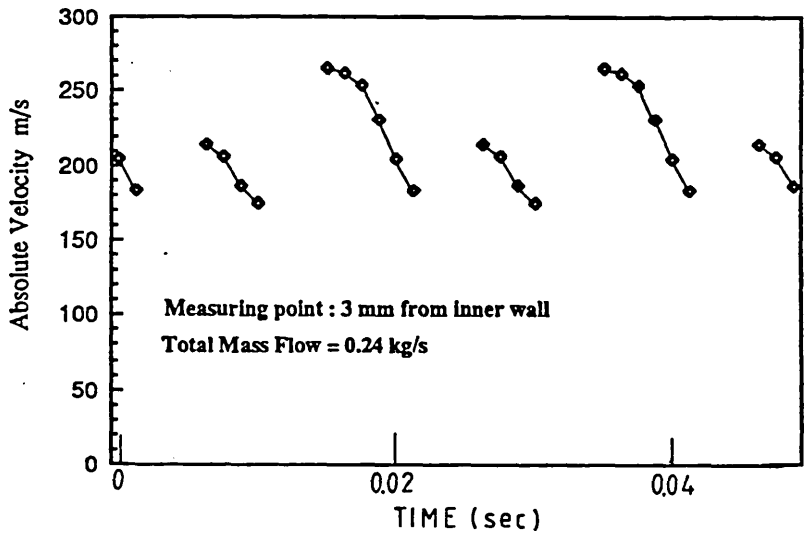
(c)

Unsteady flow characteristics at rotor inlet

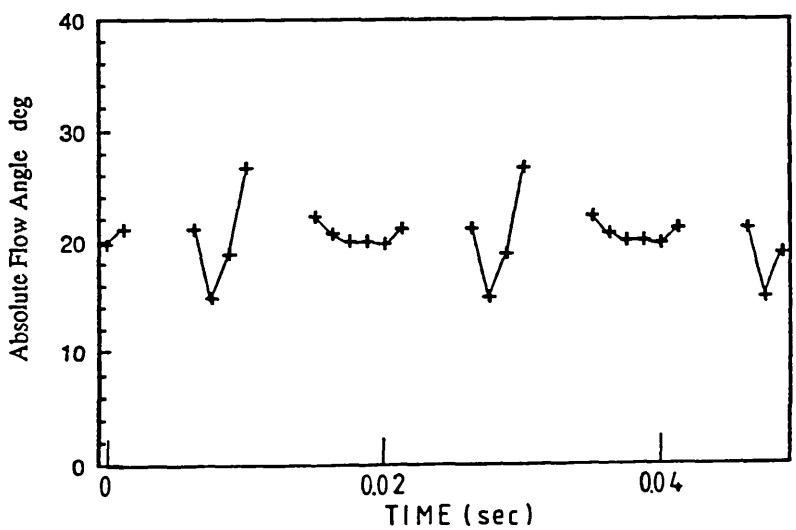
Fig. 6.4



(a)



(b)



(c)

Unsteady flow characteristics at rotor inlet

Fig. 6.5

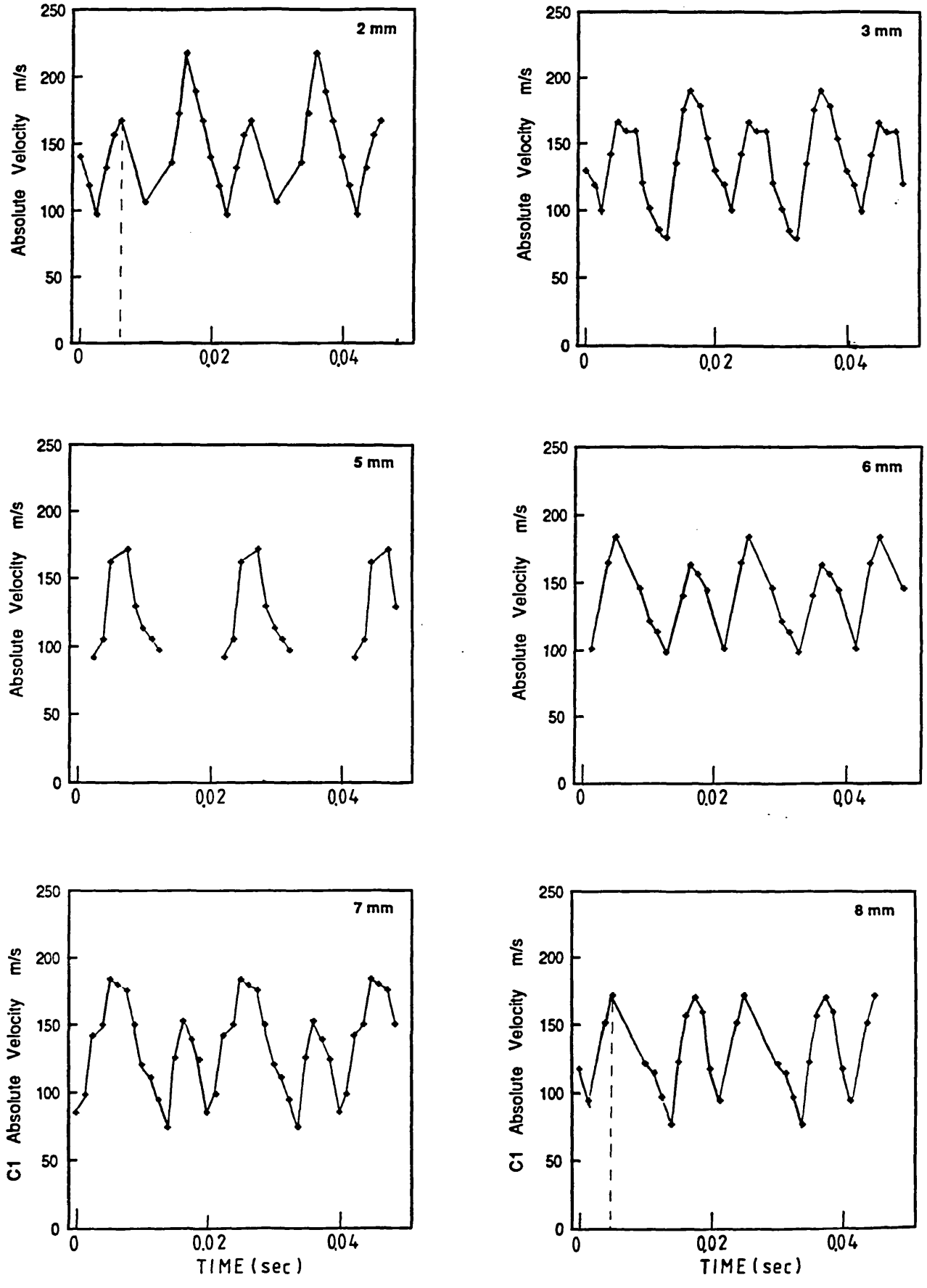


Fig 6.6 **Absolute velocity across volute exit** Total Mass Flow = 0.13 Kg/s

Rotor Inlet
180° out of phase 34000 RPM
Pulse Frequency 50Hz
180° Azimuth Angle

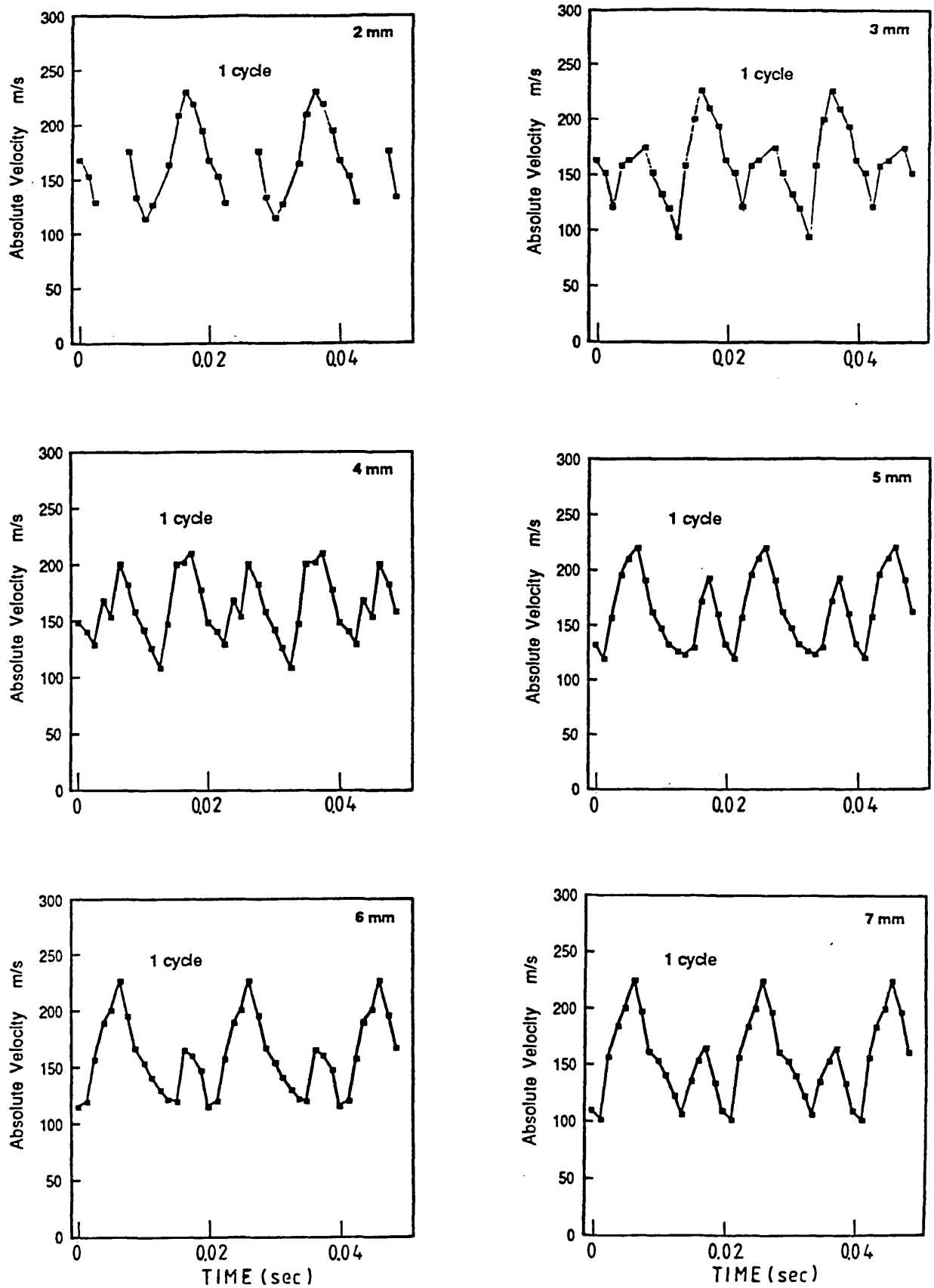


Fig 6.7 **Absolute velocity across volute exit**

Total Mass Flow = 0.17 Kg/s

Rotor Inlet
180° out of phase
Pulse Frequency 50Hz
180° Azimuth Angle

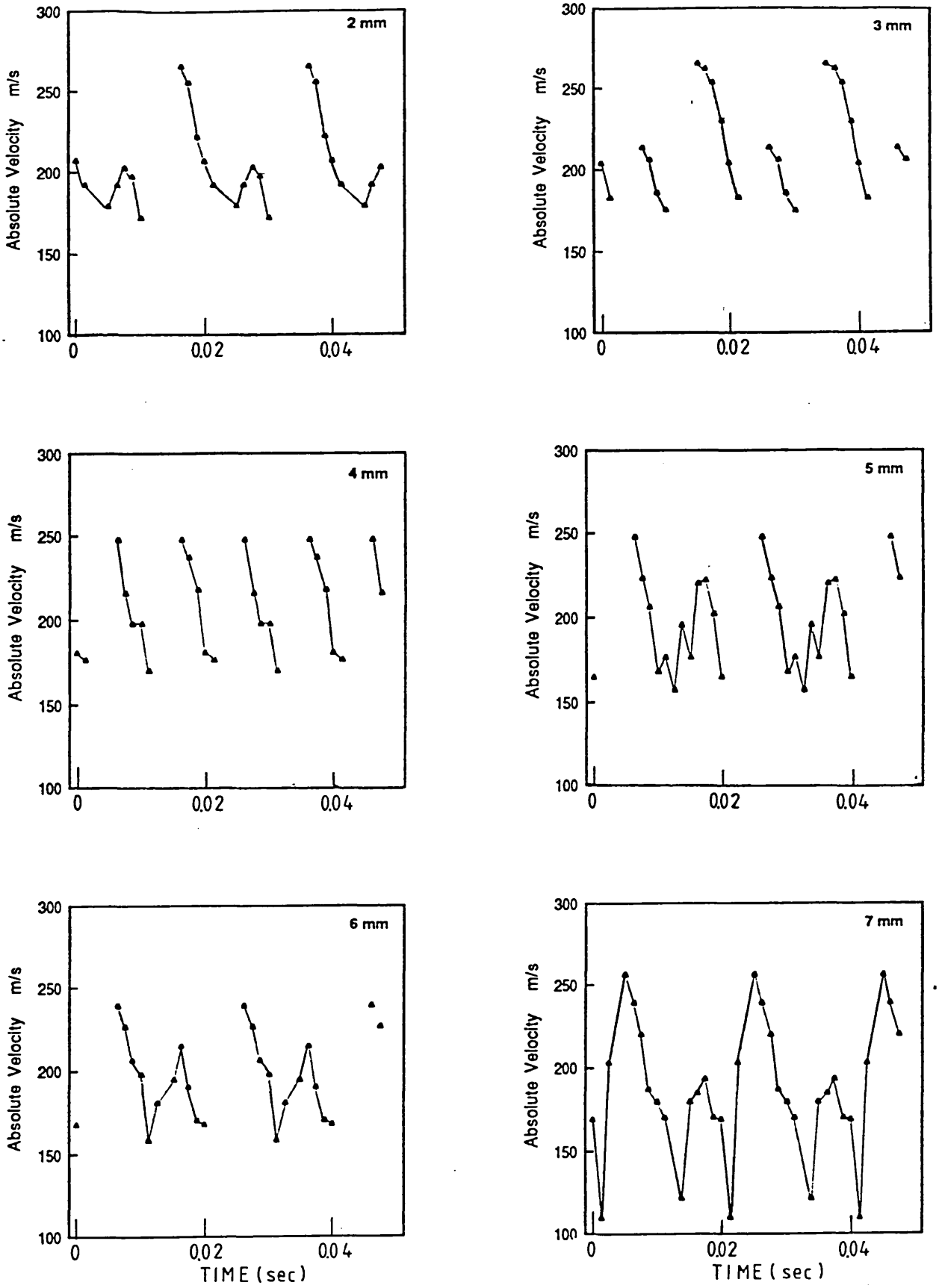
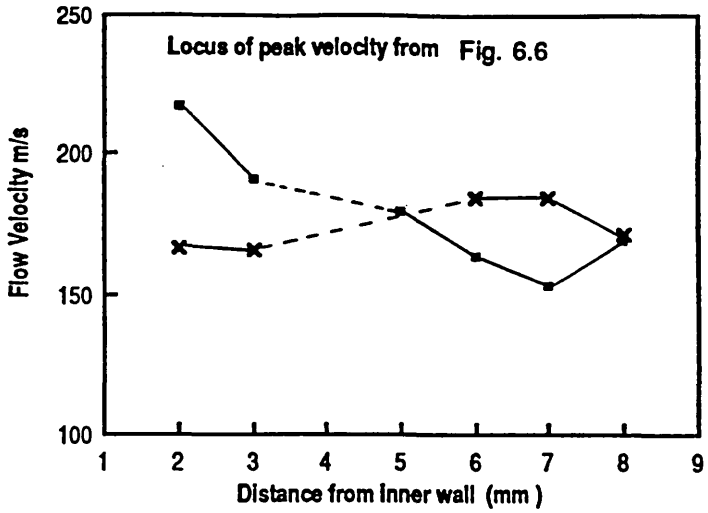


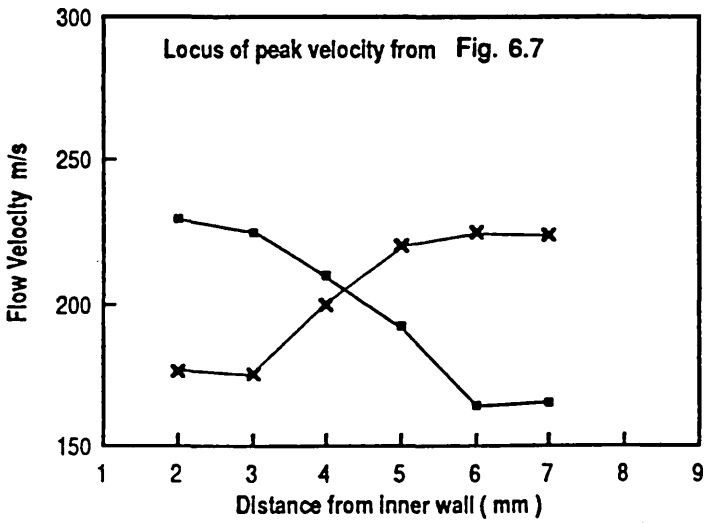
Fig 6.8 Absolute velocity across volute exit

Total Mass Flow = 0.24 Kg/s

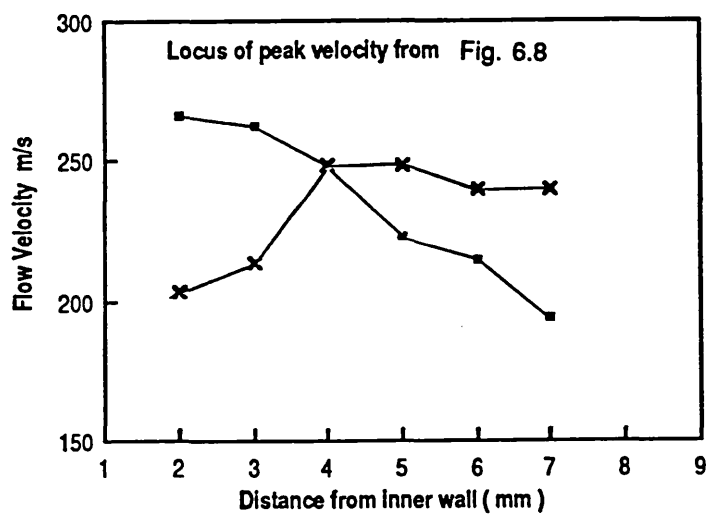
Rotor Inlet
180° out of phase 34000 RPM
Pulse Frequency 50Hz
180° Azimuth Angle



(a)



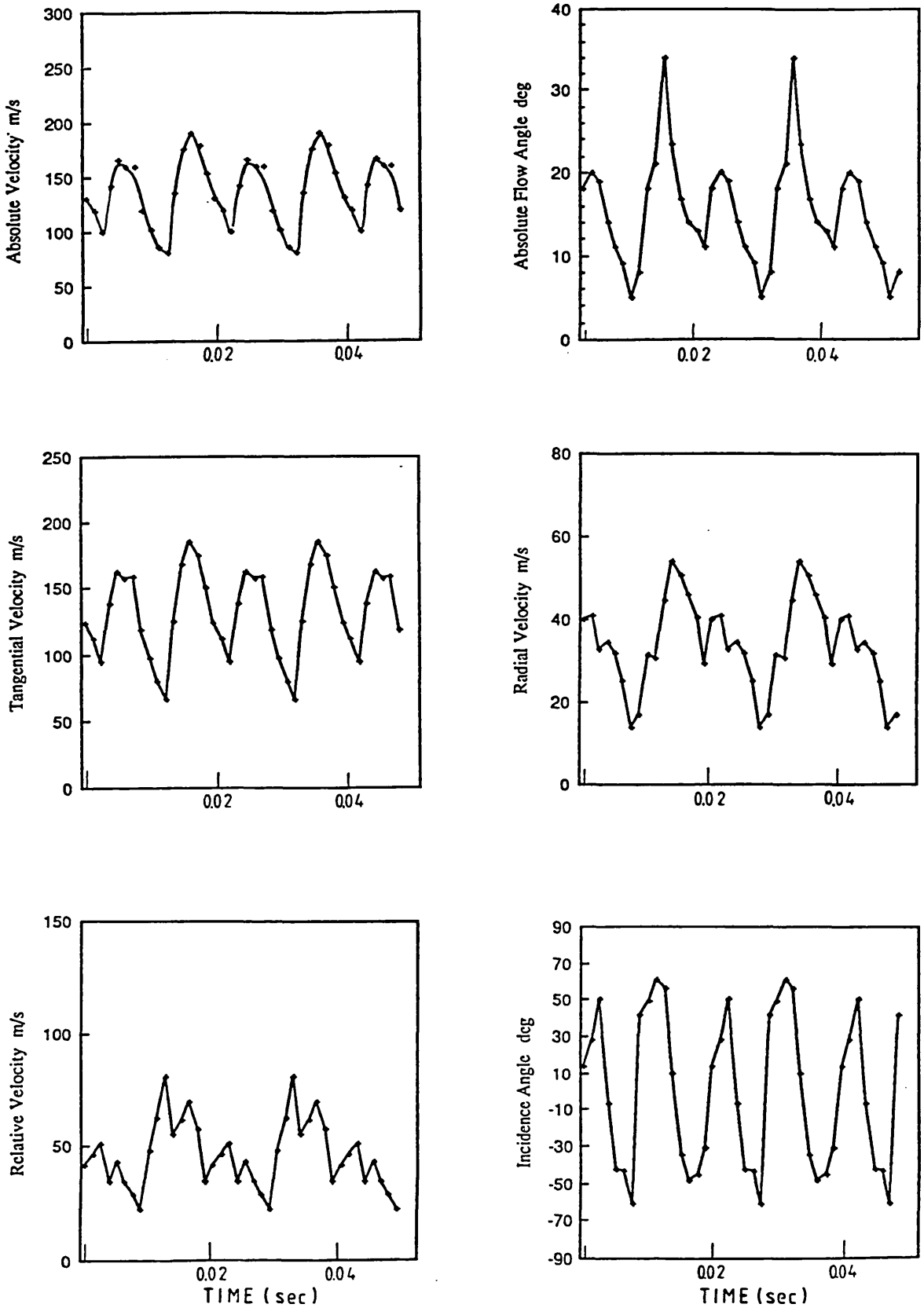
(b)



(c)

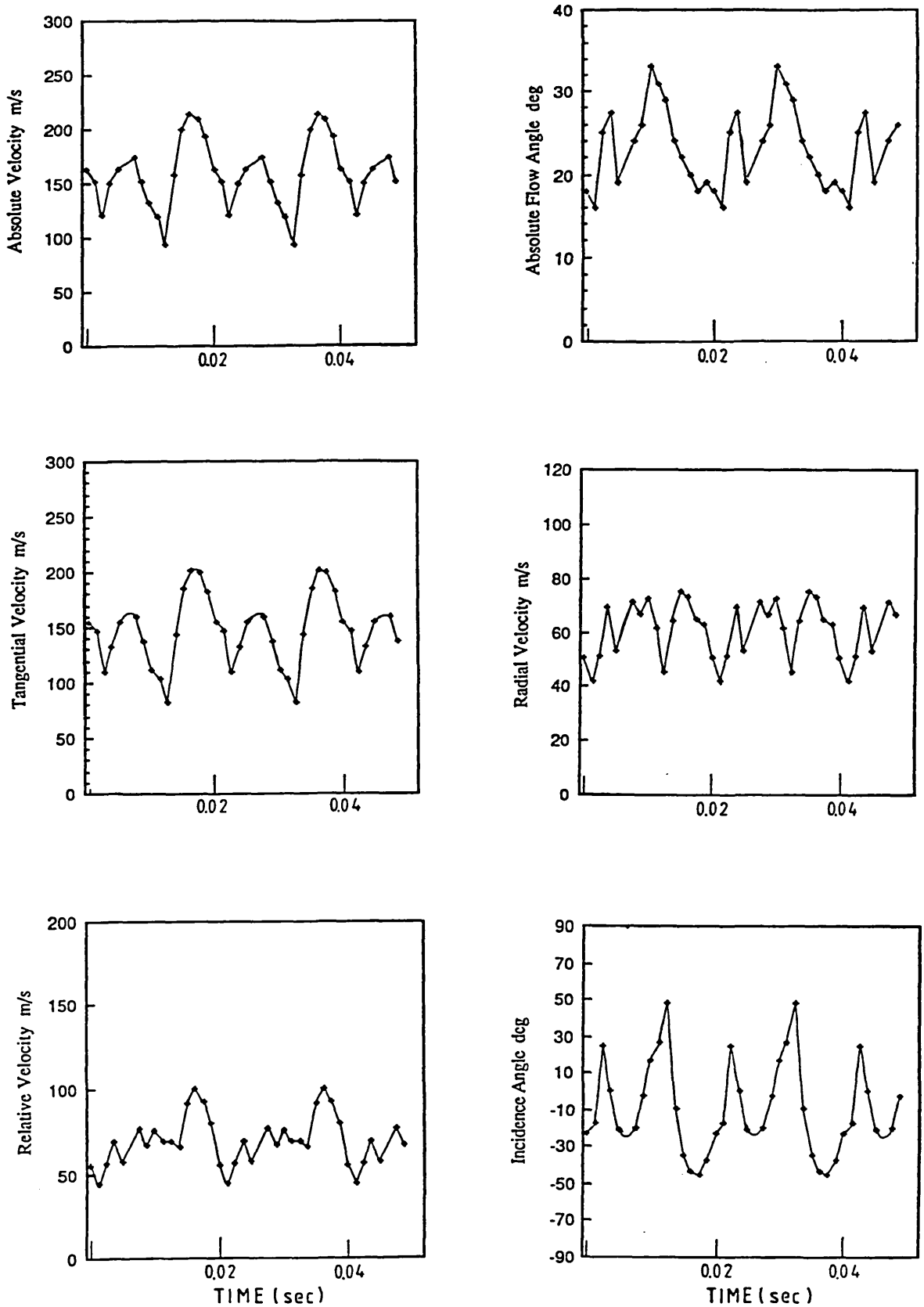
x Peak velocity at 7ms
• Peak velocity at 17ms

Fig 6.9 Loci of peak velocity



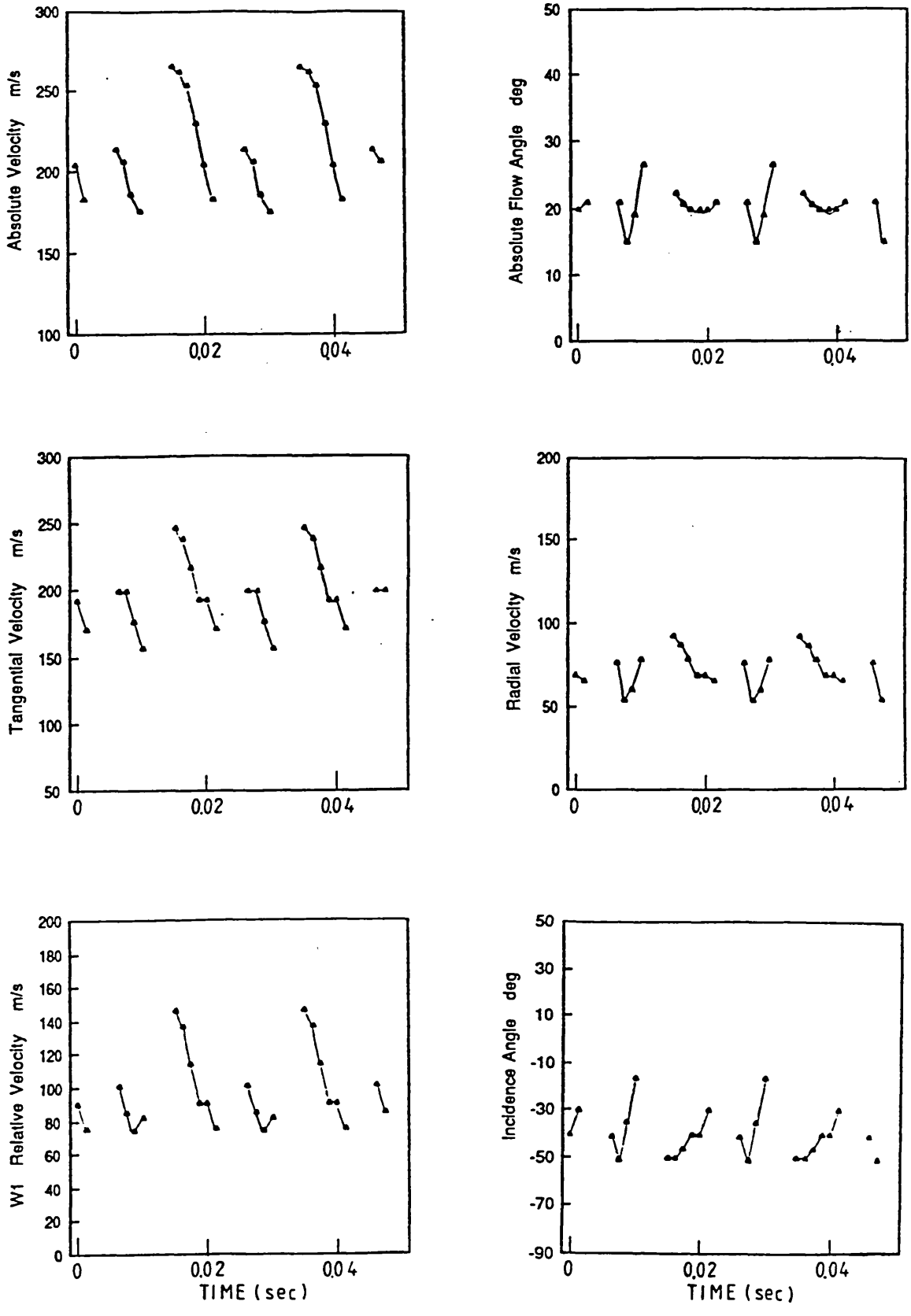
Measuring point : 3mm from inner wall
Total Mass Flow : 0.13 kg/s

Fig 6.10 Instantaneous gas flow characteristics



Measuring point : 3mm from inner wall
Total Mass Flow : 0.17 kg/s

Fig 6.11 Instantaneous gas flow characteristics



Measuring point : 3mm from inner wall
Total Mass Flow : 0.24 kg/s

Fig 6.12 Instantaneous gas flow characteristics

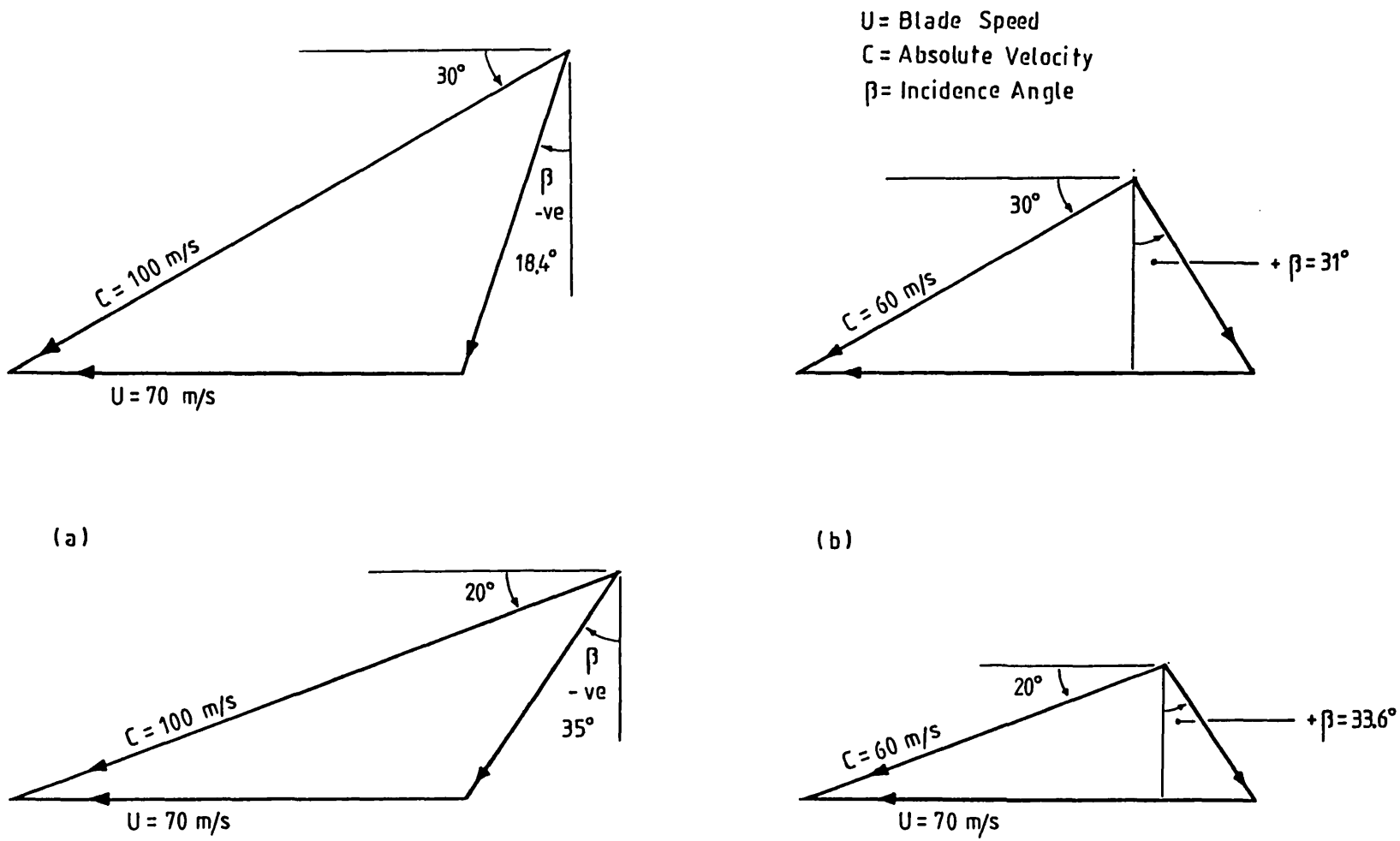
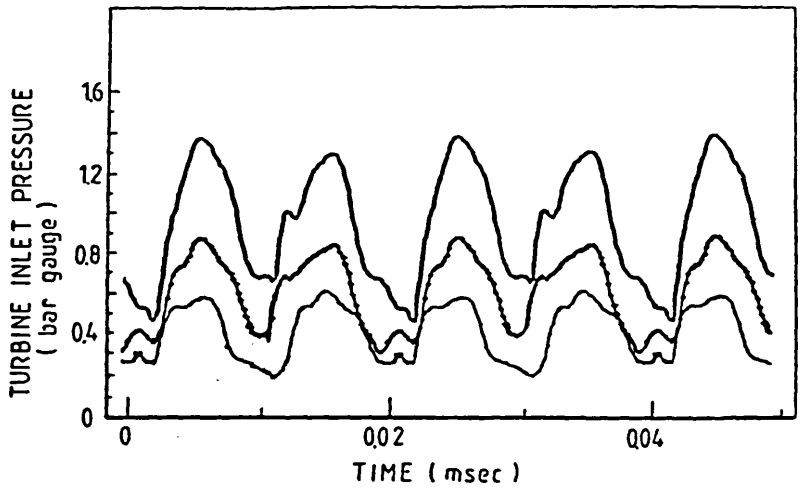
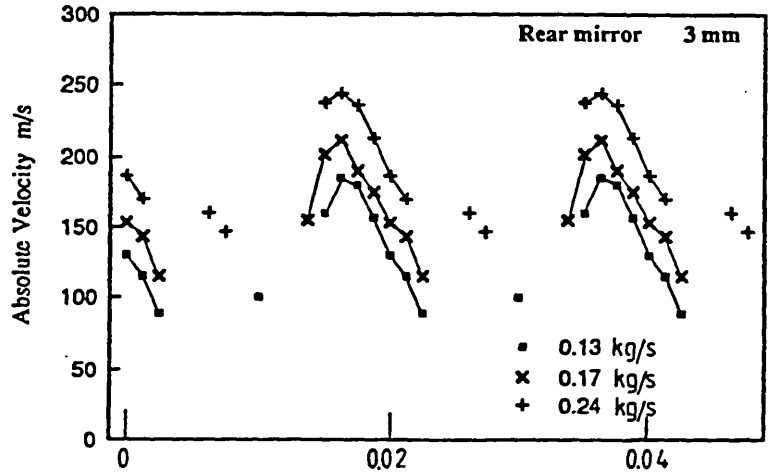
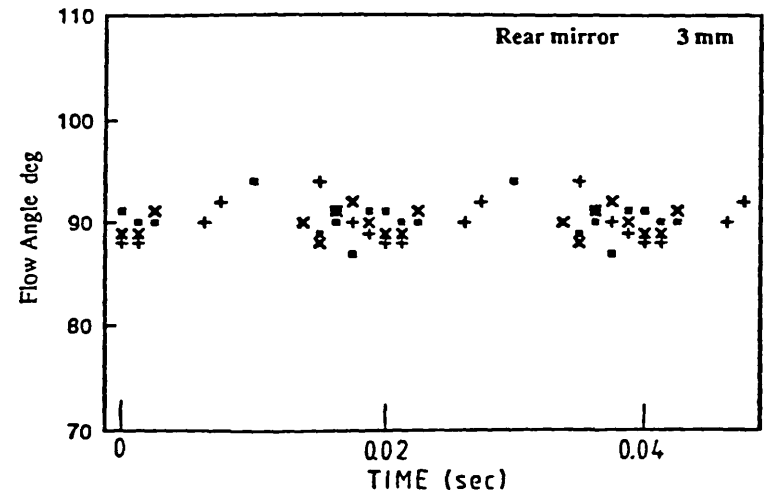


Fig 6.13 Velocity triangles

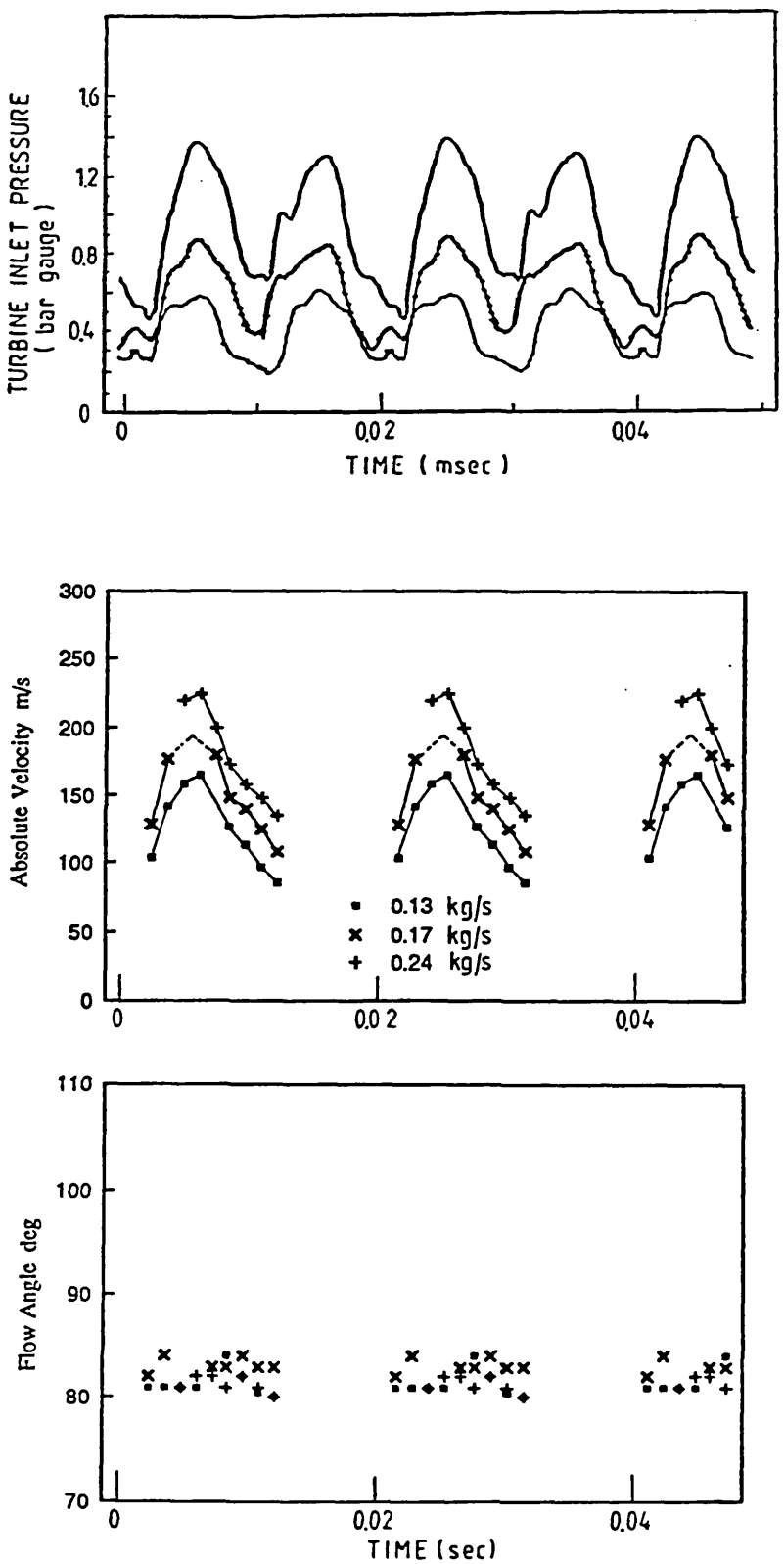






Note : 90° flow angle means flow does not deviate from the radial plane i.e zero axial component of velocity, see Fig. 4.20

Fig 6.14 Measuring flow via mirror at 3mm point



Note : 90° flow angle means flow does not deviate from the radial plane i.e zero axial component of velocity, see Fig. 4.20

Fig 6.15 Measuring flow via mirror at 7mm point

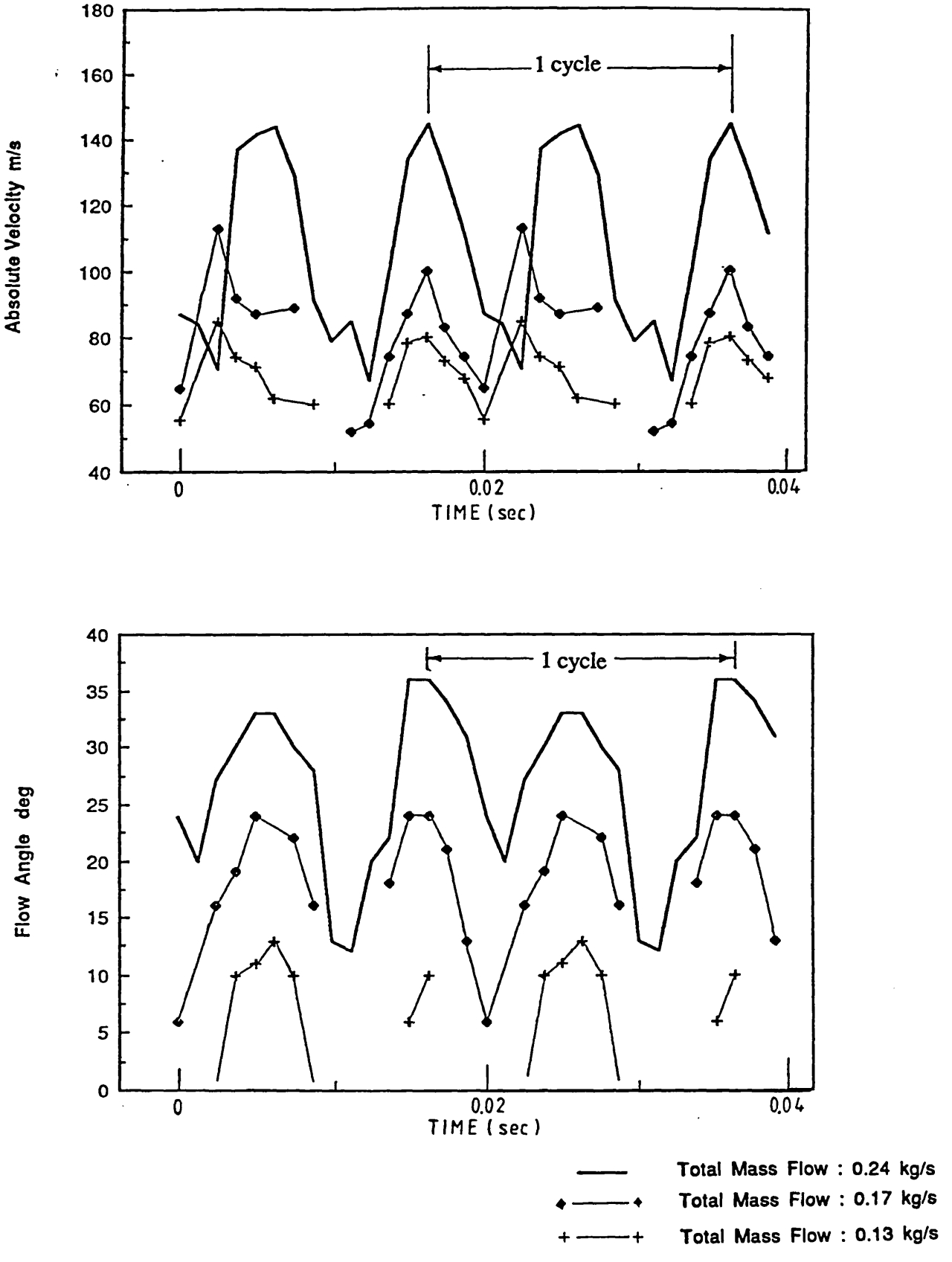
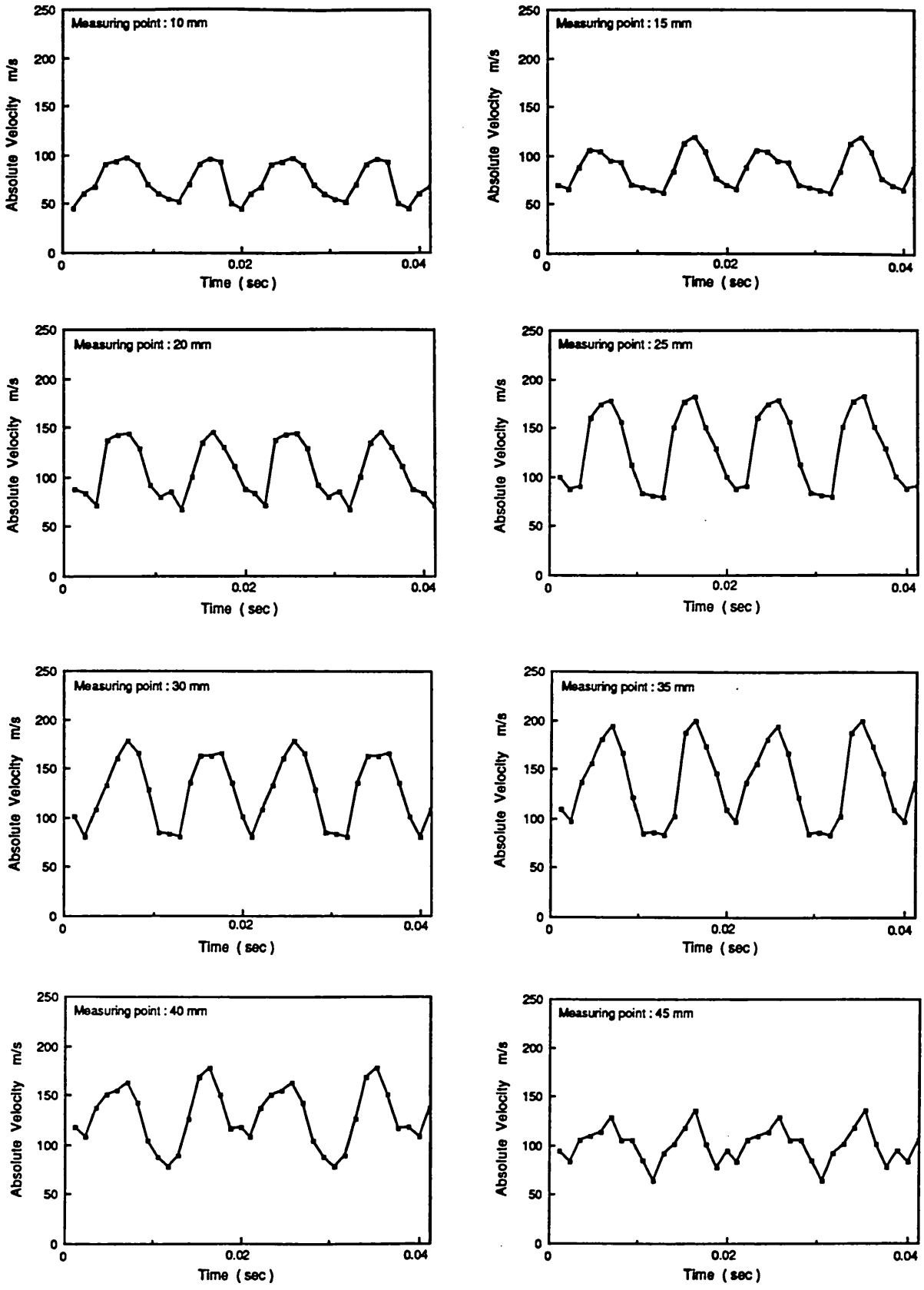


Fig 6.16 Unsteady flow characteristics at rotor exit



Total Mass Flow = 0.24 Kg/s

Fig 6.17 Instantaneous flow velocity across exit duct

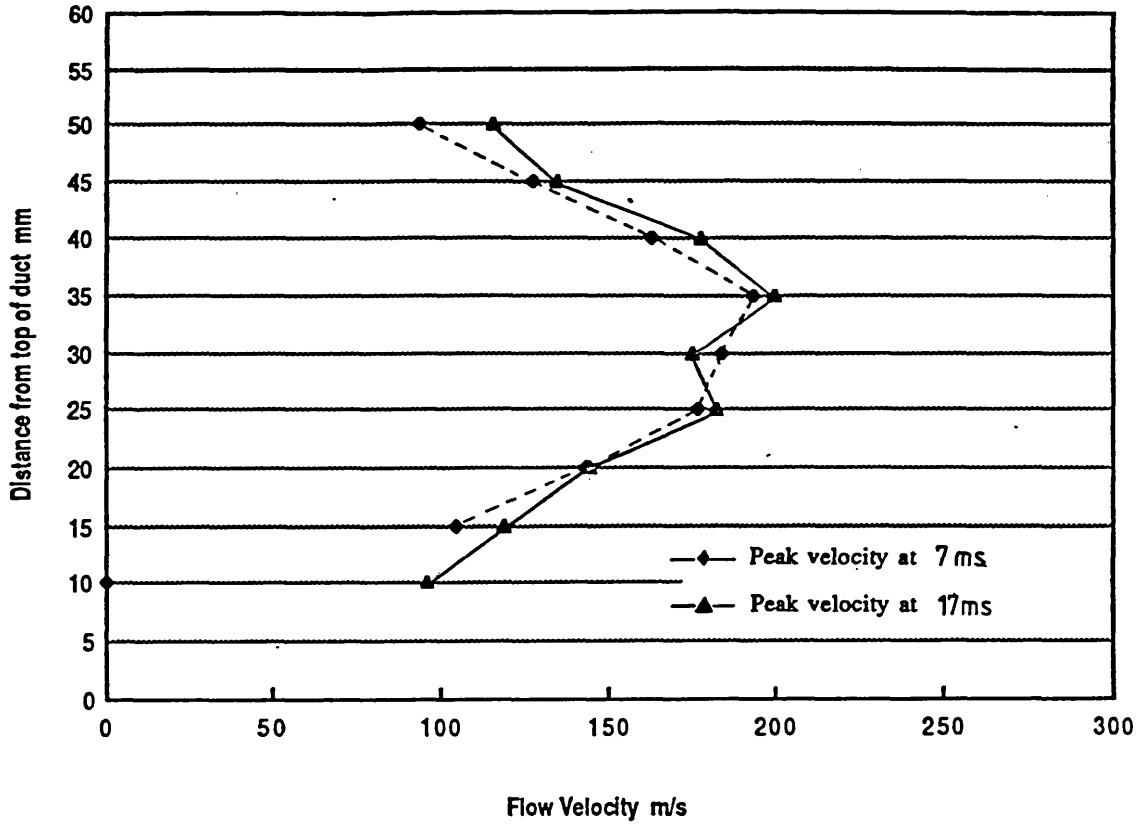
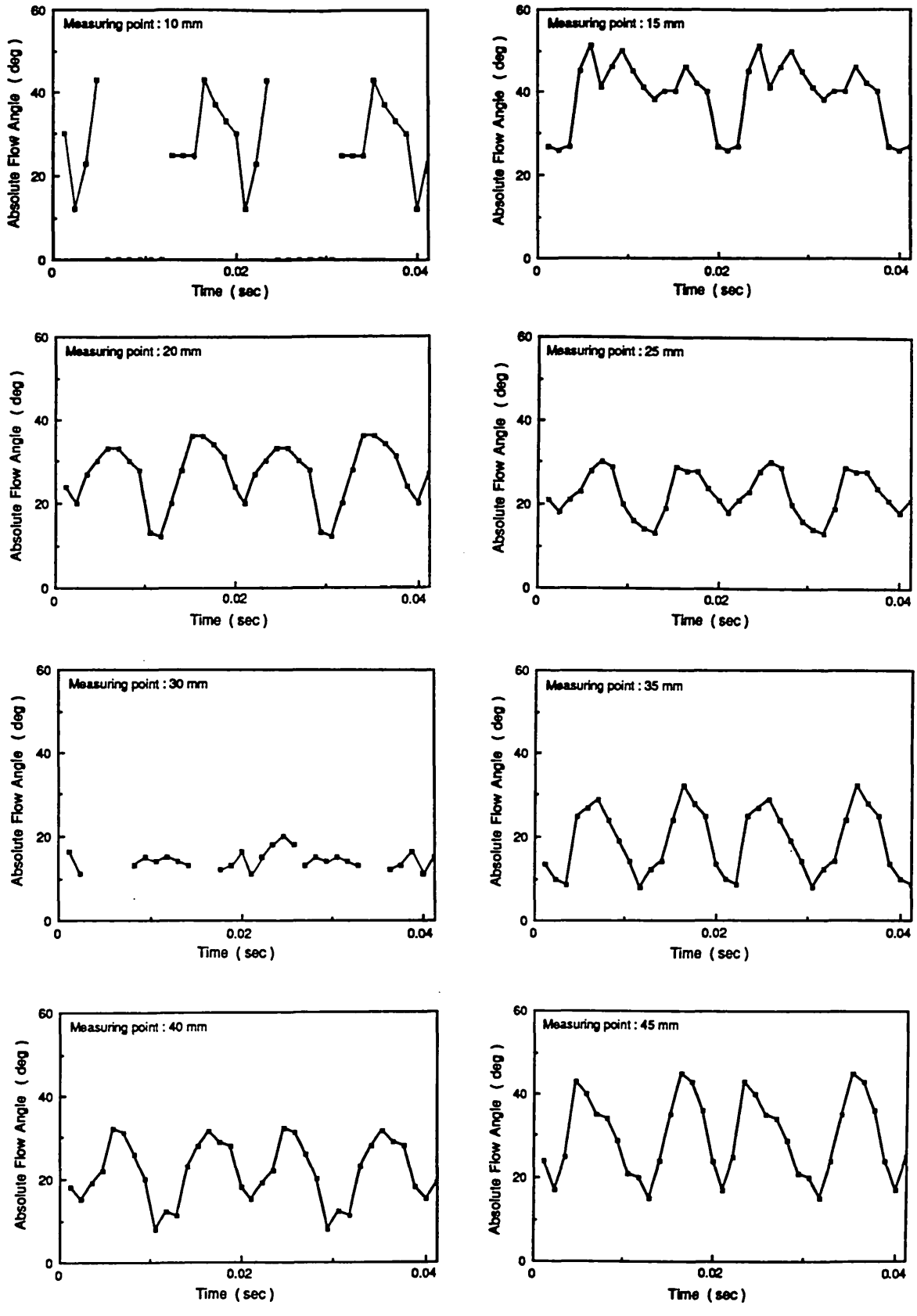
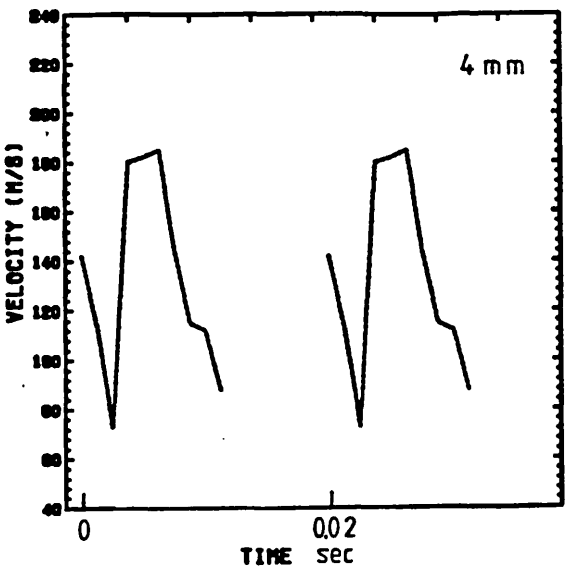


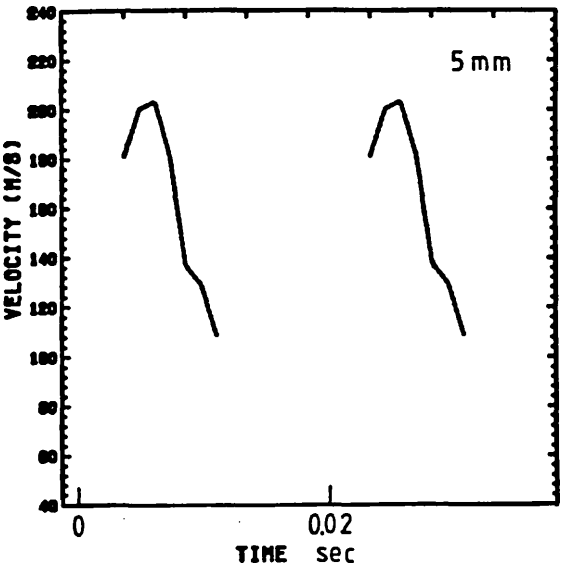
Fig 6.18 Loci of peak velocity at rotor exit

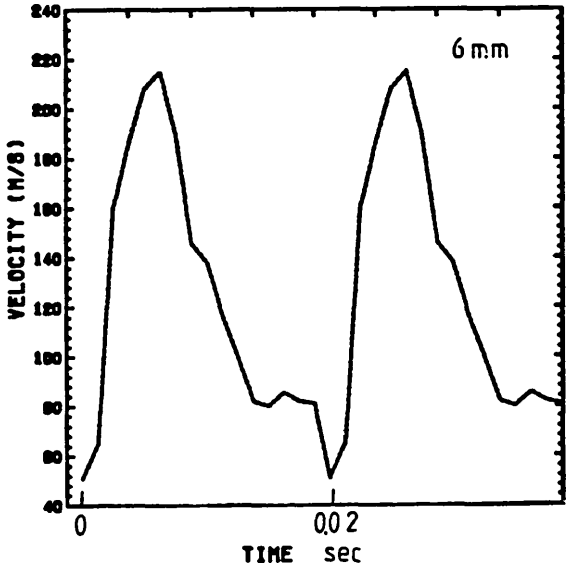


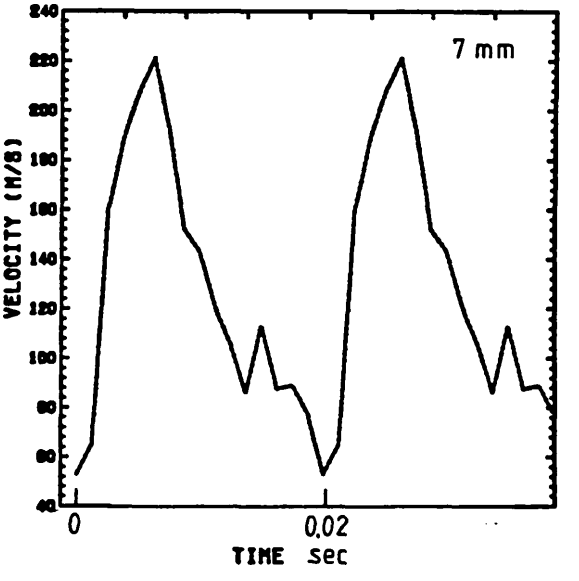
Total Mass Flow = 0.24 Kg/s

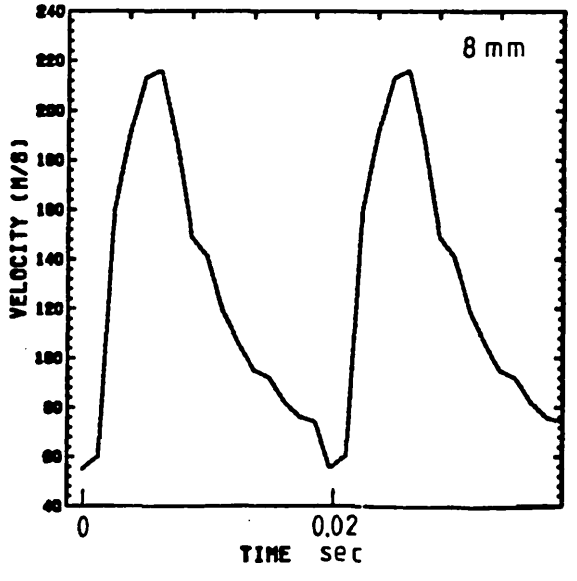
Fig 6.19 Instantaneous flow angle across exit duct







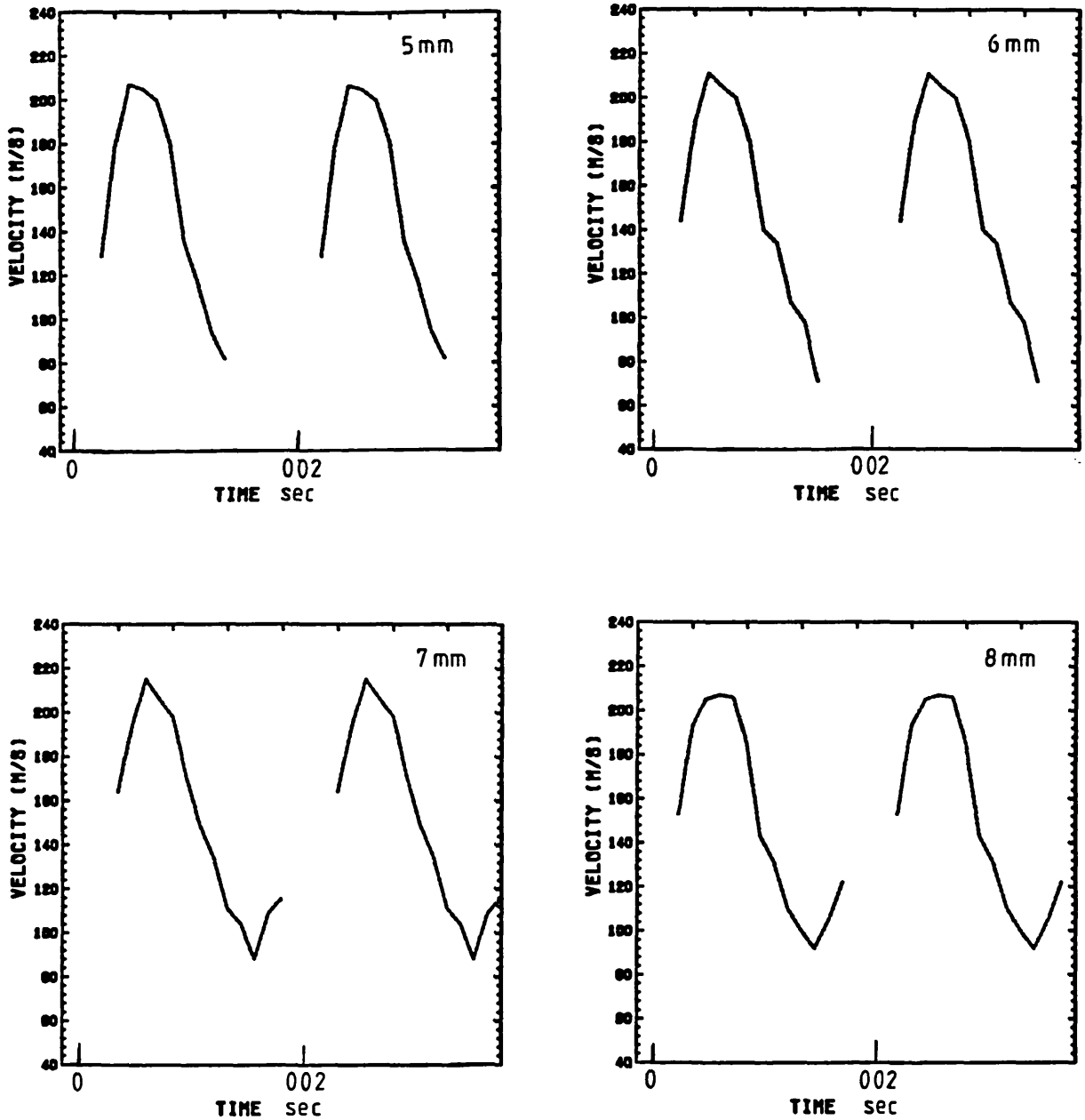




Azimuth Angle = 90°

SWϕ = 80mm

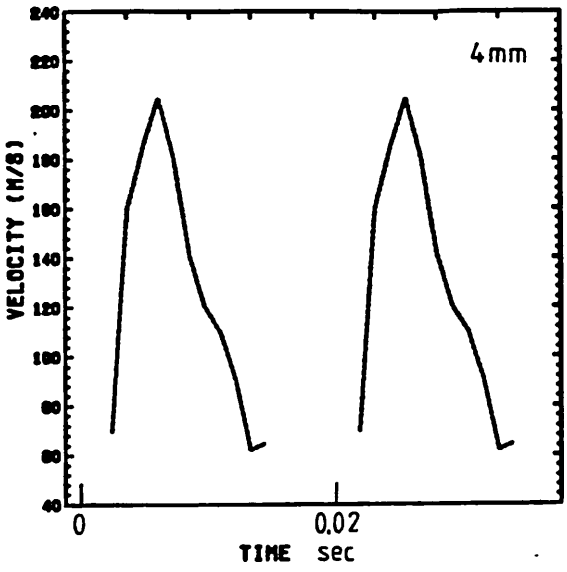
Fig 6.20a

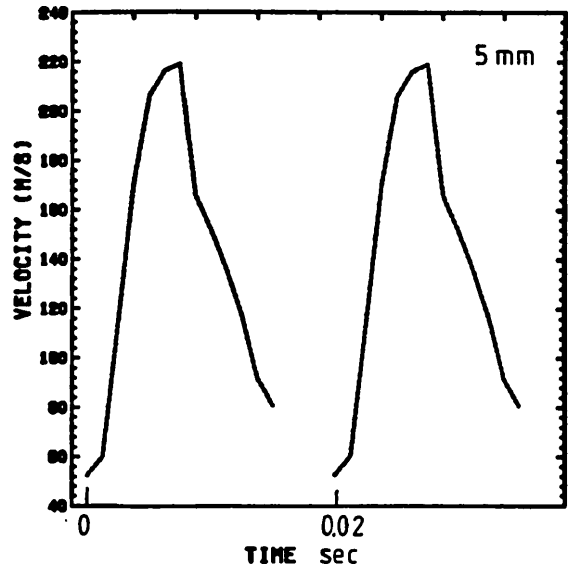


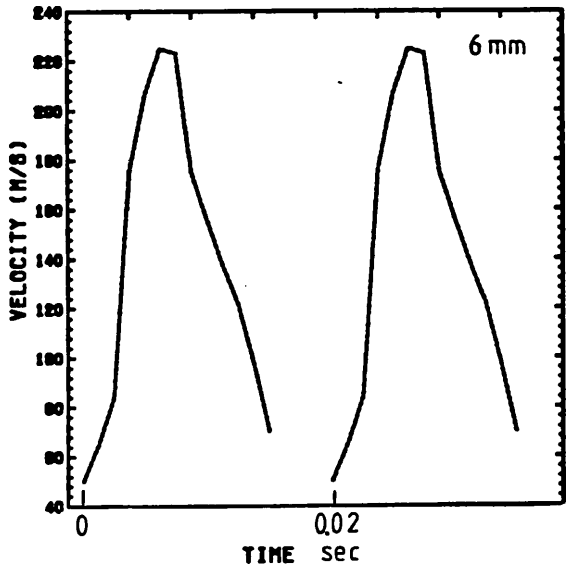
Azimuth Angle = 180°

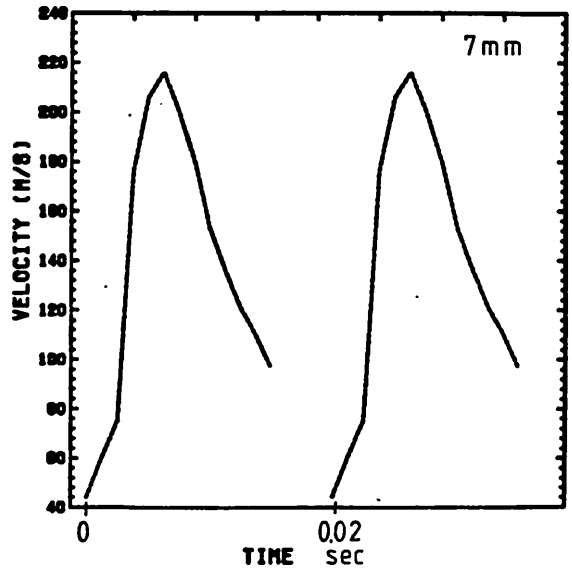
SWϕ = 80mm

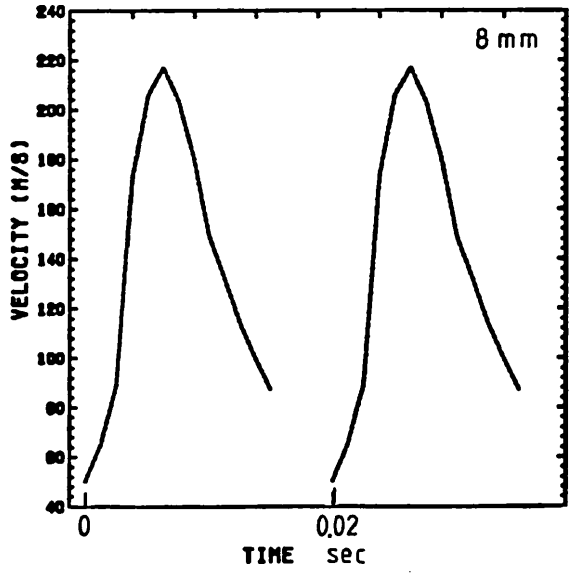
Fig 6.20b







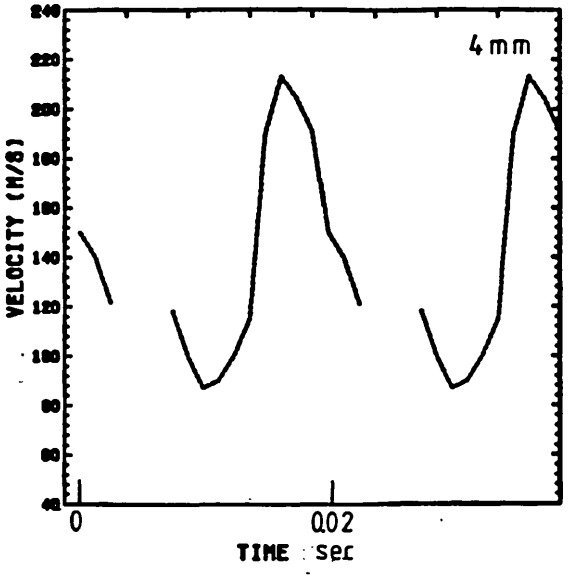


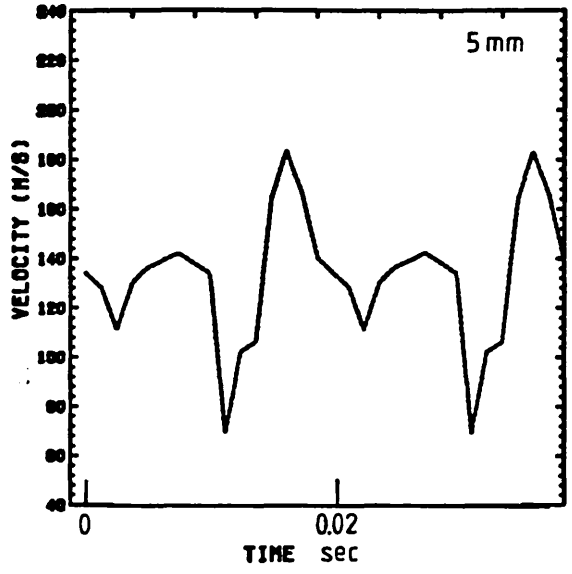


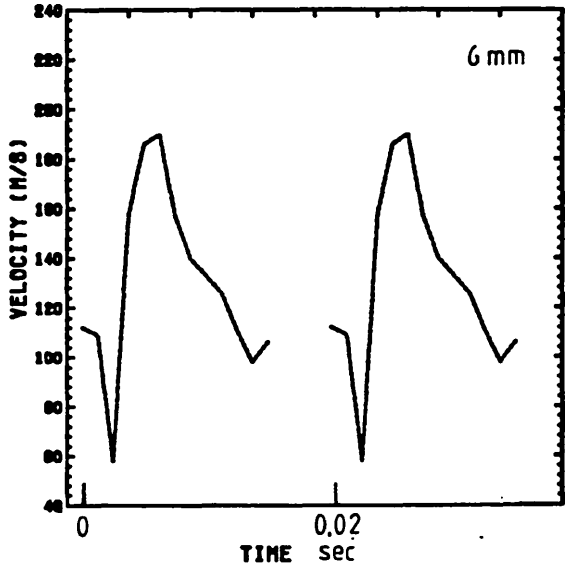
Azimuth Angle = 270°

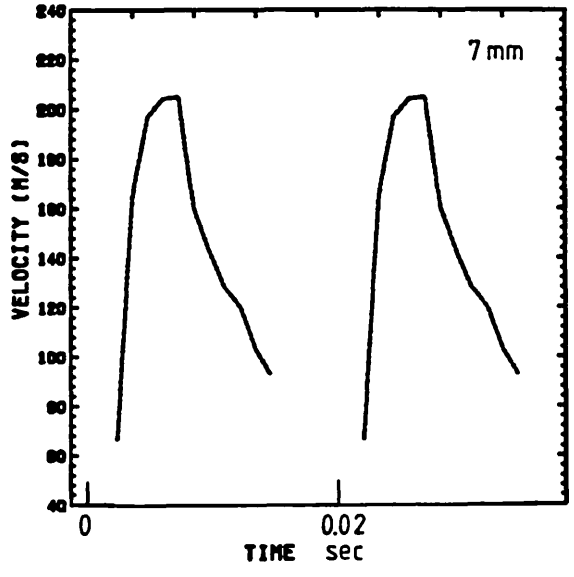
SWϕ = 80mm

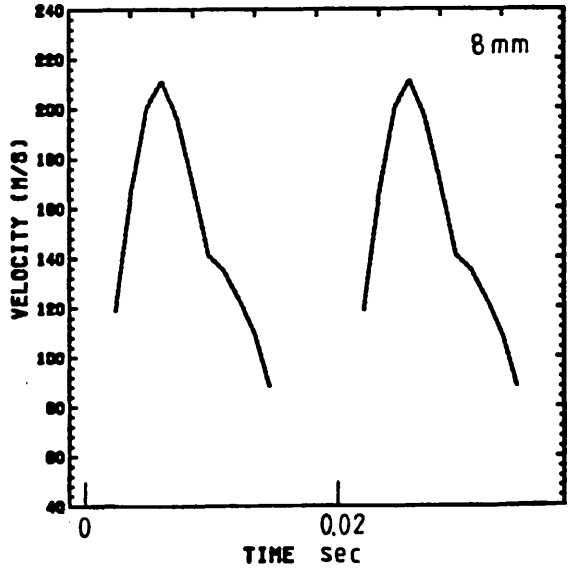
Fig 6.20c







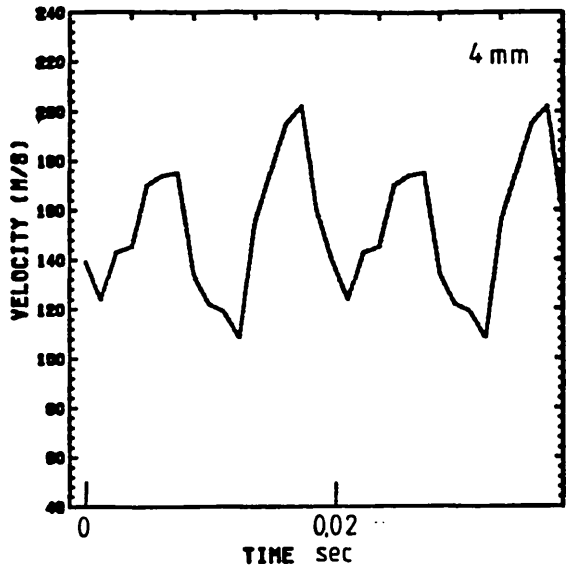


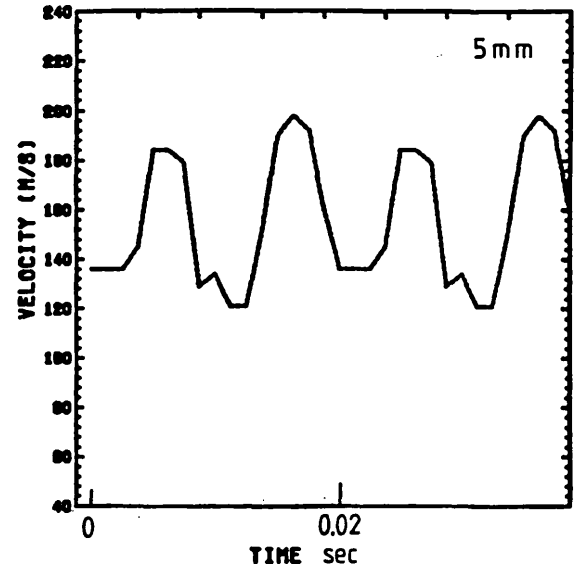


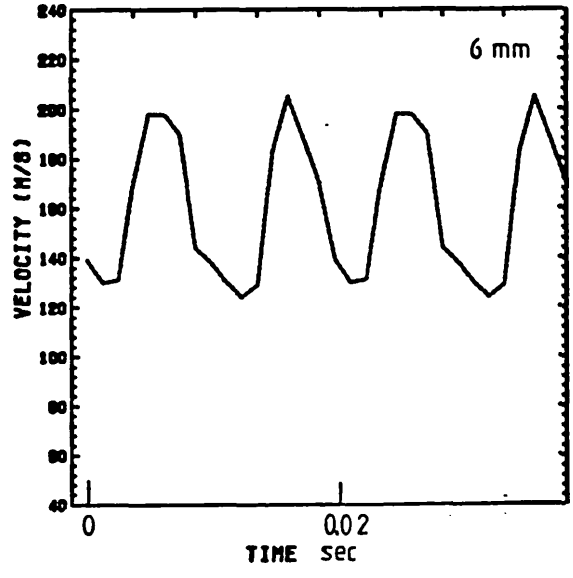
SWϕ = 86mm

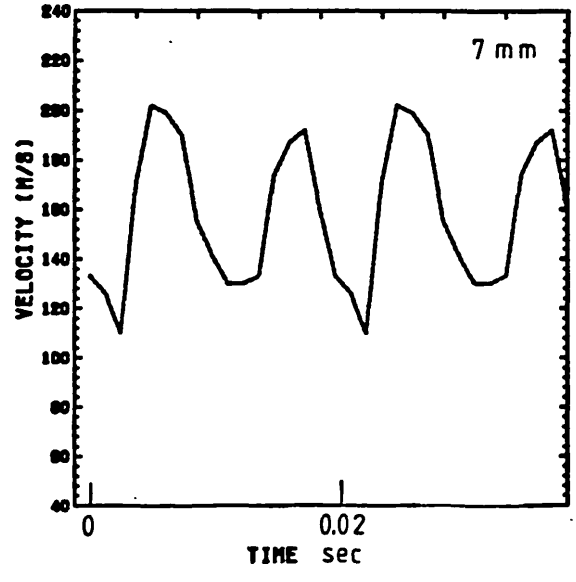
Azimuth Angle = 270°

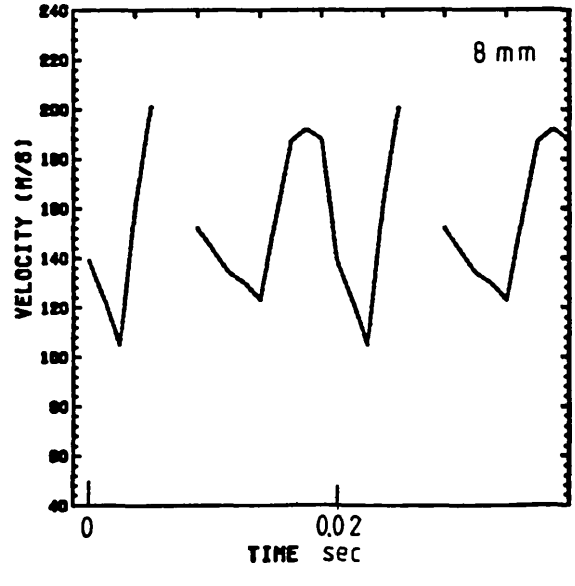
Fig 6.21a







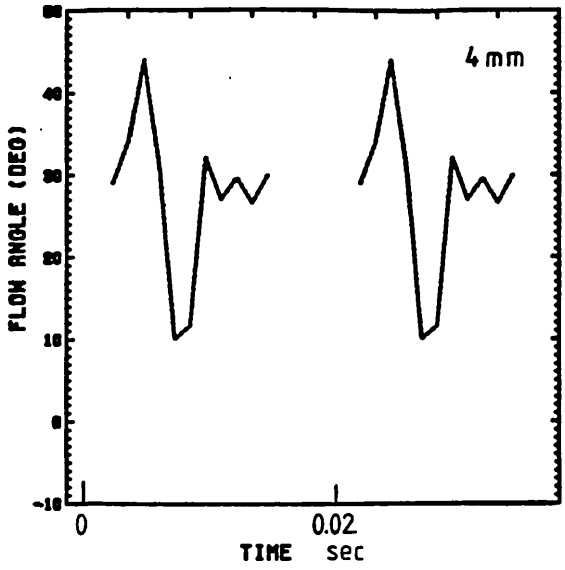


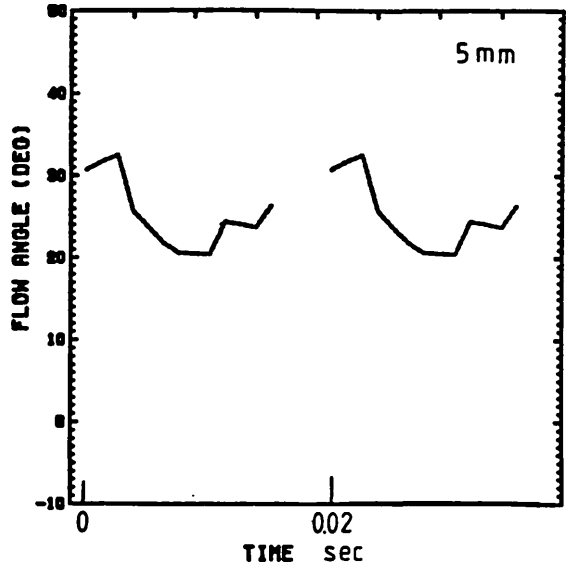


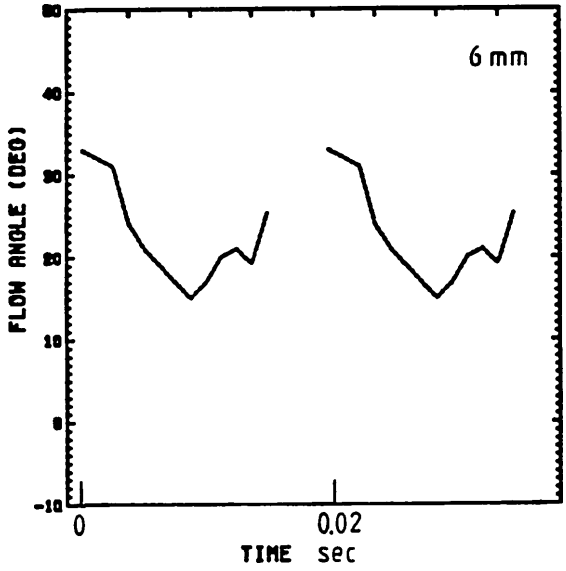
SWϕ = 96mm

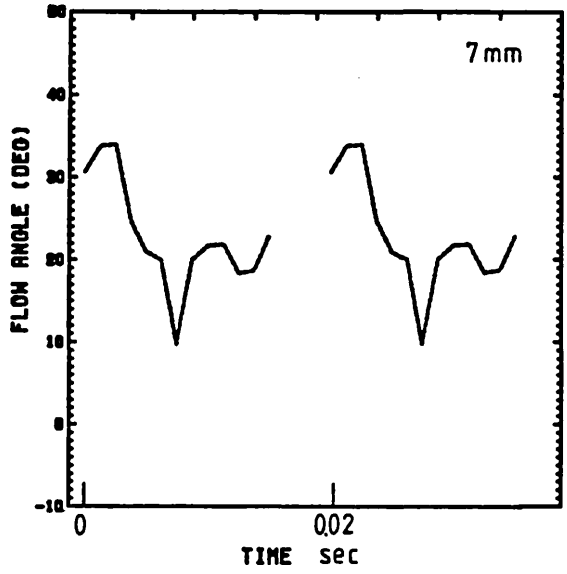
Azimuth Angle = 270°

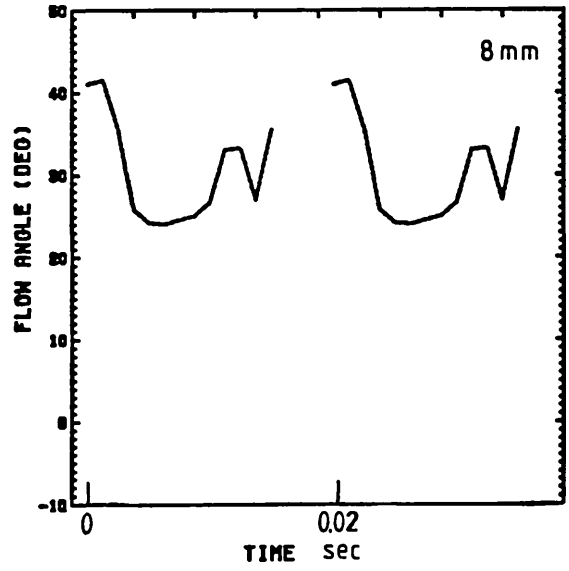
Fig 6.21b







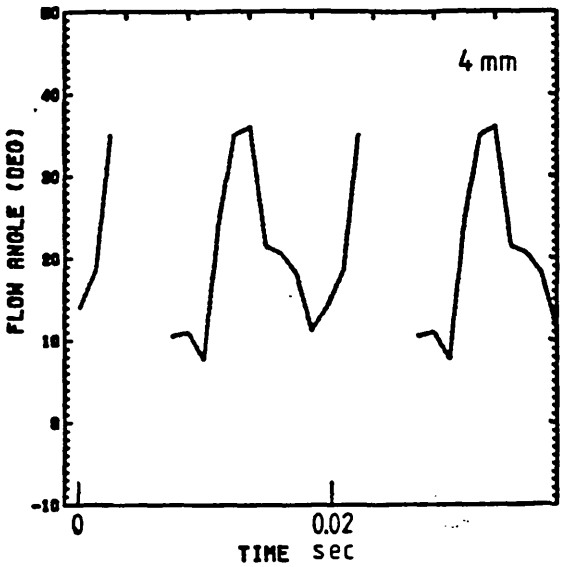


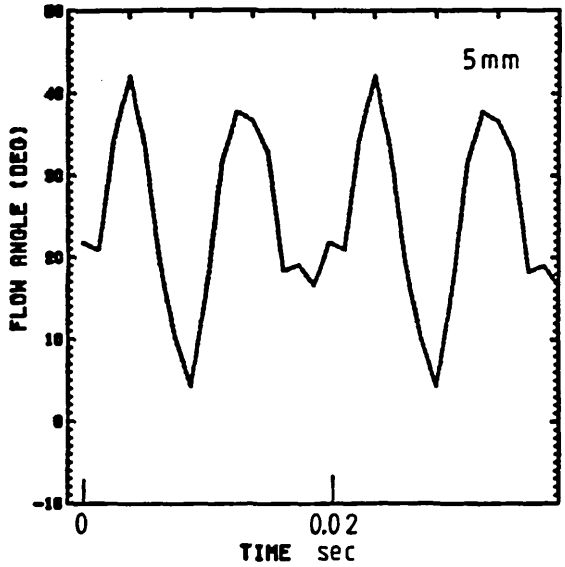


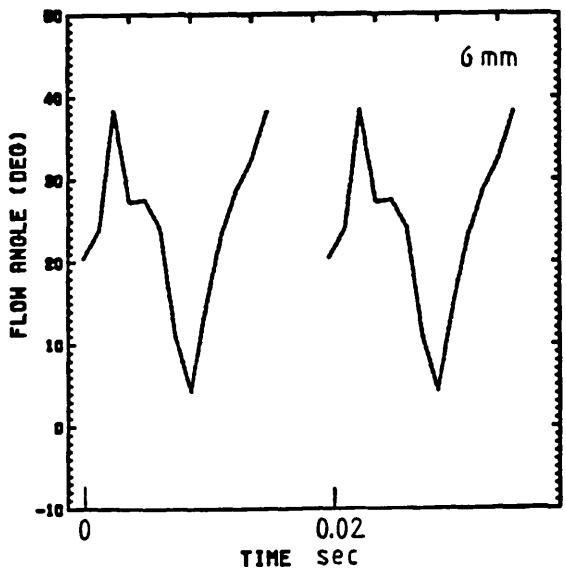
SWϕ = 80mm

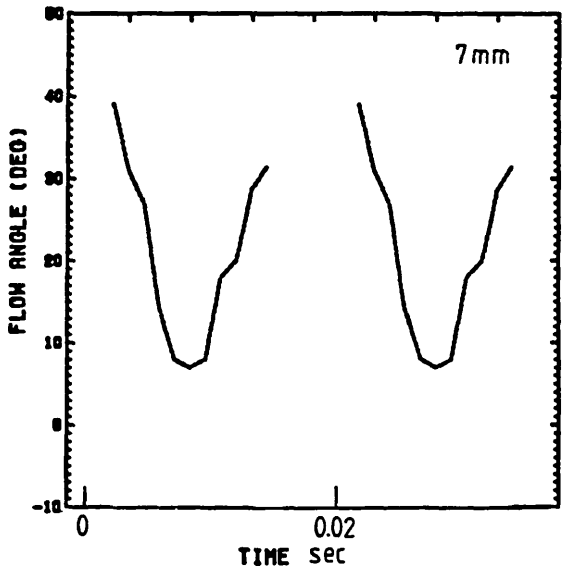
Azimuth Angle = 270°

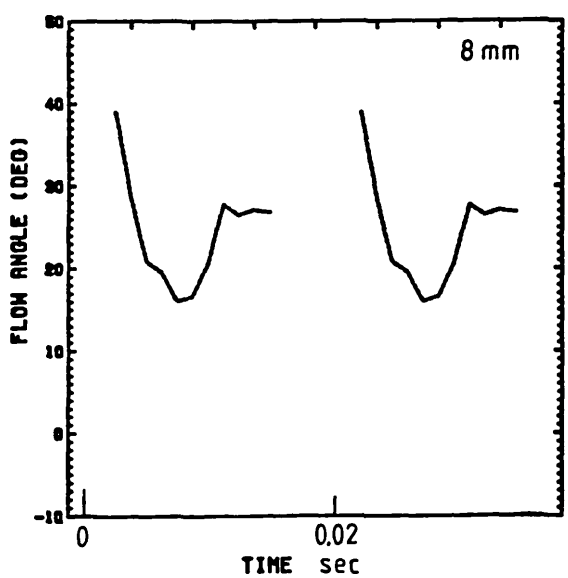
Fig 6.21c







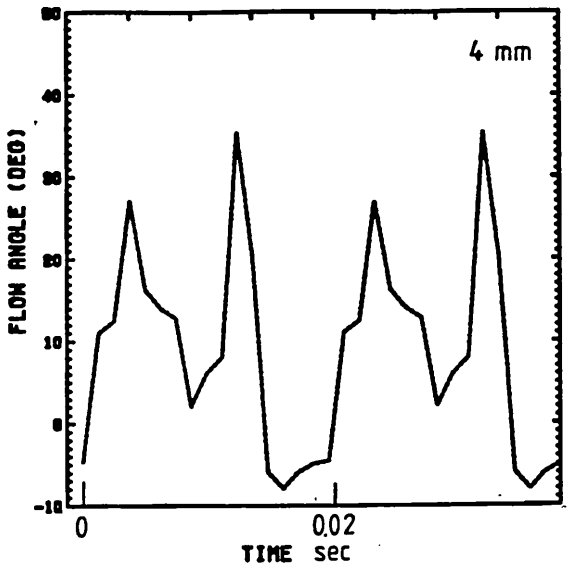


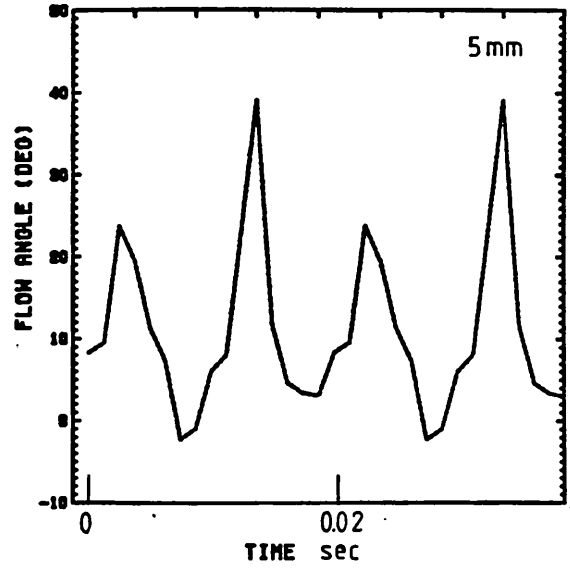


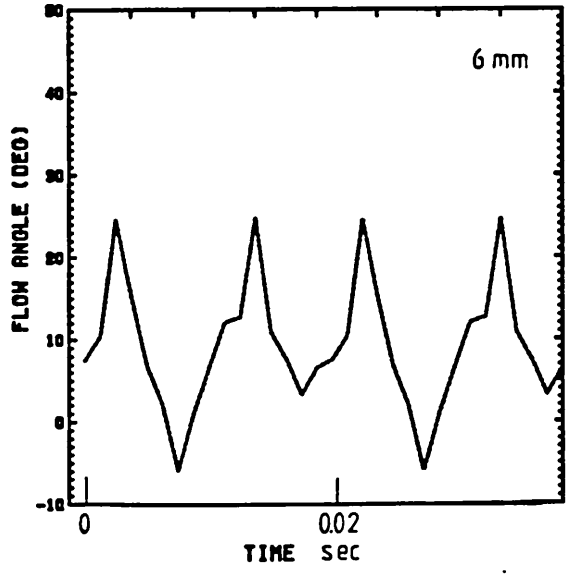
SWϕ = 86mm

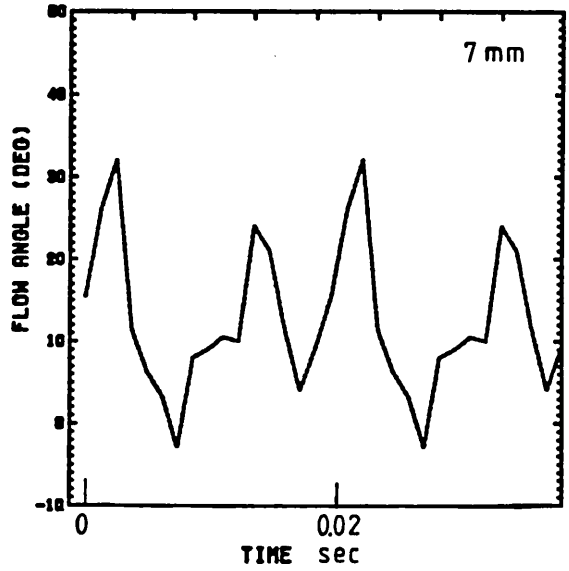
Azimuth Angle = 270°

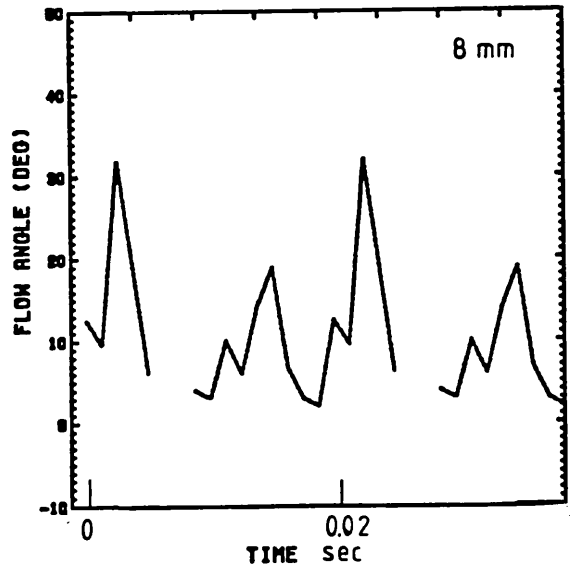
Fig 6.21d











SWϕ = 96mm

Azimuth Angle = 270°

Fig 6.21e

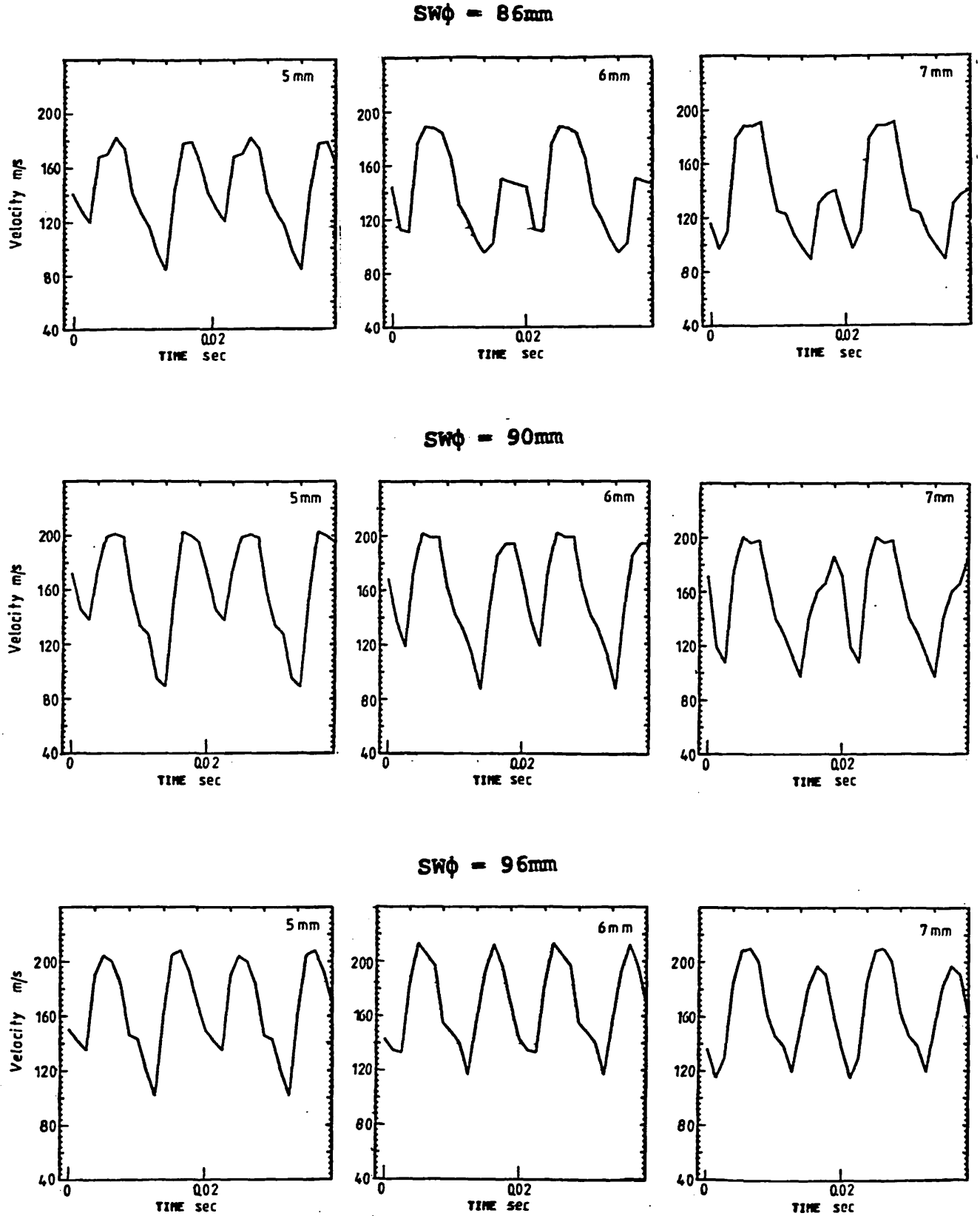


Fig 6.22 Comparison of flow characteristics with different separating wall diameter

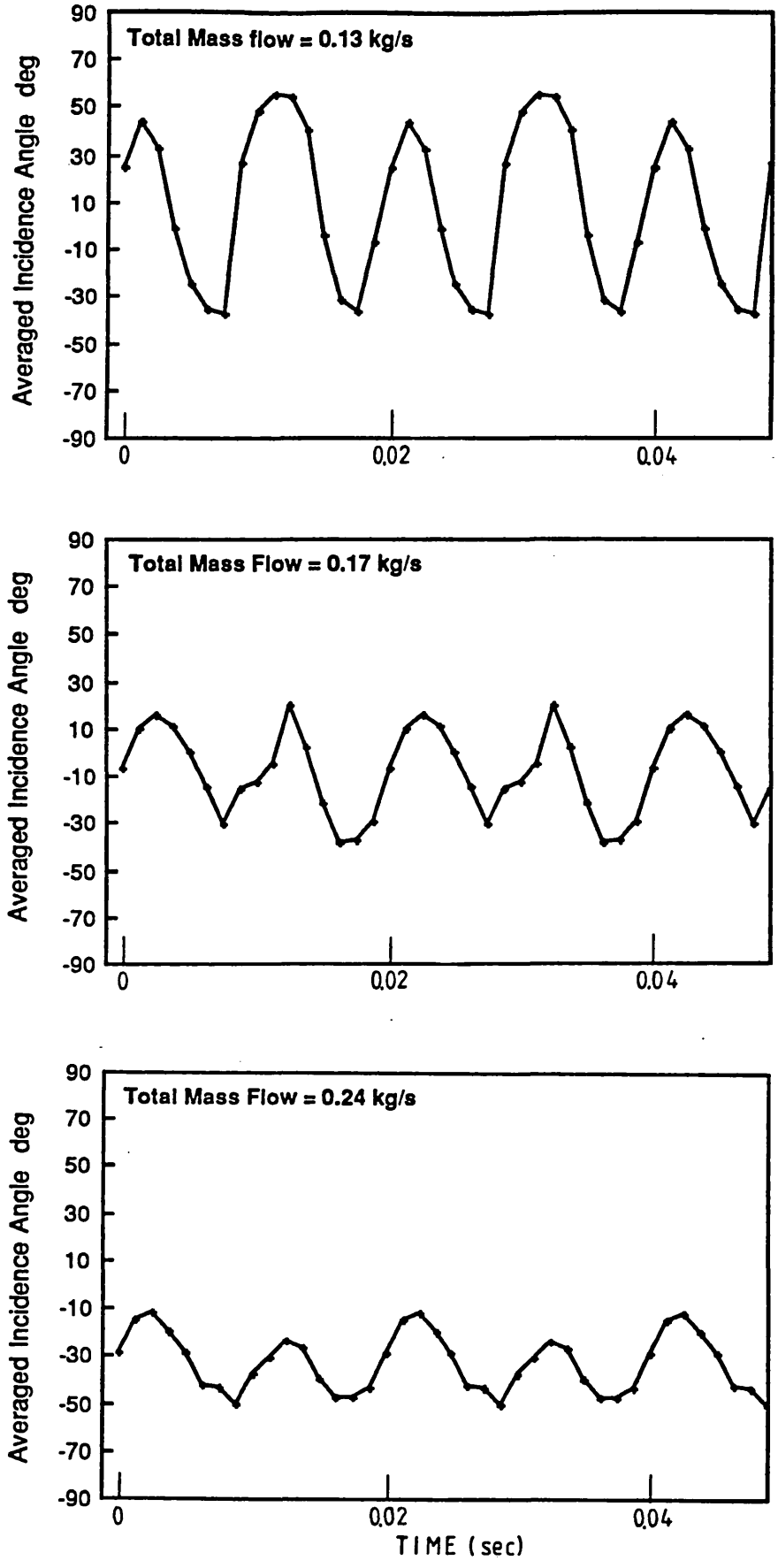


Fig 6.23 Instantaneous incidence angle

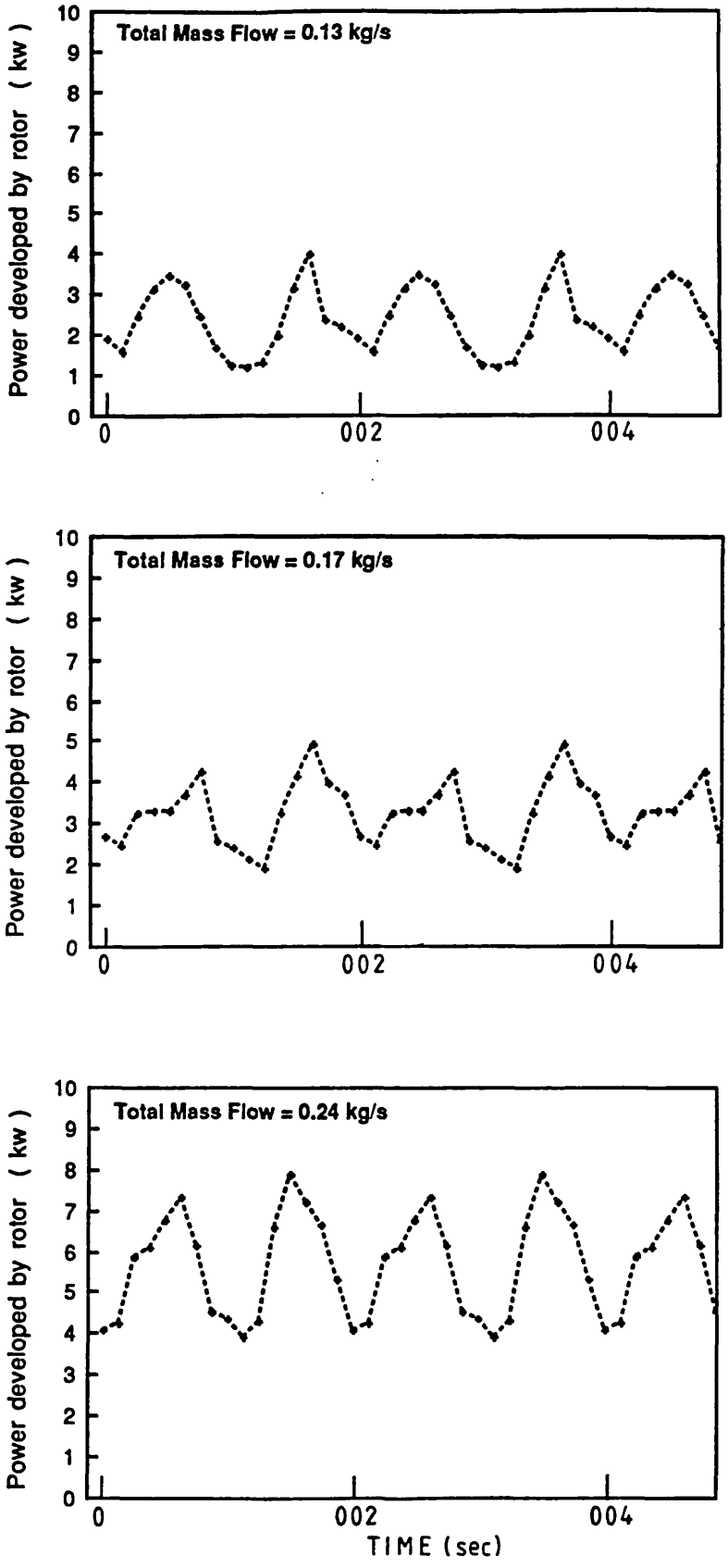


Fig 6.24 Instantaneous power developed by rotor

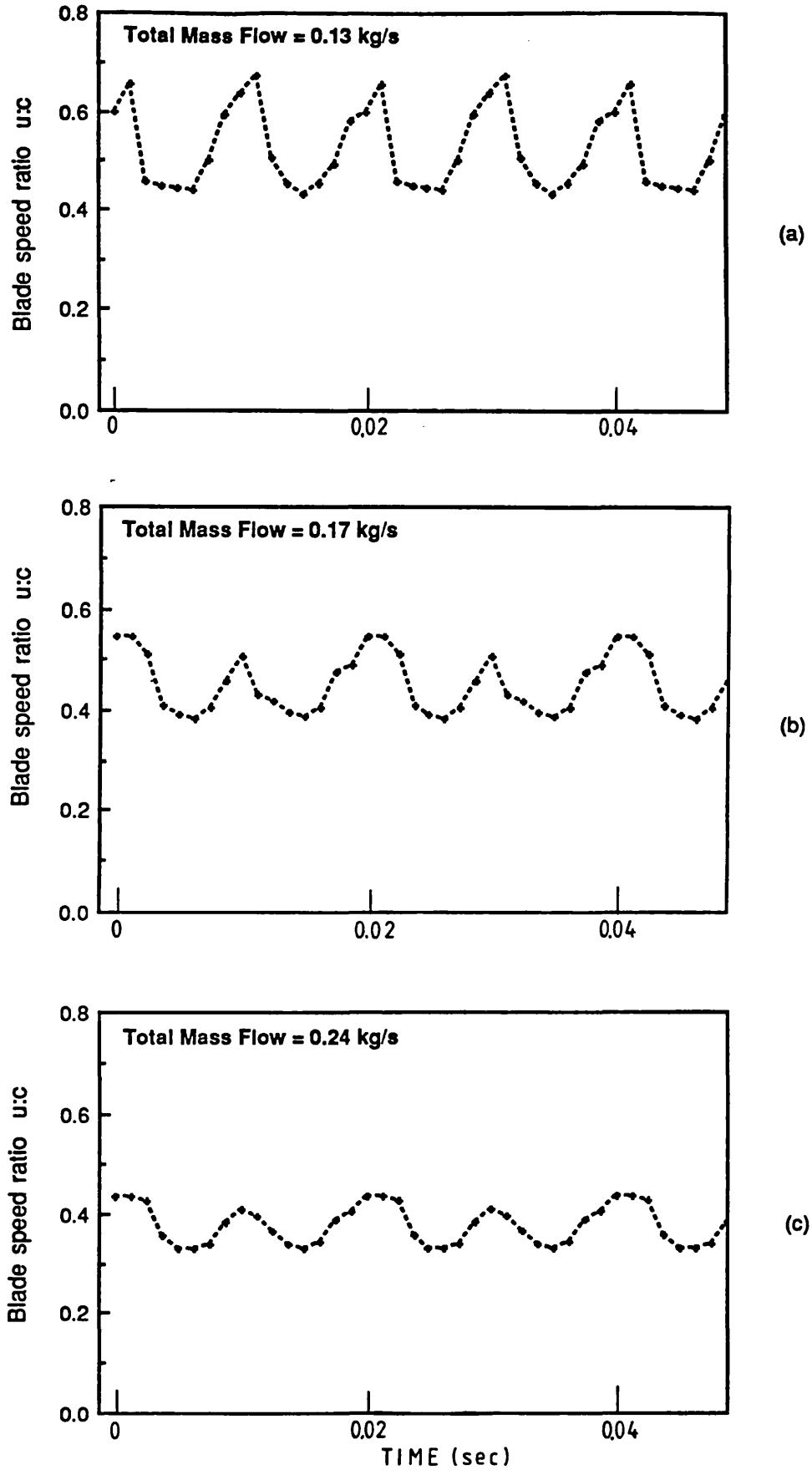


Fig 6.25 Instantaneous blade speed ratio

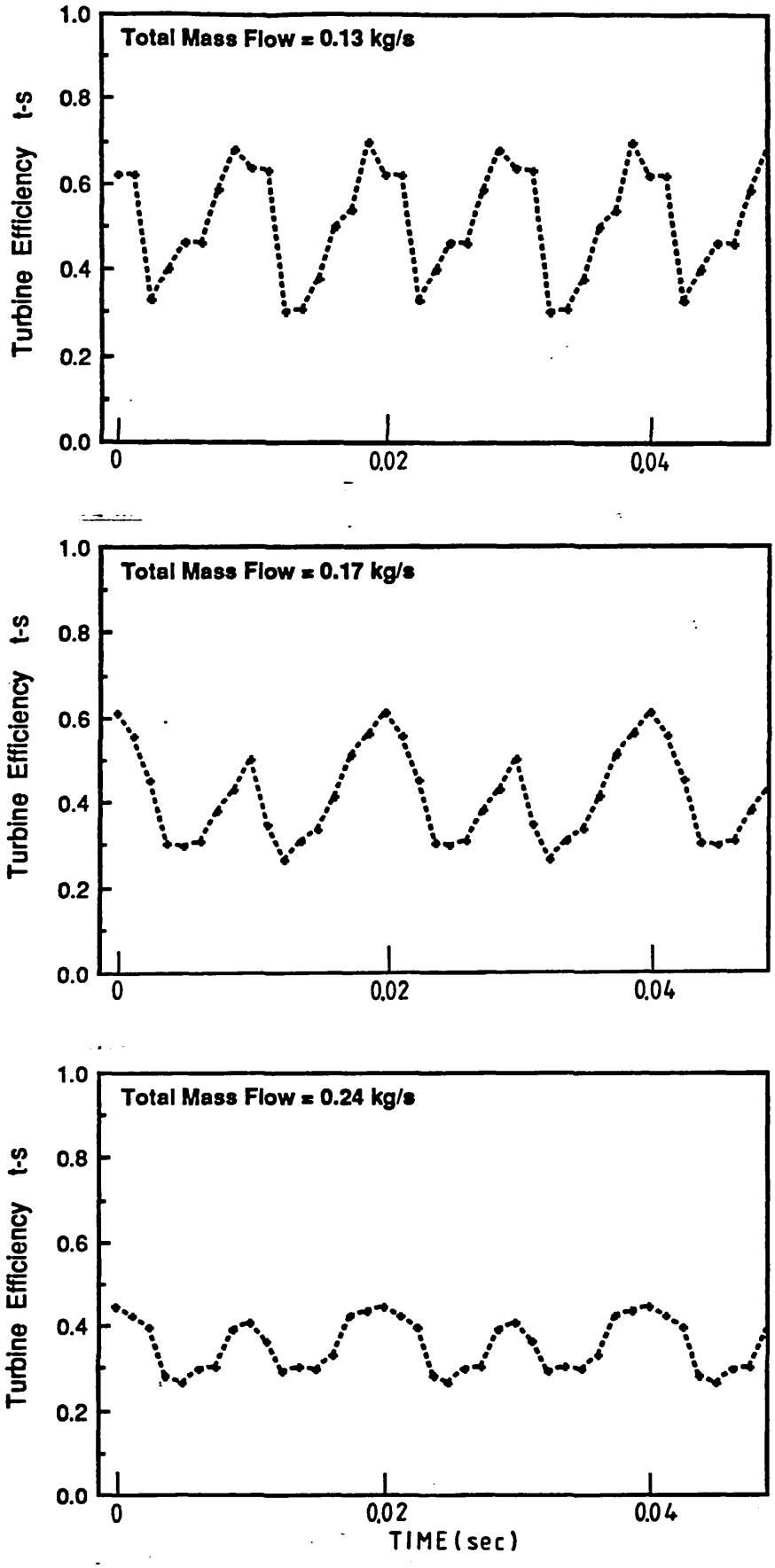


Fig 6.26 Instantaneous turbine efficiency (t-s)

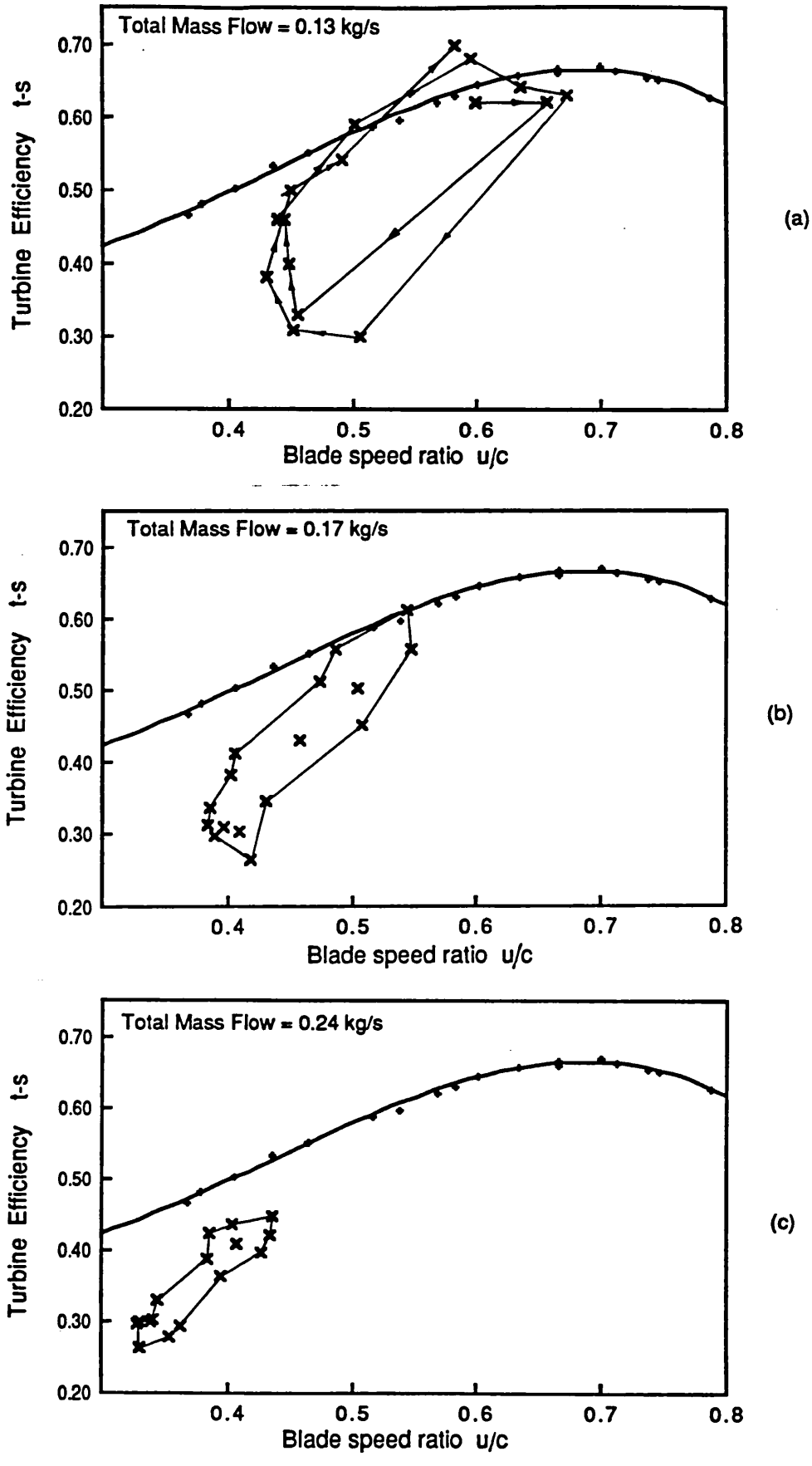


Fig 6.27 Instantaneous turbine efficiency vs blade speed ratio

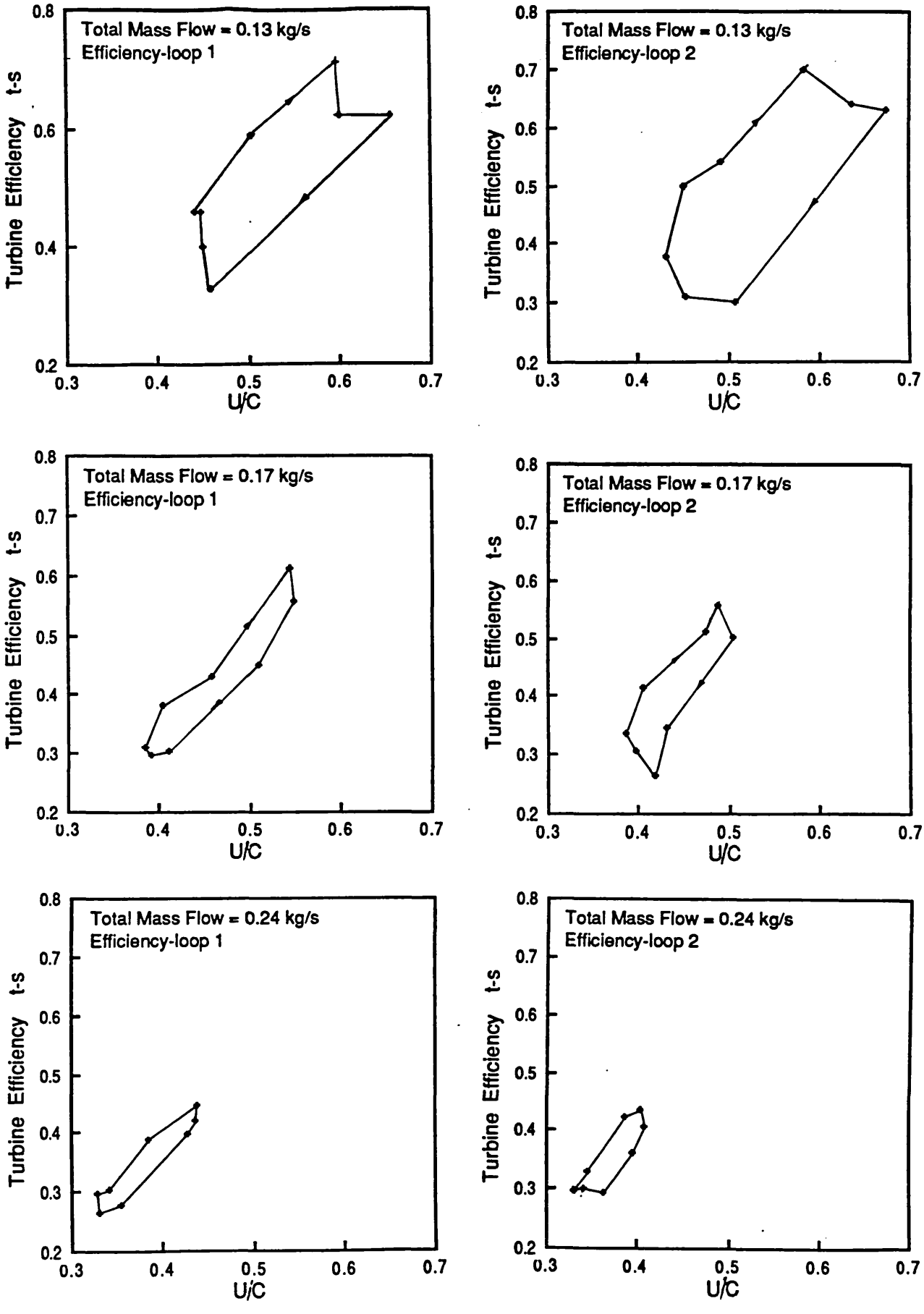
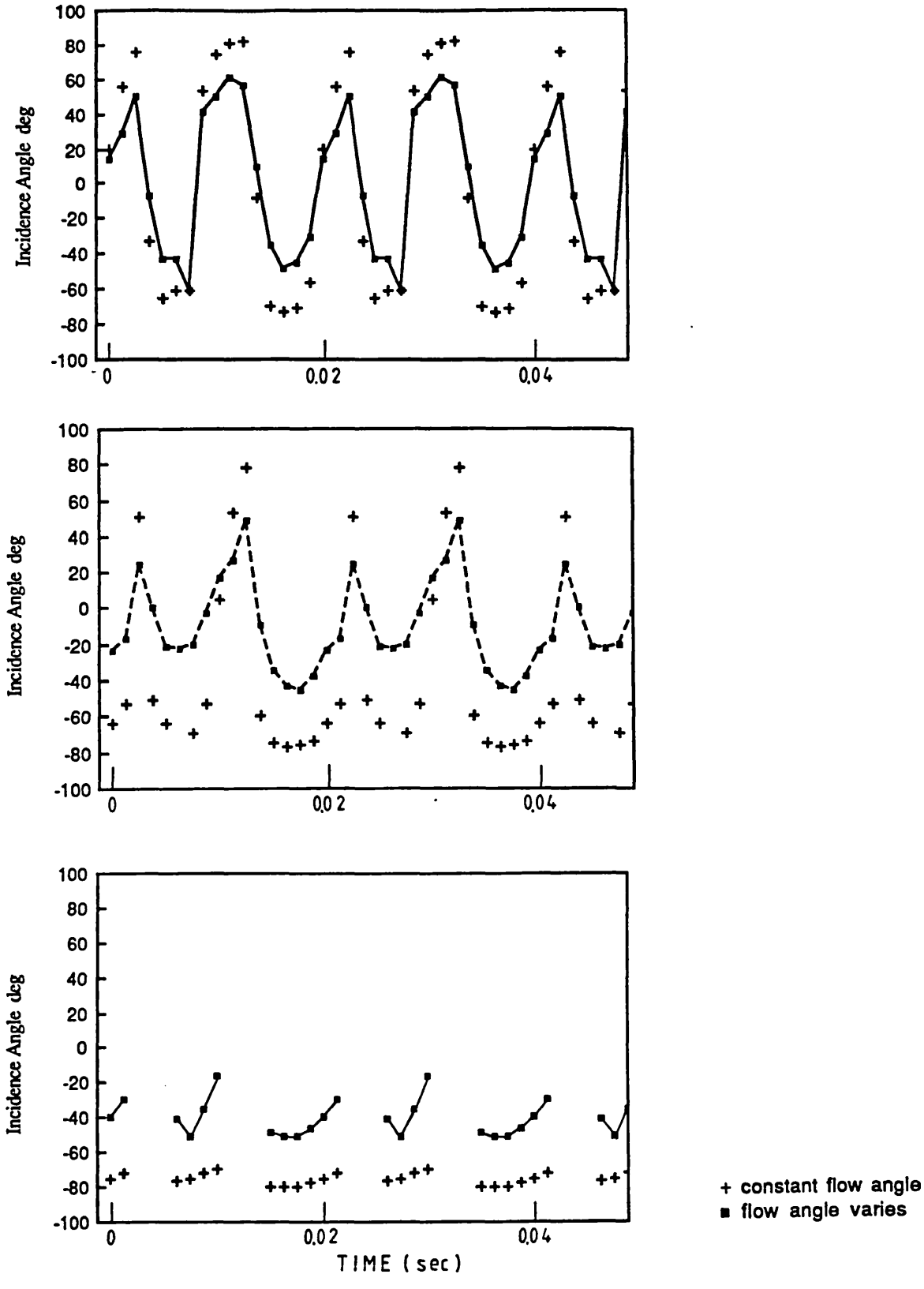
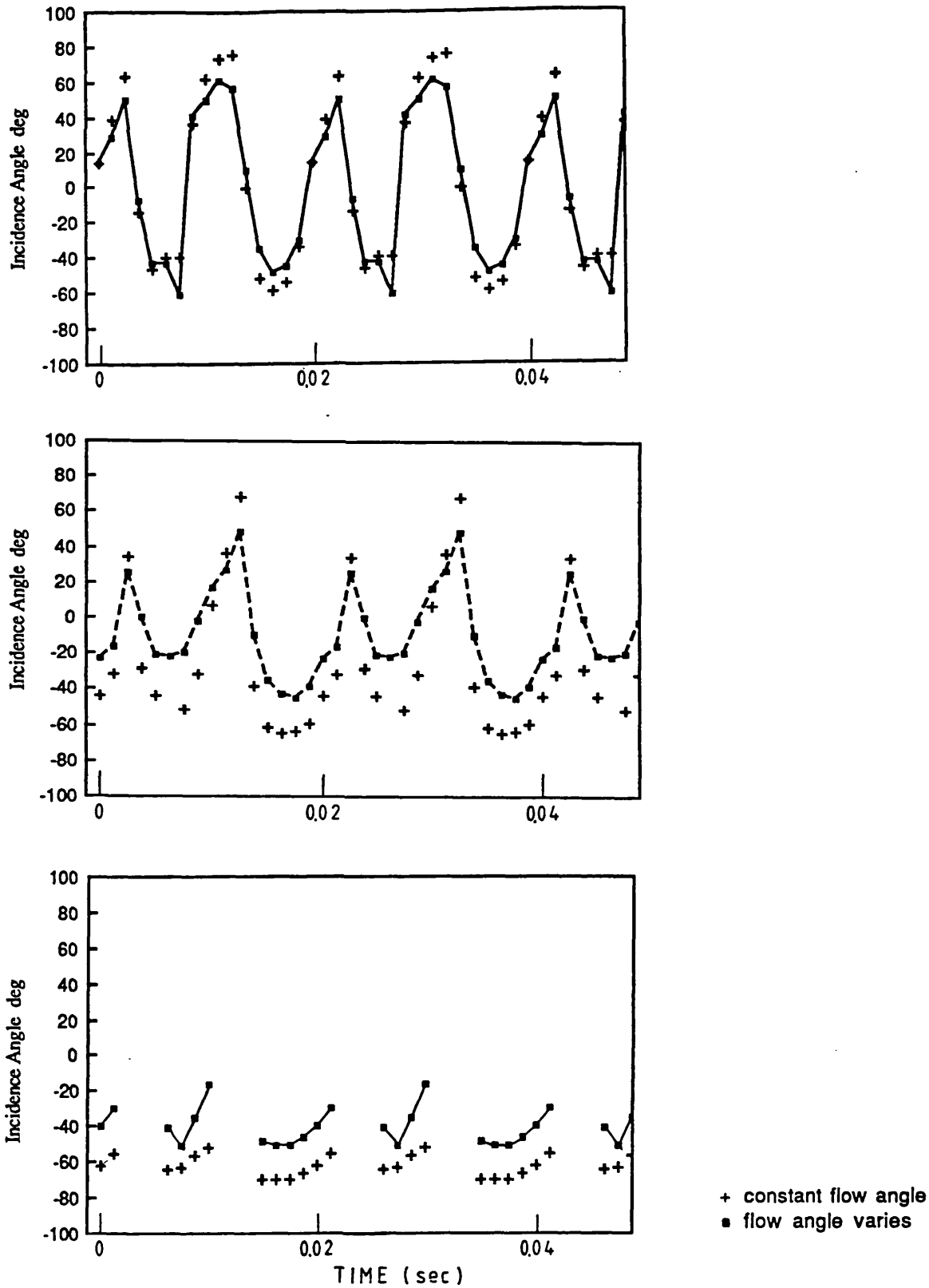


Fig 6.28 Instantaneous efficiency-loop



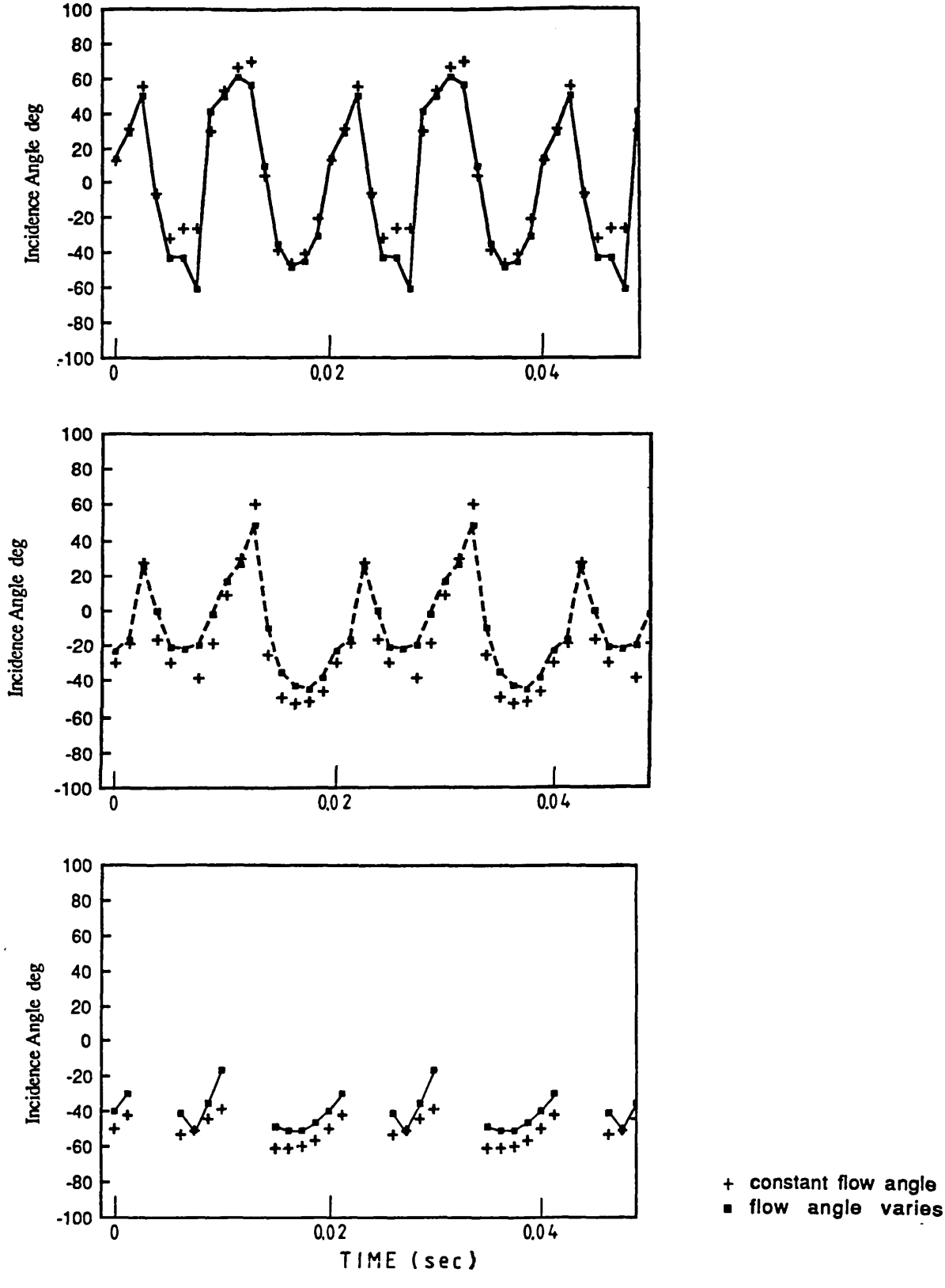
Constant flow angle = 5°

Fig 6.29 Incidence angle with constant absolute flow angle



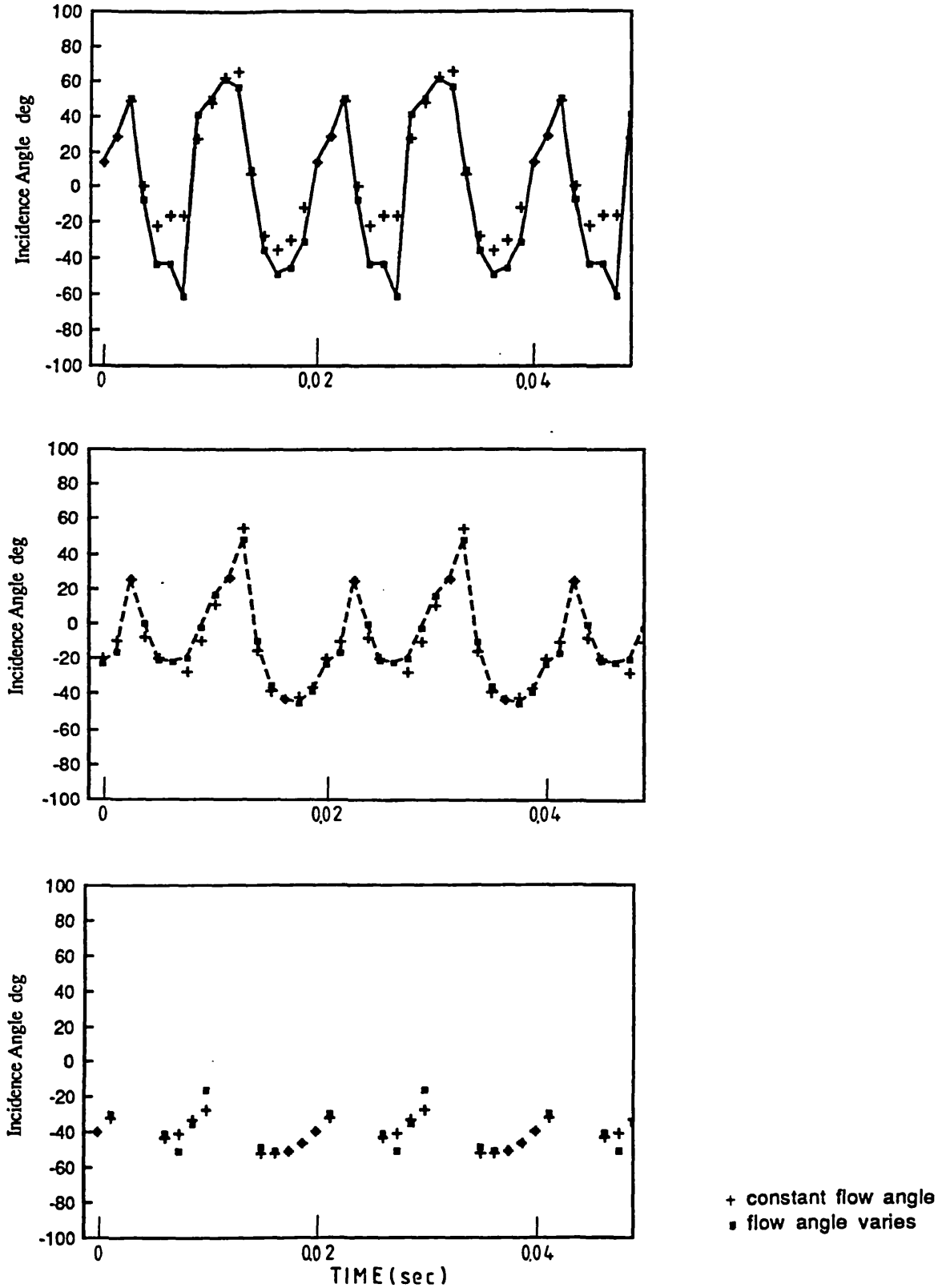
Constant flow angle = 10°

Fig 6.30 Incidence angle with constant absolute flow angle



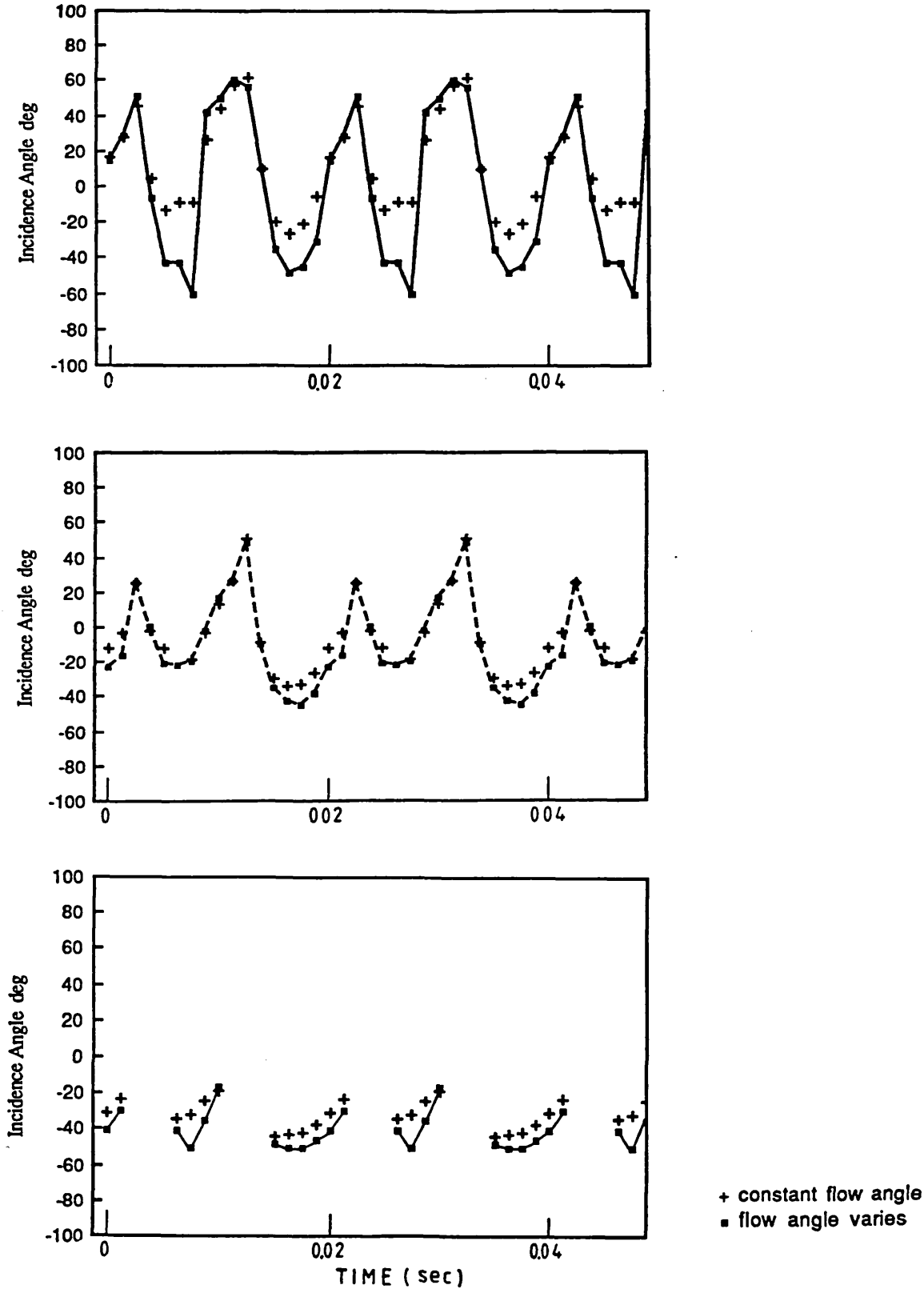
Constant flow angle = 15°

Fig 6.31 Incidence angle with constant absolute flow angle



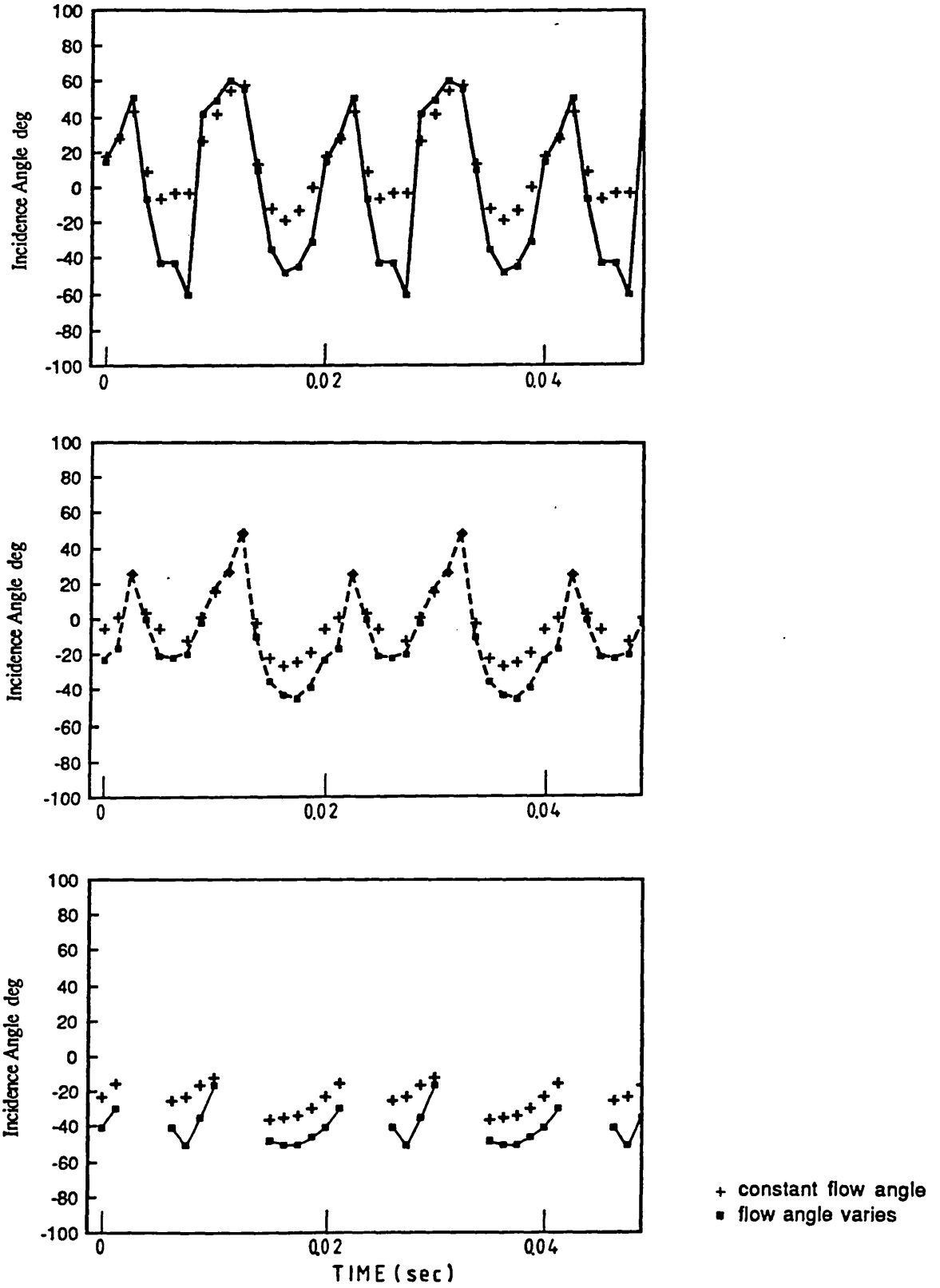
Constant flow angle = 20°

Fig 6.32 Incidence angle with constant absolute flow angle



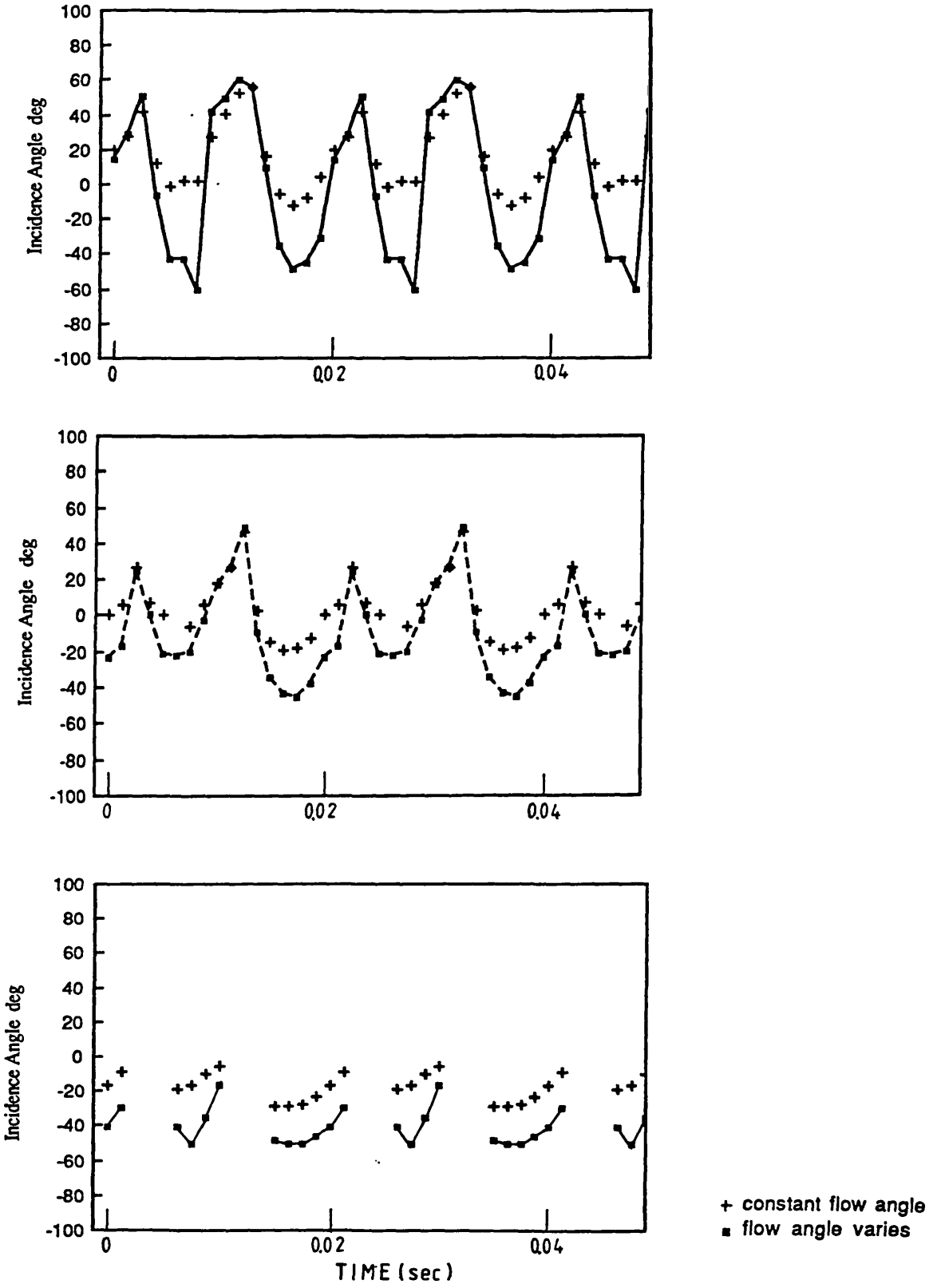
Constant flow angle = 25°

Fig 6.33 Incidence angle with constant absolute flow angle



Constant flow angle = 30°

Fig 6.34 **Incidence angle with constant absolute flow angle**



Constant flow angle = 35°

Fig 6.35 Incidence angle with constant absolute flow angle

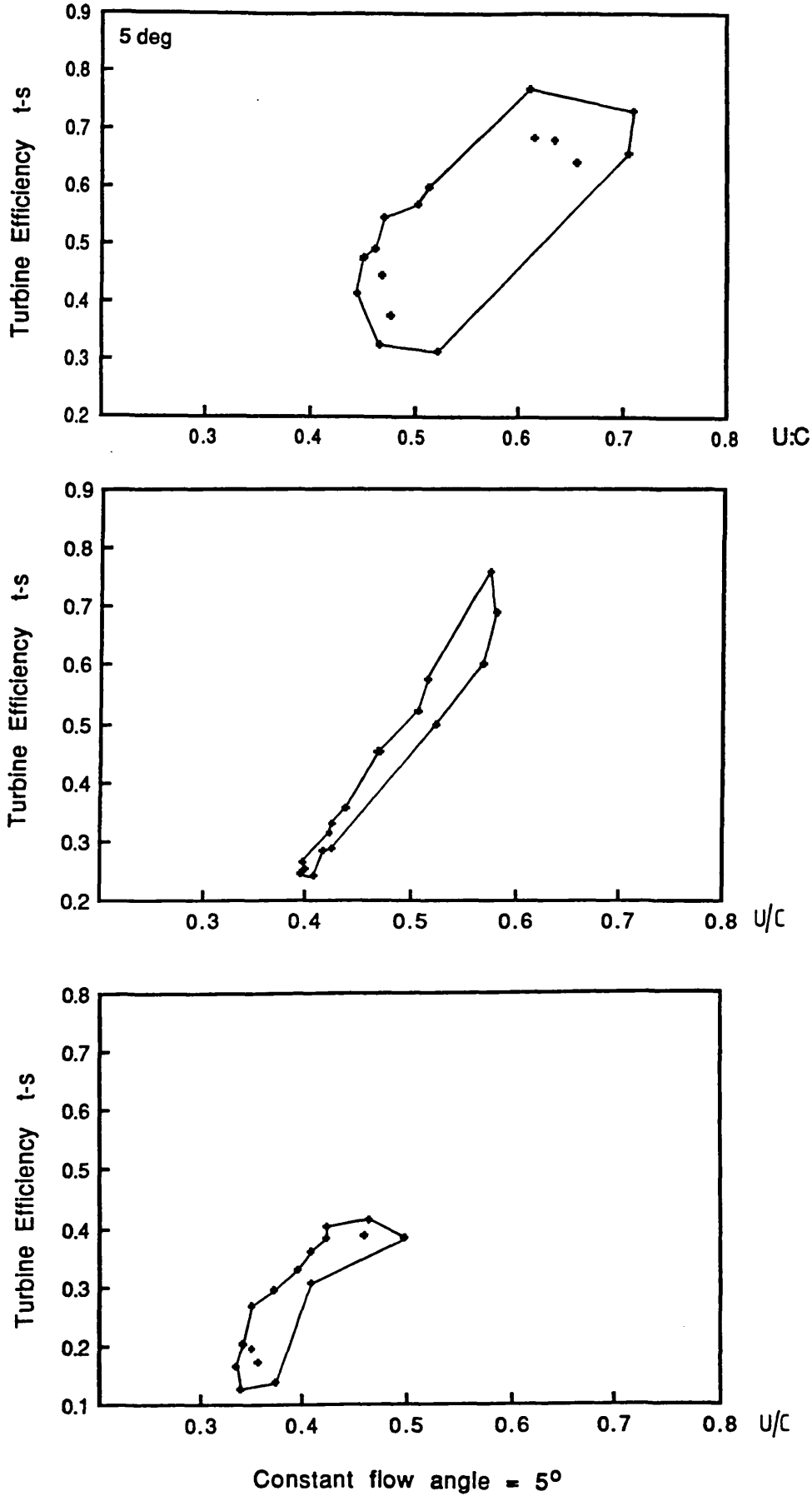


Fig 6.36 **Turbine Efficiency with constant absolute flow angle**

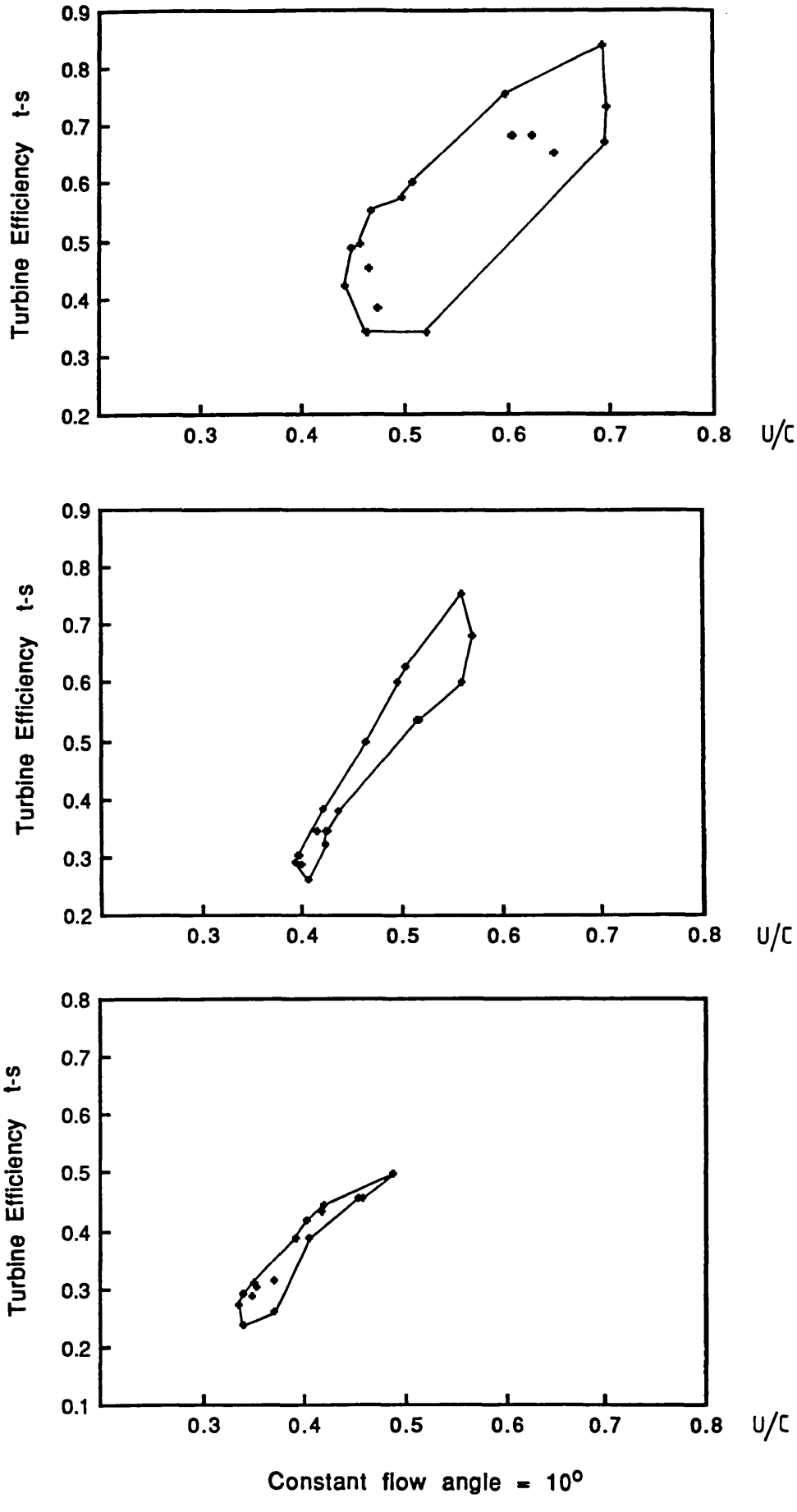


Fig 6.37 Turbine Efficiency with constant absolute flow angle

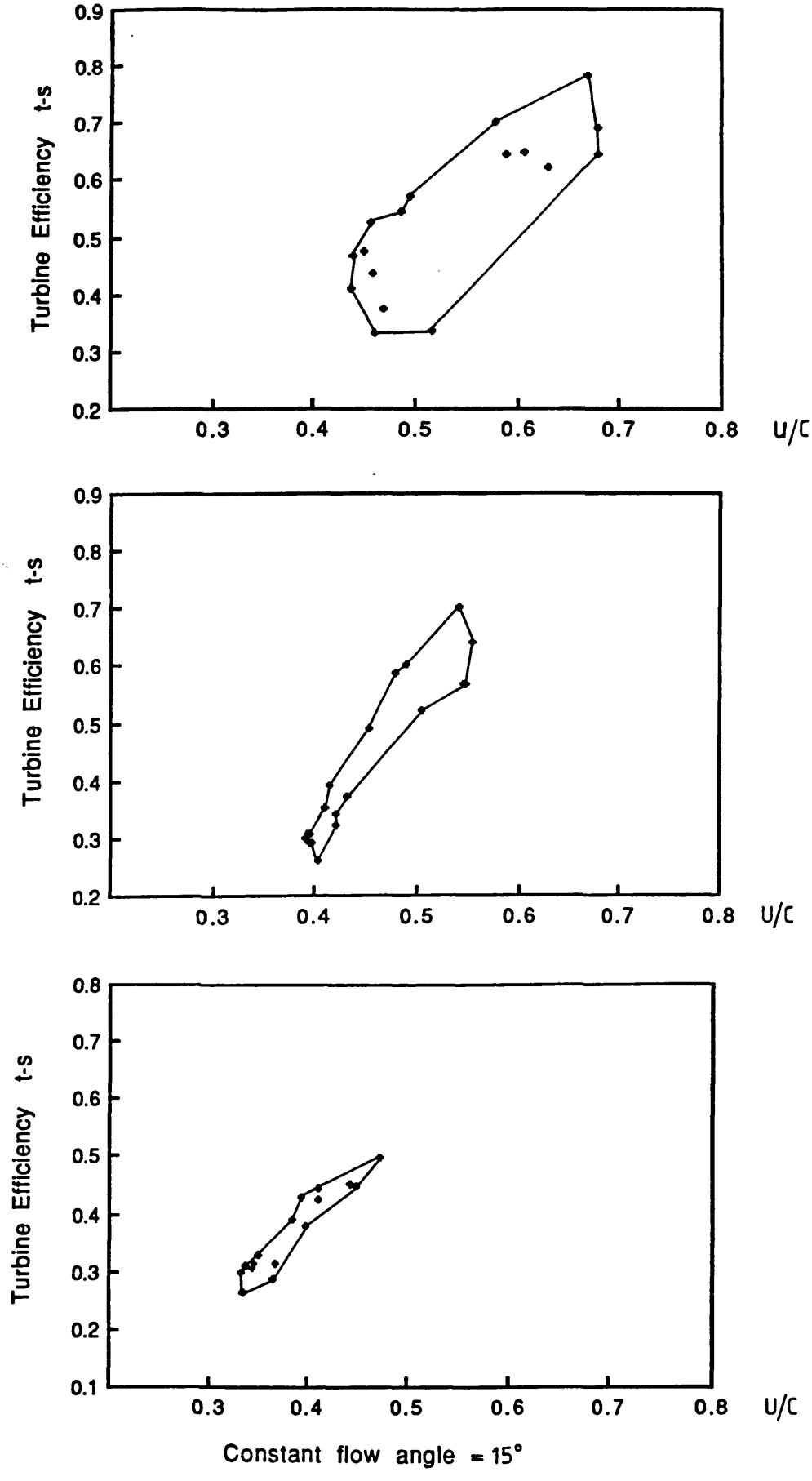


Fig 6.38 Turbine Efficiency with constant absolute flow angle

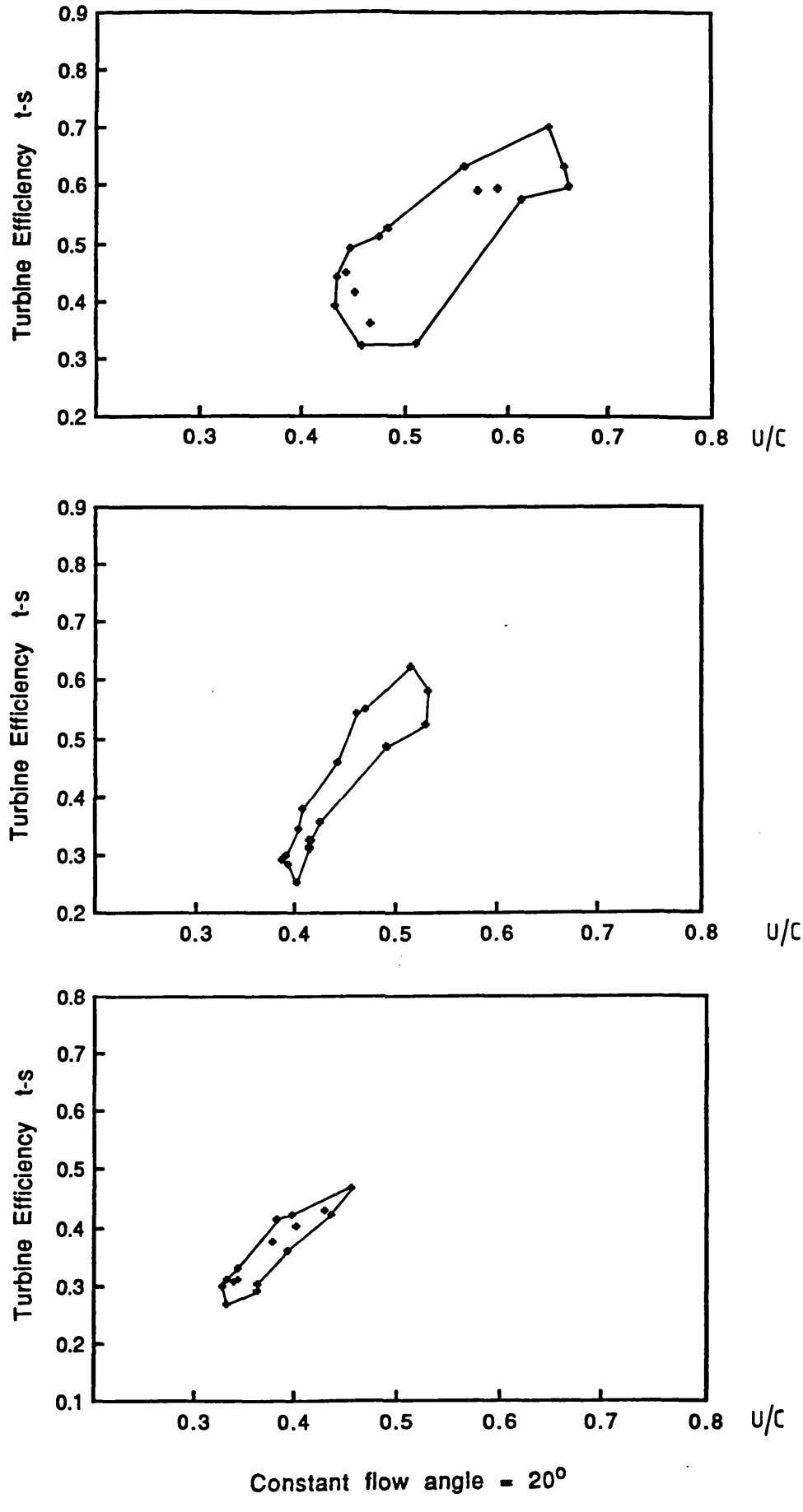


Fig 6.39 Turbine Efficiency with constant absolute flow angle

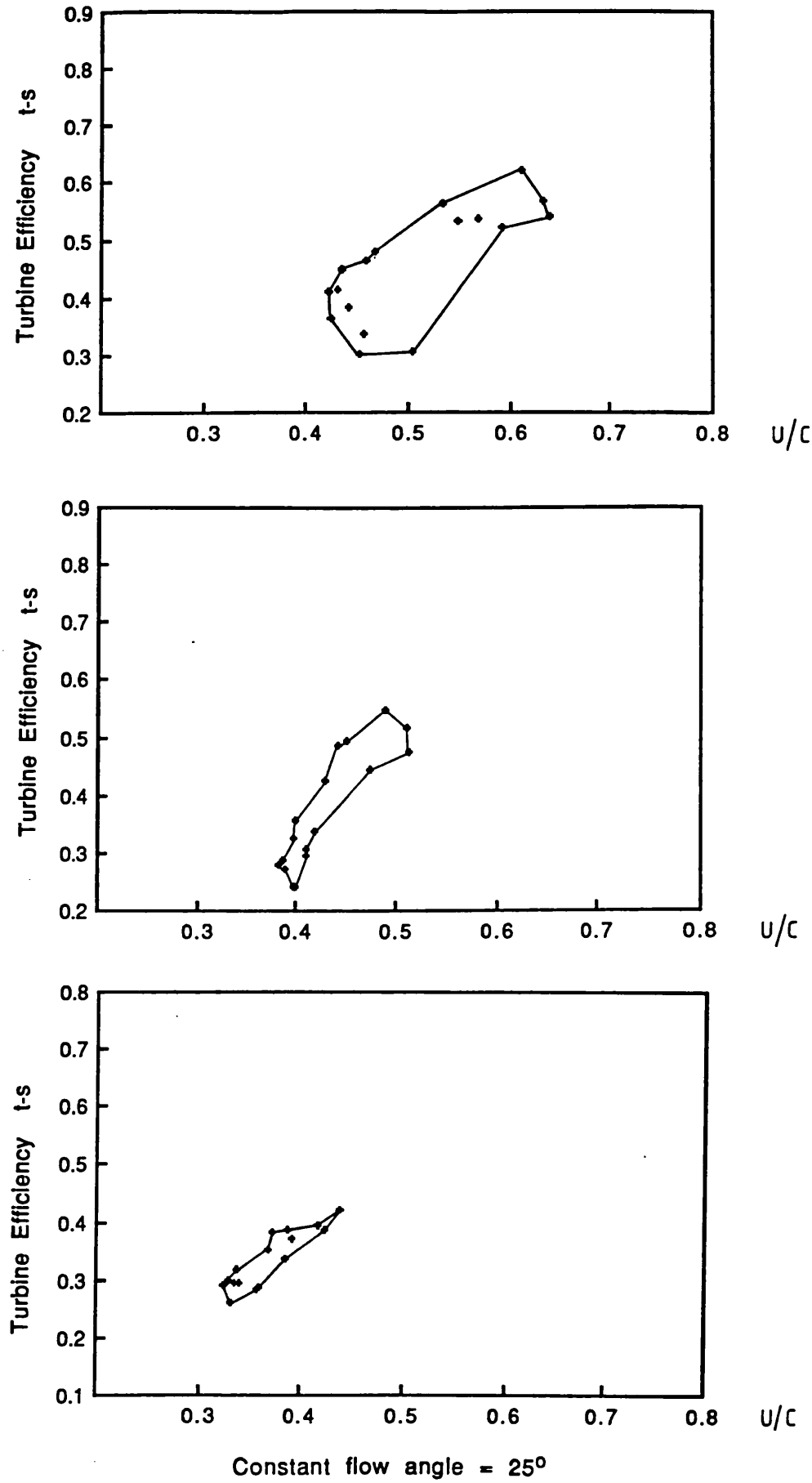


Fig 6.40 Turbine Efficiency with constant absolute flow angle

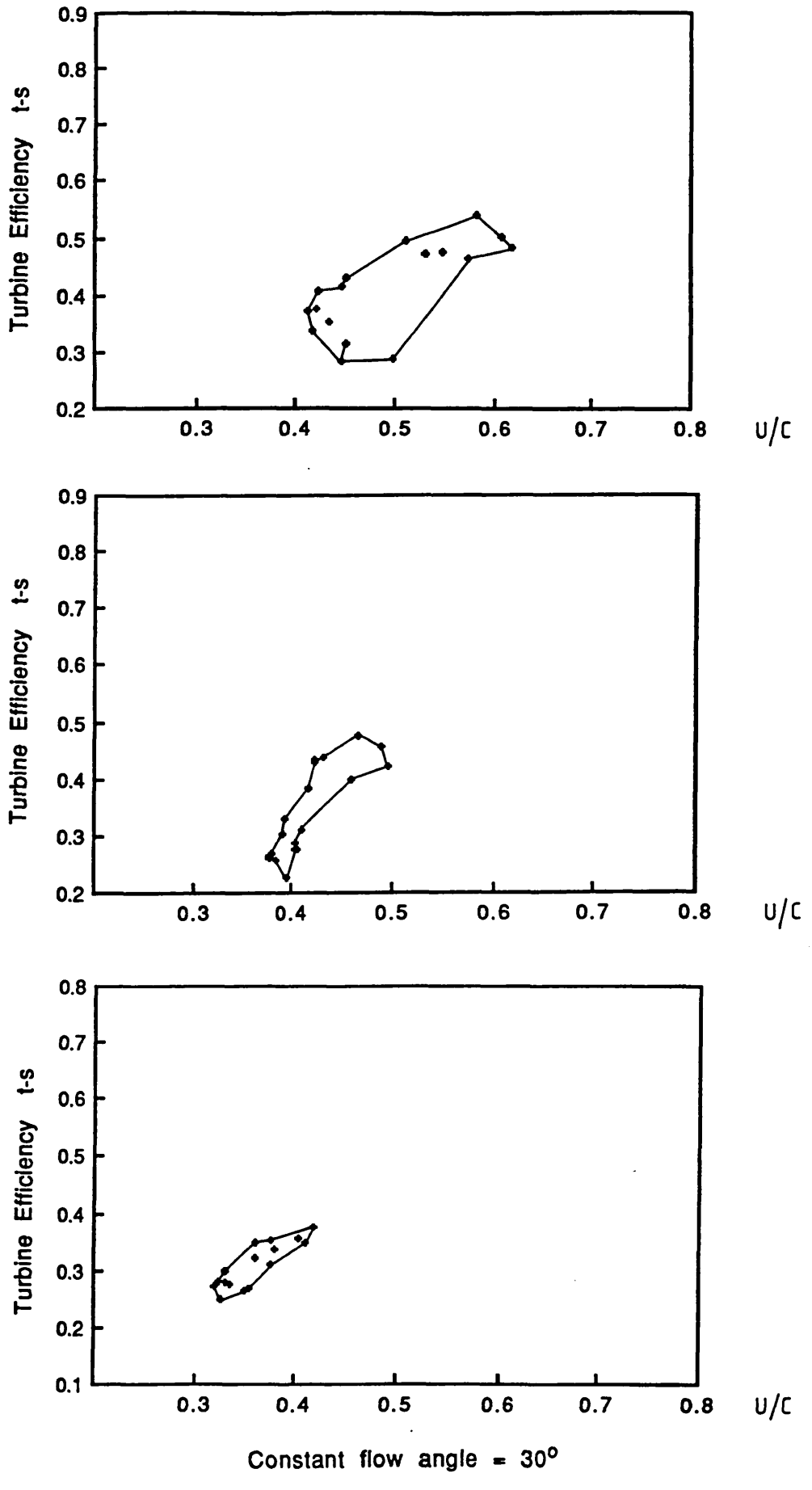


Fig 6.41 Turbine Efficiency with constant absolute flow angle

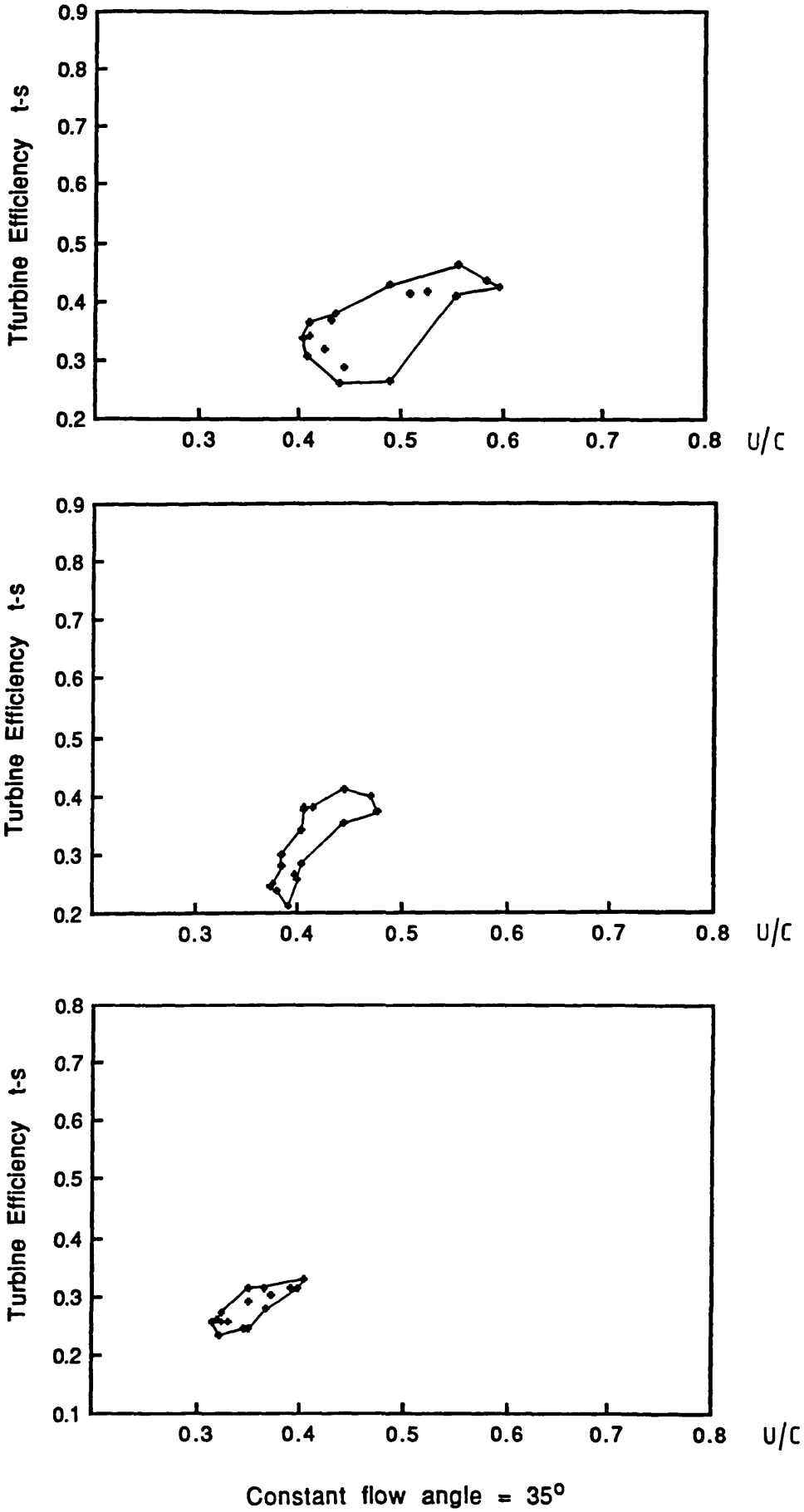


Fig 6.42 Turbine Efficiency with constant absolute flow angle

CHAPTER 7

SUMMARY OF ACHIEVEMENTS, CONCLUSIONS AND SUGGESTIONS FOR FUTURE WORK

This chapter summarizes what has been accomplished and important findings from this work. Suggestions are also made as to how the present investigation could be improved and explored in the future in order to extend the understanding of the fluid dynamics in particular to unsteady flow.

7.1 Summary of Achievements

Flow in a vaneless twin-entry radial-inflow turbocharger turbine has been studied in detail both under steady and unsteady flow conditions. Turbocharger turbine designers have until now been restricted to steady flow test information for development. As a result the variations through a pulse of flow in important regions have not been understood or even perceived. Therefore these are not likely to be included in development of the turbine. The present flow investigations have revealed important characteristics of the flow in particular under unsteady flow conditions.

A turbocharger turbine housing has been instrumented to enable detailed measurements to be made of the flows at rotor inlet and exit, using an L2F velocimeter. The absolute velocity and flow angle in the turbine housing were measured. The instrumented turbine allows these measurements to be made at different azimuth angles. At the rotor inlet, measurements were made across the volute at 1mm intervals. In addition, mirrors were used to deflect the L2F beam so that it is possible to

measure the same point in the flow from different angles, and hence to investigate the presence of axial components of velocity at rotor inlet. At the rotor exit, measurements were primarily made at 30mm downstream of the rotor trailing edge. Measurements have also been made very close to the rotor trailing edge (4mm downstream) and compared with those made further downstream.

Results were obtained for steady flow conditions with equal and partial admission in the volute entries, both at rotor inlet and exit. The results also covered three different turbine operating points. Turbine performance under these operating conditions was monitored. From these measurements, it has been possible to correlate the turbine performance and the gas flow characteristics. Important correlations are observed between the turbine performance and the gas flow characteristics at rotor inlet and exit.

The unsteady flow tests were carried out at a pulse frequency of 50 Hz. The total time-averaged mass flow to the turbine was monitored at a distance of approximately 15m upstream of the rotary pulse generator. The pressure pulse in each of the two limbs is set at 180^{o} out of phase. This reproduces the flow conditions in many common turbochargers, such as a twin-entry turbine fed from a multi-cylinder engine with divided manifold. The pulse generator uses a rotating disc, which has been developed to produce a pressure pulse shape that is similar to a typical exhaust pulse in an engine. The results are presented for different flow conditions, as well as applying different volute separating wall diameters. The presence of axial components of velocity has also been presented. Measurements were obtained for rotor inlet and exit. From these measurements, it has been possible to derive the time-varying velocity triangles. These reveal very large variations of incidence through a pulse at rotor entry, and similarly large changes in rotor exit swirl, even when operating at a nominal

design condition. From the time-varying velocity triangles at both rotor inlet and exit, it has been possible to estimate the time-varying power developed by the rotor and hence time-varying turbine efficiency. Therefore it has been possible to correlate the time-varying turbine performance and gas flow characteristics at both rotor inlet and exit. These investigations have provided a better understanding of the origin of losses associated with pulse flow.

7.2 Conclusions

7.2.1 Steady Flow Tests

The steady flow characteristics have been investigated with different flow conditions and different separating wall diameters. Through-flow velocity and axial velocity components at rotor inlet were measured for equal and partial admission. The turbine performance has been monitored in particular to study the influence on the flow characteristics under partial admission conditions.
The flow investigation can be summarized as follows :

1. The flow characteristics for different flow condition under equal admission flow shows the incidence angle to vary spatially as follows :

u/c	Turbine efficiency	Rotor incidence variation across volute exit	Rotor incidence arithmetic average
0.70	67%	23° to 35°	28°
0.67	67%	20° to 45°	30°
0.57	62%	30° to -10°	16.5°
0.44	53%	10° to -40°	-11.3°

The flow in the volute exit is three dimensional. Under equal admission conditions the axial component is a minimum. As flow in one limb becomes more dominant the axial component increases. The maximum deviation of the flow from the radial plane at extreme partial admission is about 20°.

2. With increasing separating wall diameter, the flows from the two limbs are able to mix at a higher radius. Thus under extreme partial admission conditions, the flow does not reverse in the volute. Flow reversal is, however, noted in the volute exit with smaller separating wall diameters, SWϕ = 80mm and 86mm (R/R_{tip} = 1.067 and 1.147), Figs.5.26b and 5.27b.

3. With the series of partial admission tests, a correlation between the flow characteristics and turbine performance shows that the minimum turbine efficiency occurs at extreme incidence angles. In addition, Figs.5.10 and 5.11 show that under this condition (outer limb fully close) the flow deviation from the radial plane is a maximum. This contibutes to the poor specific work and hence lower turbine efficiency.
The optimum incidence angle (averaged across the volute) for equal admission flow is 28°.

4. At the rotor exit measurements made at 30mm from the rotor trailing edge show that flow in the duct swirls with varying flow conditions. At near the design condition, the swirl is a minimum. Swirl increases as the operating conditions departs from design point.
The flow variation at the rotor inlet (even at extreme partial admission conditions) does not have an appreciable affect on the flow characteristics at the rotor exit.

5. The rotor exit flow characteristics measured close to the rotor trailing edge are different from those measured further

downstream. Closer to the rotor exit, the flow angle is larger.

6. Flow measurements made close to the rotor exit are only possible for the top half of the rotor exit blade (shroud side). This indicates that the flow in the hub region (lower half of the rotor exit blade) is highly disturbed due to blade wake and the effect of the reducing through-flow area near to the hub.

7. Applying a constant mass flow to the turbine and varying the partial admission condition, the turbine efficiency and u/c value change. The range of this change is comparable to those instantaneous efficiency measured by Dale (39).

7.2.2 Unsteady Flow Test

1. Rotor inlet

.The absolute velocity and flow angle vary with the pressure pulse. The variation of flow angle is significant from 5° to 34° at close to design operating point, Fig.6.3c.
.From the absolute velocity, flow angle and blade speed, velocity triangle can be constructed, showing the variations of tangential and radial components of velocity, incidence and relative velocity.
. A very large variation of incidence angle is noted even at near design operation, from 60° to -65°, Fig.6.10. This represents a large variation of incidence losses.
.The magnitude of the velocity pulses varies with different measuring points across the volute exit.

Measurements on the tangential-radial plane clearly show two pulses from the pressure pulse generator, one in each limb. Measuring the same point in the flow on a tangential-axial

plane shows only one pulse. Analysis of the results suggest that the missing pulse probably has a high axial component of velocity in the measuring plane. This, together with the effect of the L2F focal volume rotating on a 30° plane, resulted in insufficient quality data to produce the second pulse.
A comparison of Figs.5.10 and 6.9 suggests that the unsteady gas flows are instantaneously very similar to the steady flow at corresponding partial admission conditions. An important conclusion from this analysis is that under pulsating flow the fluid is in dynamic equilibrium, i.e the turbine is "quasi-steady"

2. Rotor exit

In the steady flow tests, rotor exit measurements show that the swirl increases as the flow condition departs from design point. When the flow condition is near to the design point, a minimum swirl is noted. Under unsteady flow conditions, the extent of the swirl varies within a pulse. From Fig.6.16 the variation of flow angle is observed as follows:

up to 12°	for 0.13 kg/s mass flow
5° to 23°	for 0.17 kg/s mass flow
12° to 36°	for 0.24 kg/s mass flow

The pulses in terms of absolute velocity and flow angle are well defined. For flow conditions away from the design point, it is clear that the swirl becomes more severe and the variation is greater. This swirl decreases as the operating point moves nearer to the design conditions.
By plotting the peak velocity of the flow characteristics across the exit duct, the result shows a variation that is similar to those obtained under steady flow tests. This also gives some indication that the fluid flow remains in dynamic

equilibrium whilst the flow is pulsating.

3 Effect of different separating wall diameters.

. With a small separating wall diameter, SWϕ = 80mm (R/R_{tip} = 1.067), the flow from a pressure pulse in inner limb has not been able to mix well with flow from outer limb as it crosses to the outer limb region. This resulted in what is consistently observed as a single velocity pulse arising from the pressure pulse in outer limb. This observation is made at 270° azimuth angle.

. At 180° azimuth angle there is little effect on the flow characteristics with different separating wall diameters except for SWϕ = 80mm (R/R_{tip} = 1.067).

. With SWϕ = 86mm (R/R_{tip} = 1.147) the flow characteristics change noticeably from 180° to 270° azimuth angle. Two velocity pulses are observed at 180° azimuth angle. As the flow moves to 270° azimuth angle mainly one velocity pulse is observed. The single velocity pulse in this case arises from pressure pulse in either the outer or inner limb depending on the measuring point.

4 Turbine performance

A method to derive the time-varying turbine performance using the unsteady flow characteristics measured at rotor inlet and exit has yielded some useful observations. There is certainly room for improvement in the method to estimate the flow characteristics immediately after the rotor exit. However this method does provide some indications of the unsteady flow turbine characteristics and these are comparable to results obtained by Dale's investigation. The following conclusions are

obtained from the observation made :

. The power developed by the rotor varies in time with the pressure pulse. Maximum power occurs around the low u/c region. As the time-averaged flow departs from the design conditions the power developed by the rotor increases (due to higher turbine inlet pressure) while the u/c values decrease.

. At off-design conditions, the time-variation of power is greater than at near design condition. But the u/c variation is greater at near design point condition.

. Large variations of incidence angle are noted particularly at the design point condition. The rotor incidence affects the power developed by the rotor. This, together with the variation in power developed, probably contributes to the large variation of turbine efficiency. The variation of turbine efficiency is a maximum at near design point conditions. This variation is reduced as flow departs from design flow condition but the general efficiency trends decrease as well.

. Combining the instantaneous turbine efficiency with corresponding u/c values produces efficiency loops. At near the design point condition, this loop is comparatively broad. This is due to the large variation of turbine efficiency and u/c values. Under this condition the turbine operates partially above and below the steady efficiency curve.

. As the time-average flow departs from design point, the efficiency loops gradually falls below the steady efficiency curve. The loop is also narrower and extends over smaller range of turbine efficiency and u/c.

. The variation of turbine efficiency versus u/c can be

identified as two efficiency loops, with each resulting from the pressure pulse in one limb.

. At off-design flow conditions, a lower turbine efficiency is associated with a negative incidence of between -14° to -52°. Under this condition higher swirl is also noted at the rotor exit, Fig.6.16.

. By applying a constant flow angle to the unsteady flow characteristics, a nozzled turbine operating under pulsating flow conditions can be modelled. As this angle increases, the incidence angle becomes less negative, bringing it closer to the optimum value (as measured under steady flow conditions). However the turbine efficiency decreases appreciably above about a 20° angle setting. At an angle of 5°, the efficiency loop under under off-design conditions is lower than when the flow angle is allowed to fluctuate. An optimum angle setting for this turbine appears to be at 10° to 15°.

7.3 Future Work

The L2F velocimeter has proved to be reliable in the gas flow measurement and its sychronizing facility in particular is very useful in taking measurements in between rotor blades and pulse flow measurements. The present study of turbine performance and gas flow characteristics in a vaneless twin entry turbine has produced some interesting results. This study can be extended to single entry turbines, nozzled turbines and mixed-flow turbines, so that a comparison of the gas flow characteristics can be made. The investigation of gas flow characteristics under pulsating and steady flow conditions (with a series of partial admission conditions) has produced useful understanding and these test conditions can also be applied in future work.

The results from unsteady flow characteristics reveal large variations of rotor inlet absolute flow velocity and angle, rotor incidence, and hence turbine performance. These results indicate the areas where further research can be directed.

1. Mixed Flow Turbine

The present study shows that under extreme partial admission flow conditions the axial component of velocity at rotor inlet becomes significant and there is evidence that this also occurs during pulsating flow. The time-varying power developed by the rotor shows that maximum power occurs at low u/c values. Under these conditions, a mixed flow turbine may cope better with higher axial components of inlet velocity. In a mixed flow rotor, the inlet is partially radial and axial direction so that the flow entering the rotor has both radial and axial component. A mixed flow turbine can have non-zero inlet blade angle and still maintain radial blades in section (important for stress). The forward sweep angle which gives reduce degree of reaction allows the maximum efficiency to move to a lower u/c value. The development of mixed flow turbine to achieve peak efficiency at low u/c values (0.5 to 0.6) will maximise exhaust pulse energy. This suggests an area for further research with mixed flow turbine, in particular to investigate the unsteady gas flow characteristics to correlate with the unsteady turbine performance.

2. Modify Turbine Housing

Unsteady flow tests with different separating wall diameters indicate that with the divider very close to the rotor tip only one pulse can be measured. This effect is more obvious at 270° azimuth angle, possibly caused in part by the reduced flow area

in this region. The current design of twin-flow housing has the volute divided 360° meridionally. The thickness of the divider remains constant throughout, thus at higher azimuth angle regions the through-flow area becomes even smaller. If the divider wall can be eliminated around the high azimuth angle region, it is possible that both pressure pulses can contribute to the power developed by the rotor.
A design of such turbine housing is in Fig.7.1 showing a gradual termination of the divider wall from 180° azimuth angle onwards.

3. Single Entry Turbine

The present studies are confined to twin-entry turbines. But most small automotive turbochargers for spark-ignition engines utilize single entry turbines. In the twin-entry turbine investigation the interaction of the flows in the two volute entries when both are pulsed in anti-phase (simulating a common pulse turbocharging arrangement) are very clearly seen. Any improvement on development in single entry turbines may also require an understanding of the flow interaction from the alternating pressure pulses arriving at the rotor. With a single entry turbine the investigation of the presence of an axial component of velocity at rotor inlet will be more direct due to the absence of the divider wall.

4. Nozzled Turbine

A constant flow angle has been applied to the measured unsteady flow characteristics. With a fixed flow angle and varying absolute velocity, this simulates an unsteady flow test in a nozzled turbine. This has produced some interesting results, and indicates that the optimum nozzle setting is 10° to 15°. Variable geometry turbines using vaned nozzles are becoming

more closely investigated in particular for the commercial automotive application. An understanding of the gas flow characteristics and the correlation with turbine performance in this area will be useful in the development of such turbines.

5. Measurement betweeen blades under steady flow condition

Gas flow measurements between blades has been successfully carried out on compressors by using the L2F sychronizing facility to phase lock measurements with the blade frequency (45,46,50). This technique applied to turbine rotors has not been published in the open literature. The objective of this work is to have an understanding of the gas flow behaviour before and after entering the turbine rotor. This work should be extented to partial admission flow, in particular at extreme flow conditions.

6. Instantaneous pressure at volute exit.

Instantaneous pressures are measured before the turbine inlet. These results have been applied to derive the turbine performance using flow characteristics measured at volute exit, thus assuming the instantaneous pressure to remain constant across the volute exit. But results have shown that flow charcteristics vary across the volute exit and interaction of the flow in the volute entries is clearly seen. Thus variation of instantaneous pressure at the volute may occur due to flow interaction from the volute entries. Investigation in this area will be another step towards understanding the unsteady flow characteristics in the turbine and will provide important boundary conditions in unsteady computational fluid dynamics work. Work in this area is already in progress.

7. Analytical methods.

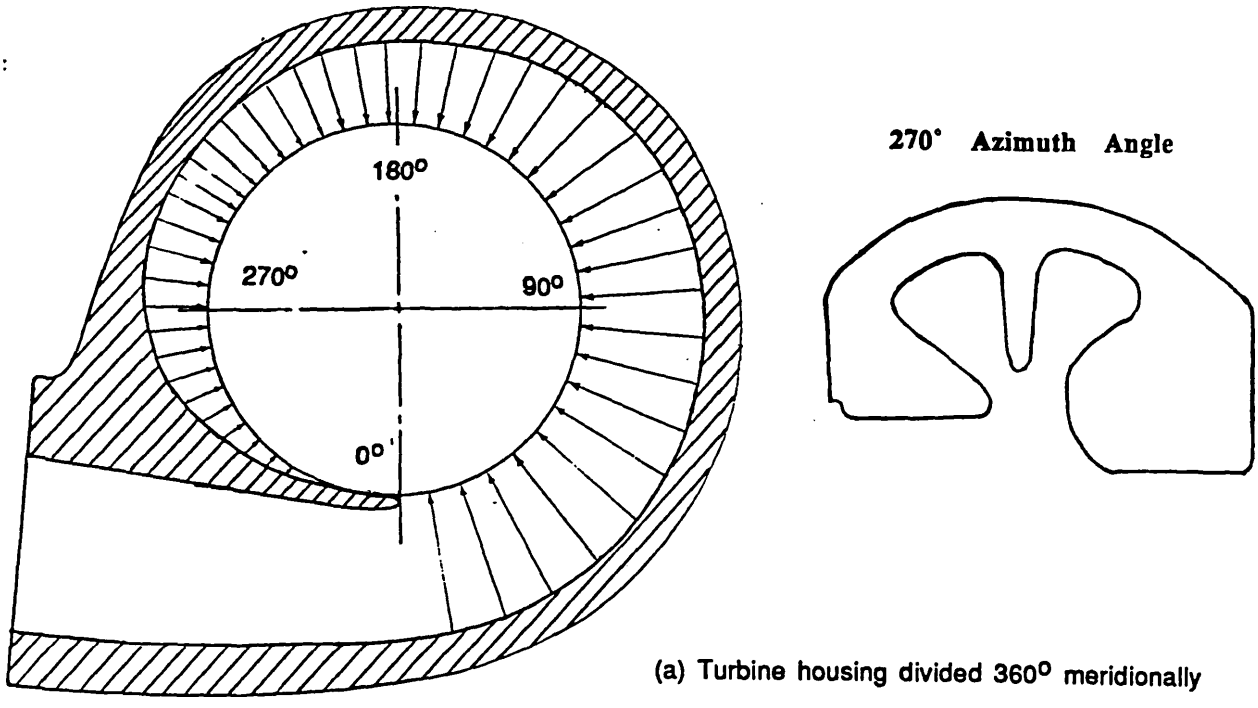
Analytical methods have been developed to model the flow in radial turbines. But these are at present restricted to steady flow application. However any model developed will require experimental data for comparison. The present work has provided unsteady flow experimental data for future development of analytical methods to model unsteady flow in turbines.

7.4 Final Remarks

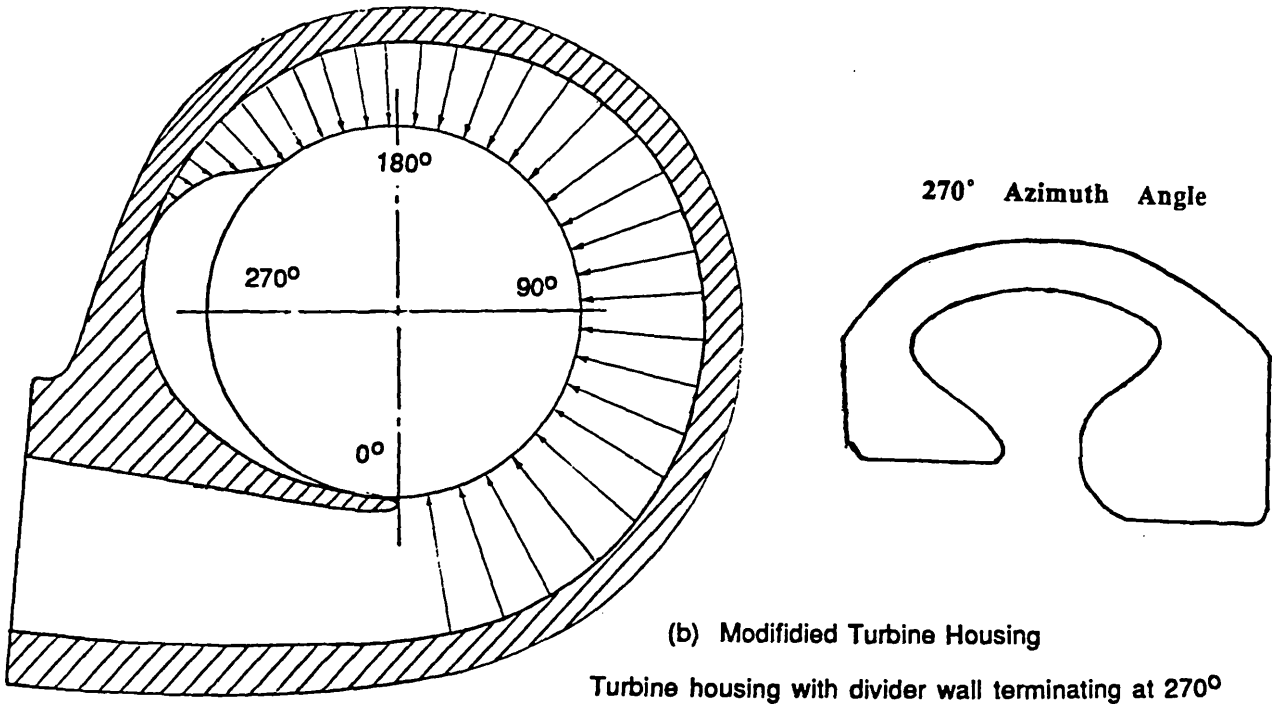
The objectives of this work stated in the introduction have been generally achieved. The gas flow characteristics under steady flow conditions have been investigated in detail with a series of partial admission flow conditions also introduced. Unsteady flow tests have produced unique gas flow information and revealed important variations of flow conditions through a pulse.

The time-varying turbine efficiencies show significant variation from the steady flow performance, which has implications both for the design of radial inflow turbines and for engine-turbocharger matching.

In view of these findings, it becomes more obvious that further developments of turbines for pulse turbocharging should be based more closely on the unsteady flow characteristics and performance. This work has taken a first step towards the unsteady flow investigation in turbocharger turbines, but there are large areas remaining for further investigation.



(a) Turbine housing divided 360° meridionally



(b) Modifidied Turbine Housing

Turbine housing with divider wall terminating at 270°

Fig 7.1 Sectional view of turbine housing

References

1. Kastner L.J. and Bhinder F.S.
   A method for predicting the performance of a centripetal gas turbine fitted with a nozzleless volute casing
   ASME Paper NO 76-GT-65

2. Wallace F.J. , Cave P.R. and Miles J.
   Performance of inward radial flow turbines under steady flow condition with special reference to high pressure ratios and partial admission.
   Proc. Instn. Mech. Engrg. Vol 184 pt1 No 56 1969-1970

3. Futral S.M. and Wasserbauer C.A.
   Off-design performance prediction with experimental verification for radial inflow turbine.
   NASA report TND 2621 1965

4. Benson R.S.
   An anaylsis of the losses in a radial ga turbine
   Proc. Instn. Mech. Engrg. Vol 180 Pt 3J 1966 pp 44-53

5. Hiett G.F. and Johnston I.H.
   Experiments concerning the aerodynamic performance of inward flow radial turbine
   Proc. Instn. Mech. Engrg. Vol 178 Pt 3I 1964 pp 28-41

6. Baines N.C. , Wallace F.J. and Whitfield A.
   A unified approach to the one dimensional analysis and design of radial flow turbine
   ASME Paper No 76-GT-100, 1976

7. Chapple P.M. , Flynn P.F. and Mulloy J.M.
Aerodynamic design of fixed and variable geometry nozzleless turbine casing.
Trans. ASME, Journal of Engineering for Power, Vol 102, Jan 1980

8. Bhinder F.S.
Investigation of flow in the nozzleless spiral casing of a radial inward flow gas turbine
Proc. Instn. Mech. Engrg. Vol 184 Pt 3G 1969-1970

9. Ellison L.F. and Partridge J.M.
Vane vibration in radial flow turbocharger
Instn. Mech. Engrg.
C76/78 ,Turbocharging and Turbochargers 1978

10. Scrimshaw K.H.
Scale effects in small geometrical similar radial gas turbine with particular reference to bladeless volute phenomena
PhD Thesis , King's College, london 1981

11. Tabakoff W. , Vittal V.B.R. and Wood B.
Three dimensional flow measurements ia a turbine scroll
NASA report 167920, July 1982

12. Tabakoff W. , Vittal V.B.R. and Wood B.
Three dimensional flow measurements in a vaneless radial turbine
NASA report CR-167994, August 1982

13. Tabakoff W. , Vittal V.B.R. and Wood B.
Three dimensional flow measurements in a turbine scroll
ASME Journal of Engineering for Gas Turbine and Power
Vol 106 1984 pp 516-522

14. Khalil I.M. , Tabakoff W. and Hamed A.
Losses in the radial inflow turbines
Trans. ASME Journal of Fluid Engineering
Vol 98 Sept 1976 pp 364-373

15. Malak M.F. , Hamed A. and Tabakoff W.
Three Dimensional Flow Field measurements in a radial inflow turbine scroll using LDV
ASME 86-GT-122 , 1986

16. Miller E.C. , L'Ecuyer M.R. and Benisek E.F.
Flowfield surveys at the rotor inlet of a radial inflow turbine
ASME 87-ICE-52 , 1987

17. Miller E.C. and L'Ecuyer M.R.
Flowfield surveys at the inlet and exit of a radial inflow turbine rotor
Thermal Science and Propulsion Center
Purdue University, Technical Report ME-TSPC-TR 85-12, Dec 1985

18. Lymberopoulos N. , Baines N.C. and Watson N.
Flow in a single and twin-entry radial turbine volutes
ASME Paper No 88-GT-59 , 1988

19. Kofskey M.G and Wasserbauer C.A
Experimental performance evaluation of a radial inflow turbine over a range of specific speed
Technical Note, NASA TN D-3742 , 1966

20. Kofskey M.G and Wasserbauer C.A
Experimental evaluation of a 3.5 inch radial turbine designed for a 10 kilowatt space power system
Technical Note, NASA TN D-5550 , 1969

21. Futral S.M, and Holeski D.E
Experimental results of varying the blade-shroud clearance in a 6.02 inch radial inflow turbine
Technical Note, NASA TN D-5513 , 1970

22. Futral S.M and Wasserbauer C.A
Experimental Performance evaluation of a 4.59 inch radial inflow turbine with and without splitter blades.
Technical Note, NASA TN D-7015 , 1970

23. Kofskey M.G and Nusbaum W.J
Effects of specific speed on experimental performance of a radial inflow turbine
Technical Note, NASA TN D-6605 , 1972

24. Mizumachi N. , Endo T. and Kitano M.
A study of aerodynamic characteristics of rotating blades in a radial inflow turbine.
Trans. JSME. Vol 41 1975

25. Tindal M.J. , Williams T.J. and Khalil A.I.
Flow in the volute of small radial turbines
ASME 87-ICE-48 , 1987

26. Benson R.S. and Scrimshaw K.H.
An experimental investigation of non steady flow in a radial gas turbine
Proc. Instn. Mech. Engrs. Vol 180 Pt.3J 1965-1966

27. Wallace F.J. and Blair G.
The pulsating performance of inward flow radial turbines under non-steady flow conditions
ASME Paper No 65-GTP-21, 1965

28. Timmis P.H.
A study of the performance of a twin-entry radial turbine operating under steady and unsteady conditions
MSc Thesis 1968, UMIST

29. Mizumachi N. , Yoshiki H. and Endo T.
A study on performance of radial turbine under unsteady flow conditions
Report of the Institute Of Industrial Science
University of Tokyo, Vol 28 Dec 1979

30. Pischinger F. and Wunsche A.
The characteristics behaviour of radial turbines and its influence on the turbocharging process
CIMAC Tokyo 1977

31. Wallace F.J. , Adgey J.M. and Blair G.P.
Performance of inward radial flow turbines under non-steady flow conditions
Proc.Instn. Mech. Engrs. Vol 184 Pt.1 No.10 , 1969-1970

32. Wallace F.J. and Miles J.
Performance of inward radial flow turbines under unsteady flow conditions with full and partial admission
Proc. Instn. Mech. Engrs. Vol 185 paper C77/71 1970-1971

33. Benson R.S.
Nonsteady flow in a turbocharger nozzleless radial gas turbine
SAE 740739, 1974

34. Miyashita T. et al
Performance of inward radial Flow turbine under unsteady flow conditions.
IHI Engineering Review, Vol 7 No.1 , Jan 1974

35. Kosuge H. et al
Performance of radial flow turbines under pulsating flow coditions
Trans ASME Journal of Engineering for Power
Vol 75-GT-30, Jan 1976

36. Wallace F.J. and Adgey J.
Theoretical assessment of the non-steady flow performance of inward radial flow turbines
Proc. Instn. Mech. Engrs , 1978-1968

37. Benson R.S.
Non steady flow in radial turbines with wave action in the turbine exhaust
I Mech E, April 1976 Paper C63/76

38. Dale A. and Watson N.
Vaneless radial turbocharger turbine performance
Turbocharging and Turbochargers, Paper No C110/86, I Mech E 1986,

39. Dale A.
Radial vaneless turbocharger turbine performance
PhD Thesis, Imperial College, Lond. U., 1990

40. Dale A. , Watson N and Cole A.C
The development of a turbocharger turbine test facility.
I Mech E seminar on " Experimental methods in Engine Research and Development" March 1988

41. Capobianco M. and Gambarotta A.
Influence of the pulsating flow operation on the turbine characteristics of a small internal combustion engine
I Mech E Paper No. C372/019, 1989

42. Acton O. and Capobianco M.
Performance of a radial flow turbocharger turbine.
Proceeding of the Eighth Conference on Fluid Machinery,Vol 1
Scientific Society of Mechanical Engineer
AKADEMIAA KIADO, Budapest, 1987

43. Schodl R.
A laser dual-beam method for flow measurement
in turbomachinery
ASME, Paper No 74-GT-157 , 1974

44. Schodl R.
A laser dual focus velocimeter for turbomachine applications
Advanced Testing Techniques in Turbomachines
VKI Lecture Series 78, April 14 - 18, 1975

45. Eckardt D.
Detailed flow investigationa within a high-speed centrifugal
compressor impeller
Trans. ASME, Journal of Fluid Engrg, Sept 1976, pp 390-402

46. Schodl R.
A laser-two-focus (L2F) velocimeter for automatic flow vector
measurements in the rotating components of turbomachines
Trans. ASME, Journal of Fluid Engrg, Dec 1980, pp 412-419

47. Masaya Tanaka et al
Application of laser 2 focus velocimeter to turbomachines
IHI Engineering Review, Vol 12 No 2, April 1981

48. Elder R.L., Forster C.P. and Gill M.E.
Application of doppler and transit laser anemometry in
small turbomachines
AGARD CP-399,

49. Forster W., Schodl R. and Kruse H.
Evaluation of L2F measurement in unsteady turbine flow
AGARD CP-399,

50. Young M.Y. and Spraker W.A.
Laser velocimeter measurements in a turbocharger compressor
Turbocharging and Turbochargers, I Mech E 1986, Paper No C95/86

51 Watson N. and Janota M.S.
Turbocharging the internal combustion engine.
1982

52. Polytec L2F, Laser Two Focus Velocimetry
Technical Manual 1985

MEASURING PROCEDURE

Measurement with L2F beam in axial direction

Measurements were made along an axial axis. The L2F focal volume is focused on the inner wall. Measuring points were subsequently made with reference to the inner wall.
When the L2F focal volume is focused on a solid dark surface, the 2 spots can be observed on the "back plate" of the L2F unit (the photo-multiplier has to be removed). Once the focal volume is out of focus the two spots will disappear. Accuracy of this setting is about 0.2mm. The two spots can be set to rotate. Constant intensity of the spots indicates consistent flatness of the focused surface.
The axis of measurement is consistently maintained at the centre of the window for all measurements. This is achieved by first focusing the L2F focal volume on a plug that sits in squarely in the optical window access. At the centre of the plug is a tiny bright spot to guide the L2F beam.
Measurement with L2F beam in the axial direction is straight forward. The position of the focal volume has to be noted always. If in doubt, the position of the focal volume can be checked with respect to the reference plane.

Measurement with L2F beam at 30° to the vertical axis

Measuring the same point in the flow from two directions can create a 3D representation of the flow. The L2F beam is deflected such that measurement can be made from another angle.

It is critical to ensure that the focal volume is on the same point in the flow from this angle. This is not straight forward. A reference gauge and a target disc were used to guide the L2F beam to the required position. The L2F unit can be traversed in three directions : vertical, horizontal and axial. All these movements are required here for the exercise shown in Figs.A1 and A2. Fig.A1 shows the set-up with front mirror in position and Fig.A2 with rear mirror in position. These two arrangements have different traverse as tabulated in Tables A1 and A2.

Fig.A3 shows the reference gauge. This gauge is machined to a tolerance of 0.2mm. One end of the gauge is machined down to its centre axis. This ensures that when the L2F beam is focused on this plane from the top, it will be somewhere along the centre axis.

The machined surface is darkened and two thin lines are scribed across the surface, so that the flare will be visible when the L2F focal volume is focused on the plane and along the line. The lines are 3mm and 7mm from the tip of the gauge, which will be pressed against the inner wall. When the gauge is inside the window, the horizontal of the machined surface has to be maintained. This is ensured by machining another flat surface on the opposite end of the gauge along the same plane.

The target disk with a bright centre spot placed on the window recess and used to guide the laser beam to the centre of the window. The windows on each azimuth angle are carefully machined so that their centres are on the same plane.

The mirror is secured by a holder. This assembly is attached by two arms which can slide along a framework. The inclination of the mirror can be adjusted and locked in position. The position of the mirror is indicated in Figs.A1 and A2.

Setting of the focal volume with laser beam directed via the mirror is as follows:

1. Starting with laser beam along the axial axis, move the laser beam vertically upwards and direct it onto the mirror that is already set in position.

2. Place the target disk on the window recess and focus the beam on the disk. The focused volume of the L2F beam should be roughly positioned on the centre of the disk. The two spots on the "back plate" of the L2F unit will be visible, indicating that the beam is focused on the disk.

3.The window is machined so that it is 30° to the horizontal, so the target is on a 30° plane. When focused on this plane the position of the mirror is checked by moving the focused spot around the target disk surface. The two spots on the "back plate" should always be in view. This indicates that the beam has been focused on the target disk plane and that the mirror is inclined correctly. Otherwise the mirror will have be to repositioned.

4. Move the focused beam on the centre of the disk and check for flare on the "back-plate".

5. Remove the target disk. Move L2F unit axially the necessary distance to position the focal volume of the beam in the volute.

6. Insert the gauge in the axial recess and hold against the inner wall (see Fig.A4). Ensure the machined surfaced is horizontal.

7. Focus the beam on the machined surface of the gauge. Check for the two spots on "back-plate".

8. The focused point may or may not line up with the thin line drawn on the surface. If it does, flare will be observed, otherwise two spots will be seen on the "back plate".

9. Axial and vertical movements of the traverse are required to move the focused spot on the reference line.

10. Subsequent movement from the reference line along an axial axis requires two movements. Refer to Tables A1 and A2.

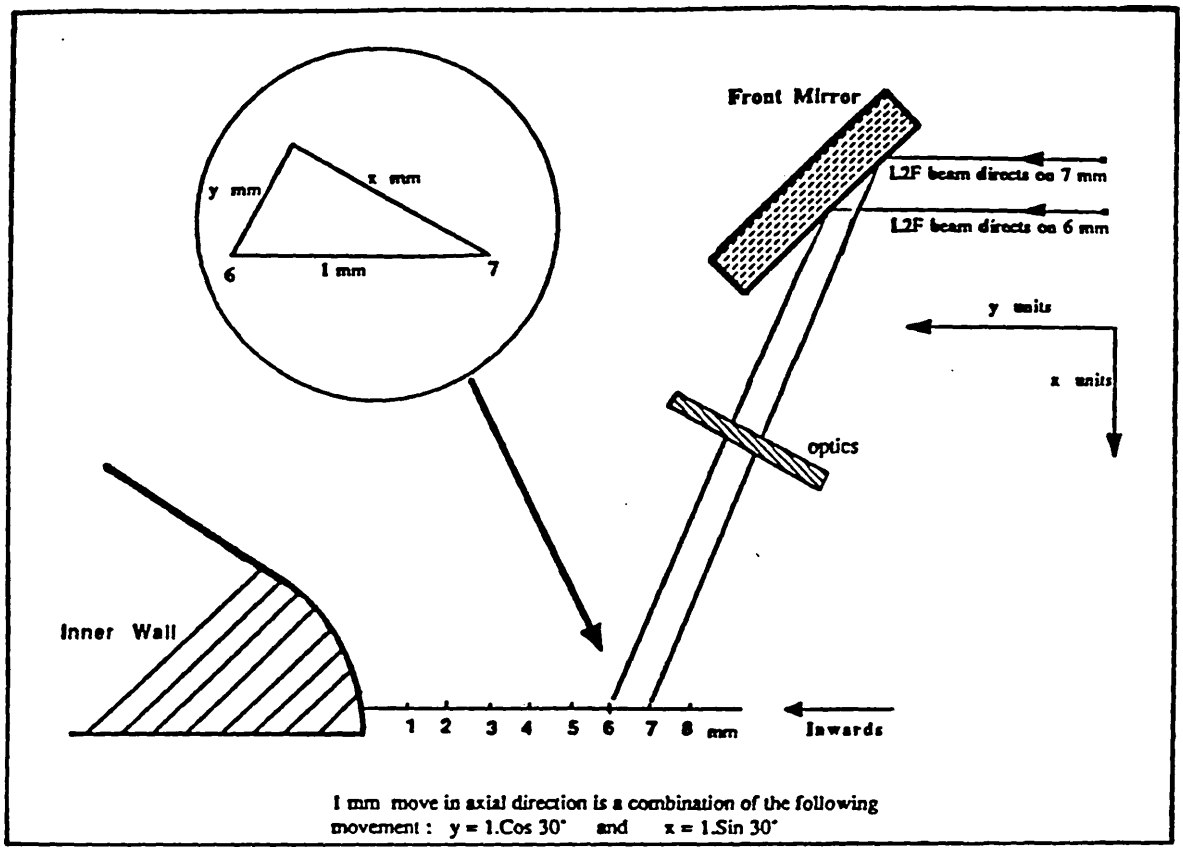


Fig A1 L2F measurement with front mirror

Table A1

Movement Inwards ←	Down x mm	Inwards y mm ←	Movement outwards	Up x mm	Outwards y mm
1 mm	0.87	0.5	1 mm	0.87	0.5
2 mm	1.73	1.0	2 mm	1.73	1.0
3 mm	2.6	1.5	3 mm	2.6	1.5
4 mm	3.47	2.0	4 mm	4 mm	2.0

This table is for traverse with Front Mirror in position at 180° section

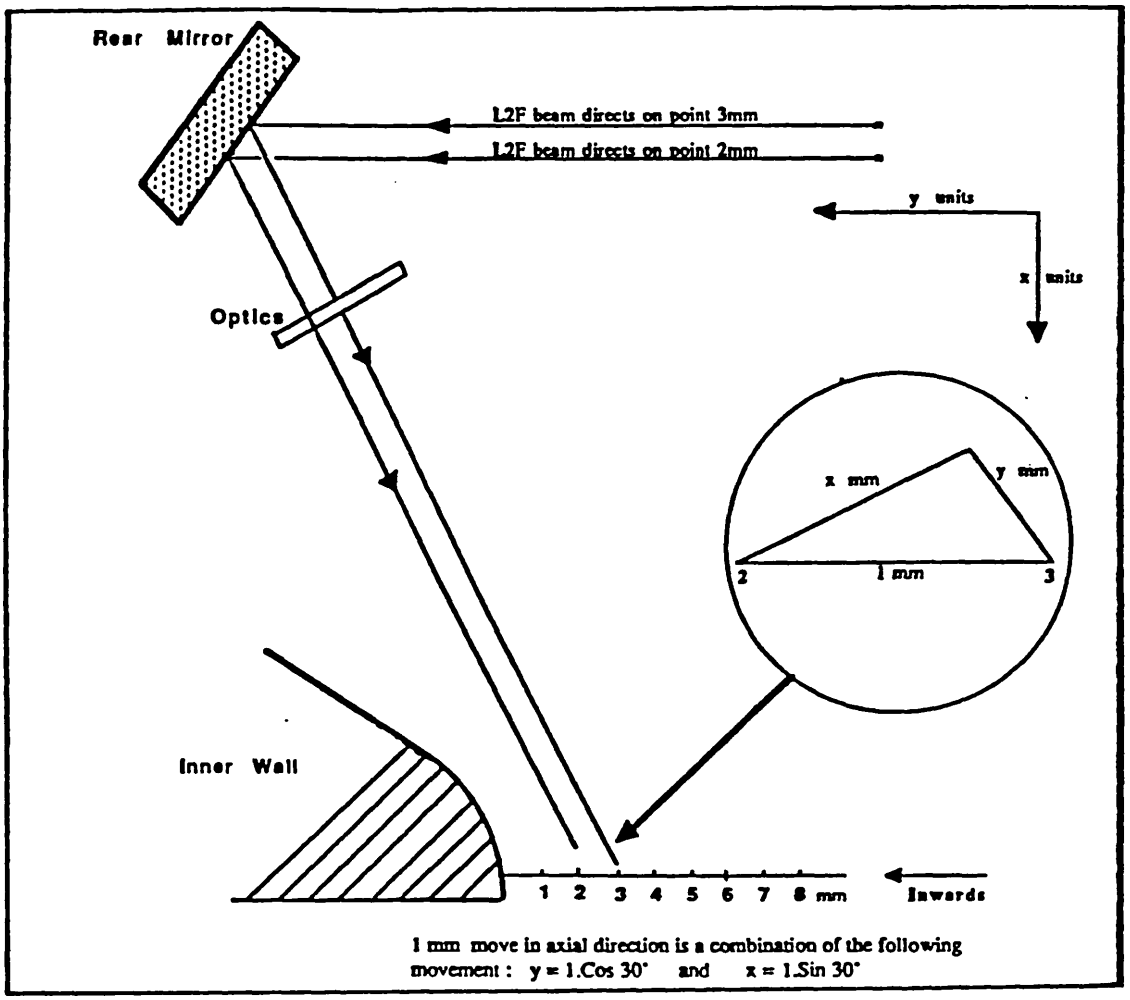


Fig A2 L2F measurement with rear mirror

Table A2

Movement Inwards ←	Down x mm	Outwards y mm	Movement outwards	Up x mm	Inward y mm ←
1 mm	0.87	0.5	1 mm	0.87	0.5
2 mm	1.73	1.0	2 mm	1.73	1.0
3 mm	2.6	1.5	3 mm	2.6	1.5
4 mm	3.47	2.0	4 mm	4 mm	2.0

This table is for traverse with Rear Mirror in position at 180° section

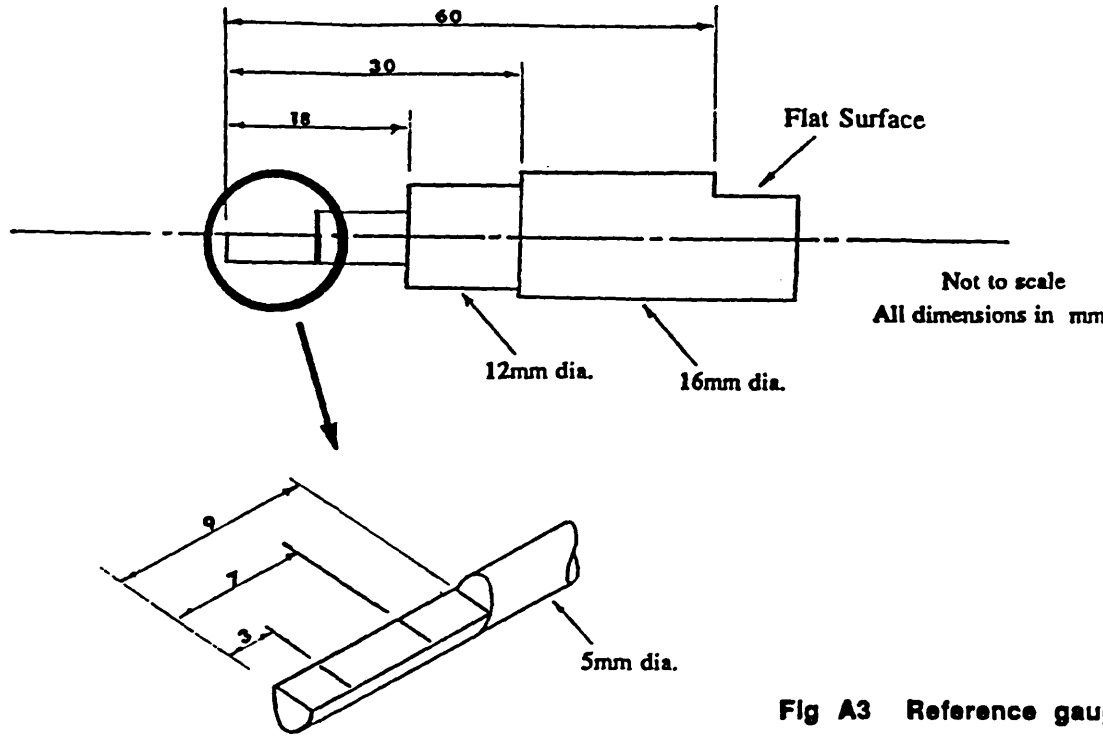


Fig A3 Reference gauge

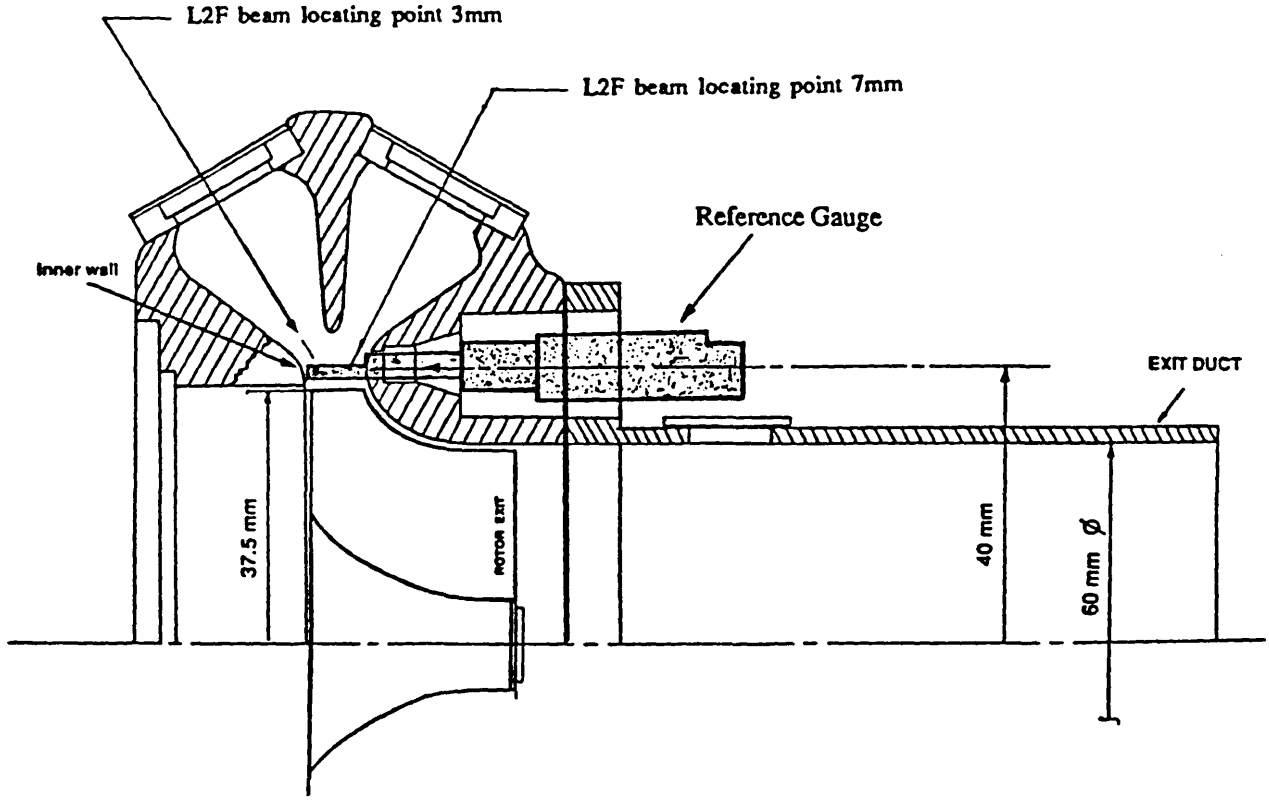


Fig A4 Locating point 3mm and 7mm with reference gauge

Effect of deflecting the L2F beam via the mirror

Appendix A described the method of how this was carried out by using either the front or the rear mirror to deflect the L2F beam. Due to the divider wall the deflection angle of the beam is 120° with front mirror and 60° with rear mirror. In both cases the L2F focal volume is rotating on a plane at 30° to the axis of the turbine. The following describes how this can affect the angle ψ (defined in Fig.B2) which includes flow with a third component of velocity.

Fig.B1 shows the L2F focal volume rotating on a 30° plane using front mirror. At the focal point the stop trigger beam (A') rotates around the start trigger beam (A). When a predetermined number of particles cross the start trigger beam, the stop trigger beam will be advanced to the next preset angle until the preselected angular scan of the flow has been covered.

If the maximum particle intensity is detected when the angle θ is at 90°, this implies that the flow has zero axial component of velocity. When the angle θ is greater than 90°, it indicates that the flow deviates in the direction towards inner limb and vice versa

$$x = s.\sin (\theta - 90°)$$

$$h = x. \sin 30°$$

$$= s. \sin 30° \sin (\theta - 90°)$$

From View A (Fig.B2) with stop trigger beam rotated to position B

$$\psi = \tan^{-1} ((l-h)/s)$$

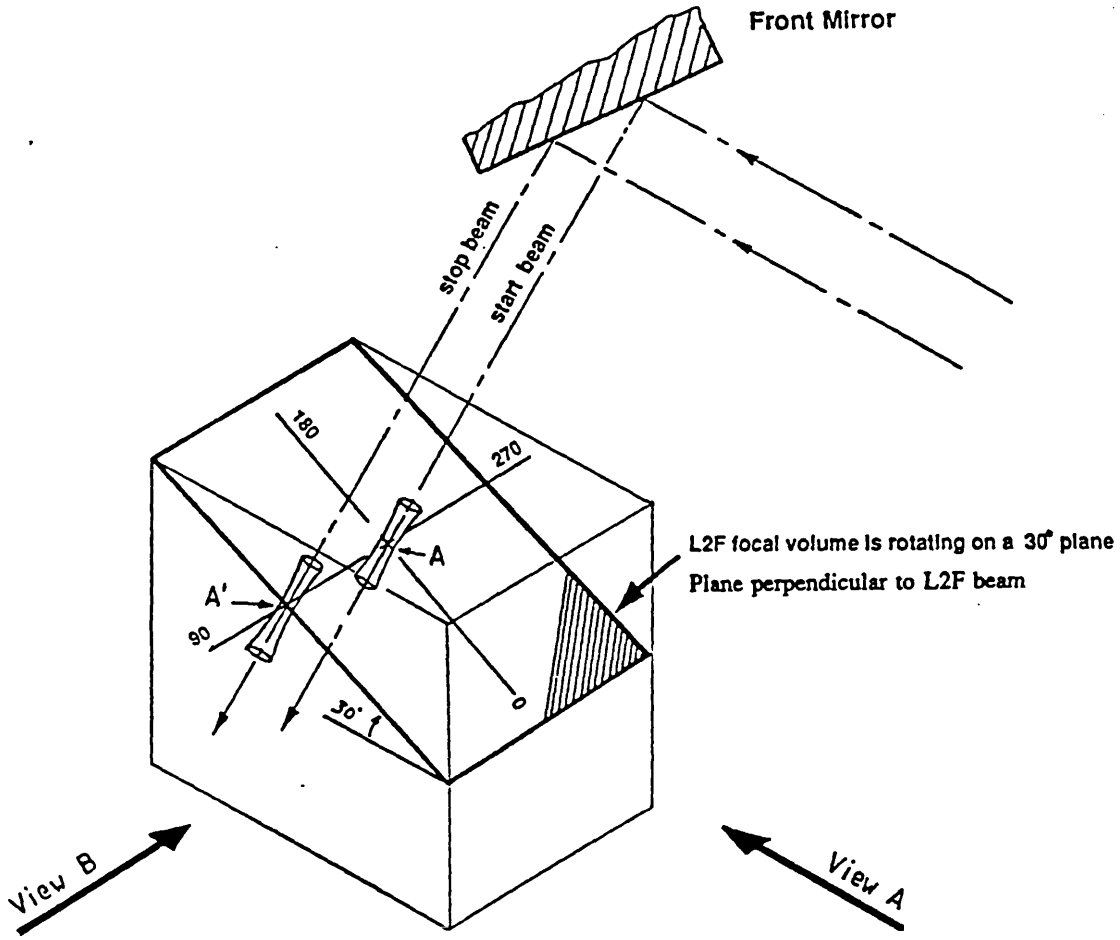
In the L2F optical system, $s=\ell$, thus

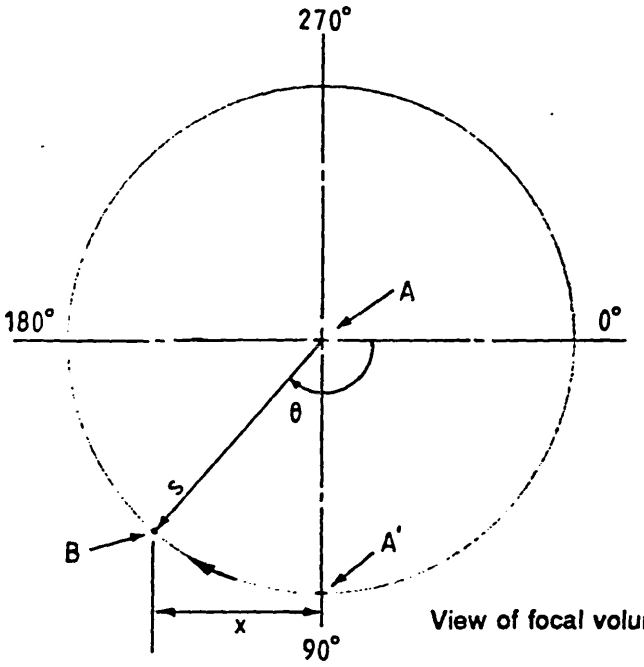
$$\psi = \tan^{-1} (1 - \sin 30^\circ . \sin (\theta - 90^\circ))$$

When angular scan θ is greater than 90° (implying an axial component of velocity in the direction towards inner limb) ψ becomes less than 45°. Table B1 shows how ψ reduces as θ increases beyond 90°.
Consider $(\theta-90^\circ) = 45^\circ$, ψ decreases to 32°. Therefore if the third component of velocity has an absolute flow angle in the region of 32° or more it becomes more difficult for the same particle to trigger both the start and stop beams and thus yield sufficient quality data to produce results.

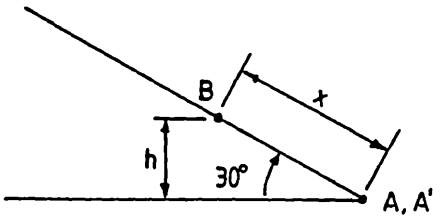
This problem can be minimized by changing the angle of deflection of the L2F beam so that the plane on which the focal volume rotates becomes more horizontal. Table B2 shows how ψ can be improved when the plane becomes more horizontal.

The analysis can be applied when using the rear mirror to deflect the L2F beam. Fig.B3 shows in this case that when angle θ is less than 90° the flow is in the direction towards the outer limb. As θ becomes less than 90°, ψ decreases.





View of focal volume on a 30° plane



View B

Fig B1 L2F measurement with front mirror

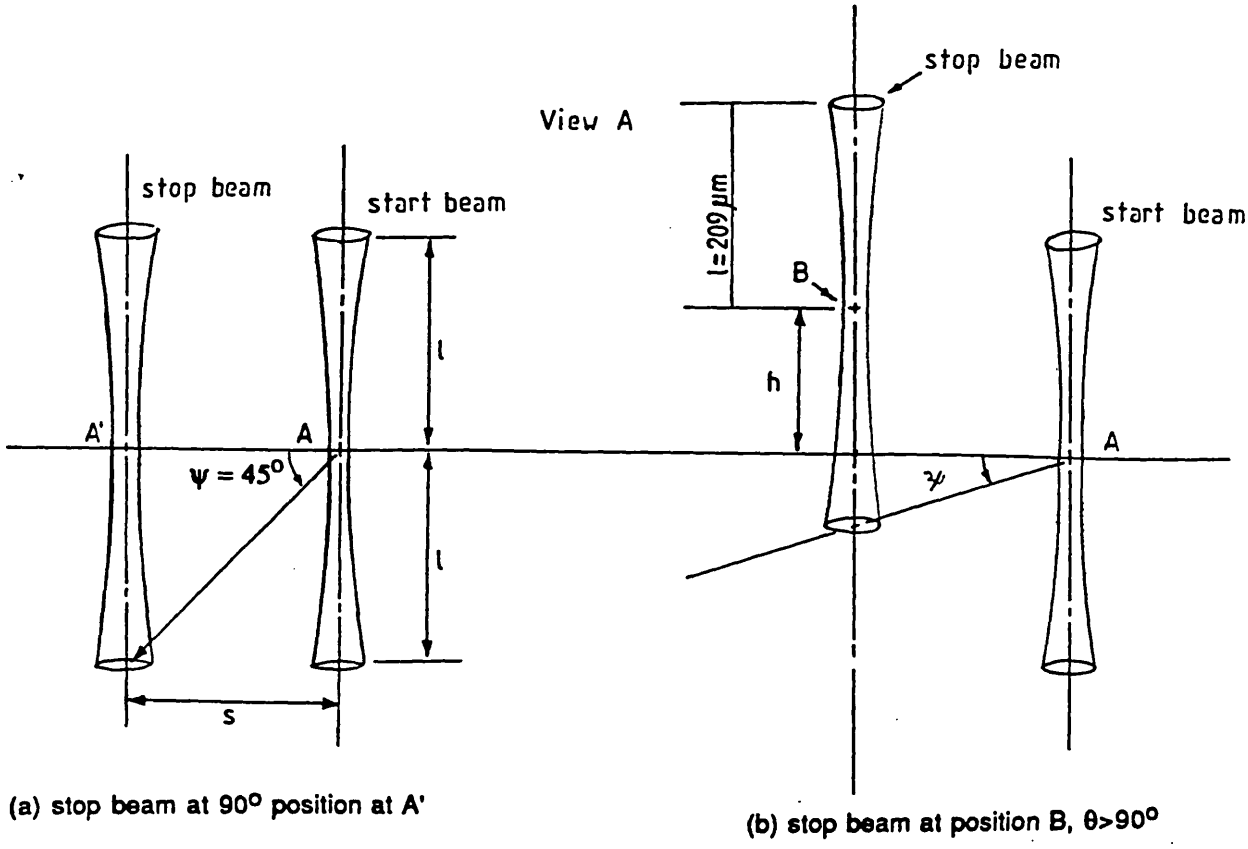


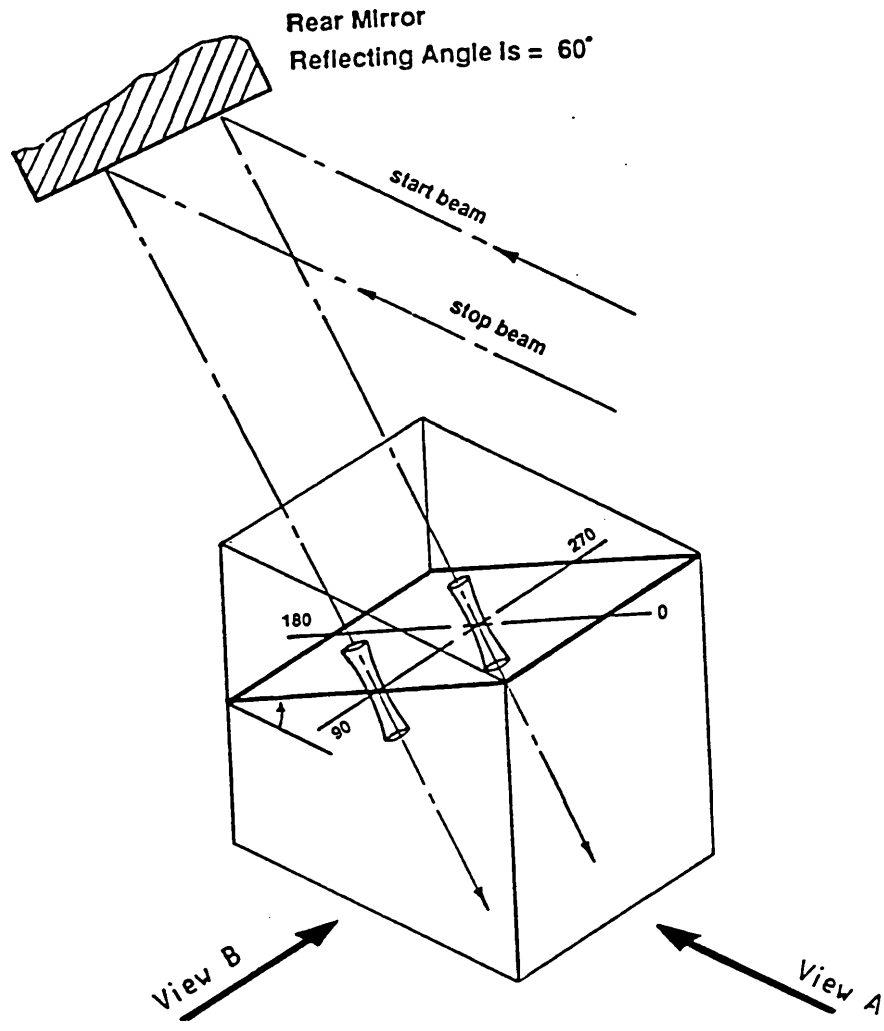
Fig B2 View A

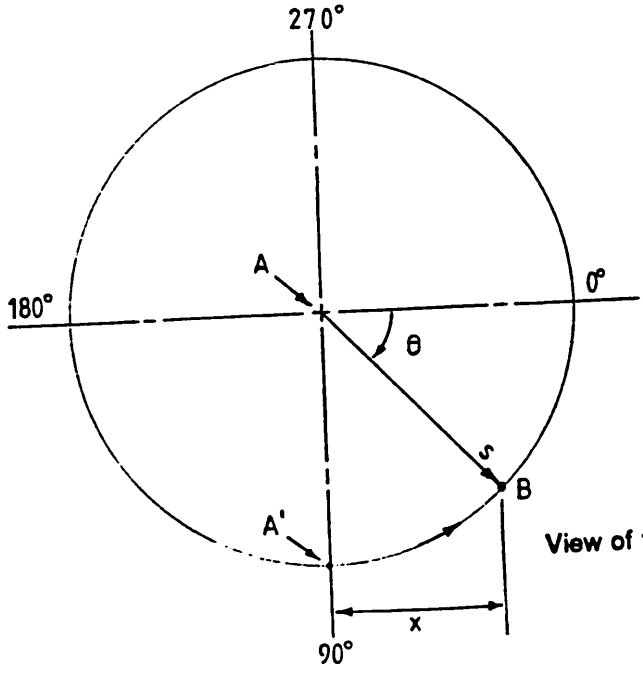
Table B1

30° Rotating plane	
θ - 90°	ψ
20°	40°
30°	37°
40°	34°
45°	32°

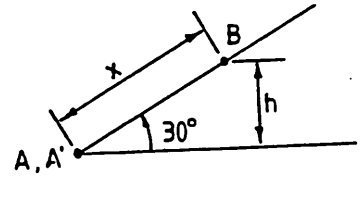
Table B2

15° Rotating plane		10° Rotating plane	
θ - 90°	ψ	θ - 90°	ψ
20°	42°	20°	43
30°	41°	30°	42
40°	40°	40°	41.6
45°	39°	45°	41.3





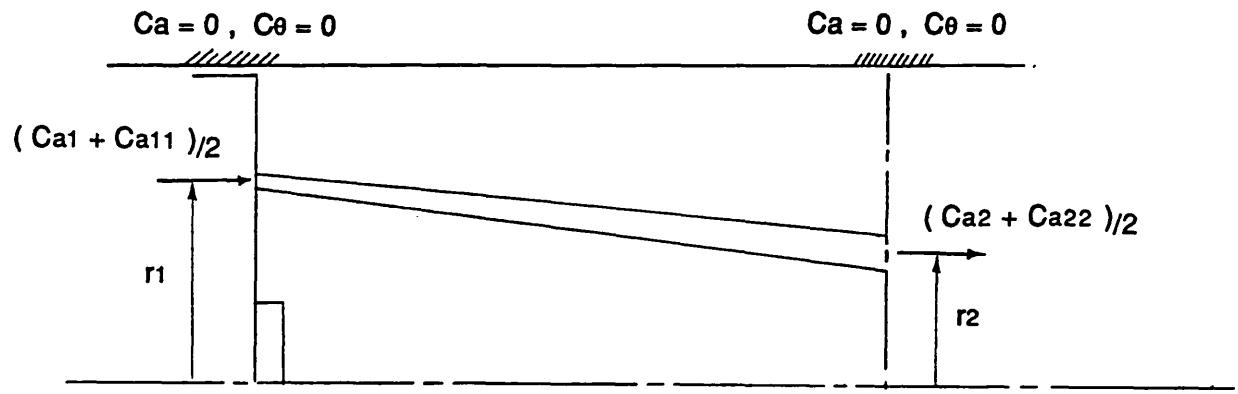
View of focal volume on a 30° plane

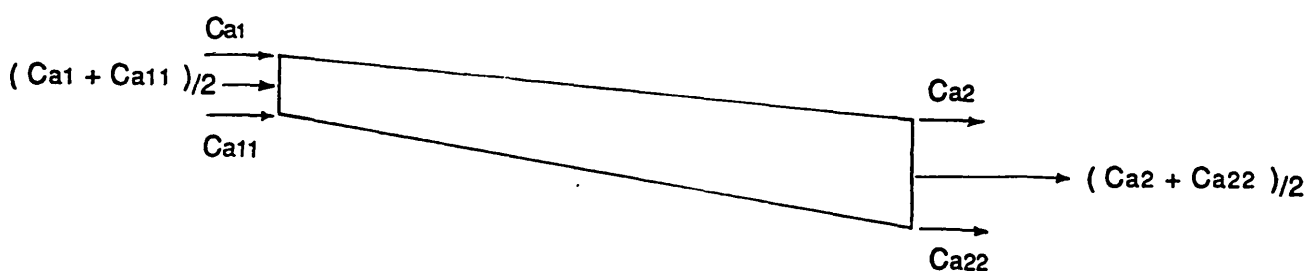


View B

Fig B3 L2F measurement with rear mirror

To calculate values immediately after rotor exit using values measured at 30mm downstream of it.





Calculate axial velocity

From continuity :

$$(C_{a1} + C_{a11})/_2 \times (\text{annulus area})_1 = (C_{a2} + C_{a22})/_2 \times (\text{annulus area})_2$$

For starting point C_{a2} and C_{a1} are assumed zero at the wall. Section 1 and 2 are divided into 30 strips. C_{a22} is a known value, hence C_{a11} can be calculated.
A weakness in this method is that as the $(\text{annulus area})_2$ tends to zero in the centre of duct it produces a singularity and forces C_{a11} to zero, which is probably unrealistic.

Calculate tangential velocity

Assume flow in the rotor exit to be free vortex.
Thus

$$r_1 . C_{\theta 1} = r_2 . C_{\theta 2}$$

$$C_{\theta 1} = (r_2 . C_{\theta 2}) / r_1$$

The method described above to calculate the velocity immediately after the rotor exit can be improved. This can be achieved by measuring the total temperature and pressure (in addition to flow velocity) at the measuring points downstream of the rotor exit and applying a two dimensional analysis in the streamtube.

To calculate unsteady turbine performance using unsteady flow characteristics measured at rotor inlet and exit.

The rate of change of angular momentum is equal to the sum of the moments of the external forces (torque). Since angular momentum is the moment of linear momentum, the rate of change is given by the product of mass flow rate, radius and velocity. Thus the torque becomes,

Torque $TQ = m(r_1 C_{\theta 1} - r_2 C_{\theta 2})$

The energy transfer (power developed by the rotor) is given by the product of torque and angular velocity.

$$W = TQ.\ \omega$$

$$W = m\ (U_1 C_{\theta 1} - U_2 C_{\theta 2}) \quad \ldots\ldots\ldots\ldots\ldots\ (1)$$

To calculate the power developed, the rotor is divided into 8 elements, Fig.D1. At the rotor inlet measurements were made across the volute exit (2m to 8mm measuring points). Data at 1mm is extrapolated. Where there are missing data within the cycle (due to poor quality signal) these are interpolated. The earlier findings in section 6.2 on the variation of the peaks of the velocity pulses across the volute exit provide a good guide to develop a time-varying representation of the unsteady flow characteristics at the rotor inlet.

At the rotor exit, measurements were made 30mm downstream of the rotor trailing edge. At the rotor exit, the unsteady flow characteristics measured across the exit duct are of the same phase, Fig.6.17. Therefore it is possible to arrange data on

the same time base and plot it as a function of distance across the exit duct. The tangential and axial components of velocity are then used to calculate values immediately after the rotor, using the method described in Appendix C. The rotor exit is also divided into 8 elements corresponding to rotor inlet.
Although it is evident that under unsteady flows condition the rotor speed fluctuates during a pulse, Dale (39) showed that the variation is very small. Therefore in the following method to calculate power developed, the rotor speed is assumed to be constant. From equ.(1) the power developed by rotor in each streamtube can be written as :

$$dW = (\delta m \; U_1 \; C_{\theta 1})_{\text{rotor inlet}} - (\delta m \; U_2 \; C_{\theta 2})_{\text{rotor exit}}$$

where

$$(\delta m)_{\text{rotor inlet}} = \rho . 2 . p . R_{tip} . \; dx . \; C_r$$

$$(\delta m)_{\text{rotor exit}} = \rho . 2 . p \; . r . \quad dr . \; C_a$$

R_{tip} = rotor tip radius

U_1 = tip speed

r_2 = radius at rotor exit

$U_2 = \omega . \; r_2$

density ρ is assumed constant i.e ($\rho_1 = \rho_2$) since the Mach number for the test condition is less than 0.3.

The turbine efficiency and blade speed ratio are defined as follows:

$$\text{Turbine Efficiency (t-s)} = \frac{\text{Power developed by rotor}}{\text{Isentropic power}}$$

$$\text{Isentropic power} = \delta m . \; C_p . \; T_{total} \; (\; 1 - (PR)^{(1-\gamma)/\gamma} \;)$$

$$U/C = \frac{\pi . \; N/60 \; . \; \text{rotor diameter}}{\sqrt{2 . \; C_p . \; T_{total} \; (\; 1 - (PR)^{(1-\gamma)/\gamma} \;)}}$$

where

$$PR = \text{turbine expansion ratio} = \frac{\text{turbine inlet total pressure}}{\text{turbine exit static pressure}}$$

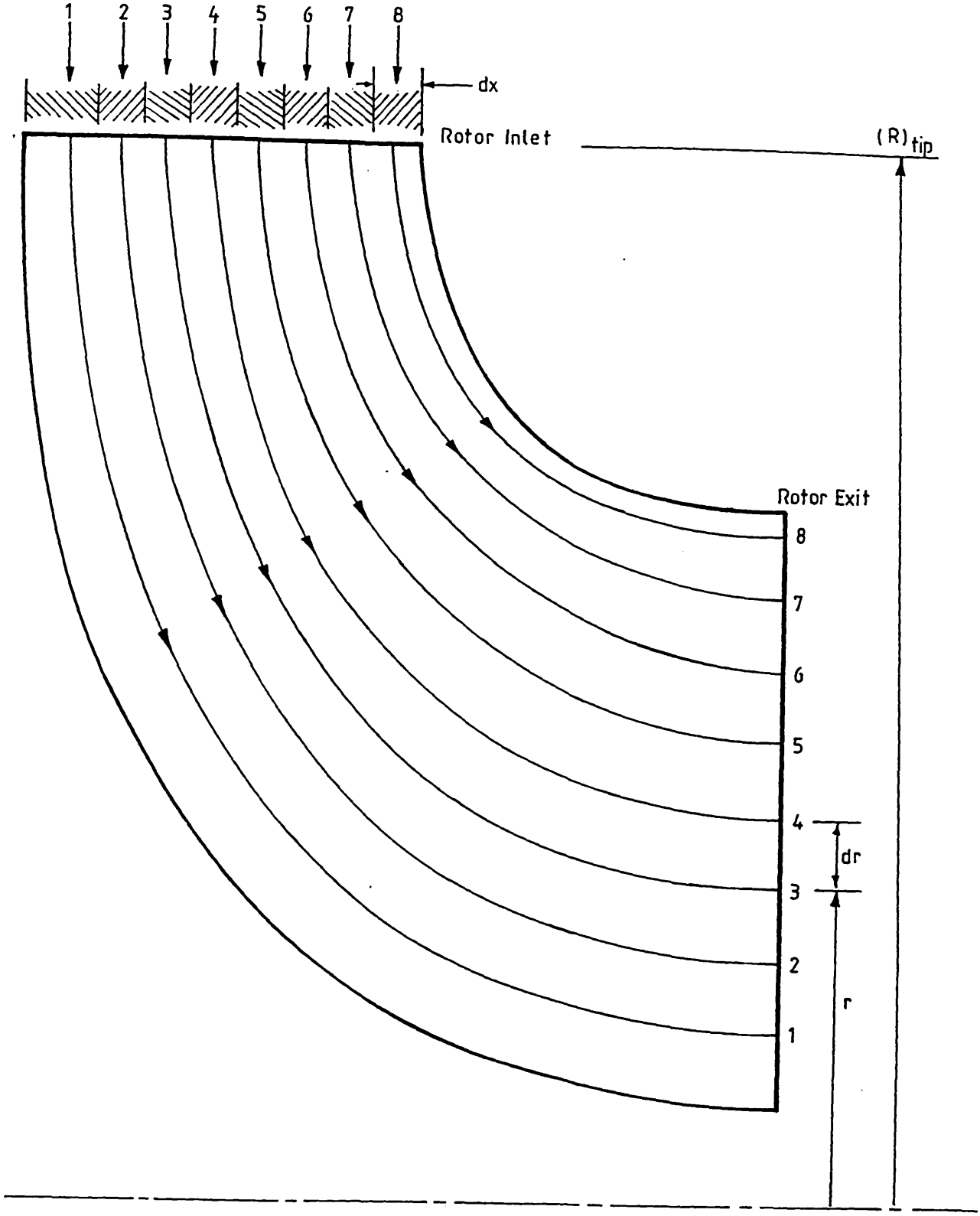
The turbine exit pressure is ambient (measured at the exit duct). Turbine inlet total pressure is derived from the instantaneous pressure (static) measured at the turbine inlet.

From steady flow test, the following parameters are applied

Total Mass Flow	γ	C_p	Ambient Pressure	Density, ρ
0.13	1.389	1.0246	1.0004	1.180
0.17	1.389	1.0236	1.0004	1.241
0.24	1.389	1.0230	1.0004	1.370

Gas constant, R = 287 J/kgK
Rotor speed, N = 34000 rev/min
Rotor tip diameter = 0.075m
Turbine Inlet Temperature = 350K
Cross sectional area of duct where instantaneous pressures were measured, A = 0.001232 m^2

Assumptions
There is no mixing between streamtubes, implying negligible secondary flow and overtip leakage. This is almost certainly not the case in actual operation.



$$\delta W = (\delta m\, U_1\, C_{\theta 1})_{\text{rotor inlet}} - (\delta m\, U_2\, C_{\theta 2})_{\text{rotor exit}}$$

where

$$(\delta m)_{\text{rotor inlet}} = \rho . 2 . \pi . R_{tip} . dx . C_r$$

$$(\delta m)_{\text{rotor exit}} = \rho . 2 . \pi . r . dr . C_a$$

Fig. D1